ELECTROMAGNETIC SURFACE WAVE PROPAGATION ON A FERROMAGNETIC INSULATOR WITH ACTIVE AND PASSIVE BOUNDARIES

by

THOMAS JAMES GERSON

A dissertation submitted to the Graduate Faculty in Engineering in partial fulfillment of the requirements for the degree of Doctor of Philosophy, The City University of New York.

1974

This manuscript has been read and accepted for the Graduate Faculty in Engineering in satisfaction of the dissertation requirement for the degree of Doctor of Philosophy.

May 16, 1974
date

Joseph S. Nadan
Chairman of Examining Committee

5/16/74
date

Jacques E. Bemeniste
Executive Officer

Professor Morris Ettenberg

Professor Carl Shulman

Professor Joseph S. Nadan
Chairman

Supervisory Committee

The City University of New York

Abstract

ELECTROMAGNETIC SURFACE WAVE PROPAGATION ON A FERROMAGNETIC INSULATOR WITH ACTIVE AND PASSIVE BOUNDARIES

by

Thomas James Gerson

Advisor: Professor Joseph S. Nadan

Electromagnetic propagation of surface waves on a ferrite slab of finite thickness magnetized parallel to the planes of its dielectric-ferrite-dielectric interfaces is investigated. It is shown that changes in the permittivities of the dielectric regions not only modify the frequency ranges and wavelengths of the dynamic modes but under certain conditions cause these modes to be cutoff or propagate in the same directions as the magnetostatic surface modes.

The propagation of electromagnetic modes on the surface of a ferrite slab backed by a perfect conductor is also considered. Surface wave propagation at frequencies greater than the ferrite-metal mode resonance frequency is predicted for thick grounded ferrite slabs thereby clarifying prior results based upon semi-infinite and magnetostatic analyses. A close relationship is shown to exist between the magnetostatic ferrite-metal mode and the dynamic modes of the semi-infinite model.

Surface electromagnetic mode propagation along the interface between a magnetic insulator and a semiconductor is also examined. The interaction between the surface wave and streaming carriers in the semiconductor is investigated to determine the effects on the predicted instability of minority carriers, finite ferrite thickness, surface space charge layers and dielectric separations between the media.

In loving memory

of my father

ACKNOWLEDGEMENTS

I would like to express my gratitude to my mentor, Professor Joseph S. Nadan, for his guidance and encouragement. I am deeply indepted also to the late Professor Bayram Vural under whose tutelage this work commenced.

Among the many people who have, by their interest in me and the progress of my work, earned my lasting gratitude are Provost Egon Brenner, Dr. Paul Fenster, the late Professor Phillip M. Brown and Professors Abraham Abramowitz, Joseph B. Aidala, Shee-Ming Chen, George Eichman, Morris Ettenberg, and Anton Steinhauser. I also wish to thank my friend and colleague Andres Fortino for his many kindnesses and his help.

Many thanks are due to Messrs. Fred Schneider and Abraham Glasser for their work in preparing the test fixtures and materials. I very much appreciate the efforts of the following people who helped me in producing this manuscript: Mr. Sam Borenstein, Mr. and Mrs. Ernest Cuni, Ms. Elizabeth Davis and Mr. Allen Halegua. The assistance provided me by Mr. David Pressman and Mrs. Venus Santiago is also appreciated.

I wish to acknowledge the support received as an NDEA Fellow, through the research programs of CUNY and the Air Force Office of Scientific Research (AFOSR-69-1700) and from the Department of Electrical Engineering at the City College.

Lastly, but certainly not least, I wish to thank my family, especially my lovely wife, for their love and support and for the sacrifices which they made so that I could complete this dissertation.

TABLE OF CONTENTS

LIST OF TABLES

LIST OF ILLUSTRATIONS

CHAPTER 1

INTRODUCTION AND BACKGROUND

The anisotropic properties of high resistivity ferrites has led to their extensive use in microwave devices. Isolators[1] and circulators.[2] based on the non-reciprocal behavior of magnetized ferrites have been developed and are important components for the microwave engineer. The relatively low losses associated with the ferrite Yittrium Iron Garnet makes this material attractive for use as the resonating element of magnetically-tuneable microwave filters.[3] The use of ferrites as substrates in microwave circuits[2,4] assures continued active interest in the microwave applications of these materials.

The magnetostatic modes supported by a slab of ferrite material magnetized in the plane of its faces have been theoretically investigated by Damon and Eshbach.[5] In this system, waves are guided along the surface in a direction transverse to the applied static magnetic field over a range of frequencies. The dispersion characteristics for propagation in the forward and reverse directions are symmetrical about the k=0 axis, the waveamplitude having its maximum at a ferrite-air interface determined by the direction of wave propagation (or the direction of applied static magnetic field). Brundle and Freedman obtained experimental verification of this theory in 1968[6]. Placing a metal plate in contact with first one and then the other surface of a transversely magnetized ferrite slab, the symmetry of the propagation characteristics

was destroyed, thereby demonstrating the unidirectional character of the magnetostatic mode of interest. Seshadri [7], considering a transversely magnetized ferrite slab with one surface in contact with a perfect conductor, pointed out that while symmetry about k=0 is destroyed, magnetostatic waves may still propagate in both directions. In addition to a magnetostatic mode similar to the Damon and Eshbach mode, a magnetostatic mode, which Young [8, 9] referred to as a ferrite-metal mode, is found to propagate in the reverse direction. (The case where the conductor is lossy has also been studied in the magnetostatic limit by DeWames and Wolfram [10].)

The study of electromagnetic wave propagation guided by the surface of a ferrite slab in some cases predates the aforementioned magnetostatic studies. In 1955, Lax and Button,[73,74] while investigating the problem of wave propagation in a rectangular waveguide containing one or two transversely magnetized ferrite slabs, considered electromagnetic mode propagation parallel to the surface of a semi-infinite ferrite slab backed by a perfect conductor. They found that such a structure could support a unidirectional mode guided along the ferrite-air interface. The mode, which they referred to as a ferrite-dielectric mode corresponds to the forward mode studied in the magnetostatic limit by Young [8, 9] and Seshadri [7]. Bressler [11], in 1959, found that in addition to the forward mode, a second mode propagating in the reverse direction also

exists. This mode exhibits a resonance as does the corresponding magnetostatic ferrite-metal mode.

The propagation characteristics of electromagnetic surface modes at a semi-infinite ferrite-dielectric interface have been investigated by Bressler[11] and Courtois et. al.[12] In addition to a mode closely resembling the magnetostatic surface mode found by Damon and Eshbach,[5] a mode propagating in the opposite direction is supported at the ferrite-dielectric interface. Courtois et. al., adopting the nomenclature used in previous investigations of mode spectra supported by longitudinally magnetized ferrite rods,[13] labelled this mode a dynamic mode since it may only be calculated by including the effects of electromagnetic wave propagation; ie. not making the magnetostatic approximation. The upper frequency limit of this dynamic mode is greater than the ferrite-metal mode resonance.

The propagation characteristics of electromagnetic surface waves supported by a slab of finite thickness with magnetization parallel to its dielectric-ferrite-dielectric interfaces is investigated. By examining the ratio of the surface wave energy densities at the top and bottom surfaces, it is demonstrated that a set of modes resembling the semi-infinite ferrite-dielectric modes is associated with each surface. When a perfect conductor is placed in intimate contact with one of the slab faces, the modes associated with this surface disappear while those associated with the opposite face are modified. For thin ferrites the dynamic mode is transformed

into a mode resembling the magnetostatic ferrite-metal mode. When the slab is sufficiently thick, it is found that the grounded slab may support surface wave propagation at frequencies greater than the ferrite-metal mode resonance frequency.

Additionally, the dispersion relationships describing electromagnetic propagation of waves guided by the surfaces of an ungrounded ferrite slab are studied to determine the effects of varying the thickness of the ferrite and of changing the permittivity of the dielectric media. It is found that the frequency range of the dynamic modes may be altered significantly by the properties of the adjacent dielectric regions; the dynamic mode may even be cutoff over the entire spectrum for certain combinations of material parameters and applied fields. The results of the finite thickness ferrite analyses are employed to evaluate data obtained from empirical transmission studies. Through the correlation of the dispersion characteristics based on an electromagnetic calculation with those obtained experimentally, it is possible to explain the observed behavior as a function of applied field for the low frequency portion of the transmission spectrum. The explanation would not have been forthcoming if the magnetostatic calculation had been used instead, for the magnetostatic approximation is not valid in this portion of the spectrum.

The possibility of obtaining an active interaction between streaming carriers and slow waves supported by the spin system of a magnetically ordered material has prompted considerable interest.[14-26] In 1964,

Spector and Trivelpiece [16] described an experiment in which they attempted to obtain oscillations through interaction of backward waves supported by polycrystalline ferrite slabs and an electron beam drifting between them. While their results were negative, this was attributed to the relatively high loss associated with the polycrystalline Yittrium Iron Garnet. With the development of chalcogenide spinels having both magnetic and semiconducting properties [27] another medium for possible active interactions became available. However, while evidence for an active helicon-spin wave interaction was presented by Vural and Thomas in 1968 [19], Robinson et.al. [23] have indicated that it is not possible to obtain unstable interactions with the high resistivities of the materials presently available.

In 1967, Vural et. al. suggested that an instability coulld be obtained in a structure consisting of adjacent ferrite and semiconducting layers through the interaction of surface waves supported by the ferrite with streaming carriers in the semiconductor. Robinson et. al. [23] analyzing a semi-infinite ferrite-semiconductor system in the magnetostatic limit developed an instability onset criterion. With the aid of this condition and further mathematical analysis they predicted that structures consisting of adjacent layers of indium antimonide and Yittrium Iron Garnet were potentially unstable at room temperature for X-band frequencies. Schlömann [18], investigating the propagation of magentostatic surface waves along the interface between a low-loss ferrite and

a high-mobility current carrying semiconductor film, also concluded that an instability could be obtained at room temperature using YIG and InSb under certain conditions.

Electromagnetic propagation of surface waves along the interface of a semi-infinite semiconductor-ferrite structure is investigated both with and without drift to determine how the dispersion characteristics are modified; of particular interest are the directions of propagation above and below resonance. Examining the longitudinal and transverse wavenumbers in the interaction region the validity of the magnetostatic approximation is verified. Using this approximation the instability onset condition obtained by Robinson et. al. [23] is extended to include the effects of multiple carrier species. By simplifying the resultant expression an instability onset condition nomograph is developed and examined for a number of commericially available semiconductor materials. The effects of finite geometry on the interaction, e.g. when the semiconductor and ferrite are separated by a thin dielectric, when a surface space charge region is present at the semiconductor surface, or when the ferrite is thin, are also considered.

A series of experiments is described in which techniques required for the proper evaluation of possible surface wave interactions supported by a ferrite spin system and drifting carriers in a semiconducting medium are developed. These techniques are used and the resultant data is compared to that obtained for the ferrite slab transmission studies enabling

positive identification of the ferrite-semiconductor surface wave.

CHAPTER 2

ELECTROMAGNETIC WAVE PROPAGATION AT THE SURFACE OF A SEMI-INFINITE FERROMAGNETIC MATERIAL

2.0 Introduction

In this chapter the dispersion relations discribing electromagnetic surface wave propagation at the interface between two insulators, one magnetic, the other non-magnetic are investigated. Through the use of these relations the characteristics of the surface modes are determined as the permittivity of the dielectric is varied. Analysis of the limiting frequencies of the surface wave spectrum leads to the discovery of a new surface mode, the forward dynamic mode.

2.1 Characterization Of A Non-Conducting Magnetic Region

The analytical investigation of electromagnetic phenomena occuring at the interface between adjacent materials requires suitable characterization of each of the media in terms of macroscopic observables. These quantities are then related by Maxwell's equations,[28]

$$\nabla \times \bar{E} = -\frac{\partial \bar{B}}{\partial t}, \tag{2-1}$$

$$\nabla \times \bar{H} = \bar{J} + \frac{\partial \bar{D}}{\partial t}, \tag{2-2}$$

$$\nabla \cdot \bar{D} = \rho, \tag{2-3}$$

$$\nabla \cdot \bar{B} = 0, \tag{2-4}$$

through the constitutive relations

$$\bar{D} = \epsilon_0 \bar{E} + \bar{P}, \tag{2-5}$$

and

$$\bar{B} = \mu_0 (\bar{H} + \bar{M}). \tag{2-6}$$

For the insulating materials herein considered, the convection current density, $\bar{J}$, and free charge density, ρ, are zero. If it is assumed that the polarizability of these materials is isotropic, then the electric displacement, $\bar{D}$, and the electric field intensity, $\bar{E}$, are linearly related through a scalar permittivity,

$$\bar{D} = \epsilon \bar{E}, \tag{2-7}$$

where

$$\epsilon_r = \frac{\epsilon}{\epsilon_0}, \tag{2-8}$$

is the permittivity of the medium relative to that of free space.

As Equation 2-6 indicates, the magnetic flux density, $\bar{B}$, in a magnetic material is dependent on the magnetic field intensity, $\bar{H}$, as well as the magnetic moment density, $\bar{M}$. Although the origins of magnetic behavior are quantum mechanical, a continuum model may be employed to describe $\bar{M}$, if the wavelengths of the system response are much larger than atomic dimensions.[21] Thus the behavior of the magnetic medium may be related to Maxwell's equations through a phenomenological theory.

There are several classes of materials which display magnetic order below certain critical temperatures. The manner in which their behavior is manifested is dependent on their crystalline lattice as well as the constituent atoms of the basis.

In ferromagnetic materials, the magnetic moments of all of the magnetic ions are aligned parallel to each other at low temperatures. This ordering is shown schematically in Figure 2-1(a). As the temperature of the material is increased, the arrangement of the magnetic moments is disturbed by thermal agitation, such spontaneous ordering no longer existing above a critical temperature known as the Curie point, T_c.

Antiferromagnetism is characterized by the antiparallel arrangement of magnetic dipoles. The two orientations of the spins form a pair of interpenetrating sublattices such that at low temperatures no net magnetic moment is exhibited.[20] A schematic representation of antiferromagnetic order is depicted in Figure 2-1(b). As the temperature of the material is increased beyond the Neel temperature, the antiferromagnetic order disappears.

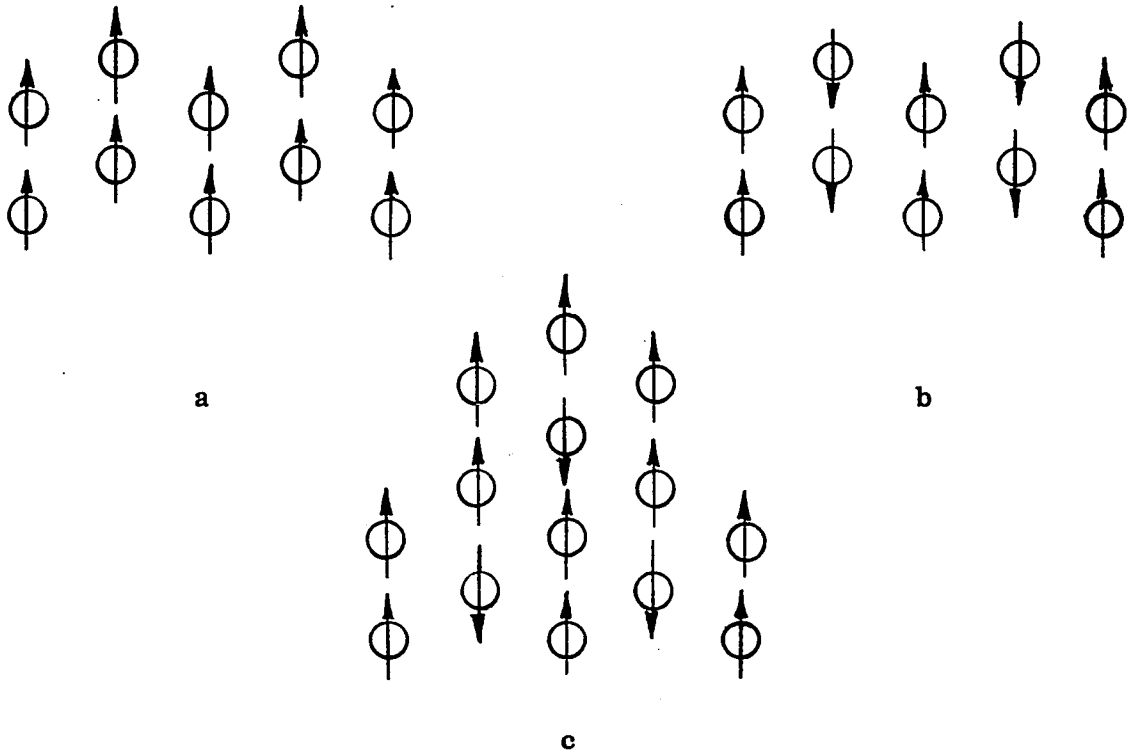

Figure 2-1 Schematic Representation of (a) Ferromagnetic (b) Antiferromagnetic (c) Ferrimagnetic Ordering [29]

A material having two interpenetrating, oppositely directed sublattices, which, unlike an antiferromagnetic system, are unequal is termed a ferrimagnet, Figure 2-1c. As with ferromagnetic crystals, ferrimagnetic materials display a net magnetization.

The magnetic materials to be considered herein are a class of ceramics called ferrites. They are ferrimagnetic materials having high resistivities. Certain ferrites, such as Yittriim Iron Garnet, (YIG). have such high resistivities (10^{12} ohm-cm. at room temperature[31]) that they may be thought of as magnetic insulators. As a result of this property, the eddy current loss in the materials is negligible even at microwave frequencies.[32] Furthermore, the insulating characteristic of these ferrites prevents "shorting out" of adjacent devices or circuits, thus enabling them to be used as substrates in integrated circuits applications.[2,4]

At microwave frequencies many of the ferrite materials behave as though they were ferromagnetic. Their characteristics are determined by the motion of the net magnetization interacting with electromagnetic excitations. The fine structure of the ferrimagnetic order of these materials, which is manifested in interactions between the interpenetrating sublattices, generally occurs at frequencies which are in the infrared or optical regions of the spectrum.[30] Although certain other ferrites do display ferrimagnetic behavior in the microwave region[33] , they are not being considered in this work. Hence, in the following discussion no distinction is made between ferri and ferromagnetism.

The microscopic moments producing the net magnetization in ferrite materials are associated with transition and rare earth metal ions which are distributed interstitually within the crystal.[30] These ions characteristically have incomplete inner shells. Thus, although their valance bands are complete, a net magnetic moment persists due to the motion of electrons in the inner shell.

In an atom or ion in free space, the motion of electrons results in two contributions to the total magnetic moment. The motion of the electrons about the nucleus gives rise to an orbital magnetic moment given by

$$\bar{m}_{or} = -\frac{e\hbar}{2m_o}\bar{L}_e, \qquad 2\text{-}9$$

where e and m_o are the respective charge and mass of the electron, $\hbar$ is Plank's constant divided by 2π, and $\hbar\bar{L}_e$ is the orbital momentum of the electron.[30] In addition a magnetic moment is also associated with the spin of the electron about is own axis

$$\bar{m}_s = -\frac{e\hbar}{m_o}\bar{S}_e, \qquad 2\text{-}10$$

where $\hbar\bar{S}_e$ is the spin angular momentum. The total angular momentum, $\hbar\bar{J}_m$, is given by the vectorial addition of $\hbar\bar{L}_e$ and $\hbar\bar{S}_e$[34] and is related to the magnetic moment through the relation

$$\bar{m} = -g\frac{e\hbar}{2m_o}\bar{J}_m, \qquad 2\text{-}11$$

where g is the spectroscopic splitting factor.[35]

In a crystal, the orbital momentum of the magnetic ion is affected by the presence of neighboring ions. The interaction with the crystal field is such that, for transition ions, the average orbital momentum is approximately zero.[30] The magnetic behavior of these materials is due

primarily to the spinning motion of the electrons.[35] The net ionic moment can therefore be expressed as

$$\bar{m} = -\gamma\hbar\bar{J}_m \cong -\gamma\hbar\bar{S}_e, \qquad 2\text{-}12$$

where

$$\gamma = \frac{ge}{2m_o}, \qquad 2\text{-}13$$

is the magnetomechanical or gyromagnetic ratio. The typical values of g and γ for various ferrite materials are listed in Table 2-1.[30]

In a magnetic material, the spins of neighboring ions are coupled together by a quantum mechanical exchange interaction. This interaction gives rise to a force which acts to align the magnetic moments in either a parallel (ferromagnetic) or an antiparallel (antiferromagnetic) arrangement. Although exchange is a short range interaction, decreasing exponentially with distance[36], it is the mechanism that determines how disturbances of magnetic order propagate in the medium; i.e. through the coupling of successive spins.

Before propagation in a ferromagnetic medium is considered, however, the relationship between magnetic moments and external fields must be considered. If a microscopic magnetic moment is placed in a magnetic field, it is subjected to a torque given by

$$\bar{T} = \bar{m} \times (\mu_o\bar{H}_o). \qquad 2\text{-}14$$

where the magnitude of the flux density of the field is $\mu_o H_o$.[37] The torque causes a time rate of change of angular momentum,

$$\hbar\frac{d\bar{S}_e}{dt} = \bar{m} \times (\mu_o\bar{H}). \qquad 2\text{-}15$$

Since

$$\bar{m} = -\gamma\hbar\bar{S}_e, \qquad 2\text{-}12$$

the equation of motion of the magnetic dipole momentum is therefore

$$\frac{d\bar{m}}{dt} = -\gamma\left[\bar{m} \times (\mu_o\bar{H}_o)\right]. \qquad 2\text{-}16$$

TABLE 2-1

TYPICAL VALUES OF g AND γ FOR VARIOUS FERRITE MATERIALS[30]

	g	γ $\frac{\text{rad./sec.}}{\text{weber/m}^2}$
Yittrium Iron Garnet (YIG) ($Y_3 Fe_5O_{12}$)	2.00	1.75×10^{11}
Magnesium.Ferrite ($Mg Fe_2 O_4$)	2.06	1.81×10^{11}
Mangenese Ferrite ($Mn Fe_2 O_4$)	2.2	1.93×10^{11}
Nickel Ferrite ($Ni Fe_2 O_4$)	2.4	2.11×10^{11}

Thus, if the magnetic moment is not colinear with the external field, it will precess about the field lines. The frequency of precession is given by the Larmor frequency

$$\omega_o = \mu_o \gamma H_o \,. \qquad 2\text{-}17$$

Considering now the effect of an array of N such dipoles in a volume dv, centered at a point r, a magnetic moment density or magnetization may be defined as[38]

$$\bar{M}(\bar{r}) = \lim_{dv \to 0} \frac{\sum_{i=1}^{N} \bar{m}_i (\bar{r} - \bar{r}_i)}{dv} \,, \qquad 2\text{-}18$$

where $\bar{m}_i$ is the magnetic moment of the ith atom located at r_i in the crystal lattice. Rewritting Equation 2-16 in terms of this macroscopic quantity yields

$$\frac{d\bar{M}}{dt} = -\gamma \left[\bar{M} \times (\mu_o \bar{H}_e) \right], \qquad 2\text{-}19$$

where, in taking the summation, $\bar{H}_o$, the static externally applied field is replaced by $\bar{H}_e$, the effective magnetic field intensity experienced by the magnetic moment density within the crystal. The effective field is expressed as

$$\bar{H}_e = \bar{H}_o + \bar{H}_a + \bar{H}_d + \bar{H}_{ex}, \qquad 2\text{-}20$$

where, in addition to the applied static magnetic field, $\bar{H}_a$ is the anisotropy field, $\bar{H}_d$ is the demagnetizing field and $\bar{H}_{ex}$ is the effective field resulting from exchange interactions between the ionic spins.[21]

All crystalline magnetic materials display anisotropy due to the interaction of the magnetic ions with the crystalline electric fields set up by the neighboring ions. These fields have symmetries determined by the location of the ions in the lattice. The electric fields do not

couple directly to the spin angular momenta; but rather they couple directly to the orbital momenta of the ions.[30] Hence, if spin-orbit coupling is appreciable, an indirect coupling between the spin angular momentum and the crystalline electric fields may result.

Some magnetic ions, such as Fe^{3+} ions, which have no orbital angular momentum, should not display anisotropy. Materials such as magnesium ferrite and yttrium iron garnet (YIG), in which, ideally, the only magnetic ions are Fe^{3+} therefore display relatively small anisotropy effects.[30]

As a consequence of the anisotropy, the magnetization, in the absence of an external field, boundary effects and other discontinuities, aligns itself in preferred directions with respect to the crystal axes. Thus, the resultant magnetic behavior of the crystal varies with the direction of the applied magnetic fields relative to the orientation of the crystal. Since the effect of an applied magnetic field is the exertion of a torque on the precessing spin system, and since the anisotropy also causes a torque on the spin system if it points in other than easy directions, the effect of the anisotropy may be reduced to an equivalent field, $\overline{H}_a$, aligned with the easy axis.[39] "If the orienting effect of the anistropy is weak compared to that of the applied fields, the concept of an anisotropy field can be used for arbitrary directions of $\overline{M}$ relative to the crystal axes".[30]

The component of the effective field termed the demagnetizing field, $\bar{H}_d$, arises whenever the magnetization is inhomogeneous. Its origin can be explained simply by noting that

$$\nabla \cdot \bar{B} = 0, \qquad 2\text{-}4$$

which, since

$$B = \mu_0(\bar{H} + \bar{M}), \qquad 2\text{-}6$$

can be expressed as

$$\nabla \cdot \bar{H} = -\nabla \cdot \bar{M} = \rho_m, \qquad 2\text{-}21$$

where ρ_m is a magnetic charge density. Thus, changes in magnetization caused by inhomogeneities, whether in the crystal or at the boundaries, are, in effect, the scalar sources of the magnetic field termed the demagnetizing field. It is evident from the above discussion that this field is highly dependent on the shape of the sample. An expression for the demagnetizing field of a rectangular slab of insulating ferromagnetic material is derived in Appendix I.

The fourth term in Equation 2-20 is due to the short-range quantum mechanical spin-spin interaction between the magnetic ions. As stated previously, this interaction maintains the alignment of spins and is the ordering mechanism of ferromagnetic materials. Although microscopic in origin, the effects of exchange may be incorporated into the macroscopic model through an effective exchange field,

$$H_{ex} = \Lambda \nabla^2 \bar{M}, \qquad 2\text{-}22$$

where Λ, the exchange parameter, is given by

$$\Lambda = \frac{k_B T_c a_1^2}{\mu_B M_o}, \qquad 2\text{-}23$$

where k_B is the Boltzman constant, μ_B is the Bohr magneton, a_1 is the lattice constant and M_o is the saturation magnetization.[21]

In thermal equilibrium, the direction of the magnetization vector, $\bar{M}$, coincides with the direction of the internal effective field, $\bar{H}_e$. If $\bar{M}$ is displaced from the direction of $\bar{H}_e$, the energy of the sample is increased. Consider, as an example, the situation in the bulk of a ferrite of infinite extent, with $\bar{H}_o$ aligned with the easy axis. If $\bar{M}$ and $\bar{H}_e$ are not colinear, but are displaced from each other by some angle Θ, Equation 2-19 indicates that the magnetic moment precesses about the direction of the magnetic field with a frequency given by,

$$\omega_e = \mu_o \gamma H_e, \qquad 2\text{-}24$$

as shown schematically in Figure 2-2. This precession is uniform throughout the sample. If now an r.f. field, $\bar{H}(t)$, of frequency ω_e, polarized such that its magnetic field lies in a plane perpendicular to the direction of H_e, is applied, the magnetization will experience an additional torque,

$$t_m = \left[\bar{M} \times \mu_o \bar{H}(t)\right]. \qquad 2\text{-}25$$

This torque is perpendicular to $\bar{M}$ and will always be in such a direction as to increase the precession angle, Θ, between $\bar{M}$ and $\bar{H}_e$, increasing the energy of the system.[40] This increased energy is absorbed from the r.f. field. However, the precession angle cannot increase ad infinitum and energy is transferred from the precessional mode to

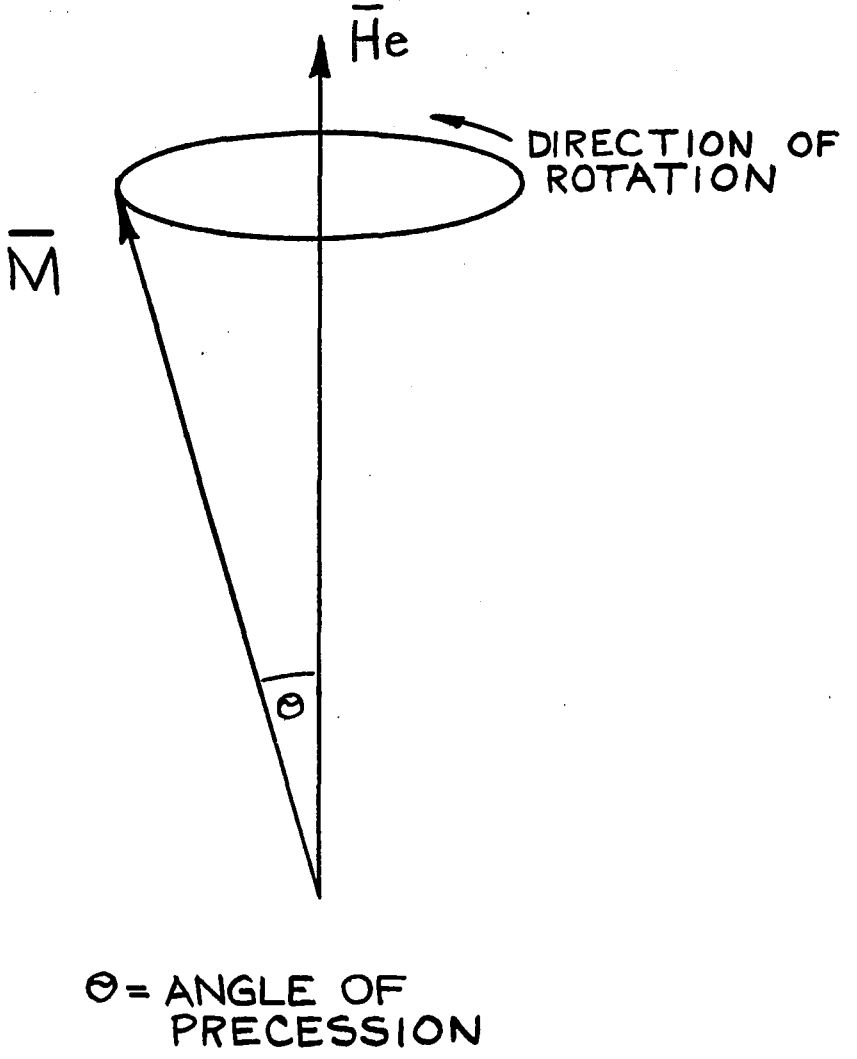

Figure 2-2 - Precession of Magnetization About The Effective Magnetic Field

other modes of the system. Similarly, when the r.f. field is turned off, the precession angle decreases as the sample returns to equilibrium. The relaxation results from the coupling of the spins to other spin modes, as well as the interaction between the spins and the lattice vibrations. Materials, such as YIG., in which the coupling between the spins and the crystalline electric fields is weak, are therefore relatively low loss materials.[41]

A quantitative assessment of the losses associated with a particular sample of magnetic material may be obtained through ferromagnetic resonance experiments in which the sample under test is exposed to an r.f. field. The power absorbed by the sample as a function of the applied d-c magnetic field is measured and may be plotted. The width of this resonance curve at one-half the maximum absorbed power is termed the linewidth, ΔH. The linewidth of a magnetic material is a function of test frequency, temperature, impurity content, surface preparation and orientation of the sample. The room temperature linewidth of specially prepared samples of YIG, with impurity content less than 0.1 ppm. , has been measured to be less than 0.4 oersteds at 9.3 GH_z along the [111] axis.[42]

The equation of motion, which including the time varying field, has the form

$$\dot{\bar{M}} = -\gamma\left[\bar{M} \times \mu_o \bar{H}_+\right] \qquad 2\text{-}26$$

where $\bar{H}_+ = \bar{H}_e + \bar{H}(+)$, describes a lossless system. As such it does not include the effects of the various relaxation processes. The presence of these interactions may, however, be

taken into account through the addition of a phenomenological damping term,

$$\dot{\bar{M}} = -\mu_0 \gamma (\bar{M} \times \bar{H}_t) + \text{damping term} \qquad 2\text{-}27$$

The three most common terms used to describe relaxation effects are [43] the Landau-Lifshitz form,

$$-\frac{\lambda_r}{|M|^2} (\bar{M} \times \bar{M} \times \bar{H}_t), \qquad 2\text{-}27a$$

the Gilbert form,

$$+\frac{\alpha_r}{|M|} (\bar{M} \times \dot{\bar{M}}), \qquad 2\text{-}27b$$

and the Bloch-Bloembergen form,

$$-\frac{M_x \hat{x}}{\tau_2} - \frac{M_y \hat{y}}{\tau_2} - \frac{(M_z - |\bar{M}|)\hat{z}}{\tau_1}, \qquad 2\text{-}27c$$

where $\bar{H}_e$ is assumed to be $\hat{z}$ directed, and τ_1 and τ_2 are the relaxation times in the longitudinal and transverse direction respectively.

By taking the scalar product of both sides of the equation of motion, (including the relaxation terms) with $\bar{M}$ it is found that

$$\bar{M} \cdot \dot{\bar{M}} = 0 \qquad 2\text{-}28$$

for the Landau-Lifshitz and Gilbert formulations. [44] This indicates that the magnitude of $\bar{M}$ is conserved since $\dot{\bar{M}}$ is always perpendicular to $\bar{M}$. The effect of either of these damping terms is to cause $\bar{M}$ to spiral in toward H_e as shown in Figure 2-3. [45]

Taking the cross product of $\bar{M}$ with the Gilbert equation of motion, Equations 2-27 and 2-27b, results in

$$\bar{M} \times \dot{\bar{M}} = -\mu_0 \gamma \bar{M} \times (\bar{M} \times \bar{H}_t) + \frac{\alpha}{|M|} \bar{M} \times (\bar{M} \times \dot{\bar{M}}). \qquad 2\text{-}29$$

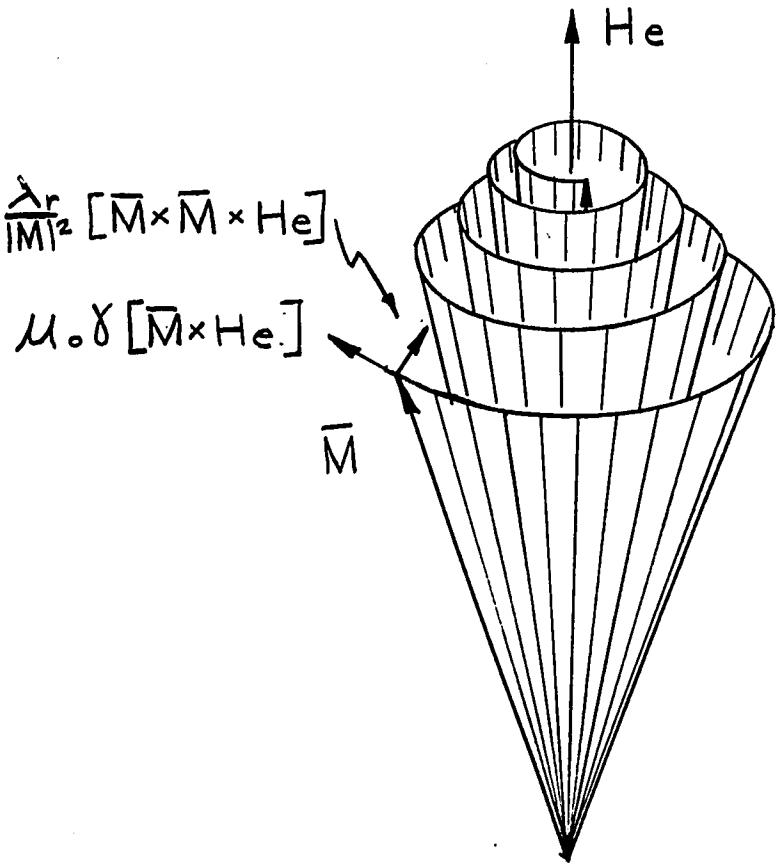

Figure 2-3 Damped Precession of Magnetization in the Absence of an r.f. Field (45)

By use of a vector identity and Equation 2-28, Equation 2-29 may be rewritten,

$$\bar{M} \times \dot{\bar{M}} = -\mu_0 \gamma \bar{M} \times (\bar{M} \times H_t) - \alpha |M| \dot{\bar{M}} \qquad 2\text{-}30$$

(Note the equivalent Equation, (8.6), in Skrotskii and Kurbatov's proof[45] is incorrect).

Multiplying both sides of Equation 2-30 by $\frac{\alpha}{|M|}$ and substituting the result into the Gilbert equation of motion yields, upon rearranging terms

$$\dot{\bar{M}} = -\gamma^* (\bar{M} \times \mu_0 \bar{H}_t) - \frac{\lambda_r^*}{|M_0|^2} [\bar{M} \times (\bar{M} \times \bar{H}_t)], \qquad 2\text{-}31$$

where

$$\gamma^* = \frac{\gamma}{1 + \alpha^2}, \qquad 2\text{-}32$$

$$\lambda_r^* = \mu_0 \gamma^* |M| \alpha, \qquad 2\text{-}33$$

and α is a parameter related to the linewidth of the material by

$$\alpha = \frac{\mu_0 \gamma \Delta H}{2 \omega}. \qquad 2\text{-}34$$

Thus the Landau-Lifshitz and Gilbert forms of the equation of motion are equivalent for $\mu_0 \gamma \Delta H \ll \omega$, a valid approximation in most ferromagnetic resonance experiments.

The Bloch-Bloembergen form of the damping term describes a relaxation process with different rates of relaxation in the transverse and longitudinal directions. However, in the small signal limit, where excursions of $\bar{M}$ from its equilibrium position are small, variations in the longitudinal direction are negligible and only the relaxation process in the transverse direction need be considered. In this limit, all three forms of the damping term yield similarly shaped resonance

absorption curves for narrow line widths. The choice of which damping term to use, for this case, is then only a matter of personal preference.

Near the surface of the magnetic material, departures from the conditions existing in the bulk occur due to the abrupt termination of the crystalline structure. As the model of a thin ferromagnetic film, Figure 2-4[46], illustrates, the saturation magnetization varies across the sample thickness, the greatest variation occuring in the surface region of thickness δ_s.[47] The resultant anisotropy is uniaxial in character, with the easy axis of magnetization parallel to the film normal.[47] When this magnetic anisotropy is strong, the spins at the surface may be immobilized or "pinned".[44] This imposes a boundary condition on the r.f. magnetic moment density which must be satisfied in addition to the conditions imposed on the electromagnetic fields by Maxwell's equations.

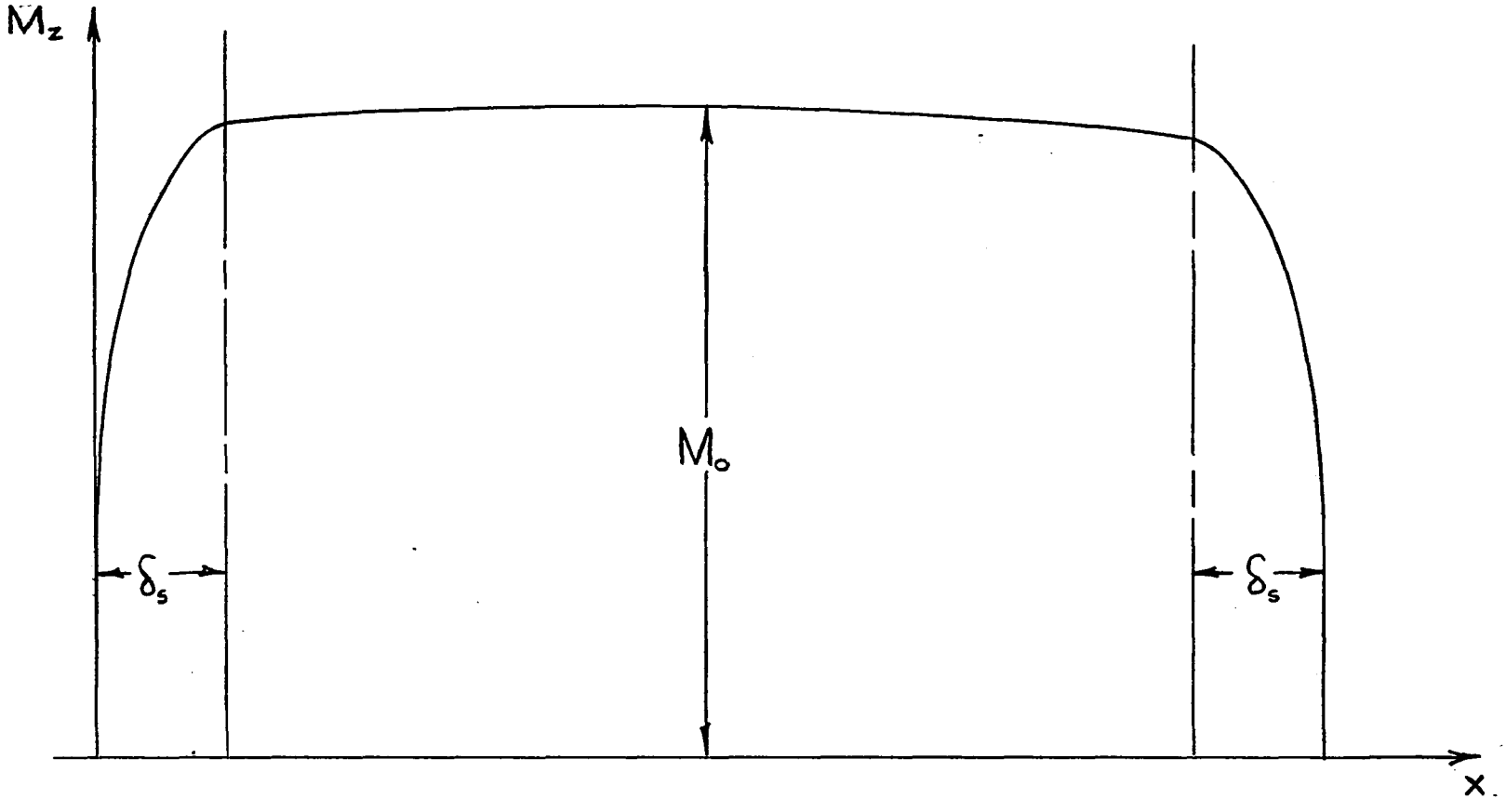

Figure 2-1 - Variation of the Saturation Magnetization Across the Thickness of a Ferromagnetic Thin Film [46]

2.2 Semi-infinite Model

In the preceding section the characteristics of the magnetic medium were discussed. In order to apply this information to the problem at hand, a suitable model is now developed. To accomplish this end, some simplifying assumptions consistent with the physics of the problem are employed.

The surface electromagnetic modes of a planar slab of insulating ferromagnetic material are to be investigated. The slab shown in Figure 2-5, is a single crystal ferrite, its easy axis being perpendicular to the $\hat{x}$-$\hat{y}$ plane in the orientation shown. The ferrite, bounded on all sides by a uniform dielectric medium of permittivity ϵ_d, is exposed to a directed static magnetic field, $\bar{H}_o$.

An exact description of the electromagnetic mode spectrum of the above described slab, requires that a self-consistent solution of Maxwell's equation be found for both media satisfying the boundary conditions at each surface of the slab. The additional complication arising from the nonuniformity of the magnetization within the ferrite makes such a problem exceedingly complex. Considerable simplification, however, can be achieved by assuming the width, c, and length, b, of the sample to be much larger than its thickness, a, and, more importantly, the excitation wavelength, λ, so that the effect of the presence of these transverse boundaries on the r.f. response is negligible.

Therefore, a centrally located region, far removed from the boundaries in the $\hat{z}$ and $\hat{y}$ directions is considered. The demagnetizing

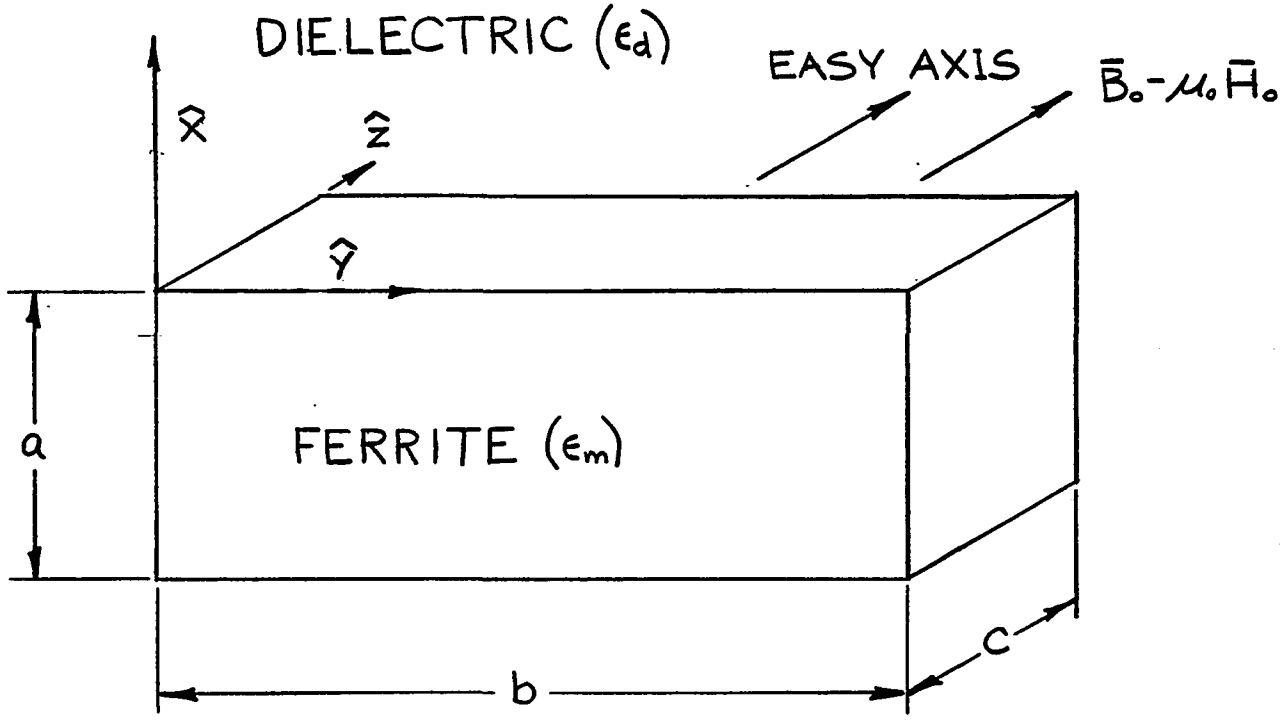

Figure 2-5 - Planar Ferrite Slab in Uniform Dielectric

field in the ferrite is uniform in the $\hat{y}$ and $\hat{z}$ directions since discontinuities in magnetization occuring at the surfaces are far from the region of interest (Appendix I). Not only does this approximation reduce the number of boundary conditions that need be imposed, it additionally leads to a reduction in the complexity of the mode structure in the small signal limit. The mode structure simplification, as is shown in the following sections, arises directly from the assumption that $\hat{z}$ directed variations may be neglected.

The principle focus of this chapter is directed toward the study of electromagnetic phenomena occuring at or near the interface of the insulaing ferromagnetic medium with the dielectric. It is convenient to begin the analysis by considering a semi-infinite model in which the boundary in the negative $\hat{x}$ direction is also assumed to be infinitely far from the region under consideration. Whereas such an approximation may not be valid if the magnetic material is a thin film, it is a reasonalbe assumption if the material is uniform over a distance which is large in comparison to the wavelength of the response. (Finite geometries are presented in Chapter 3.)

A ferrite, as illustrated in the previous section, is characterized by an almost uniform magnetization except near the surface. In the vicinity of the surface the magnetization decreases from its value in the bulk as shown in Figure 2-4. To illustrate the effect decreased surface magnetization has on the spins, a thin sample magnetized perpendicular to the plane of the interface is considered. When the sample is excited by a uniform externally applied field, the torque experienced by the surface spins is smaller than the torque experienced by the bulk spins, effectively

restricting their motion. Thus, the spins in the vicinity of the surface are said to be "pinned" since deviations from their equilibrium positions are small.[48] Spins are "pinned" when

$$M(t) \cong 0 \qquad 2\text{-}35$$

In addition to pinning caused by the non-uniformity of the magnetization[49,50] other pinning mechanisms have also been investigated. For example, spins may be pinned by the variations in the demagnetizing field in the vicinity of a rough surface.[51] Anisotropies at the surface due to the lower degree of symmetry experienced by the surface spins[52] or the formation of anti-ferromagnetic oxides[53] may also lead to surface pinning. Rado and Weertman[54] determined pinning conditions by considering a uniform ferromagnetic medium with an anisotropy at the surface. They found that when the surface anisotropy is reduced to zero the exchange interaction causes the spins to become "unpinned",[48] that is the normal derivative of the r.f. magnetization is zero,

$$\nabla_n \cdot M(t) = 0, \qquad 2\text{-}36$$

at the surface.

In general the pinning condition at the surface of a ferromagnetic material is a combination of the "pinned" and "unpinned" conditions[48] depending, in part, on the thickness of the surface region[46], material properties, surface preparation and orientation with respect to the applied field. However, experimental results[55] for single crystal YIG samples indicate that while spins are pinned at the small edges of the films, the magnetization is unpinned at the large faces. Comparison of experimental data

with theoretical calculations[56] for permalloy films magnetized in the plane of the surface, as in the model herein consided, also indicates that the surface spins are unpinned.

Thus good agreement between theory and experiment is obtained by assuming the ferrite model to be uniform with no explicit pinning mechanism at the surface. The semi-infinite model is shown in Figure 2-6.

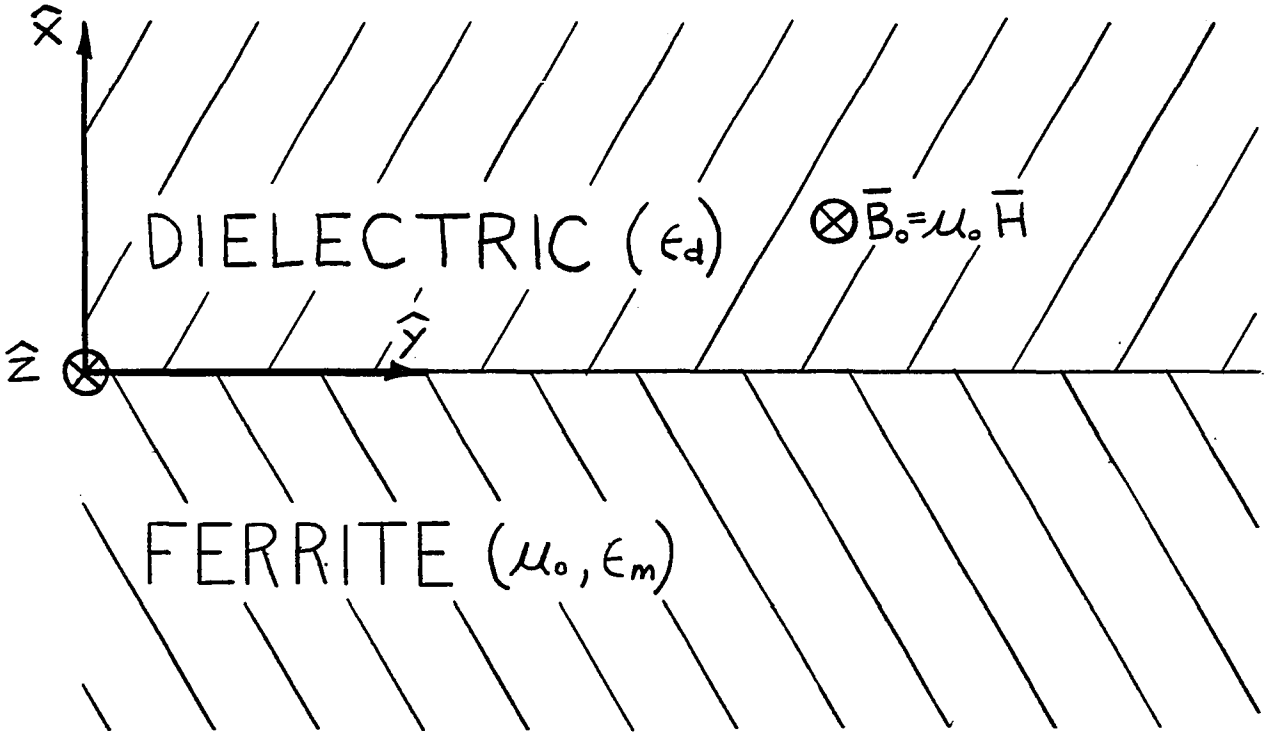

Figure 2-6 - Semi-infinite Ferrite-Dielectric Model

2.3 Dispersion Relations For Wave Propagation At The Surface Of A Semi-infinite Magnetic Medium

In this section the dispersion characteristics of surface waves propagating along the interface between a semi-infinite dielectric and an insulating ferromagnetic medium is determined. This relationship is obtained by finding a solution which satisfies Maxwell's equations in both media as well as at the boundary.

An r.f. field configuration is sought which satisfies the above requirements while displaying surface wave characteristics; that is, the amplitude of the mode reaches its maximum value at the surface.[5] Since the boundary condition at $x = \pm\infty$ requires the fields to asymptotically approach zero, a solution of the form

$$\exp\left[-\beta_{1,2}|x|\right], \qquad 2\text{-}37$$

where the real part of β is positive, is appropriate. It is further assumed that the excitation is of radian frequency ω, propagates in the positive $\hat{y}$ direction, and that variations in the $\hat{z}$ direction are negligible. The solution may be described by an expression of the form

$$\exp\left[-\beta_{1,2}|x| + j(\omega t - Ky)\right]. \qquad 2\text{-}38$$

In the dielectric material, Maxwell's equations may be expressed as

$$\nabla \times \bar{E}_d = -\mu_o \frac{\partial \bar{H}_d}{\partial t}, \qquad 2\text{-}39$$

and

$$\nabla \times \bar{H}_d = \epsilon_o \epsilon_d \frac{\partial \bar{E}_d}{\partial t}, \qquad 2\text{-}40$$

where the subscript d signifies that quantities are associated with the dielectric. For the case under consideration, where variations in the $\hat{z}$ direction are neglected, the electric and magnetic field quantities are separable into two uncoupled sets, one which is Transverse Electric (TE) with respect to the $\hat{y}$ direction and one which is Transverse Magnetic (TM) with respect to $\hat{y}$. Assuming the r.f. electric field in the dielectric to be of the form

$$\bar{E}_d = \bar{A} \exp[-\beta_d x + j(\omega t - k_d y)], \qquad 2\text{-}41$$

the TE_y components are found, using Equation 2-39, to be given by

$$E_{dz} = A_z \exp[-\beta_d x + j(\omega t - k_d y)], \qquad 2\text{-}42$$

$$H_{dx} = \frac{k_d A_z}{\omega \mu_o} \exp[-\beta_d x + j(\omega t - k_d y)], \qquad 2\text{-}43$$

and

$$H_{dy} = j\frac{\beta_d A_z}{\omega \mu_o} \exp[-\beta_d x + j(\omega t - k_d y)], \qquad 2\text{-}44$$

where the real part of $\beta_d > 0$, since the dielectric occupies the upper half-space, $x > 0$. The TM_y set is similarly found to consist of

$$E_{dx} = A_x \exp[-\beta_d x + j(\omega t - k_d y)], \qquad 2\text{-}45$$

$$E_{dy} = A_y \exp[-\beta_d x + j(\omega t - k_d y)], \qquad 2\text{-}46$$

and

$$H_{dz} = -\frac{[k_d A_x + j\beta_d A_y]}{\omega \mu_o} \exp[-\beta_d x + j(\omega t - ky)]. \qquad 2\text{-}47$$

Both the TE_y and TM_y sets thus obtained must, in addition, be consistant with Equation 2-40. Substitution of either set of field components into this Maxwell equation leads to a dispersion relation describing wave propagation in the dielectric material expressed as

$$k_d^2 - \beta_d^2 = \frac{\omega^2}{c_d^2}, \qquad 2\text{-}48$$

where c_d is the velocity of light in the dielectric (intrinsic velocity) given by

$$c_d = \frac{1}{\sqrt{\mu_o \epsilon_o \epsilon_d}} \qquad 2\text{-}49$$

Maxwell's equations for the insulating ferromagnetic medium are expressed as

$$\nabla \times \bar{E}_m = -\frac{\partial B_m}{\partial t} = -\mu_o \frac{\partial (\bar{H} + \bar{M})}{\partial t} \qquad 2\text{-}50$$

and

$$\nabla \times \bar{H}_m = \epsilon_o \epsilon_m \frac{\partial \bar{E}_m}{\partial t} , \qquad 2\text{-}51$$

where the relationship between the magnetic field intensity and the magnetic moment density is described by the equation of motion of magnetization. Using the Landau-Lifschitz form for the relaxation term, the equation of motion is

$$\dot{\bar{M}} = -\mu_o \gamma \left(\bar{M} \times \bar{H}_m \right) - \frac{\lambda_r}{|M|^2} \left(\bar{M} \times \bar{M} \times \bar{H}_m \right) . \qquad 2\text{-}27,\ 2\text{-}27a$$

For the small r.f. excitation amplitude case, the magnetic field intensity and magnetization may be expressed approximately as

$$\bar{H}_m = H_{im} \hat{z} + \bar{H}_{1m} \exp[\beta_m x + j(\omega t - k_m y)], \qquad 2\text{-}52$$

and

$$\bar{M} = M_o \hat{z} + M_1 \exp[\beta_m x + j(\omega t - k_m y)], \qquad 2\text{-}53$$

where H_i is the effective static field in the ferrite, and terms higher than first order are assumed to be very small and are neglected. The subscript m appearing in these expressions signifies that the quantity is associated with the magnetic medium. Thus, since the magnetic medium occupies the lower half-space, $x < 0$, the real part of β_m must be positive.

Substituting Equations 2-52 and 2-53 into Equation 2-27, 2-27a and retaining only first order terms results in

$$\dot{\bar{M}}_1 = z \times \left\{ \mu_o \gamma \left[H_i \bar{M}_1 - M_o (\bar{H}_{1m} + \Lambda \nabla^2 \bar{M}_1) \right] - \frac{\lambda_r}{M_o} \left[H_i \bar{M}_1 - M_o (H_{1m} + \Lambda \nabla^2 \bar{M}_1) \right] \times \hat{z} \right\} \quad 2\text{-}54$$

This expression for $\dot{\bar{M}}_1$ may be written as

$$j \left[\omega - j \left(\frac{\lambda \Omega_e}{\omega_m} \right) \right] (M_{1x} \hat{x} + M_{1y} \hat{y}) = \Omega_e \hat{z} \times \bar{M}_1 + \lambda_r (H_{1mx} \hat{x} + H_{1my} \hat{y}) - \omega_m \hat{z} \times H_{1m}, \quad 2\text{-}55$$

$$j \omega M_{1z} = 0, \quad 2\text{-}56$$

where, neglecting variations in the $\hat{z}$ direction,

$$\Omega_e = \omega_i + \omega_{ex} a_1^2 D_k, \quad 2\text{-}57$$

$$D_k = k_m^2 - \beta_m^2, \quad 2\text{-}58$$

$$\omega_{ex} = \frac{\mu_o \gamma \Lambda}{a_1^2} = \text{Exchange frequency} \quad 2\text{-}59$$

$$\omega_i = \mu_o \gamma H_i = \text{Precession frequency} \quad 2\text{-}60$$

and

$$\omega_m = \mu_o \gamma M_o = \text{Magnetization frequency} \quad 2\text{-}61$$

Typical values for ω_{ex}, a and ω_m are shown in Table 2-2.

Solving for the first order magnetic moment density in terms of the field intensity components

$$M_{1x} = \frac{\Omega_e \omega_m}{\left[\Omega_e^2 - (\omega - j \frac{\lambda_r \Omega_e}{\omega_m})^2 \right]} \left\{ \left[1 + j \frac{\lambda_r \omega}{\omega_m \Omega_e} + \left(\frac{\lambda_r}{\omega_m} \right)^2 \right] H_{1mx} + j \frac{\omega}{\Omega_e} H_{1my} \right\}, \quad 2\text{-}62$$

$$M_{1y} = \frac{\Omega_e \omega_m}{\left[\Omega_e^2 - (\omega - j \frac{\lambda_r \Omega_e}{\omega_m})^2 \right]} \left\{ -j \frac{\omega}{\Omega_e} H_{1mx} + \left[1 + j \frac{\lambda_r \omega}{\omega_m \Omega_e} + \left(\frac{\lambda_r}{\omega_m} \right)^2 \right] H_{1my} \right\}, \quad 2\text{-}63$$

$$M_{1z} = 0, \quad 2\text{-}64$$

or

$$\bar{M}_1 = \| \chi \| \bar{H}_{1m}, \quad 2\text{-}65$$

TABLE 2-2

TYPICAL VALUES OF ω_{ex} , a_1 and ω_m
FOR VARIOUS FERRITE MATERIALS

	ω_{ex} rad./sec.	a_1 Å.	ω_m rad./sec.
Yittrium Iron Garnet ($Y_3 Fe_5O_{12}$)	1.44×10^{14}	12.37	3.1×10^{10}
Magnesium Ferrite ($Mg Fe_2 O_4$)	1.69×10^{14}	8.36	2.6×10^{10}
Manganese Ferrite ($Mn Fe_2 O_4$)	1.66×10^{14}	8.51	9.3×10^{10}
Nickel Ferrite ($Ni Fe_2 O_4$)	2.70×10^{14}	8.60	6.8×10^{10}

where the tensor quantity $\|\chi\|$ is the intrinsic susceptability of the medium. The r.f. magnetic field density, B_{1m}, may be related to the r.f. magnetic field intensity through the constitutive relation

$$\bar{B} = \mu_o (\bar{H} + \bar{M}) \qquad 2\text{-}6$$

yielding a tensor permeability $\bar{B}_{1m} = \mu_o \|1 + \chi\| \bar{H}_{1m} = \mu_o \|\mu\| \bar{H}_{1m}$,

where

$$\|\mu\| = \begin{Vmatrix} \mu_{11} & +j\mu_{12} & 0 \\ -j\mu_{12} & \mu_{11} & 0 \\ 0 & 0 & 0 \end{Vmatrix}, \qquad 2\text{-}66$$

$$\mu_{11} = 1 + \frac{\Omega_e \omega_m}{\left[\Omega_e^2 - \left(\omega_m - j\frac{\lambda_r \Omega_e}{\omega_m}\right)^2\right]} \left[1 + j\frac{\lambda_r \omega}{\omega_m \Omega_e} + \left(\frac{\lambda}{\omega_m}\right)^2 \right], \qquad 2\text{-}67$$

and

$$\mu_{12} = \frac{\omega_m \omega}{\left[\Omega_e^2 - \left(\omega - j\frac{\lambda_r \Omega_e}{\omega_m}\right)^2\right]}. \qquad 2\text{-}68$$

Assuming the r.f. electric field in the ferromagnetic medium to be given by

$$\bar{E}_{1m} = \bar{G} \exp [\beta_m x + j(\omega t - k_m y)], \qquad 2\text{-}69$$

the relationships between the electric and magnetic field quantities become,

$$\nabla \times \bar{H}_{1m} = j\omega \epsilon_o \epsilon_m \bar{E}_{1m} \qquad 2\text{-}70$$

and

$$\nabla \times \bar{E}_{1m} = -j\omega \mu_o \|\mu\| \bar{H}_{1m}. \qquad 2\text{-}71$$

The $\hat{x}$ and $\hat{y}$ components of Equation 2-70 may be used to find the expressions relating the $\hat{x}$ and $\hat{y}$ components of the electric field to the $\hat{z}$ component of the magnetic field intensity,

$$E_{1mx} = -\frac{k H_{1mz}}{\omega \epsilon_o \epsilon_m}, \qquad 2\text{-}72$$

and

$$E_{1my} = j\frac{\beta_m H_{1mz}}{\omega \epsilon_o \epsilon_m}. \qquad 2\text{-}73$$

Using the $\hat{x}$ and $\hat{y}$ components of Equation 2-71, the $\hat{x}$ and $\hat{y}$ directed field intensity components may be expressed in terms of the $\hat{z}$ component of the electric field as

$$H_{1mx} = \left[\frac{k_m \mu_{11} - \beta_m \mu_{12}}{\omega \mu_0 (\mu_{11}^2 - \mu_{12}^2)} \right] E_{1mz} , \qquad 2\text{-}74$$

and

$$H_{1my} = j \left[\frac{k_m \mu_{12} - \beta_m \mu_{11}}{\omega \mu_0 (\mu_{11}^2 - \mu_{12}^2)} \right] E_{1mz} . \qquad 2\text{-}75$$

For this special case, i.e. $\frac{\partial}{\partial z} = 0$, the first order fields are separable into two uncoupled sets, one which is TM with respect to the $\hat{y}$ direction (TM_y) and one which is TE with respect to $\hat{y}$ (TE_y).

The TM_y set includes the $\hat{z}$ component of the magnetic field intensity and the $\hat{x}$ and $\hat{y}$ directed electric field components. Substitution of the expressions for E_{1mx} and E_{1my} into Equation 2-71, yields the following dispersion relation

$$k_m^2 - \beta_m^2 = \frac{\omega^2}{c_m^2} , \qquad 2\text{-}76$$

where c_m is the velocity of light in a dielectric having the same permittivity as the magnetic material and is given by

$$c_m = \frac{1}{\sqrt{\mu_0 \epsilon_0 \epsilon_m}} . \qquad 2\text{-}77$$

Thus, the TM solution is to first order, unaffected by the spin system, a direct consequence of the colinearity of the saturation magnetization and the first order magnetic field intensity. The magnetic medium appears as if it were a dielectric, with relative permittivity ϵ_m, to the small signal TM field which is propagating perpendicular to the direction in which the medium is magnetized.

The TE_y set, on the other hand, is quite strongly influenced by the spin system. This set consists of the $\hat{z}$ component of the electric field and the $\hat{x}$ and $\hat{y}$ directed magnetic field intensity components. Substituting the latter into Equation 2-70 results in the following relation describing propagation in the magnetic medium

$$k_m^2 - \beta_m^2 = \frac{\omega^2}{c_m^2} \frac{(\mu_{11}^2 - \mu_{12}^2)}{\mu_{11}} = D_k \qquad 2\text{-}78$$

This is the dispersion relation for 90° spin waves in an infinite ferromagnetic medium, with $\pm\sqrt{D_k}$ corresponding to the wavenumber.[21]

An expression for D_k as a function of frequency is obtained by rewriting Equation 2-78 using the permeability tensor component definitions, Equations 2-67 and 2-68, as

$$D_k = \frac{\omega^2\left[(\omega_i + \omega_m + \omega_{ex}a_1^2 D_k)^2\left(1+\frac{\lambda_r^2}{\omega^2}\right)^2 - \omega^2\right] + j\frac{2\omega\lambda_r}{\omega_m}(\omega_i + \omega_m + \omega_{ex}a_1^2 D_k)}{c_m^2\left[(\omega_i + \omega_{ex}a_1^2 D_k)(\omega_i + \omega_m + \omega_{ex}a_1^2 D_k)\left(1+\frac{\lambda_r^2}{\omega^2}\right) - \omega^2\right] + j\left[2\frac{\omega\lambda_r}{\omega_m}(\omega_i + \omega_m + \omega_{ex}a_1^2 D_k)\right]} \qquad 2\text{-}79$$

a third degree equation in D_k. At each value of frequency, therefore, not one but three solutions are possible. Thus, the general solution for a surface wave propagating with phase velocity

$$v_y = \frac{\omega}{\mathrm{Re}[k_m]}, \qquad 2\text{-}80$$

consists of a linear combination of three terms with differing transverse wave vector values,[57,58]

$$E_{1mz} = \sum_{i=1}^{3} G_{zi} \exp[-\beta_{mi}x + j(\omega t - k_m y)]. \qquad 2\text{-}81$$

Two of the three terms are directly attributable to the exchange interaction, for if the exchange parameters in Equation 2-79 are neglected, i.e.

$$\omega_{ex}a_1^2 D_k \cong 0, \qquad 2\text{-}82$$

only one solution exists. The third term is approximately equal to the value

of D_k for the zero exchange case, varying from it only when D_k becomes large enough for the exchange term to become appreciable in comparison to ω_i, ω_m, and ω. For YIG at room temperature, ω_m is approximately 3.1×10^{10} rad/sec., and $\omega_{ex} a_i^2$ is approximately 2.2×10^{-4} m^2 rad/sec.; ω_i is chosen to correspond to the mode and frequency range of interest.

An assumption commonly employed in the literature on the microwave properties of ferromagnetic materials, (References 7, 59-64) whether explicitly stated or implied, is that the phase velocity is sufficiently small that electromagnetic propagation is negligible. With the neglect of propagation Maxwell's equations reduce to those of Magnetostatics[65]

$$\nabla \cdot \bar{B} = 0, \qquad 2\text{-}83$$

and

$$\nabla \times \bar{H} = 0, \qquad 2\text{-}84$$

When exchange energy is neglected under these circumstances, the modes are called magnetostatic [66] (or pure magnetostatic[48]) modes. The zero exchange term of Equations 2-79 and 2-81 is not a magnetostatic mode but rather an electromagnetic mode since effects of propagation have been included. Whereas the electromagnetic zero exchange mode closely resembles the magnetostatic mode in the short wavelength region, it is shown in Section 2-4 and Chapter 3 that significant results may be obtained in the long wavelength region by the inclusion of electromagnetic wave propagation.

Having determined expressions relating the field components, subject to the constraints imposed by Maxwell's equations and the characteristics of each of the adjacent media, attention is now focussed upon the

interface, for if the composite structure solution is to be self-consistant, Maxwell's equations must be satisfied there as well. Since both media are insulating, neither can give rise to a surface charge nor surface current at x=0. Thus the boundary conditions are given by

$$\hat{x} \times (\bar{E}_{1m} - \bar{E}_d) = 0, \qquad 2\text{-}85$$

and

$$\hat{x} \times (\bar{H}_{1m} - \bar{H}_d) = 0. \qquad 2\text{-}86$$

Applying Equation 2-85 to the r.f. electric field expressions at x=0 yields

$$E_{1mz} = \sum_{l=1}^{3} G_{zl} \exp[j(\omega t - k_m y)] = A_z \exp[j(\omega t - k_d y)] = E_{dl}, \quad x = 0 \qquad 2\text{-}87$$

resulting in

$$E_l = \sum_{l=1}^{3} G_{zl} = A_z \qquad 2\text{-}88$$

and

$$k = k_m = k_d . \qquad 2\text{-}89$$

Imposing the second electromagnetic boundary condition on the r.f. magnetic field intensity components leads to

$$H_{lmy} = \sum_{l=1}^{3} \left[\frac{k\mu_{lzl} - \beta_{ml}\mu_{lxl}}{\omega\mu_o(\mu_{lxl}^2 - \mu_{lzl}^2)} \right] G_{zl} \exp[j(\omega t - ky)] = j\frac{\beta_l E_l}{\omega\mu_o} \exp[j(\omega t - ky)] = H_{dy}, \quad x = 0 \qquad 2\text{-}90$$

yielding

$$\beta_d = \sum_{l=1}^{3} \left[\frac{k\mu_{lzl} - \beta_{ml}\mu_{lzl}}{(\mu_{lxl}^2 - \mu_{lzl}^2)} \right] \frac{G_{zl}}{E_l} . \qquad 2\text{-}91$$

In the absence of exchange effects (only one value of l) the dispersion relations for the dielectric and ferrite media, Equations 2-48 and 2-78 respectively, together with Equation 2-91, the electromagnetic boundary condition, are sufficient to determine the electromagnetic surface wave mode spectrum. However, when exchange effects are considered, two

additional waves exist in the ferromagnetic medium, so that determination of the surface wave spectrum requires additional conditions to be imposed at the interface.[67] The additional conditions are obtained by applying the appropriate pinning conditions (on $\bar{M}(t)$ and its normal derivative) at the ferrite surface.

The effect of exchange on the surface modes of YIG films has been studied by Wolfram and DeWames [68] employing the equations of magnetostatics. They report only slight differences between results calculated for a pinning condition involving linear combinations of $\nabla_n \cdot \bar{M}(t)$, $H(t)$, and $M(t)$ and results obtained by considering the spins to be "unpinned".

Sparks [48] , in discussing the effects of surface pinning on the modes of a thin ferromagnetic film, indicates that of the three modes of the general solution, one is off frequency and has a small amplitude. He additionally shows how the remaining two modes, one a magnetostatic surface wave which decreases exponentially towards the interior, the other an exchange mode which oscillates rapidly away from the surface, combine to satisfy the pinning conditions at the surface. However, since the rapidly oscillating exchange mode integrates to zero,[66] the intensity and frequency of the surface wave is essentially independent of surface pinning.[48]

The insensitivity of the surface wave to the pinning conditions indicated by the theoretical results cited above, is further confirmed by experimental observations. Microwave propagation experiments [6, 59] have shown that good agreement is obtained when experimental results are compared to magnetostatic surface wave calculations with pinning neglected. Thus, taking the variation of the microwave magnetization in the semi-

infinite ferrite to be

$$M(t) \longrightarrow \exp(+\beta_m x), \qquad x < 0 \qquad 2\text{-}92$$

is not only physically interpretable as a surface wave, but also satisfies the electromagnetic boundary conditons and agrees well with the previously referenced experimental observations.

Neglecting pinning coupled exchange effects reduces the equations describing surface wave propagation at the interface to

$$\beta_d = \frac{k\mu_{12} - \beta_m \mu_{11}}{(\mu_{11}^2 - \mu_{12}^2)}, \qquad 2\text{-}93$$

and

$$k^2 - \beta_d^2 = \frac{\omega^2}{c_d^2}, \qquad 2\text{-}94$$

$$k^2 - \beta_m^2 = \frac{\omega^2}{c_m^2} \frac{(\mu_{11}^2 - \mu_{12}^2)}{\mu_{11}}, \qquad 2\text{-}95$$

where in contrast to the work of Courtois et al.[12], the permeability tensor components have the correct sign[69], and Equation 2-95 is modified by exchange. (Courtois et al. varied the permittivity of the dielectric but restricted the $\epsilon_d \mu_d$ product to unity. The case where $\mu_d = 1$ and ϵ_d may take on various values is a more realistic situation.) Similar results, excluding exchange, have also been obtained by Bresler,[11] who considered surface waves guided along a ferrite-air interface.

The single mode approximation is valid as long as the surface wave is not so closely confined to the surface that the transverse exchange term becomes important as in thin films or at extreams of the spectrum. At this limit the transverse exchange term, $\omega_{ex} a_i^2 \beta^2_m$ (from $\omega_{ex} a_i^2 D_k$ in Equation 2-79), becomes appreciable in comparison to ω[70]. Thus, the region of validity of surface waves described by Equations 2-93, 2-94 and

2-95 is

$$\omega >> \omega_{ex} a_1^2 \beta_m^2 . \qquad 2\text{-}96$$

For YIG this corresponds to approximate upper limits of the magnitude of β_m of 3×10^6/m. at S - band and 5.5×10^6/m. at X-band.

The equations describing the single-mode exchange-modified surface wave dispersion characteristics are solved by first finding the value of D_k with the smallest magnitude. (The other two solutions of Equation 2-95 correspond to exchange modes and are neglected.) Since the transverse wavenumber in the ferrite may be expressed (from equation 2-95) in terms of D_k and k as

$$\beta_m = \pm \sqrt{k^2 - D_k} , \qquad 2\text{-}97$$

β_m may be eliminated from Equation 2-93 resulting in

$$\beta_{d\pm} = \frac{k\mu_{12} \mp \mu_{11} \sqrt{k^2 - D_k}}{(\mu_{11}^2 - \mu_{12}^2)} , \qquad 2\text{-}98$$

where the permeability tensor components are evaluated using the value of D_k specified.

Two equations relating β_d and k remain to be solved. Squaring both sides of Equation 2-98.

$$\beta_{d\pm}^2 = \frac{(\mu_{11}^2 + \mu_{12}^2) k^2 \mp 2k\mu_{11}\mu_{12}\sqrt{k^2 - D_k} - \mu_{11}^2 D_k}{(\mu_{11}^2 - \mu_{12}^2)^2} , \qquad 2\text{-}99$$

and substituting this result in Equation 2-94 yields

$$\left[1 - \frac{(\mu_{11}^2 + \mu_{12}^2)}{(\mu_{11}^2 - \mu_{12}^2)^2}\right] k^2 + \frac{2\mu_{11}\mu_{12} k \sqrt{k^2 - D_k}}{(\mu_{11}^2 - \mu_{12}^2)^2} + \frac{\mu_{11}^2 D_k}{(\mu_{11}^2 - \mu_{12}^2)^2} - \frac{\omega^2}{c_d^2} = 0, \qquad 2\text{-}100$$

and

$$\left[1 - \frac{(\mu_{11}^2 + \mu_{12}^2)}{(\mu_{11}^2 - \mu_{12}^2)^2}\right] k^2 - \frac{2\mu_{11}\mu_{12} k \sqrt{k^2 - D_k}}{(\mu_{11}^2 - \mu_{12}^2)^2} + \frac{\mu_{11}^2 D_k}{(\mu_{11}^2 - \mu_{12}^2)^2} - \frac{\omega^2}{c_d^2} = 0. \qquad 2\text{-}101$$

The solution of Equation 2-100 and 2-101 proceeds by multiplying the

former by the latter, resulting in the elimimination of the radical term. (Had the radical term been eliminated previously by taking the product of β_{d+} and β_{d-} errors may have resulted since this product does not equal β_d^2 .) The dispersion relation describing surface wave propagation along the interface between a semi-infinite dielectric and insulating ferromagnetic material is therefore

$$\left[(\mu_{11}^2-\mu_{12}^2)^2-2(\mu_{11}^2+\mu_{12}^2)+1\right]k^4 + 2\left\{\frac{\mu_{11}^2 D_k}{(\mu_{11}^2-\mu_{12}^2)}\left[(\mu_{11}^2-\mu_{12}^2)-1\right]-\frac{\omega^2}{c_d^2}\left[(\mu_{11}^2-\mu_{12}^2)^2-(\mu_{11}^2+\mu_{12}^2)\right]\right\}k^2 + \left\{\frac{\mu_{11}^2 D_k}{(\mu_{11}^2-\mu_{12}^2)}-\frac{\omega^2}{c_d^2}(\mu_{11}^2-\mu_{12}^2)\right\}^2 = 0 \quad , \qquad 2\text{-}102$$

a biquadratic equation in k. Two of the roots of the equation correspond to waves propagating in the forward or $+\hat{y}$ direction while the remaining roots propagate in the reverse direction. In order to determine which of these roots correspond to surface wave solutions the transverse wavenumbers must be examined. Not only must the transverse wavenumbers have positive real parts, the wavenumber set k, β_m and β_d must, in addition, self-consistantly satisfy the dispersion relations.

The following algorithm selects only those sets of longitudinal and transverse wavenumbers which correspond to self-consistent solutions of the dispersion relation, Equations 2-93, 2-94 and 2-95.

1. For each root, k_l , of Equation 2-102, Equation 2-97 is solved for

$$\beta_{ml1,2} = \pm\sqrt{k^2 - D_k} \quad , \qquad 2\text{-}103$$

2. Substituting each of the two values of β_{ml} into Equation 2-93, two corresponding values of β_{dl} are found

$$\beta_{dl1,2} = \frac{k_l \mu_{12} - \beta_{ml1,2}\mu_{11}}{\mu_{11}^2 - \mu_{12}^2} \quad . \qquad 2\text{-}104$$

3. Alternately, two values of β_{dl} are obtained by evaluating the expression

$$\beta_{dl\,3,4} = \pm \sqrt{k_l^2 - \frac{\omega^2}{c_d^2}} \quad . \qquad 2\text{-}105$$

4. β_{dl1} and β_{dl2} are compared with β_{dl3} and β_{dl4} . If either $|\beta_{dl1} - \beta_{dl3}|$, $|\beta_{dl1} - \beta_{dl4}|$, $|\beta_{dl2} - \beta_{dl3}|$ or $|\beta_{dl2} - \beta_{dl4}|$ is less than some test value, chosen in conformity with the precision and accuracy of the calculation, that value of β_{dl} and its corresponding value of β_{ml} are the transverse wavenumbers associated with the longitudinal wavenumber, k_l. If none of the terms is smaller than the test value, the solution is not self-consistant and k_l is not a valid solution of the dispersion relations.

Having determined which sets of k_l , β_{ml} and β_{ml} satisfy the dispersion relations, there remains only the task of determining which, if any, of these solutions are surface waves. This is simply accomplished by noting that the values of k_l corresponding to surface waves are associated with transverse wavenumbers having positive real parts.

The algorithm described above is diagramatically displayed in flow chart form in Figure 2-7 and has been used to compute the semi-infinite ferrite-dielectric surface mode spectra shown in Figure 2-8. These dispersion characteristics are computed for magnetic material parameters appropriate to YIG, i.e. $\epsilon_m = 14$, $M_o = 1750$ O_e., $T_c = 550^\circ K$, a = 12.37 Å, g = 2.0, with the internal field chosen to be 196.7 O_e (to obtain $\frac{d\omega}{dk} \cong 0$ at $3GH_z$.) Loses in the ferrite are neglected in order to

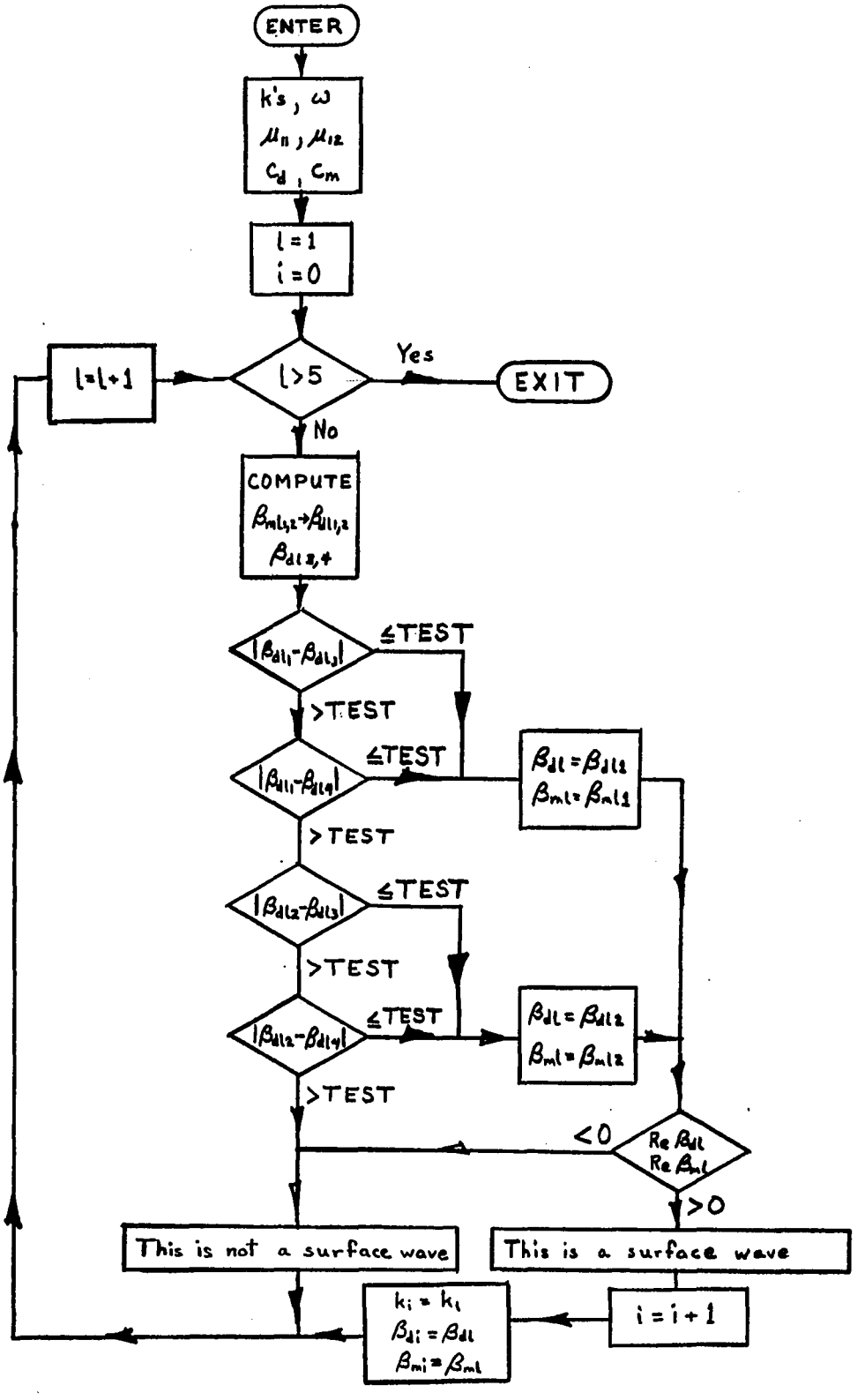

Figure 2-7 - Algorithm for Determination of Surface Modes

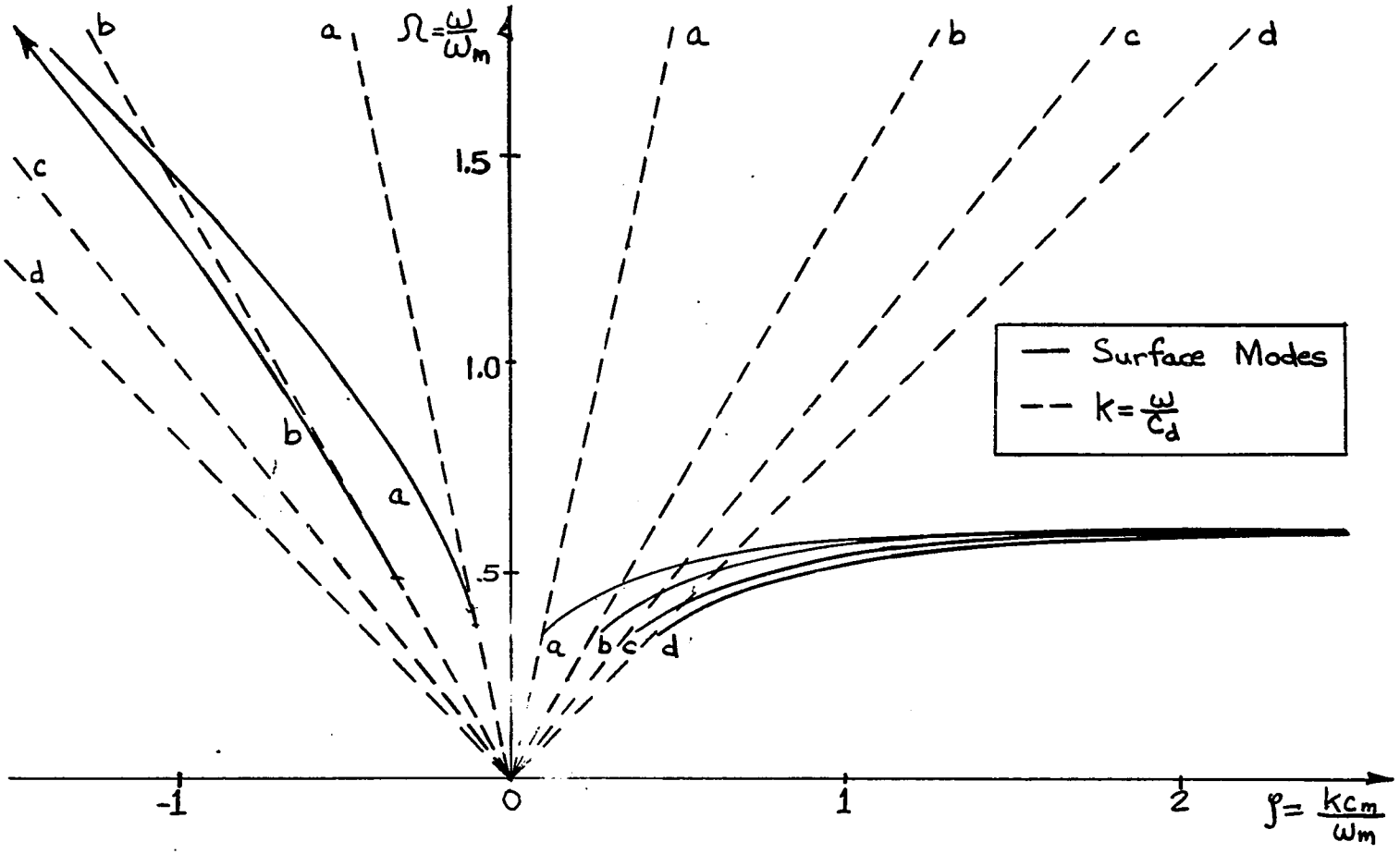

Figure 2-8 - Semi-infinite Ferrite-Dielectric Surface Mode Spectrum;
(a) $\epsilon_d = 1$, (b) $\epsilon_d = 7$, (c) $\epsilon_d = 14$, (d) $\epsilon_d = 21$.

facilitate comparisons with results based on approximate analyses to follow in Section 2.4. The curves correspond to relative dielectric permittivity values $\epsilon_d = 1$, $\epsilon_d = \frac{\epsilon_m}{2}$, $\epsilon_d = \epsilon_m$ and $\epsilon_d = \frac{3\epsilon_m}{2}$. The graph is normalized to ferrite material parameters, the vertical axis being the normalized frequency $\Omega = \frac{\omega}{\omega_m}$, the horizontal axis being the normalized wavenumber $\beta = \frac{kc_m}{\omega_m}$.

Examining the spectra to the right of the $\beta = 0$ axis, corresponding to waves with positive $\hat{y}$ directed phase velocities, it is observed that while all four curves appear to have the same lower cutoff frequency, the wavenumber at cutoff is different for each curve. As the intrinsic velocity of the dielectric medium is decreased, the magnitude of the phase velocity is decreased, its maximum always being less than c_d. As the frequency is increased the wavenumber of the forward traveling mode increases, all of the $\beta > 0$ curves approaching a resonance, $\frac{\partial \omega}{\partial k} \cong 0$, at the same frequency, approximately 3GHz. for the parameters chosen. (A discussion of the limiting frequencies of the surface wave spectrum appears in Section 2-4.).

One might expect , in analogy with bulk modes, that as k becomes large the exchange energy should become appreciable, manifesting itself as an upward curving of the dispersion characteristic in the large k limit.[71] It is interesting to note that the exchange modified model under consideration does not exhibit this behavior. The model , in which pinning conditions at the surface have been neglected, shows that the forward surface mode is relatively unaffected by exchange. However, as the longitudinal, and hence

transverse wavenumbers becomes large, the energy of wave is restricted more and more to the vicinity of the ferrite-dielectric interface. Under these conditions it becomes necessary to satisfy the pinning conditions in addition to the electromagnetic boundary conditions at the surface.

The curves appearing in the $y < 0$ region of Figure 2-8, the reverse or negative $\hat{y}$ propagating mode is now considered. As with the forward mode, the magnitude of the phase velocity of the reverse mode is smaller than the intrinsic velocity of the dielectric. In contrast to the "slow" forward mode, however, the magnitude of the phase velocity of the reverse mode always exceeds the intrinsic velocity of the ferrite. The restriction of the reverse mode to the region $\frac{\omega}{c_d} \leq |k| < \frac{\omega}{c_m}$ causes its wave propagation characteristics to be highly sensitive to the relative permeability and permittivity parameters. Not only is the frequency range of the reverse mode altered by changing the intrinsic velocities of the materials, the mode itself does not exist if $c_d \leq c_m$. Thus only two reverse mode curves, corresponding to $\epsilon_d = 1$ and $\epsilon_d = \frac{\epsilon_m}{2}$ appear in Figure 2-8.

This result, the ability to control the frequency range of the reverse mode or eliminate it entirely through the appropriate selection of material parameters and (as shown in Section 2-4) the appropriate choice of operating frequency is extreamly important to the proper interpretation of experimental results (Chapter 3).

2.4 Approximations For Analytical Investigations

In this section the equations describing wave propagation along the interface between semi-infinite dielectric and insulating ferromagnetic media are considered using certain approximation techniques. By comparing the resultant dispersion characteristics with those computed in the previous section, regions of validity for the approximations are obtained. Where there is good agreement, the approximate relations provide a means for investigation of the surface wave modes analytically.

The dispersion relations are first analyzed in the magnetostatic regime, with exchange and losses assumed to be negligible. Using Equations 2-83 and 2-84, the equations of magnetostatics, in which propagation effects are neglected, the following equations relating the longitudinal and transverse wavenumbers are obtained

$$k^2 = \beta_d^2, \qquad 2\text{-}106$$

and

$$k^2 = \beta_m^2. \qquad 2\text{-}107$$

As can be seen by comparing Equations 2-106 and 2-107 with Equations 2-94 and 2-95 the magnetostatic approximation is valid in regions where the phase velocity is much smaller than the intrinsic velocity of both media and, additionally,

$$k^2 \gg \left| \frac{\omega^2}{c_m^2} \frac{\mu_{11}^2 - \mu_{12}^2}{\mu_{11}} \right|, \qquad 2\text{-}108$$

for the ferrite. As indicated in Section 2.3, these conditions are not simultaneously satisfied for the reverse mode. On the other hand, the magnitude of the phase velocity of the forward mode, considered in Section 2.3, is always less than the intrinsic velocities of the ferrite and dielectric media. As is shown subsequently, the additional condition given by Equation 2-108, is satisfied in the vicinity of the mode's resonance frequency. The magnetostatic approximation may therefore be employed in this region. Substituting

$$k = \beta_m \qquad 2\text{-}109$$

and

$$k = \beta_d \qquad 2\text{-}110$$

into Equation 2-93, the magnetostatic surface mode dispersion relation for the semi-infinite ferrite-dielectric structure is found to be

$$1 + (\mu_{11} + \mu_{12}) = 0 \qquad 2\text{-}111$$

Since exchange and losses are neglected the permeability tensor component definitions, Equation 2-67 and 2-68, are given by

$$\mu_{11} = 1 + \frac{\omega_m \omega_i}{\omega_i^2 - \omega^2} \,, \qquad 2\text{-}112$$

$$\mu_{12} = \frac{\omega_m \omega}{\omega_i^2 - \omega^2} \,. \qquad 2\text{-}113$$

Substitution of these definitions into Equation 2-111 yields the resonant frequency of the forward surface mode,

$$\omega_{res} = \omega_i + \frac{\omega_m}{2} \,. \qquad 2\text{-}114$$

(If the permeability of the dielectric is not μ_o, the resonance frequency is altered[12]).

While the analysis employed here yields information concerning the upper frequency limit of the forward surface mode, no information is obtained concerning the sensitivity of the wavelength to frequency or to changes in the intrinsic velocity of the dielectric. An alternate technique[21], in which the magnetostatic approximation is taken only in the ferrite yields somewhat more insight into the behavior of the forward surface mode. Substituting Equation 2-109 into Equation 2-93 an expression is obtained relating β_d to k,

$$\beta_d = \frac{-k}{\mu_{11} + \mu_{12}} . \qquad 2\text{-}115$$

This equation may be used to eliminate β_d from Equation 2-94, resulting in the following approximate dispersion relation

$$k^2 = \frac{\omega^2}{c_d^2} \frac{(\mu_{11} + \mu_{12})^2}{[(\mu_{11} + \mu_{12})^2 - 1]} . \qquad 2\text{-}116$$

Upon simplification Equation 2-116 becomes

$$k^2 = \frac{\omega^2}{c_d^2} \frac{[\omega_i + \omega_m - \omega]^2}{2\omega_m(\omega_i + \frac{\omega_m}{2} - \omega)} , \qquad 2\text{-}117$$

where k must be greater than zero in order to satisty the boundary condition at $-\infty$. In agreemanet with the previous analysis, Equation 2-117 indicates that the surface wave has a resonance at $\omega_{res} = \omega_i + \frac{\omega_m}{2}$, the wavelength becoming infinitely large as this resonance frequency is approached. Near ω_{res}, the condition given by Equation 108 may be reexpressed

$$k^2 >> \left| \frac{\omega^2}{c_m^2} \left(3 + 4\frac{\omega_i}{\omega_m}\right) \right| , \qquad 2\text{-}118$$

or

$$V_{ph} < \frac{c_m}{\sqrt{3 + 4\frac{\omega_i}{\omega_m}}} . \qquad 2\text{-}119$$

This condition is satisfied as k becomes infinite, showing that the magnetostatic approximation is valid in the vicinity of the resonance.

The wavenumber increases as the intrinsic velocity of the dielectric is decreased (see Equation 2-117). This is in agreement with the results of the electromagnetic calculations performed in Section 2.3. However, comparison of these results with Equation 2-117 reveals that Equation 2-117 yields incorrect information about the lower cutoff frequency of the surface mode. This cutoff occurs in the long wavelength region in which the magnetostatic approximation is no longer valid.

In order to gain further insight into the behavior of the surface modes in the long wavelength region, the dispersion relations obtained through an electromagnetic calculation, Equations 2-93, 2-94 and 2-95, are considered with the effects of exchange and losses neglected. The dispersion characteristics, computed using the algorithm of Section 2.3 for the same parameters as the $\epsilon_d=1$ curve of Figure 2.8, are plotted in Figure 2.9. The curves corresponding to $k=\frac{\omega}{c_d}$, $k=\frac{\omega}{c_m}$ and $k^2=\frac{\omega^2}{c_m^2}\frac{(\mu_m^2-\mu_n^2)}{\mu_n}$ are also plotted on the same set of normalized axes. To distinguish between the forward and reverse modes, which are plotted in the same quadrant, the s notation, introduced by Seshadri[7] is employed. Defining the term s as

$$s=\frac{k}{|k|}, \qquad 2\text{-}120$$

The forward mode is labeled $s=+1$ and the reverse mode $s=-1$. (This notation may be extended to lossy cases as well through a more general definition

$$s=\mathrm{SGN}[\mathrm{Re}\,k]. \qquad 2\text{-}121$$

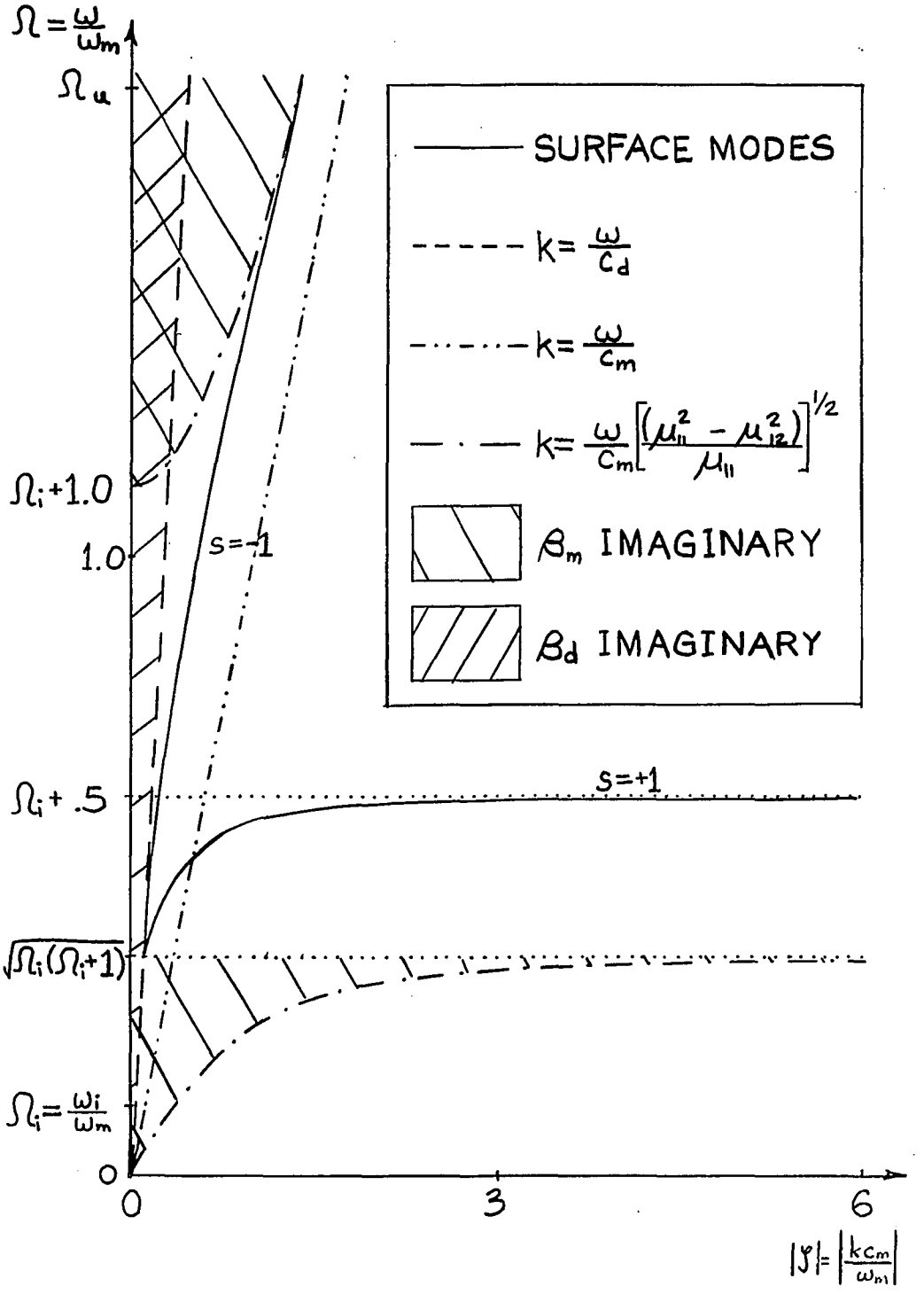

Figure 2-9 Dispersion of Semi-infinite Model Surface Modes

Comparison of Figure 2-9 and the $\epsilon_d = 1$ curves of Figure 2-8 indicate that they are identical. The differences caused by the inclusion of exchange, which occur in the region of the lower frequency limit are relatively insignificant, being too small to be observed on the scale on which the figures are presented.

The frequency range of the surface modes is determined by observing the behavior of the transverse wavenumbers as the frequency is varied. The boundary conditions stipulating that the response exist simultaneously in both media and that it vanish at $x = \pm\infty$ impose the constraint that both β_m and β_d be finite positive real numbers in the surface wave passband. At the limiting frequencies, this condition is not fulfilled determining the extent of the surface wave spectrum.

Examination of Equation 2-94 reveals that $\beta_d = 0$ when the phase velocity of the wave equals the intrinsic velocity of the dielectric. Thus, for β_d to be a positive real number the magnitude of the phase velocity of the surface wave must be less than the intrinsic velocity of the dielectric.

Examination of Equation 2-95 reveals that the difference between squares of the longitudinal and transverse wavenumbers is positive below the frequency $\omega = \sqrt{\omega_i(\omega_i + \omega_m)}$ and above the frequency $\omega = \omega_i + \omega_m$. Thus β_m is imaginary in these regions if the magnitude of the phase velocity is greater than the phase velocity of waves represented by the $\beta_m = 0$ $\left(k^2 = \frac{\omega^2}{c_m^2}\frac{(\mu_{11}^2 - \mu_{12}^2)}{\mu_{11}}\right)$ curves of Figure 2-9.

Since the surface waves being investigated are forward and reverse modes (as opposed to backward modes) the lower frequency limit occurs when either

$\beta_d = 0$ or $\omega = \sqrt{\omega_i(\omega_i + \omega_m)}$. If it is assumed that $\beta_d = 0$ then Equations 2-94 and 2-93 become

$$k^2 = \frac{\omega^2}{c_d^2} \quad , \qquad 2\text{-}122$$

and

$$k = \beta_m \frac{\mu_{11}}{\mu_{12}} \, . \qquad 2\text{-}123$$

Since $\mu_{11} > 0$ and $\mu_{12} < 0$ in the region $\omega > \sqrt{\omega_i(\omega_i + \omega_m)}$, the $s = -1$ mode lower frequency limit occurs when $\beta_d = 0$. This frequency is determined by substituting Equation 2-122 and 2-123 into Equation 2-95 yielding,

$$\frac{\omega^2}{c_d^2}\left[1 - \frac{\mu_{11}^2}{\mu_{12}^2}\right] = \frac{\omega^2}{c_m^2}\frac{(\mu_{11}^2 - \mu_{12}^2)}{\mu_{11}} \quad , \qquad 2\text{-}124$$

which, upon simplification results in

$$\epsilon_m \mu_{11} = \epsilon_d \, . \qquad 2\text{-}125$$

Equation 2-125 may be solved for the lower frequency limit yielding,

$$\omega_l \Big|_{s=-1} = \sqrt{\frac{(\epsilon_m - \epsilon_d)\omega_i^2 + \epsilon_m \omega_m \omega_i}{(\epsilon_m - \epsilon_d)}} \, . \qquad 2\text{-}126$$

The reverse mode is not cutoff at this lower limit but rather ceases to have surface wave properties. Its characteristic merges smoothly into the dispersion characteristic corresponding to propagation within the bulk of an infinite dielectric medium, $k = -\frac{\omega}{c_d}$.

Examination of Equation 2-126 reveals that if $\epsilon_m > \epsilon_d$, the lower frequency limit of the $s = -1$ wave must be above the frequency $\omega = \sqrt{\omega_i(\omega_i + \omega_m)}$, the resonance frequency of 90^0 spin-waves in an infinite ferromagnetic medium ("slow" portion of the $\beta_m = 0$ curve of Figure 2-9). As ϵ_d approaches ϵ_m , the lower frequency limit increases, Equation 2-126 having a pole at $\epsilon_m = \epsilon_d$. If $\epsilon_m < \epsilon_d < \epsilon_m \frac{(\omega_i + \omega_m)}{\omega_i}$, Equation 2-126 yields an

imaginary solution indicating that the reverse mode does not exist for these conditions. These results are in agreement with the reverse mode dispersion characteristics plotted in Figure 2-8.

For the large dielectric constant case, such that $\epsilon_d > \epsilon_m \frac{(\omega_i + \omega_m)}{\omega_i}$ ($\epsilon_d > 138$ for the parameters used in plotting Figures 2-8 and 2-9) the solution to Equation 2-126 is real, indicating the existance of another surface mode. Since the limiting frequency for this new mode occurs for $\omega < \omega_i$, a region where both μ_{11} and μ_{12} have the same sign, Equation 2-123 stipulates that k be greater than zero. In contrast to the $s = +1$ mode discussed above in connection with the magnetostatic approximation, the new $s = +1$ mode cannot be found through a magnetostatic analysis but rather only by an electromagnetic calculation. Adopting the nomenclature used in investigations of mode spectra supported by longitudinally magnetized rods[13], the former is termed "magnetostatic" while the latter is designated as "dynamic". The reverse mode also falls into the "dynamic" mode category, since it too may only be calculated by including the effects of electromagnetic wave propagation.

Having determined the lower frequency limits of the dynamic modes, the lower cutoff of the "magnetostatic" $s = 1$ or $s = 1_m$ mode is now considered. Since $\beta_d \neq 0$ at this cutoff, its lower cutoff frequency is

$$\omega_{co}\Big|_{s=+1_m} = \sqrt{\omega_i(\omega_i + \omega_m)} \quad . \qquad 2\text{-}127$$

As this lower limit is approached, μ_{11} becomes very small. Thus, just above the cutoff, the transverse wavenumber of the $s = +1$ mode is, from Equation 2-95,

$$\beta_m \cong \frac{\omega}{c_m}\sqrt{\frac{\mu_{12}^2}{\mu_{11}}} \quad . \qquad 2\text{-}128$$

Subsitution of Equation 2-128 into Equation 2-93 indicates that the transverse wavenumber in the dielectric is related to the longitudinal wavenumber by

$$\beta_d \cong -\frac{k}{\mu_{12}} \quad . \qquad 2\text{-}129$$

Thus, the wavenumber of the $s=+1$ mode at cutoff may be determined by subsitution of Equation 2-129 into Equation 2-94 yielding, upon simplification,

$$k_{co}\Big|_{s=+1_m} = \frac{\omega_i + \omega_m}{c_d}\sqrt{\frac{\omega_i}{\omega_m}} \quad . \qquad 2\text{-}130$$

With the exception of its lower limit, the reverse dynamic (or $s=-1_d$) mode satisfies the inequality $\frac{\omega}{c_d} < |k| < \frac{\omega}{c_m}$ over its frequency range. Therefore its upper limit can only occur when $\beta_m = 0$. At this point, which occurs at a frequency greater than $\omega = \omega_i + \omega_m$, the $s=-1_d$ mode is no longer indentifiable as a surface wave, it characteristic having merged with the "fast" portion of the bulk 90^0 spin wave curve.

The upper frequency limit of the $s=+1_m$ wave occurs at the resonance frequency $\omega_{res} = \omega_i + \frac{\omega_m}{2}$, where the magnetostatic analysis appearing earlier in this section is appropriate. Since the $s=+1_d$ mode is not found in the magnetostatic limit, its upper frequency limit occurs when $\beta_m = 0$ where its dispersion characteristic merges with the "slow" branch of the bulk 90^0 spin wave mode. Thus the frequency range of the forward dynamic mode never overlaps that of the forward magnetostatic mode.

The surface wave spectrum at the interface of a semi-infinite dielectric medium, $\epsilon_d = 210$, and a semi-infinite ferromagnetic insulator, with material

and field parameters as in Figures 2-8 and 2-9, is plotted in Figure 2-10. Both modes shown are forward modes as expected. As before the magnetostatic mode is resonant at 3 GHz., the effect of increasing the permittivity of the dielectric being most apparent in the long wavelength region where it results in a larger value of k . The dispersion characteristic of the forward dynamic mode is shown to closely resemble the characteristic corresponding to $k=\frac{\omega}{c_d}$. Close examination reveals that its phase velocity is slower than the intrinsic velocity of the dielectric (as expected for a surface wave); this property is most noticeable in the region where the $s=+1_d$ surface mode merges with the "slow" branch of the bulk 90^0 spin wave (or $\beta_m=0$) mode.

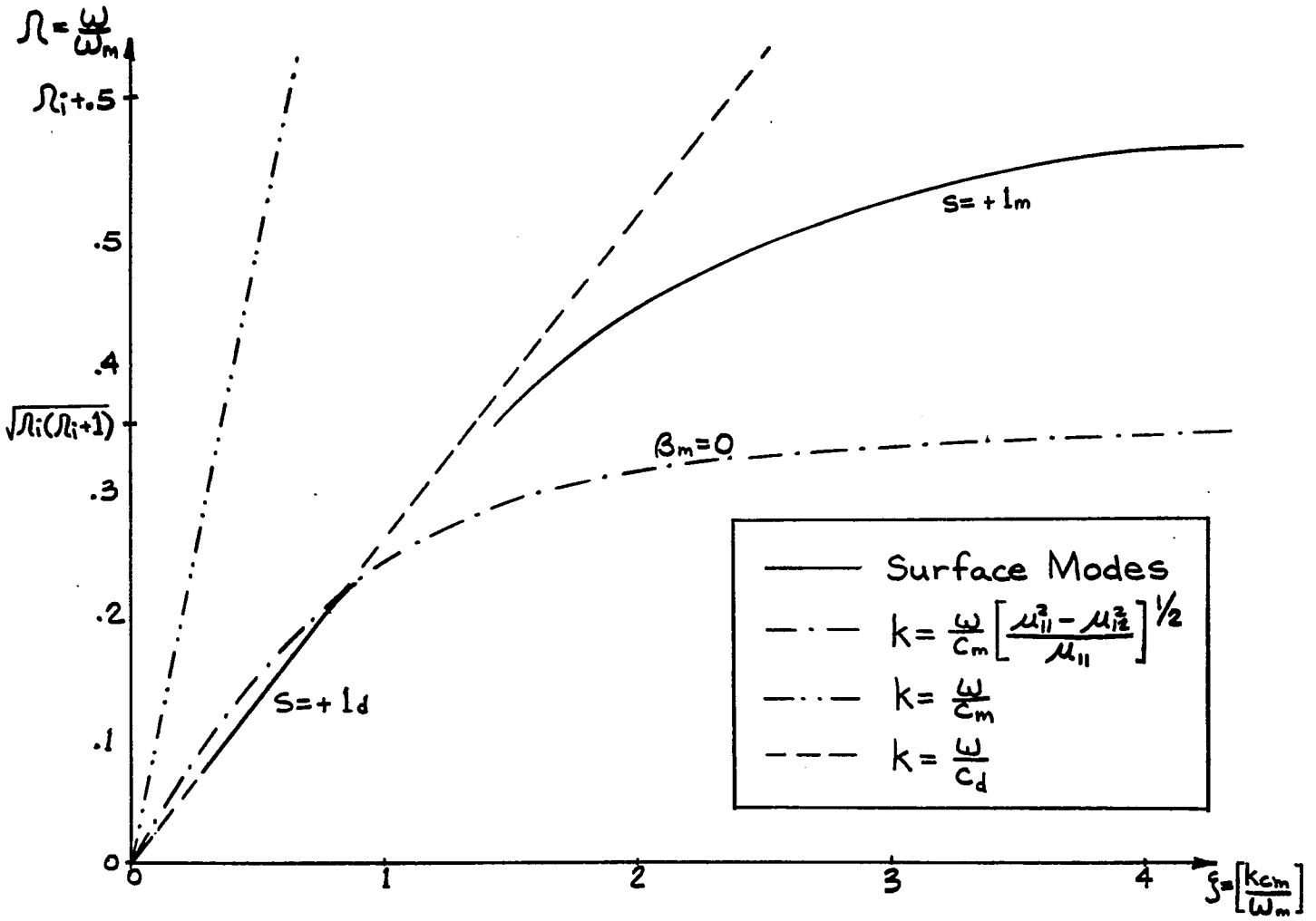

Figure 2-10 - Semi-infinite Ferrite-Dielectric Surface Mode Dispersion Characteristics For Large Dielectric Constant Case

CHAPTER 3
SURFACE ELECTROMAGNETIC MODES OF A FERRITE SLAB

3.0 Introduction

Electromagnetic wave propagation at a surface of a semi-infinite ferrite slab bounded by a uniform dielectric was investigated in Chapter 2. In the present chapter, the electromagnetic surface wave spectrum of a ferrite slab of finite thickness is considered. The results of this analysis are compared with surface wave calculations obtained through the magnetostatic approximation as well as with the semi-infinite ferrite results of the previous chapter. It is shown in Section 3.1 that control of the frequency range of the dynamic surface modes, as demonstrated in the semi-infinite case, is also possible when the ferrite is of finite thickness. This is shown to have a bearing on the interpretation of experimental results discussed in Section 3.3.

In Section 3.2 the case of a ferrite slab having one of its faces in intimate contact with a perfect conductor is considered. Studying the structure in both the thick film and magnetostatic limits allows certain inconsistancies between dispersion characteristics derived in these limits to be resolved. Additionally, it is shown that the frequency ranges of forward and reverse "magnetostatic" modes may be made to be non-overlapping, a result which is of importance in the proper interpretation of experimental data on surface wave propagation.

3.1 Electromagnetic Surface Wave Propagation On a Planar Ferrite Slab With Dielectric Loading

The surface electromagnetic modes of a planar slab of single crystal ferrite material of magnetization M_0 are to be investigated. The slab, shown in Figure 3-1, is of thickness a and is assumed to be infinite in extent in the $\hat{y}$ and $\hat{z}$ directions. The ferrite is bounded at its x=0 and x=-a surfaces by uniform dielectric media of permittivities ϵ_1 and ϵ_2 respectively. A static magnetic field is applied in the $\hat{z}$ direction, resulting in a magnetic field intensity, $\overline{H}_i$, assumed uniform within the ferrite.

The development of the equations describing the response of the structure of Figure 3-1 to electromagnetic excitation closely follows the procedures of Chapter 2. Since dielectric # 1 occupies the upper half space, $x > 0$, the relations between the field quantities in this region are

$$E_{d1z} = A_z \exp\left[-\beta_{d1} x + j(\omega t - ky)\right], \qquad 3\text{-}1$$

$$H_{d1x} = \frac{kA_z}{\omega\mu_o} \exp\left[-\beta_{d1} x + j(\omega t - ky)\right], \qquad 3\text{-}2$$

and

$$H_{d1y} = j\frac{\beta_{d1}}{\omega\mu_o} A_z \exp\left[-\beta_{d1} x + j(\omega t - ky)\right], \qquad 3\text{-}3$$

where consistancy with Maxwell's equations (2-39 and 2-40) requires that β_{d1} be related to k through the relation

$$k^2 - \beta_{d1}^2 = \frac{\omega^2}{c_{d1}^2} \qquad 3\text{-}4$$

c_{d1} being the velocity of light in dielectric # 1.

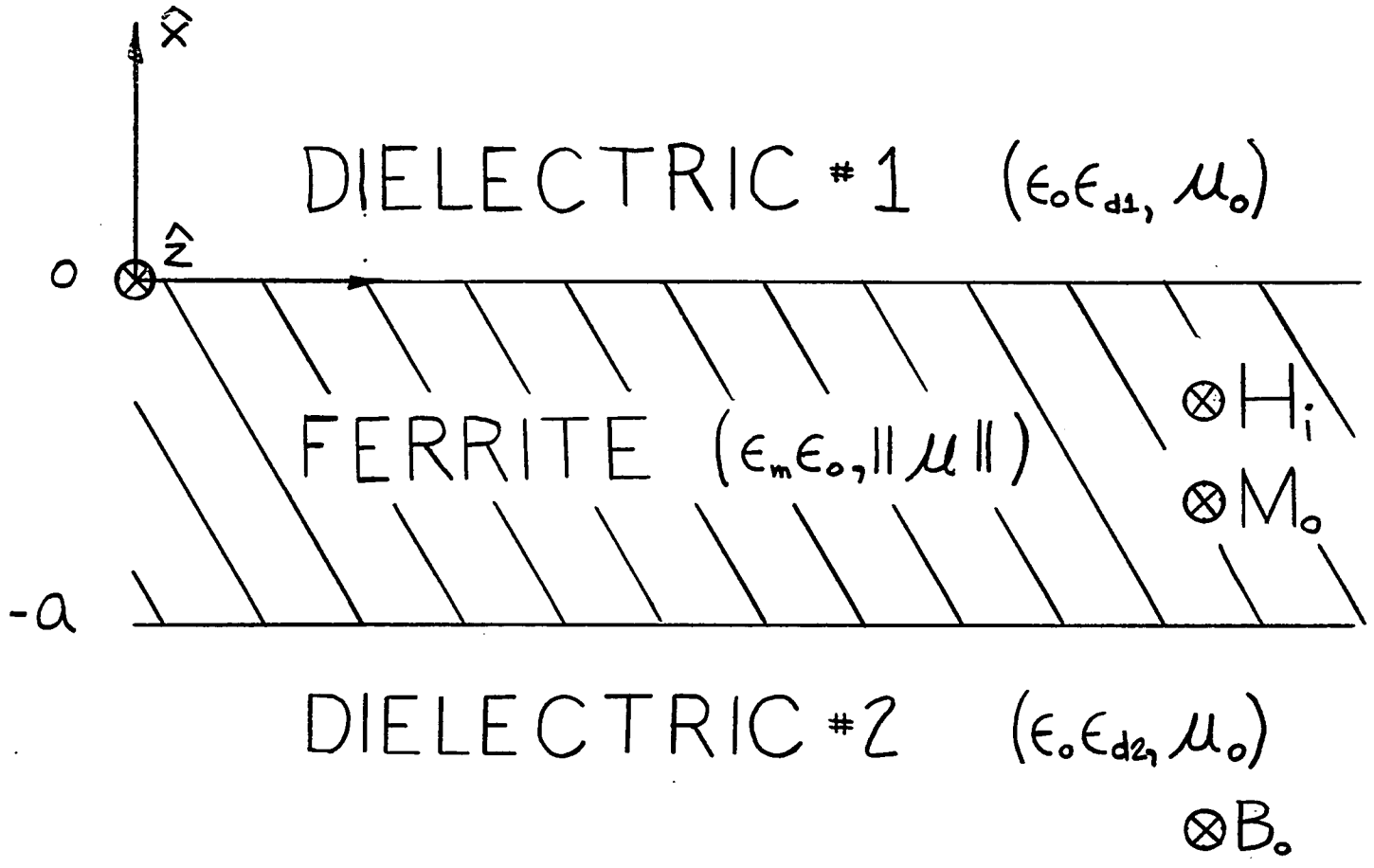

Figure 3-1 - Finite Thickness Ferrite Model

Similarly, the relations between the field quantities in dielectric # 2 are

$$E_{d2z} = R_z \exp\left[+\beta_{d2}(x+a) + j(\omega t - ky)\right], \qquad 3\text{-}5$$

$$H_{d2x} = \frac{kR_z}{\omega\mu_o} \exp\left[+\beta_{d2}(x+a) + j(\omega t - ky)\right], \qquad 3\text{-}6$$

and

$$H_{d2y} = -j\frac{\beta_{d2}}{\omega\mu_o} R_z \exp\left[+\beta_{d2}(x+a) + j(\omega t - ky)\right], \qquad 3\text{-}7$$

where the real part of $\beta_{d2} > 0$, since dielectric # 2 occupies the region $x < -a$. The transverse and longitudinal wavenumbers in the medium are related through the equation

$$k^2 - \beta_{d2}^2 = \frac{\omega^2}{c_{d2}^2} \quad . \qquad 3\text{-}8$$

For a plane wave solution to exist, the waveform in the ferrite slab must have the same phase velocity as the excitations in the adjacent dielectric media. Assuming the electric field in the ferrite to be of the form

$$E_{1mz} = \left[G\cosh\beta_m x + L\sinh\beta_m x\right]\exp\left[j(\omega t - ky)\right], \qquad 3\text{-}9$$

the magnetic field intensity components are found, through Equation 2-39, to be given by

$$H_{1mx} = \frac{\left[(k\mu_{11}G - \beta_m\mu_{12}L)\cosh\beta_m x + (k\mu_{11}L - \beta_m\mu_{12}G)\sinh\beta_m x\right]}{\omega\mu_o(\mu_{11}^2 - \mu_{12}^2)}\exp\left[j(\omega t - ky)\right] \qquad 3\text{-}10$$

and

$$H_{1my} = j\frac{\left[(k\mu_{12}G - \beta_m\mu_{11}L)\cosh\beta_m x + (k\mu_{12}L - \beta_m\mu_{11}G)\sinh\beta_m x\right]}{\omega\mu_o(\mu_{11}^2 - \mu_{12}^2)}\exp\left[j(\omega t - ky)\right] \qquad 3\text{-}11$$

Substitution of E_{1mz}, H_{1mz}, and H_{1my} into Equation 2-40 leads to the condition that

$$k^2 - \beta_m^2 = \frac{\omega^2}{c_m^2} \frac{(\mu_{11}^2 - \mu_{12}^2)}{\mu_{11}} . \qquad 2\text{-}95$$

An equation relating the transverse wavenumbers associated with each of the media may be obtained by applying the boundary conditions on the electric and magnetic fields at the ferrite-dielectric interfaces. Applying the condition that the tangential r.f. electric field be continuous across any plane, first at x=0 and then at x=-a, yields

$$A_z = G , \qquad 3\text{-}12$$

and

$$R_z = A_z \cosh Q_m - L \sinh Q_m , \qquad 3\text{-}13$$

respectively, where

$$Q_m \equiv \beta_m a. \qquad 3\text{-}14$$

Equating the tangential components of the r.f. magnetic field intensity at x=0 leads to

$$A_z \beta_{d1} = \frac{(k\mu_{12} A_z - \beta_m \mu_{11} L)}{(\mu_{11}^2 - \mu_{12}^2)} . \qquad 3\text{-}15$$

This equation relating A_z and L may be used to eliminate L from Equation 3-13 yielding an expression relating the amplitude of a mode at x=-a with its amplitude at x=0,

$$\frac{R_z}{A_z} = \cosh Q_m - \left[\frac{k\mu_{12} - \beta_{d1}(\mu_{11}^2 - \mu_{12}^2)}{\beta_m \mu_{11}}\right] \sinh Q_m . \qquad 3\text{-}16$$

Although the term β_{d2} does not explicitly appear in the above expression, changes in the permittivity of dielectric # 2 alter the R_z/A_z ratio through the interrelationship of the transverse and longitudinal wavenumbers. An expression displaying this interdependency is obtained by applying the boundary condition on the $\hat{y}$ component of the r.f. magnetic field intensity at x=-a and using Equations 3-15 and 3-16. The resultant equation,

$$\beta_m \mu_{11}(\beta_{d1}+\beta_{d2})(\mu_{11}^2-\mu_{12}^2)\coth Q_m = \left\{(k^2\mu_{12}^2-\beta_m^2\mu_{11}^2)+k\mu_{12}(\beta_{d2}-\beta_{d1})(\mu_{11}^2-\mu_{12}^2) - \beta_{d1}\beta_{d2}(\mu_{11}^2-\mu_{12}^2)^2\right\}, \qquad 3\text{-}17$$

together with Equations 3-4, 3-8 and 2-95 defines the mode spectrum supported by the layered structure.

To facilitate comparison with previous results, analysis of Equation 3-17 is performed in the limit of zero loss with exchange neglected. Imposing an additional constraint by searching only for solutions having real values of β_m restricts the possible modes to waves whose amplitude varies as a sum of exponentials across the thickness of the ferrite. These modes display surface wave characteristics since their amplitude is a maximum at one of the ferrite-dielectric interfaces.

In the short wavelength region (large k), where the phase velocity of the response is much smaller than the intrinsic velocities of the ferrite media, and additionally

$$k^2 \gg \left| \frac{\omega^2}{c_m^2} \quad \frac{\mu_{11}^2-\mu_{12}^2}{\mu_{11}} \right|, \qquad 2\text{-}108$$

the relationships between the longitudinal and transverse wavenumbers are

$$k^2 \cong \beta_m^2 \quad , \qquad 3\text{-}18$$

$$k^2 \cong \beta_{d1}^2 \quad , \qquad 3\text{-}19$$

and

$$k^2 \cong \beta_{d2}^2 \quad . \qquad 3\text{-}20$$

In this, the magnetostatic limit, where $\nabla \times \bar{H} \cong 0$, Equation 3-17 reduces to

$$2\mu_{11} \coth Q_m = -\left[(\mu_{11}^2 - \mu_{12}^2) + 1\right] , \qquad 3\text{-}21$$

which may be reexpressed, using the permeability tensor component definitions, Equations 2-111 and 2-112, in the form obtained by Damon and Esbach[60]

$$\omega^2 = \omega_i^2 + \omega_i \omega_m + \frac{\omega_m^2}{2[1+\coth|k|a]} . \qquad 3\text{-}22$$

Equation 3-22 is plotted in Figure 3-2 for a ferrite of thickness .5mm having saturation magnetization of 1750 Gauss and spectroscopic splitting factor g=2.0 (appropriate for YIG). The internal magnetic field intensity is chosen to be 197.6 Oe. and the graph is normalized to ferrite material parameters in conformity with the dispersion relation plots of Chapter 2.

The magnetostatic dispersion relation, Equation 3-22, predicts that the mode spectrum extends from a lower cutoff frequency, $\omega_{co} = \sqrt{\omega_i(\omega_i + \omega_m)}$, where k=0 (a contradiction to the assumptions expressed by Equations 3-18, 3-19 and 3-20), to an upper frequency limit of

$$\omega_{res} = \omega_i + \frac{\omega_m}{2} , \qquad 2\text{-}113$$

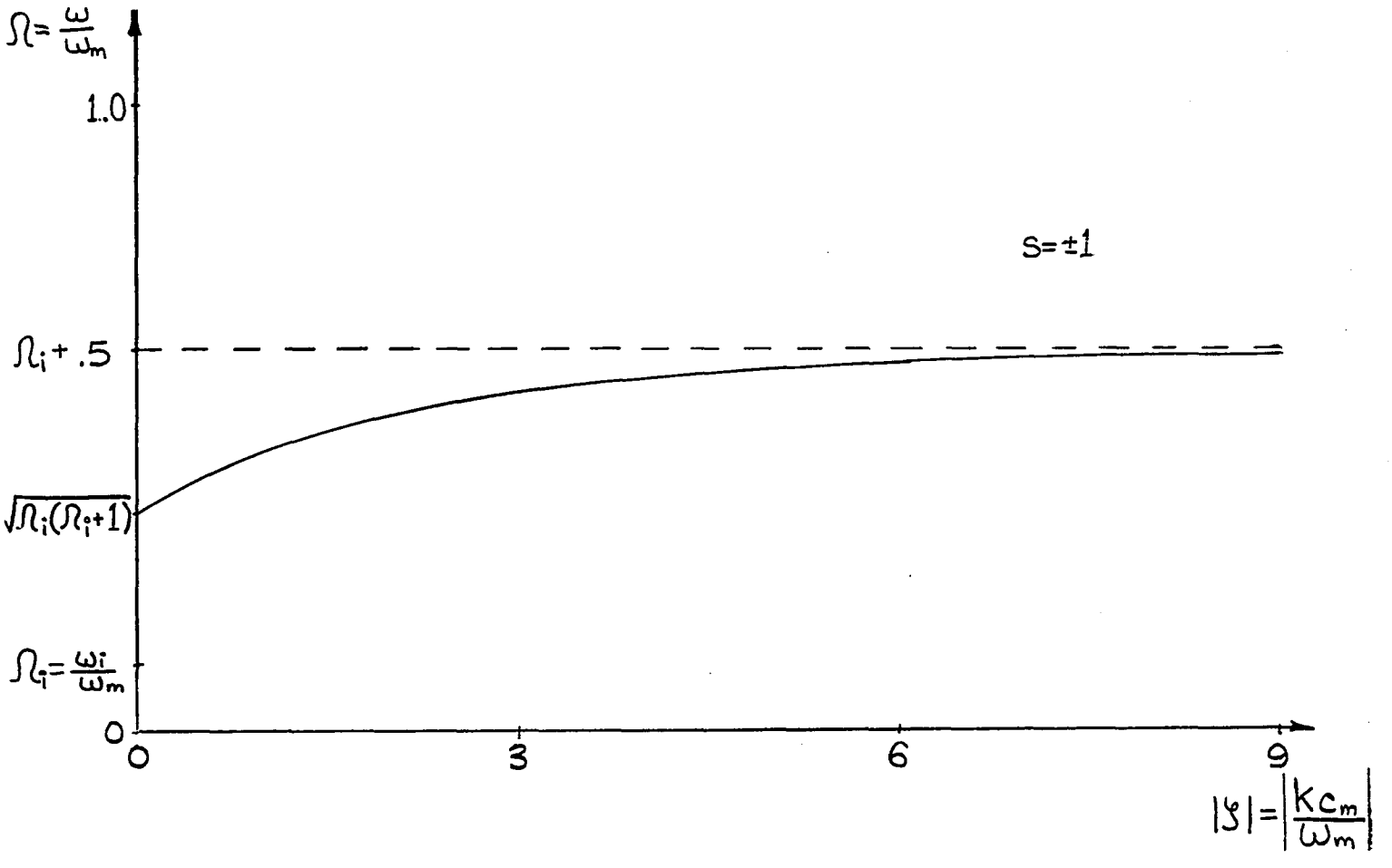

Figure 3-2 - Magnetostatic Surface Mode Spectrum Of A Finite Thickness Ferrite Slab

where the surface wave is resonant. Within this passband surface waves may propagate in either the + or - $\hat{y}$ directions, however, the properties of these forward and reverse waves are different. The ratio of the mode amplitude at the bottom surface to that at the top surface is dependent on the direction of propagation. Applying Equations 3-16, 3-18 and 3-19 and employing the direction parameter, s, defined by Equation 2-117, one obtains

$$\frac{R_z}{A_z} = \cosh|k|a - \left[\frac{s\mu_{12} - (\mu_{11}^2 - \mu_{12}^2)}{\mu_{11}}\right]\sinh|k|a . \quad 3\text{-}23$$

Reexpressing this result through the use of the permeability tensor component definitions, Equations 2-111 and 2-112, results in

$$\frac{R_z}{A_z} = \cosh|k|a + \left[\frac{\omega^2 + s\omega\omega_m - (\omega_i + \omega_m)^2}{\omega^2 - \omega_i(\omega_i + \omega_m)}\right]\sinh|k|a . \quad 3\text{-}24$$

The relative energy density at the bottom surface as a function of frequency is plotted in Figure 3-3 for both the forward and reverse modes. It is observed that most of the energy associated with the mode propagating in the positive direction (s=+1) is concentrated near the top surface, the interface of the ferrie with dielectric #1. Similarly, most of the energy associated with the s=-1 mode is concentrated near the ferrite-dielectric #2 interface.

If the direction of $\bar{H}_i$ is reversed, the directions of propagation of the modes associated with the top and bottom faces reverses. Thus, the direction of propagation of the surface magnetostatic modes of a ferrite slab is such that the vector $\bar{k}\times\bar{H}_i$ coincides with the outward directed normal.

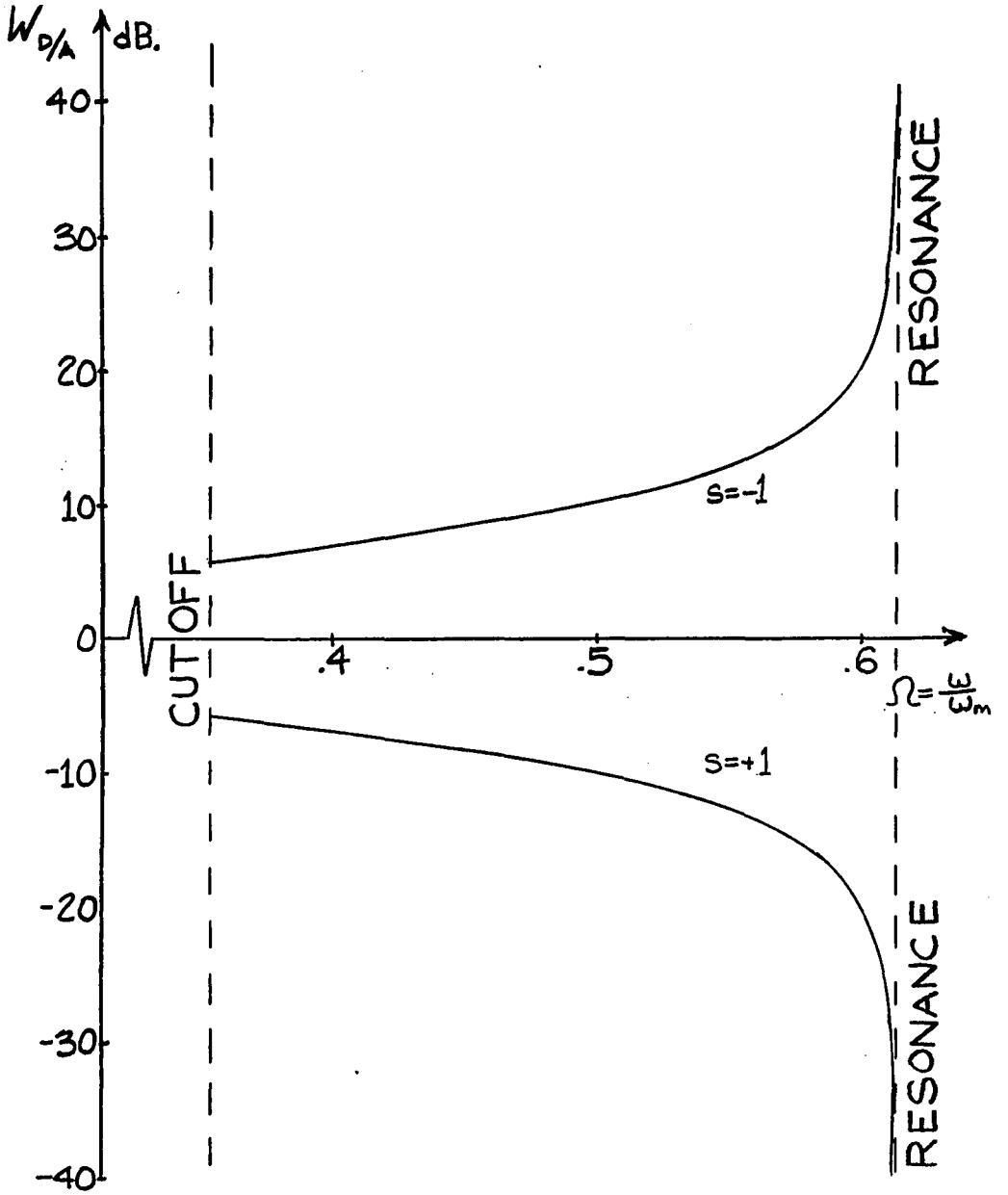

Figure 3-3 - Relative Energy Density - Bottom/Top for Magnetostatic Approximation

The magnetostatic dispersion relationship, Equation 3-22, from which an explicit expression for $|k|a$ may be obtained, predicts that the wavenumber thickness product is independent of the thickness of the ferrite. Hence, from Equation 3-18, $\beta_m a$ does not vary as a is increased. One may therefore conclude that although the wavelength of the response is affected by varying the ferrite thickness, the relative surface wave amplitudes at the two surfaces are unaffected, a limit inherent to the magnetostatic approximation.

The symmetry of the dispersion relations about k=0 and the symmetry about the 0db axis of Figure 3-3, suggests that the characteristics of the s=+1 surface wave with respect to the top face are identical to the characteristics of the s=-1 mode with respect to the bottom face. For any frequency within the passband, R_z/A_z for the s=-1 mode should be reciprocal of R_z/A_z for the s=+1 mode. This conclusion, however, is a consequence of having performed the analysis in the magnetostatic limit and is not true in general. For electromagnetic surface waves on opposing faces of the ferrite slab, symmetry considerations dictate that the exact correspondance of properties described above is obtained only when the permittivities of the top and bottom dielectric media are equal. For this case

$$\beta_{d1} = \beta_{d2} = \beta_d \qquad 3\text{-}25$$

and Equation 3-17 reduces to

$$2\mu_{11}\beta_d\beta_m \coth Q_m = \frac{k^2\mu_{12}^2 - \beta_m^2\mu_{11}^2 - \beta_d^2(\mu_{11}^2 - \mu_{12}^2)^2}{(\mu_{11}^2 - \mu_{12}^2)} . \qquad 3\text{-}26$$

(A similar expression was derived by Bresler[11] in investigating surface

mode propagation at the ferrite-air interfaces of a transversly magnetized slab in an infinite parallel plane waveguide). The solutions of Equation 3-26 are symmetrical about the k=0 axis leading to

$$\left.\frac{R_z}{A_z}\right|_{s=+1} = \cosh Q_m - \left[\frac{|k|\mu_{12} - (\mu_{11}^2 - \mu_{12}^2)\beta_d}{\beta_m \mu_{11}}\right] \sinh Q_m , \qquad 3\text{-}27$$

for a forward traveling mode, and

$$\left.\frac{R_z}{A_z}\right|_{s=-1} = \cosh Q_m + \left[\frac{|k|\mu_{12} + (\mu_{11}^2 - \mu_{12}^2)\beta_d}{\beta_m \mu_{11}}\right] \sinh Q_m , \qquad 3\text{-}28$$

for reverse traveling modes. Multiplying Equation 3-27 by Equation 3-28 one obtains

$$\left.\frac{R_z}{A_z}\right|_{s=+1} \times \left.\frac{R_z}{A_z}\right|_{s=-1} = \cosh^2 Q_m - \left[\frac{k^2\mu_{12}^2 - (\mu_{11}^2 - \mu_{12}^2)^2\beta_d^2}{\beta_m^2 \mu_{11}^2}\right] \sinh^2 Q_m + 2\left[\frac{(\mu_{11}^2 - \mu_{12}^2)\beta_d}{\beta_m \mu_{11}}\right] \sinh Q_m \cosh Q_m . \qquad 3\text{-}29$$

The second term on the right-hand side of Equation 3-29 may be reexpressed, using Equation 3-26, as

$$\left[\frac{k^2\mu_{12}^2 - (\mu_{11}^2 - \mu_{12}^2)^2\beta_d^2}{\mu_{11}^2 \beta_m^2}\right] \sinh^2 Q_m = \left[\frac{2\mu_{11}(\mu_{11}^2 - \mu_{12}^2)\beta_d \beta_m \coth Q_m + \mu_{11}^2\beta_m^2}{\mu_{11}^2 \beta_m^2}\right] \sinh^2 Q_m . \qquad 3\text{-}30$$

Noting that

$$\cosh^2 Q_m - \sinh^2 Q_m = 1 , \qquad 3\text{-}31$$

Equation 3-29 may be expressed as

$$\left.\frac{R_z}{A_z}\right|_{s=+1} \times \left.\frac{R_z}{A_z}\right|_{s=-1} = 1 - \left[\frac{2\mu_{11}(\mu_{11}^2 - \mu_{12}^2)\beta_d \beta_m \coth Q_m}{\mu_{11}^2 \beta_m^2}\right] \sinh^2 Q_m + 2\left[\frac{(\mu_{11}^2 - \mu_{12}^2)\beta_d}{\mu_{11}\beta_m}\right] \sinh Q_m \cosh Q_m . \qquad 3\text{-}32$$

Equation 3-32 may be simplified to yield

$$\left.\frac{R_z}{A_z}\right|_{s_z+1} \times \left.\frac{R_z}{A_z}\right|_{s_z-1} = 1 \quad , \tag{3-33}$$

for all ferrite thicknesses as anticipated for this special case.

For thick ferrites such that

$$\beta_m \coth Q_m \cong |\beta_m| \, , \tag{3-34}$$

Equation 3-17, which includes electromagnetic propagation effects, reduces to

$$(k^2\mu_{12}^2 - \beta_m\mu_{11}^2) + [k\mu_{12}(\beta_{d2}-\beta_{d1}) - \beta_m\mu_{11}(\beta_{d1}+\beta_{d2})](\mu_{11}^2-\mu_{12}^2) - \beta_{d1}\beta_{d2}(\mu_{11}^2-\mu_{12}^2)^2 = 0 \tag{3-35}$$

This equation may be factored to yield

$$[(\mu_{11}^2-\mu_{12}^2)\beta_{d2} + k\mu_{12} + \beta_m\mu_{11}][(\mu_{11}^2-\mu_{12}^2)\beta_{d1} - k\mu_{12} + \beta_m\mu_{11}] = 0 \tag{3-36}$$

The second term of Equation 3-36 is recognized as the dispersion relationship describing surface wave propagation along a ferrite-dielectric interface where both media are semi-infinite,

$$\beta_{d1} = \left[\frac{k\mu_{12} - \beta_m\mu_{11}}{(\mu_{11}^2-\mu_{12}^2)}\right] \, , \tag{3-37}$$

this equation differing from Equation 2-93 only in the form of the subscript of dielectric medium transverse wavenumber. Since the present derivation has proceeded by considering a ferrite of finite thickness, Equation 3-36 indicates a second set of modes,

$$\beta_{d2} = -\left[\frac{k\mu_{12} + \beta_m\mu_{11}}{(\mu_{11}^2-\mu_{12}^2)}\right] \tag{3-38}$$

The mode set represented by Equation 3-37 corresponds to surface modes for the semi-infinite model with the ferrite occupying the lower half-space and dielectric #1 occupying the upper half-space; the mode set represented by Equation 3-38 describes surface wave propagation for the semi-infinite model where the lower half-space is occupied by dielectric#2. Significantly, the direction of propagation of the modes at the top and bottom faces of the ferrite is reversed.

Thus, in the thick film limit it has been found that the ferrite may support at least two and possibly four propagating surface modes for any one combination of material parameters. Of the modes associated with the top surface, the forward mode is "magnetostatic" and is labled $s=+1_m$, while the second mode, if it exists, is a "dynamic" mode whose direction of propagation depends on the relative permittivities of the media. Similarly, the modes associated with the bottom face of the slab are a reverse "magnetostatic" mode, $s=-1_m$, and possibly a forward or reverse dynamic mode.

To determine the effects of the finite film thickness on these modes, Equations 3-4, 3-8, 2-95, 3-16 and 3-17 must be solved. However, a great reduction in complexity may be achieved without sacrificing the essential details of the mode behavior if the symmetrical case, in which both dielectric media have the same parameters, is considered instead. For the symmetrical case Equations 3-26, 2-94, 2-95, and 3-16 are applicable. The process of solving these equations is further simplified by noting that the dispersion relationships are symmetrical in k and β_m. In addition, the mode amplitude relations are also symmetrical

in β_m. Thus, having neglected losses and having confined the search to modes exhibiting surface wave characteristics, only those solutions corresponding to positive real values of β_m need be considered.

Squaring both sides of Equation 3-26 and substituting Equations 2-94 and 2-95 into the resultant expression, an equation in one variable, β_m, is obtained as

$$\beta_m^4\left\{4\mu_{11}^2\coth^2 Q_m-\left[1+(\mu_{11}^2-\mu_{12}^2)\right]^2\right\}$$
$$+\beta_m^2\left\{4\mu_{11}^2\left(D_k-\frac{\omega^2}{c_d^2}\right)\coth^2 Q_m+2\left[1+(\mu_{11}^2-\mu_{12}^2)\right]\left[D_k\left(\frac{\mu_{12}^2}{\mu_{11}^2-\mu_{12}^2}-\mu_{11}^2+\mu_{12}^2\right)+\frac{\omega^2}{c_d^2}(\mu_{11}^2-\mu_{12}^2)\right]\right\}$$
$$+\left\{D_k\left[\frac{\mu_{12}^2}{(\mu_{11}^2-\mu_{12}^2)}-(\mu_{11}^2-\mu_{12}^2)\right]+\frac{\omega^2}{c_d^2}(\mu_{11}^2-\mu_{12}^2)\right\}^2=0, \qquad 3\text{-}39$$

In the thick ferrite limit, $Q_m\to\infty$, and Equation 3-39 reduces to

$$\beta_m^4\left\{4\mu_{11}^2-\left[1+(\mu_{11}^2-\mu_{12}^2)\right]^2\right\}$$
$$+\beta_m^2\left\{4\mu_{11}^2\left(D_k-\frac{\omega^2}{c_d^2}\right)+2\left[1+(\mu_{11}^2-\mu_{12}^2)\right]\left[\frac{D_k\mu_{12}^2}{(\mu_{11}^2-\mu_{12}^2)}-\left(D_k-\frac{\omega^2}{c_d^2}\right)(\mu_{11}^2-\mu_{12}^2)\right]\right\}$$
$$+\left[D_k\frac{\mu_{12}^2}{(\mu_{11}^2-\mu_{12}^2)}-\left(D_k-\frac{\omega^2}{c_d^2}\right)(\mu_{11}^2-\mu_{12}^2)\right]^2=0 \qquad 3\text{-}40$$

This equation is biquadratic in β_m and has at most two roots on the positive real β_m axis. This upper limit also applies in the case where the ferrite is of finite thickness.

A flow chart illustrating the major steps in the numerical evaluation of Equation 3-39 is shown in Figure 3-4. The technique employed involves the division of the positive β_m axis into a number of segments. Proceeding along the axis, the end points of each successive interval are substituted into a trial function consisting of the left hand side of Equation 3-39. In general, the value of this trial function is positive or negative, the function having a zero only at

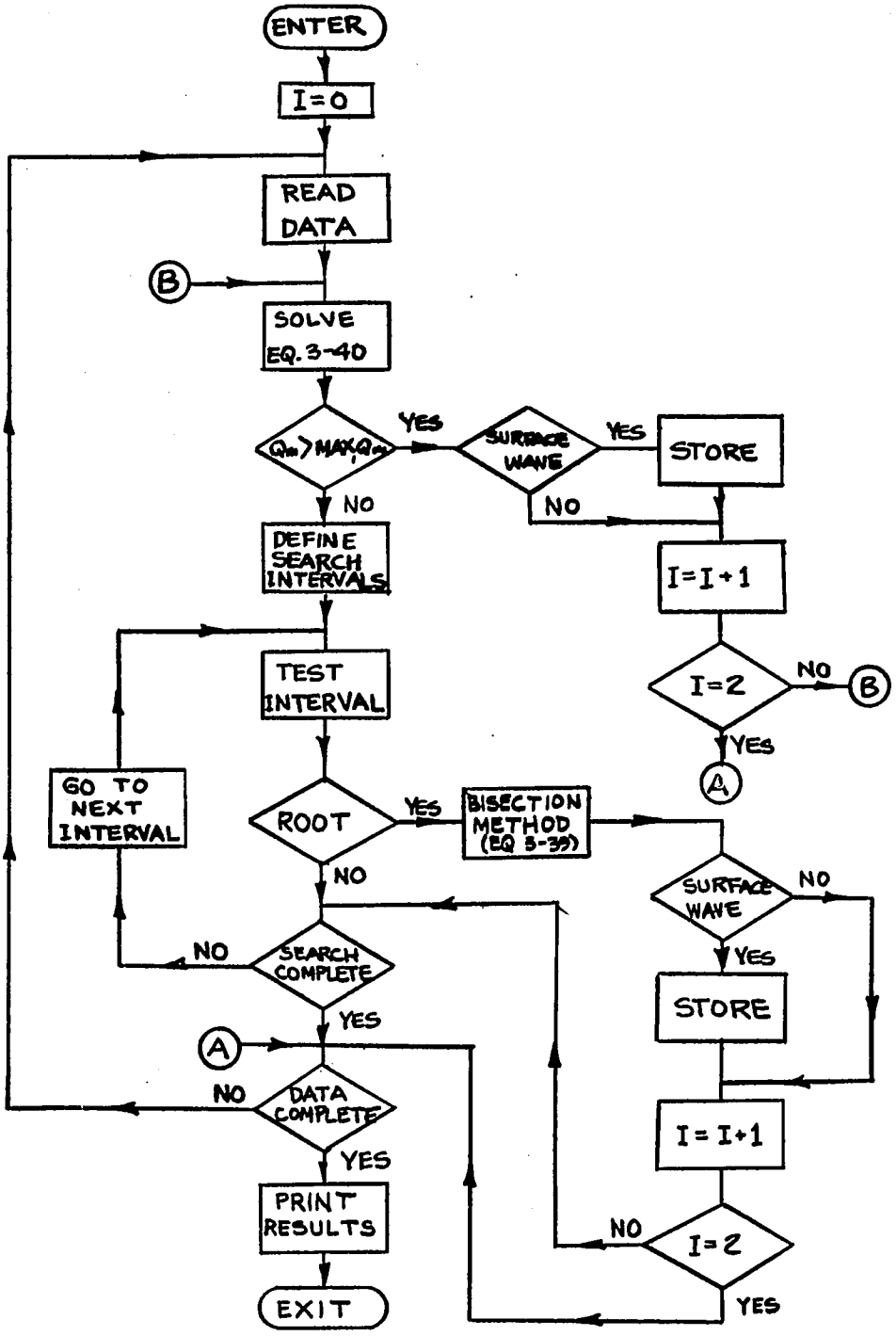

Figure 3-4 - Flow Chart for Numerical Evaluation of Finite Ferrite Surface Wave Characteristics

points corresponding to roots of Equation 3-39. If there is a difference in sign between the end point trial functions, a root of the equation lies within the interval. If there is no change of sign, the interval contains either no roots or two roots. This latter case may be avoided by choosing intervals sufficiently small. Upon locating a segment of the positive real β_m axis containing one root, the region is searched using the Bisection Method[72]. Refinement of the root, through successive halving of the interval being searched, continues until the magnitude of the trial function is less than some test value or a maximum number of bisections has been exceeded, both limits chosen in conformity with the precision and accuracy of the calculation.

Selection of the intervals to be searched is based upon solutions of Equation 3-40, the thick ferrite limit equation. An upper and lower limit of the search area is established by determining the maximum and minimum values that the argument of the hyperbolic cotangent may attain without causing an overflow or exceeding the maximum argument permitted. This search region may be subdivided further if the positive β_m solutions of Equation 3-40 fall within its limits. If, however, a β_m solution of Equation 3-40 is such that Q_m exceeds the maximum argument value, this solution is considered to be a solution of Equation 3-39 as well.

Having divided the search region into at most three subsections through the use of the thick ferrite solutions, each subsection is further subdivided into smaller intervals for trial function analysis. These intervals are not of equal size, the increments being varied so that the search is most intensive in those portions of the positive β_m axis neighboring the roots of Equa-

tion 3-40.

When a root of Equation 3-39 is located it is tested to determine if it corresponds to a propagating surface wave (i.e. k is real and β_d is positive). If the solution is a surface mode the longitudinal and transverse wavenumbers are stored for subsequent print out. In addition, since the solutions obtained are symmetrical about the k=0 axis, R_z/A_z is computed for both the forward and reverse propagating solutions to determine the surface with which they are associated. This process is repeated until all of the data points have been processed.

The dispersion relationship has been solved using the same material and field parameters as in Figure 3-2. The results of the numerical evaluation are plotted in Figure 3-5 for the cases a=.5mm, and a=1mm. The ferrite is bordered at its top and bottom surfaces by free space. The graph axes have been normalized with respect to the ferrite material parameters; i.e. the vertical axis being $\Omega = \frac{\omega}{\omega_m}$, the horizontal axis being the absolute value of the normalized wavenumber $|\xi| = \left|\frac{kc_m}{\omega_m}\right|$, no distinction being made to the direction of propagation because of the symmetry about k=0. The dispersion characteristics for the infinite film case are also included.

Comparing the wavenumbers of the "dynamic" modes shown in Figure 3-5, it is observed that the magnitude of the wavenumbers is reduced by decreasing the thickness of the film. In fact, for this thickness (.5mm) the magnitude of the phase velocity of these long wavelength modes is only slightly less than the intrinsic velocity in the free space regions. In contrast, the

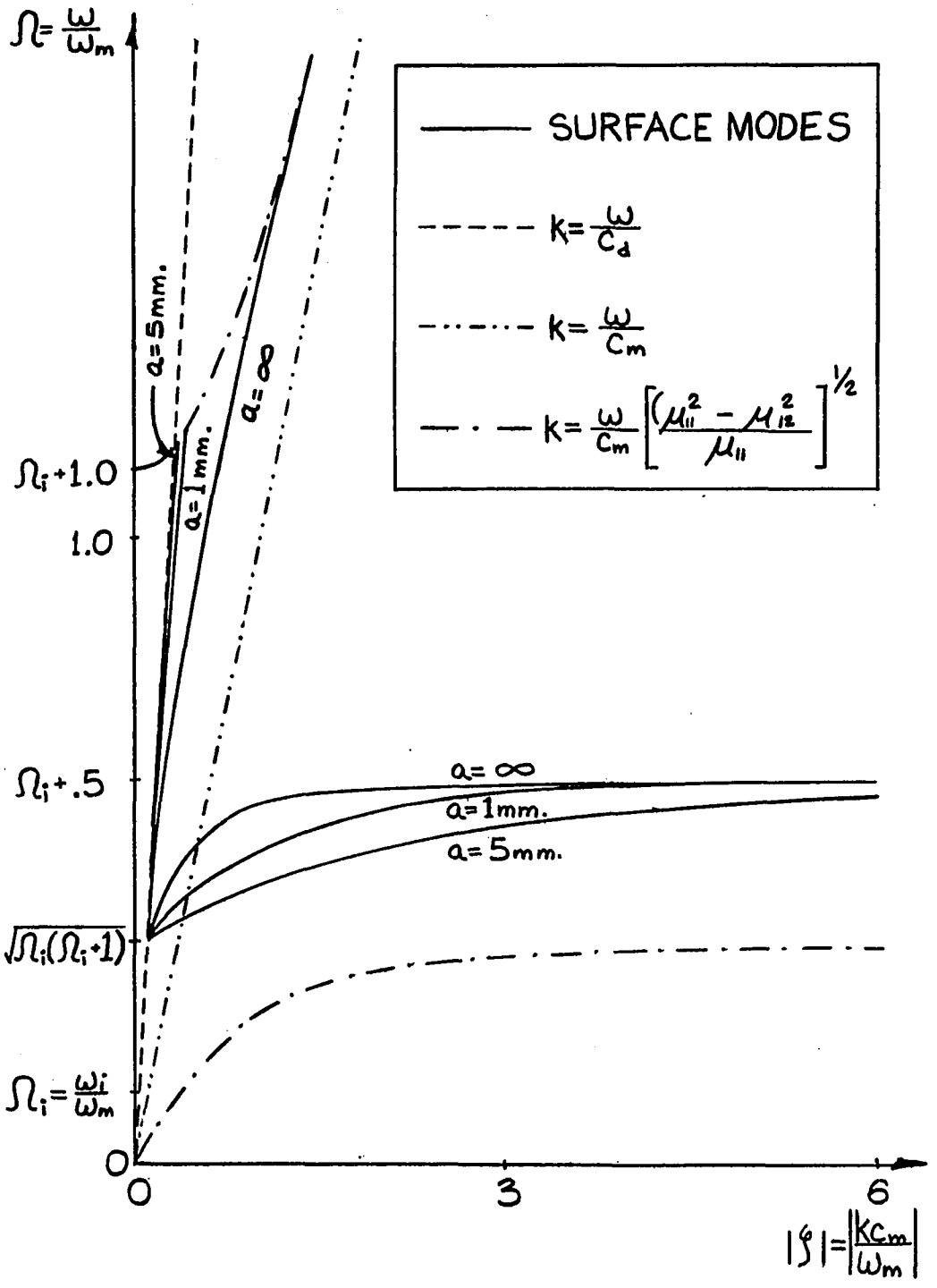

Figure 3-5 Electromagnetic Surface Wave Dispersion For A Ferrite Slab

"magnetostatic" modes suffer a decrease in wavelength over most of their spectrum due to the finite geometry. As either the lower cutoff or resonance frequency is approached, the transverse wavenumber β_m increases, concentrating the energy carried by a "magnetostatic" mode in the vicinity of one of the surfaces as shown in Figure 3-6. In these regions, the mode is less dependent on the thickness of the ferrite and approaches the infinite ferrite results.

Examination of Equation 3-16 in both the magnetostatic and thick ferrite limits indicates that a "magnetostatic" surface wave propagating in the forward direction is associated with the top face while a reverse "magnetostatic" mode is associated with the bottom surface. A check of Figure 3-6 confirms these results for a ferrite of finite thickness with electromagnetic propagation included.

In Figure 3-7 the energy density of a surface wave at the x=-a surface relative to its energy density at the bottom surface is plotted for the "dynamic" as well as the "magnetostatic" modes of Figure 3-5. In agreement with the thick ferrite results for $\epsilon_d < \epsilon_m$, the top surface supports a "dynamic" mode propagating in the reverse direction ($s=-\hat{1}_d$), while "dynamic" mode propagation at the bottom surface is in the forward direction ($s=+\hat{1}_d$).

The thick ferrite results indicate that dynamic modes do not exist if the dielectric media have permittivities such that $\epsilon_m < \epsilon_d < \epsilon_m \frac{(\omega_i + \omega_m)}{\omega_i}$. To verify that this phenomenon is observed when a ferrite of finite thickness is considered, the surface mode characteristics of a .5mm ferrite slab with symmetrical dielectric loading are calculated. The ferrite parameters remain

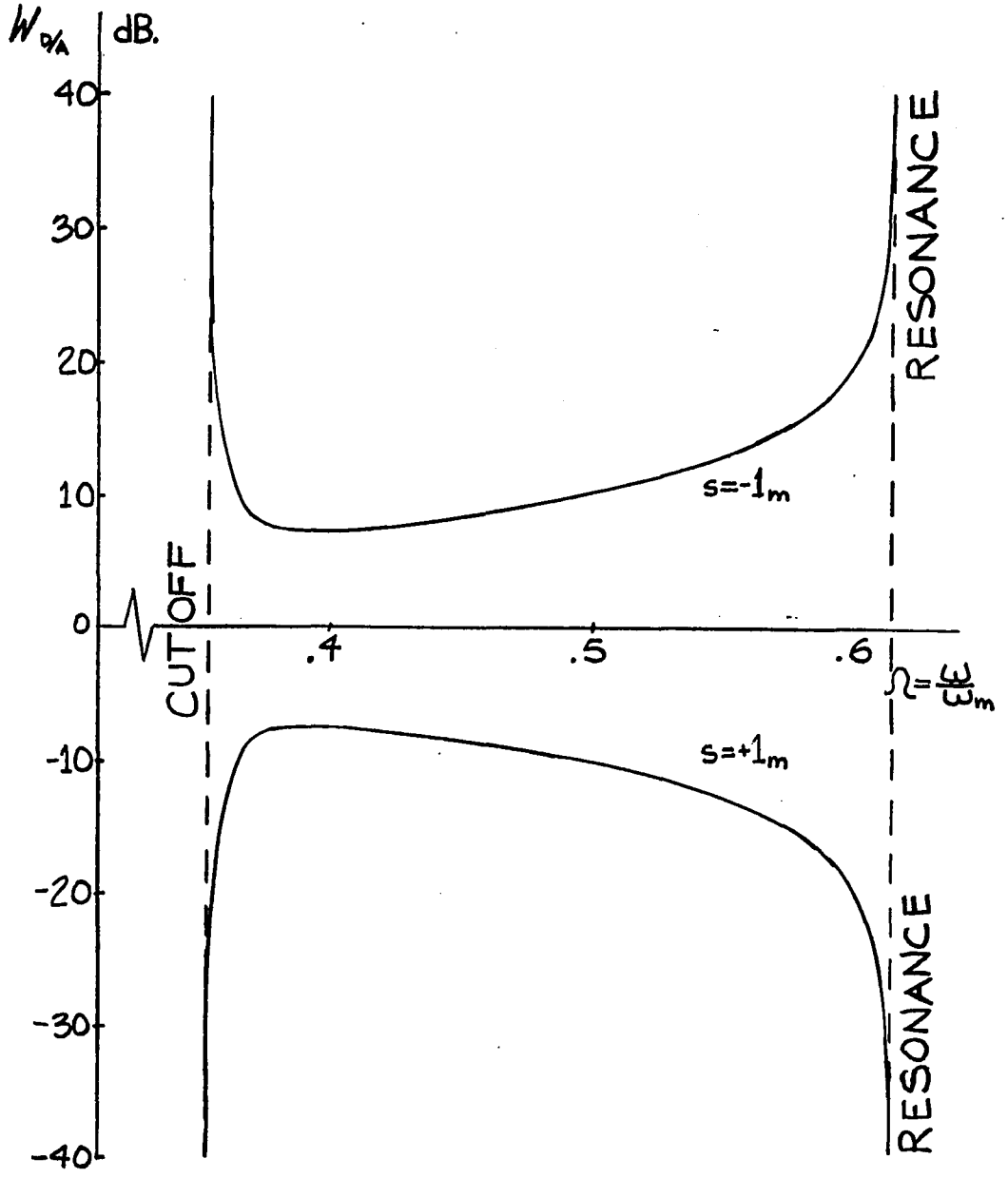

Figure 3-6 Relative Energy Density - Bottom/Top for "Magnetostic" Mode Including the Effects of Propagation, a=. 5mm.

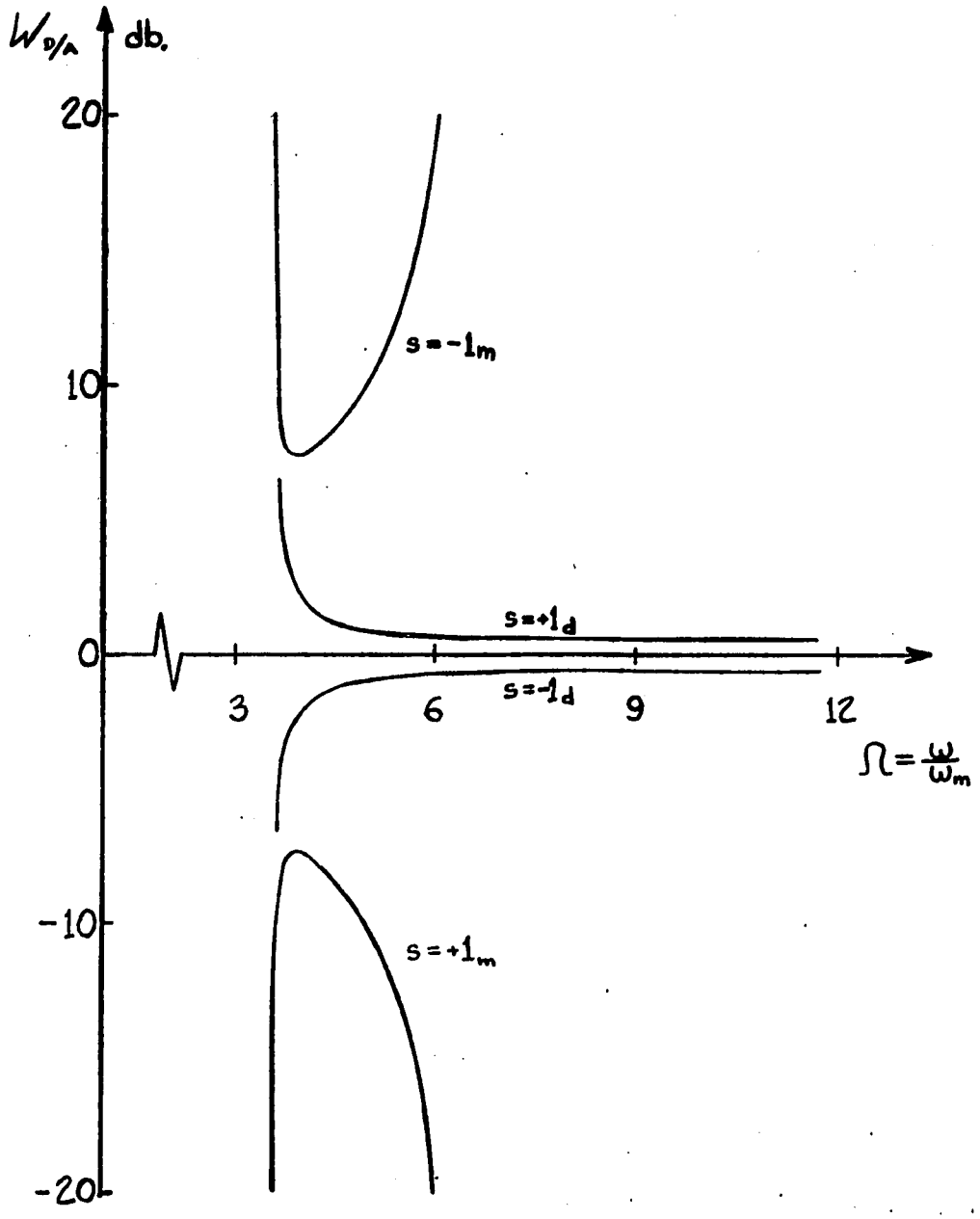

Figure 3-7 - Relative Energy Density - Bottom/Top of Surface Electromagnetic Modes of a Ferrite Slab; a=.5mm.

the same as above, while the dielectric permittivity is chosen to be $\epsilon_d = 21$. The resultant dispersion characteristics are plotted in Figure 3-8. In agreement with the thick ferrite results, only the "magnetostatic" modes exist for this set of parameters. If the dielectric permittivity is increased still further, beyond $\epsilon_m \frac{(\omega_i + \omega_m)}{\omega_i}$, it is expected from the semi-infinite results, that dynamic modes will again propagate along the ferrite surface. This is verified by the dispersion characteristics plotted in Figure 3-9, for $\epsilon_d = 210$. Now, however, the "dynamic" mode associated with the top surface is a forward mode ($s=+1_d$). The dynamic mode at the bottom surface propagates in the reverse direction. The cases shown in the last two figures are of particular interest because the surface modes associated with a particular face propagate in only one direction. This direction is such that the vector $\bar{k} \times \bar{H}_i$ coincides with the outward directed normal.

While Figures 3-5 through 3-9 have been plotted for surface waves on symmetrically loaded slabs, it is clear that if the conditions existing at the bottom face of the ferrite are modified, the modes associated with the bottom face would be more strongly affected than those associated with the top face. Not only would the modification of the environment alter the relative amplitudes of the modes at the two surfaces, it would, as the linear term in Equation 3-16 indicates, also destroy the symmetry of propagation characteristics at the upper and lower ferrite surfaces. An extreme example of this occurs when the r.f. electric field at the bottom face of the ferrite is set to zero by placing this surface in contact with a perfect conductor as in Section 3.2.

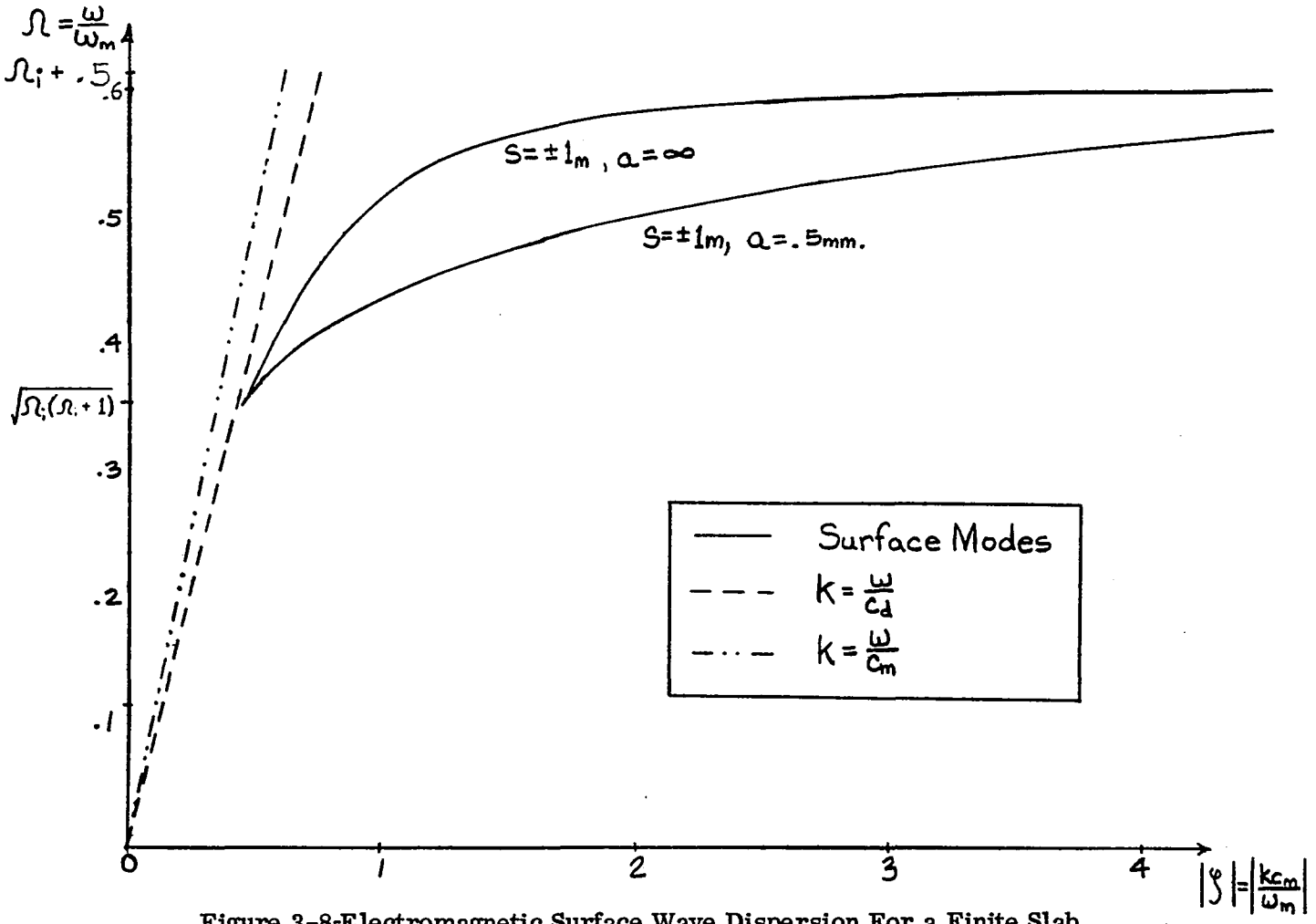

Figure 3-8-Electromagnetic Surface Wave Dispersion For a Finite Slab With Moderate Dielectric Loading

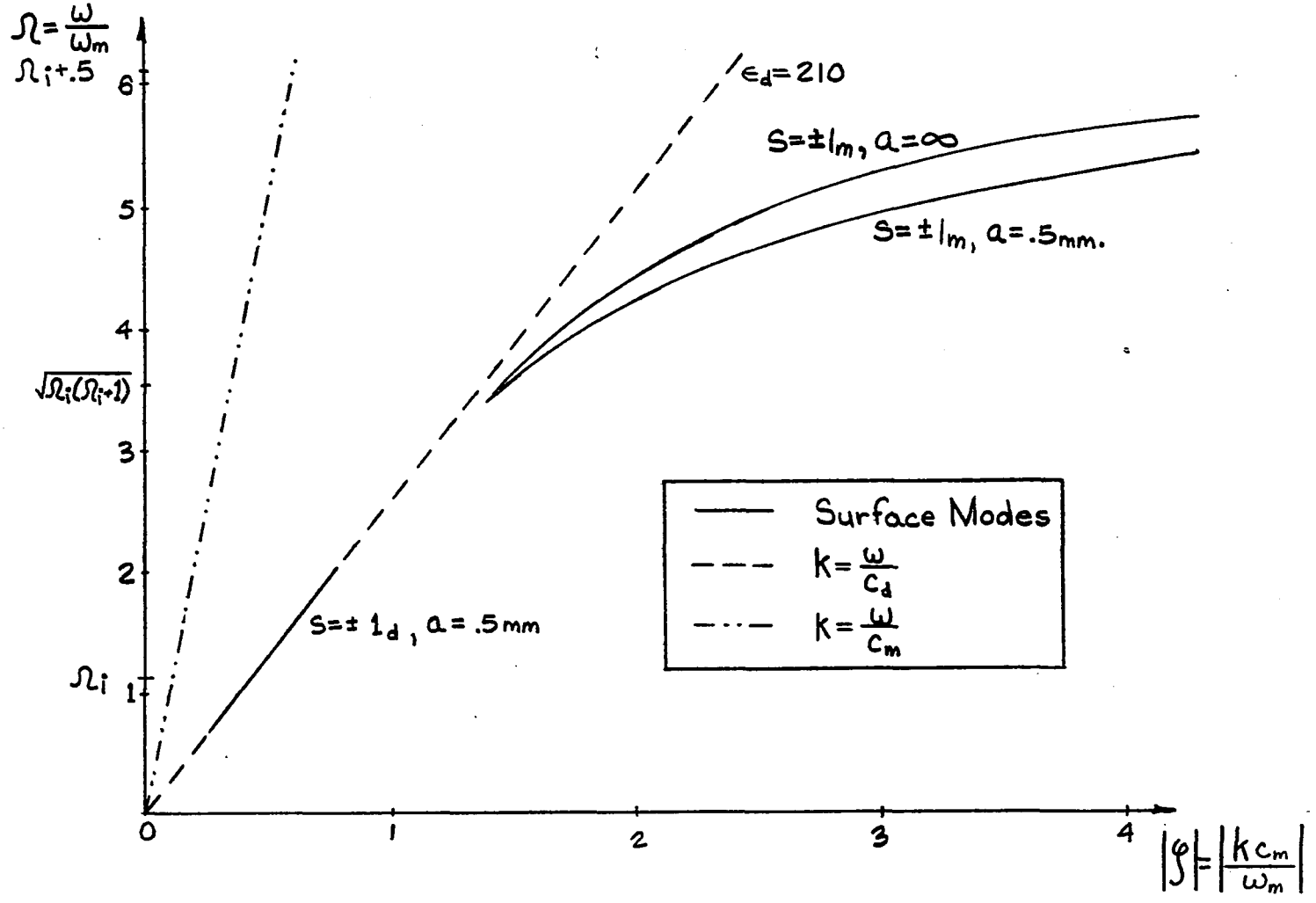

Figure 3-9 Electromagnetic Surface Wave Dispersion For A Ferrite Slab, Large Dielectric Constant Case.

3.2 Electromagnetic Surface Wave Propagation On A Grounded Ferrite Slab

The surface electromagnetic modes of a planar slab of single crystal ferrite material, grounded on one side by a perfect conductor, are investigated. The slab is of thickness a meters, and has a boundary at $x=-0$ with a uniform dielectric of semi-infinite extent. The ferrite, shown in Figure 3-10, is assumed to be infinite in extent in the $\hat{y}$ and $\hat{z}$ directions. A static magnetic field is applied parallel to the $\hat{z}$ axis resulting in a magnetic field intensity, H_i, assumed to be uniform within the ferrite.

The analysis of the ferrite slab terminated in a ground plane at $x=-a$ proceeds in a similar manner to that performed in Section 3.1. The r.f. electric field in the dielectric has exponential dependence of the form

$$E_{dz} = A_z \exp[-\beta_d x + j(\omega t - ky)] \; ; \qquad 2\text{-}41$$

the r.f. field in the ferrite may be expressed as,

$$E_{1mz} = [G \cosh \beta_m x + L \sinh \beta_m x] \exp[j(\omega t - ky)] \qquad 3\text{-}9$$

Since the boundary condition at the ferrite-metal interface requires that E_{1mz} be zero there, the r.f. electric field within the ferrite assumes the form

$$E_{1mz} = G[\cosh \beta_m x + \coth Q_m \sinh \beta_m x] \exp[j(\omega t - ky)]. \qquad 3\text{-}41$$

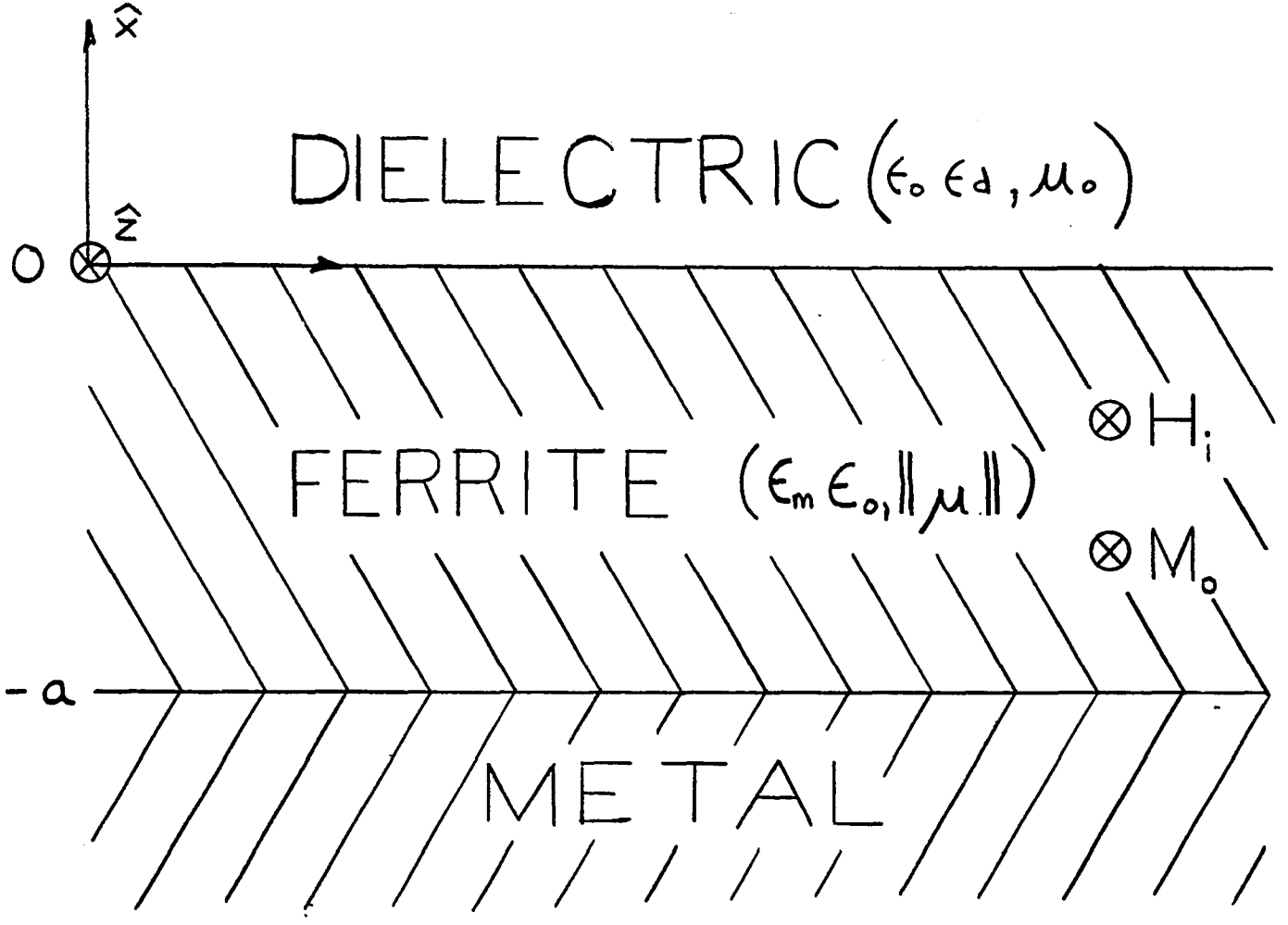

Figure 3-10 - Grounded Ferrite Model

Maxwell's equations are utilized to obtain expressions for the r.f. magnetic field intensities and the dispersion equations relating the longitudinal and transverse wavenumbers in each medium. The third equation, relating the transverse wavenumbers in the dielectric and ferromagnetic media is obtained by applying the boundary conditions on the tangential r.f. electric and magnetic field components at the $x = 0$ interface. The resultant equations are

$$k^2 - \beta_d^2 = \frac{\omega^2}{c_d^2} , \qquad 2\text{-}94$$

$$k^2 - \beta_m^2 = \frac{\omega^2}{c_m^2} \frac{(\mu_{11}^2 - \mu_{12}^2)}{\mu_{11}} \qquad 2\text{-}95$$

and

$$\beta_d = \frac{k\mu_{12} - \beta_m \mu_{11} \coth Q_m}{(\mu_{11}^2 - \mu_{12}^2)} . \qquad 3\text{-}42$$

Similar equations, with $c_d = c_o$, were obtained by Lax and Button[73,74] for a grounded ferrite slab bounded by free space. They found that the structure supports a forward propagating surface mode, termed the "ferrite-dielectric" mode. Bresler[11] in considering wave propagation along the ungrounded surface of a ferrite slab, situated at the bottom of a metallic trough, found that a grounded ferrite slab supports a reverse as well as a forward propagating mode. (Since $\frac{\partial}{\partial z} = 0$ for the lowest order mode, the presence of the metallic side walls in Bresler's work does not effect the propagation characteristics.) Forward and reverse propagation at the surface of

a grounded ferrite slab has also been investigated in the magnetostatic regime by Young[9] and Seshadri[7]. While Seshadri considered a model similar to that of Lax and Button, Young considered higher order modes in the trough configuration. This trough configuration can be thought of as a ferrite loaded waveguide with one wall of the guide removed to infinity. In fact, the equations for the lowest order TE mode in a rectangular waveguide with a ferrite slab placed across its short dimension, a configuration studied by Kales et. al.,[75] Lax et. al.[76] and Seidel and Fletcher,[77] may be transformed into equations of the form obtained by Lax and Button and Bresler. Similarly, the equations obtained by Pauchard et. al.[78] for propagation of electromagnetic surface waves in a metalized ferrite-dielectric sandwich structure, reduce to Equations 2-94, 2-95, and 3-42 for large dielectric thicknesses.

If the grounded ferrite slab of Figure 3-10 is very thick, the metal is far from the dielectric interface; under these conditions the modes associated with this surface have propagation characteristics approaching those of the semi-infinite model. In the limit as $a \longrightarrow \infty$,

$$\beta_m \coth Q_m \longrightarrow |\beta_m|, \qquad 3\text{-}32$$

Equation 3-40 reduces to

$$\beta_d = \frac{k\mu_{12} - \beta_m \mu_{11}}{(\mu_{11}^2 - \mu_{12}^2)}, \qquad 2\text{-}93$$

the dispersion relation for the semi-infinite model, as anticipated.

Examining Equation 3-42 by employing the magnetostatic approximation, one obtains

$$1 = \frac{s\mu_{12} - \mu_{11}\coth|k|a}{(\mu_{11}^2 - \mu_{12}^2)}, \qquad 3\text{-}43$$

which, if losses are neglected, may be shown to be equivalent to the results obtained by Young[9], for $n=0$, and Seshadri[7]. Using the lossless permeability tensor component definitions given by Equations 2-111 and 2-112, Equation 3-43 may be solved for $|k|$ yielding

$$|k| = \frac{1}{2a}\ln\left\{\frac{\omega_m[s\omega - (\omega_i+\omega_m)]}{2\omega^2 + s\omega\omega_m - (\omega_i+\omega_m)(2\omega_i+\omega_m)}\right\} \qquad 3\text{-}44$$

This dispersion relation is plotted in Figure 3-11 for a ferrite thickness of 0.5 mm. The ferrite parameters, internal field and normalization used in the preparation of this figure are the same as used in Figure 3-2. It is observed that the s=+1 mode spectrum extends, as in Figure 3-2, from $\omega = \sqrt{\omega_i(\omega_i+\omega_m)}$ to $\omega = \omega_i + \frac{\omega_m}{2}$ where it is resonant. The s=-1 mode spectrum also has its lower cutoff frequency at $\omega = \sqrt{\omega_i(\omega_i+\omega_m)}$. However, with one side of the ferrite grounded by a perfect conductor, the mode spectrum now extends up to the frequency $\omega = \omega_i + \omega_m$ where it is also resonant. (The situation where the conductor is not perfect has been

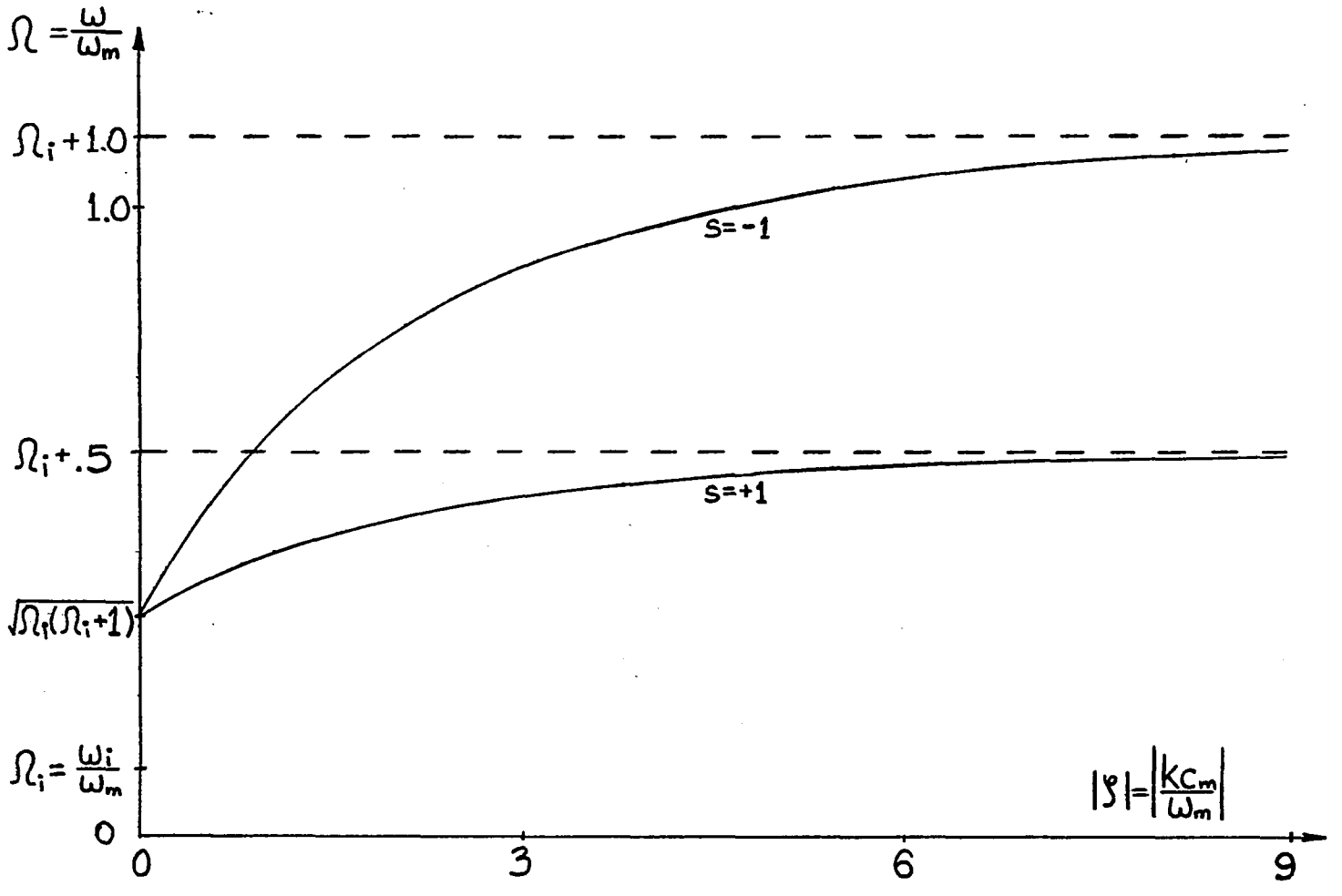

Figure 3-11 - Modes of a Grounded Ferrite Ferrite Slab Found through the Magnetostatic Approximation

treated by DeWames and Wolfram[10] in the magnetostatic limit.) Although Figure 3-11 is only plotted for a ferrite thickness of .5mm., examination of Equation 3-44 reveals that the magnetostatic model predicts that

$$k\left(\omega = \omega_i + \omega_m\right) \rightarrow -\infty \qquad 3\text{-}45$$

regardless of the thickness of the ferrite. This, however, is in direct contradiction to what is predicted in the thick ferrite case, where Equation 2-93 is applicable. Furthermore, the magnetostatic model predicts no surface wave propagation beyond the s=-1 resonant frequency, whereas analysis of the thick ferrite case indicates that surface waves may exist at frequencies greater than $\omega = \omega_i + \omega_m$ for $\epsilon_d < \epsilon_m$. The reason for these discrepancies becomes obvious when it is observed that the magnetostatic approximation predicts that as the thickness of the ferrite is increased, the magnitudes of the surface mode wavenumbers must decrease to maintain a constant $|k|a$ product. As the thickness of the ferrite becomes large, k becomes small, and the conditions assumed in applying the magnetostatic approximation are no longer satisfied. Under these conditions electromagnetic wave propagation may no longer be neglected.

The surface wave dispersion relationship is plotted in Figure 3-12 for ferrite thickness of .5mm., 2mm., 10mm., and 20mm. The ferrite parameters and applied field are unchanged from Figure 3-11. The permittivity of the dielectric region is chosen to be unity corresponding to free space.

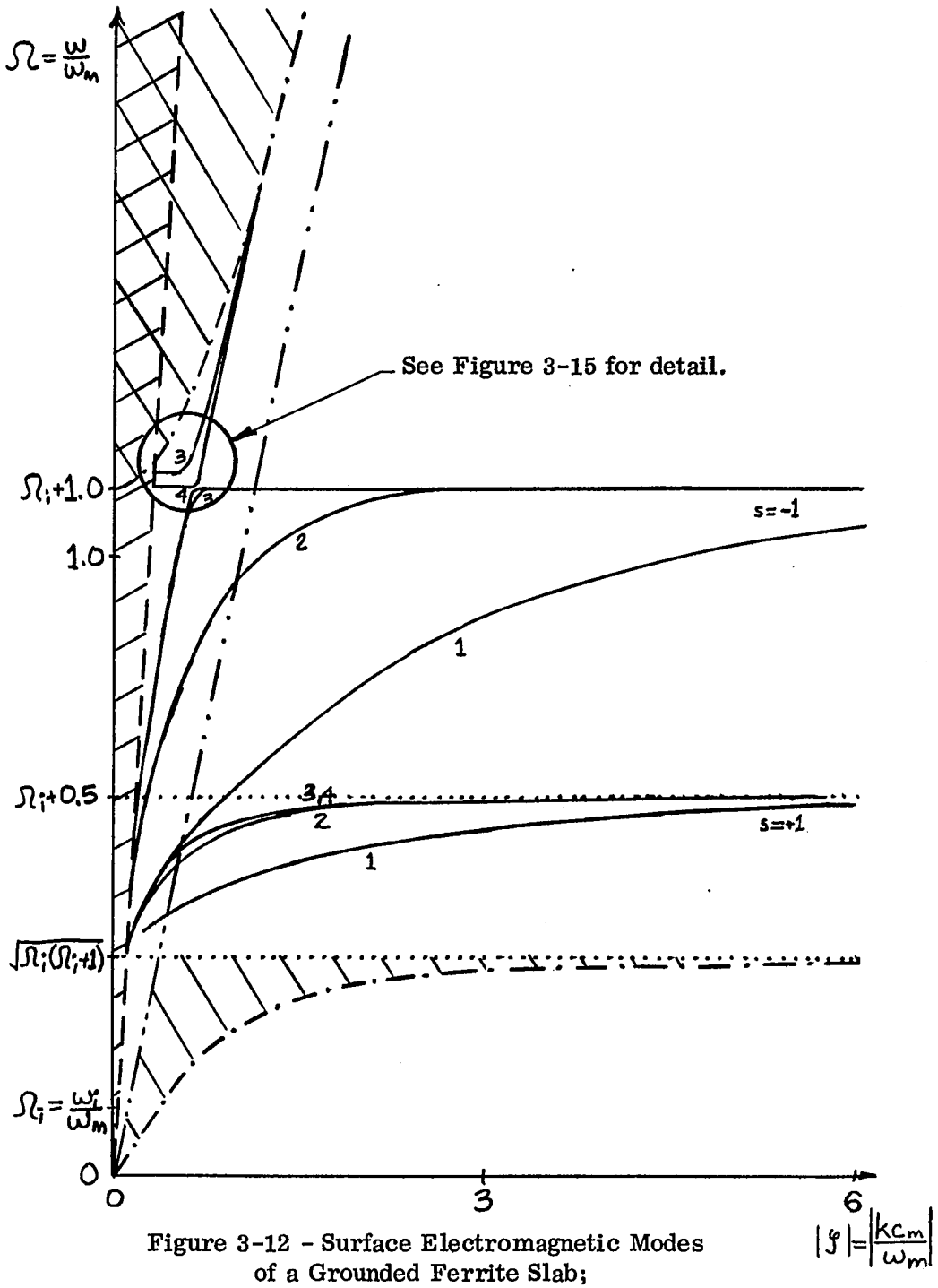

Figure 3-12 - Surface Electromagnetic Modes of a Grounded Ferrite Slab;

1. a= 0.5mm., 2. a= 2mm., 3. a= 10mm., 4. a= 20mm.

Considering first the portion of the spectrum below the s=-1 mode resonance, it is observed that with the exception of the long wavelength region, the dispersion curve for a .5mm. ferrite thickness closely resembles that found by using the magnetostatic approximation, Figure 3-11. As the thickness of the ferrite is increased, the wavenumber at any given frequency decreases, and the dispersion characteristic approaches the characteristics obtained for the thick or semi-infinite case, Figure 2-9, except that the resonance predicted by using the magnetostatic approximation is retained for all finite values of ferrite thickness. Thus, while the semi-infinite model may be appropriate near the lower end of the s=-1 mode spectrum, it is not appropriate near the $\omega = \omega_i + \omega_m$ resonance, even for relatively thick ferrites.

The metamorphosis in the character of the s=-1 mode may be best appreciated by considering the variation of the amplitudes of the r.f. field components across the thickness of the ferrite. The magnetostatic s=-1 mode has been referred to in the literature[8,9] as a "ferrite-metal"[77] mode since the wave is concentrated along the ferrite metal boundary. (It should be noted that the r.f. displacement current is neglected in the magnetostatic approximation, so that only the r.f. magnetic field intensity components are considered). In contrast to the "ferrite-metal" mode the magnetostatic s=+1 mode is termed a "ferrite-dielectric" mode because the wave is concentrated near the ferrite-dielectric boundary. By the preceeding definition both the "magnetostatic" and the "dynamic" modes of the semi-infinite model would be termed "ferrite-dielectric" modes since the magnitudes of the r. f.

electric and magnetic field components decrease exponentially away from the surface. The behavior of the field components of the s=-1 grounded ferrite surface mode is more complex, however. By rewriting Equation 3-41 as

$$E_{1mz} = G' \sinh [\beta_m (x+a)] \exp [j(\omega t - ky)], \qquad 3\text{-}46$$

where

$$G' = \frac{G}{\sinh Q_m}, \qquad 3\text{-}47$$

it is observed that the r.f. electric field has its maximum amplitude at the ferrite-dielectric interface and decreases monotonically to zero at x=-a. Determination of how the amplitudes of the r.f. magnetic field intensity components,

$$|H_{1mx}| = G' \left| \frac{k\mu_{11} \sinh \beta_m (x+a) - \beta_m \mu_{12} \cosh \beta_m (x+a)}{\omega \mu_0 (\mu_{11}^2 - \mu_{12}^2)} \right|, \qquad 3\text{-}48$$

and

$$|H_{1my}| = G' \left| \frac{k\mu_{12} \sinh \beta_m (x+a) - \beta_m \mu_{11} \cosh \beta_m (x+a)}{\omega \mu_0 (\mu_{11}^2 - \mu_{12}^2)} \right| \qquad 3\text{-}49$$

vary over the thickness of the ferrite is much more involved and requires

numerical evaluation. Curves are presented in Figures 3-13 and 3-14 showing the variation of the magnitudes of H_{1mx} and H_{1my}, respectively, across the thickness of the ferrite slab. The curves, which are drawn for five values of frequency, $\omega = \omega_i + 0.3\omega_m$, $\omega = \omega_i + 0.5\omega_m$, $\omega = \omega_i + 0.7\omega_m$, $\omega = \omega_i + 0.9\omega_m$ and $\omega = \omega_i + 0.995\omega_m$, corresponding to $\Omega = 0.4124$, $\Omega = 0.6124$, $\Omega = 0.8124$, $\Omega = 1.0124$ and $\Omega = 1.1074$ on the 10mm. s=-1 curve of Figure 3-12, are normalized with respect to their amplitudes at the ferrite-dielectric boundary. It is observed that near the lower end of the s=-1 mode frequency spectrum, the magnetic field intensity magnitudes are greatest at the ferrite-free-space interface and decrease rapidly towards the interior of the ferrite. In this region of the spectrum, the modes may be classed as "ferrite-dielectric" and the semi-infinite approximation is valid. As the frequency is increased, a transition takes place in which the minimum magnitude point of the magnetic field intensity shifts towards the ferrite-dielectric interface. For frequencies just below the s=-1 "magnetostatic" mode resonance, the wave takes on the appearance of a "ferrite-metal" mode, the magnitudes of the magnetic field intensity components having maxima at the ferrite-metal interface and decreasing monotonically as the ferrite-dielectric interface is approached. It is noted that for thicker ferrites the transition to ferrite-metal mode behavior takes place closer to the resonant frequency, the resonance becoming increasingly sharp

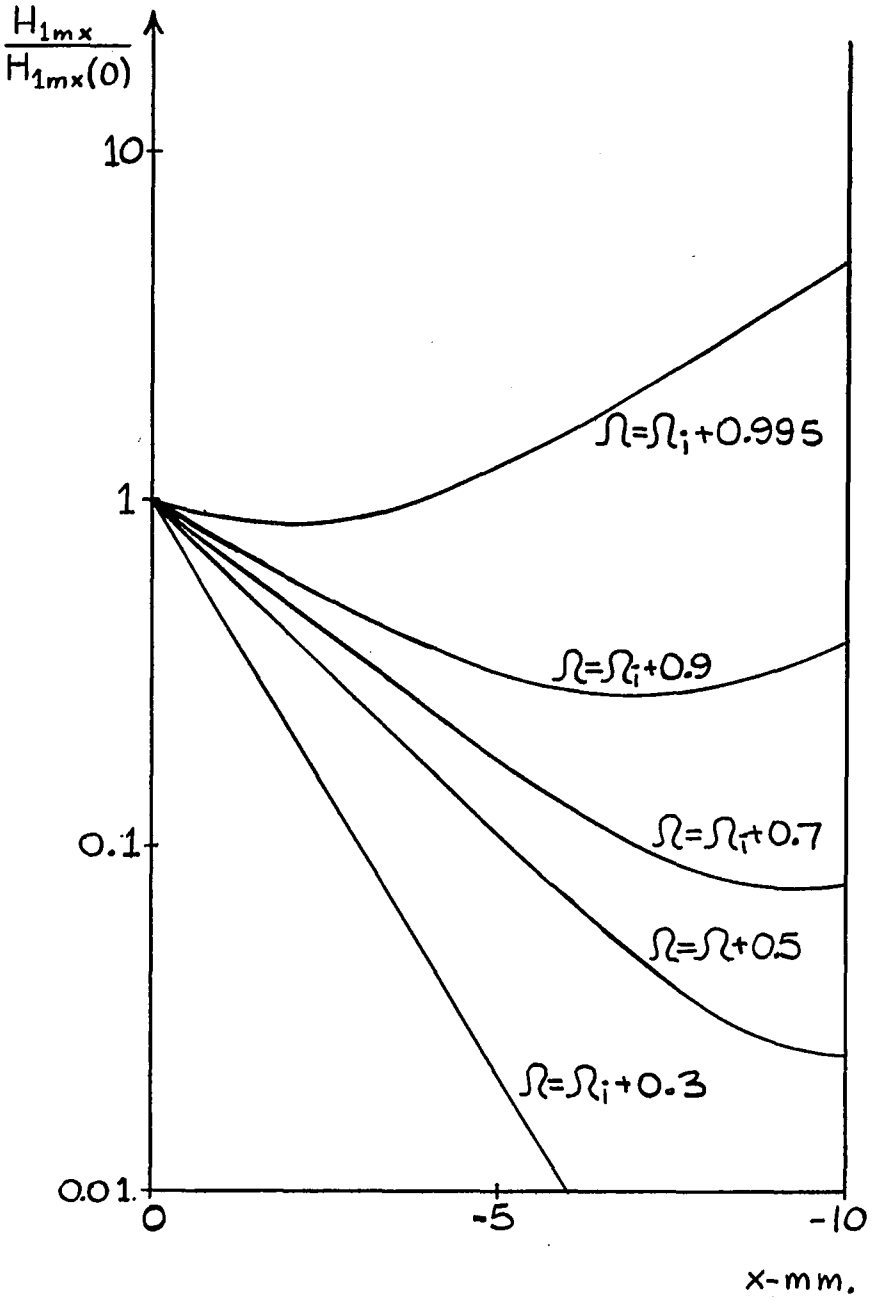

Figure 3-13 - Variation of the Magnitude of H_{1mx} Across The Thickness of 10mm. Grounded Ferrite Slab

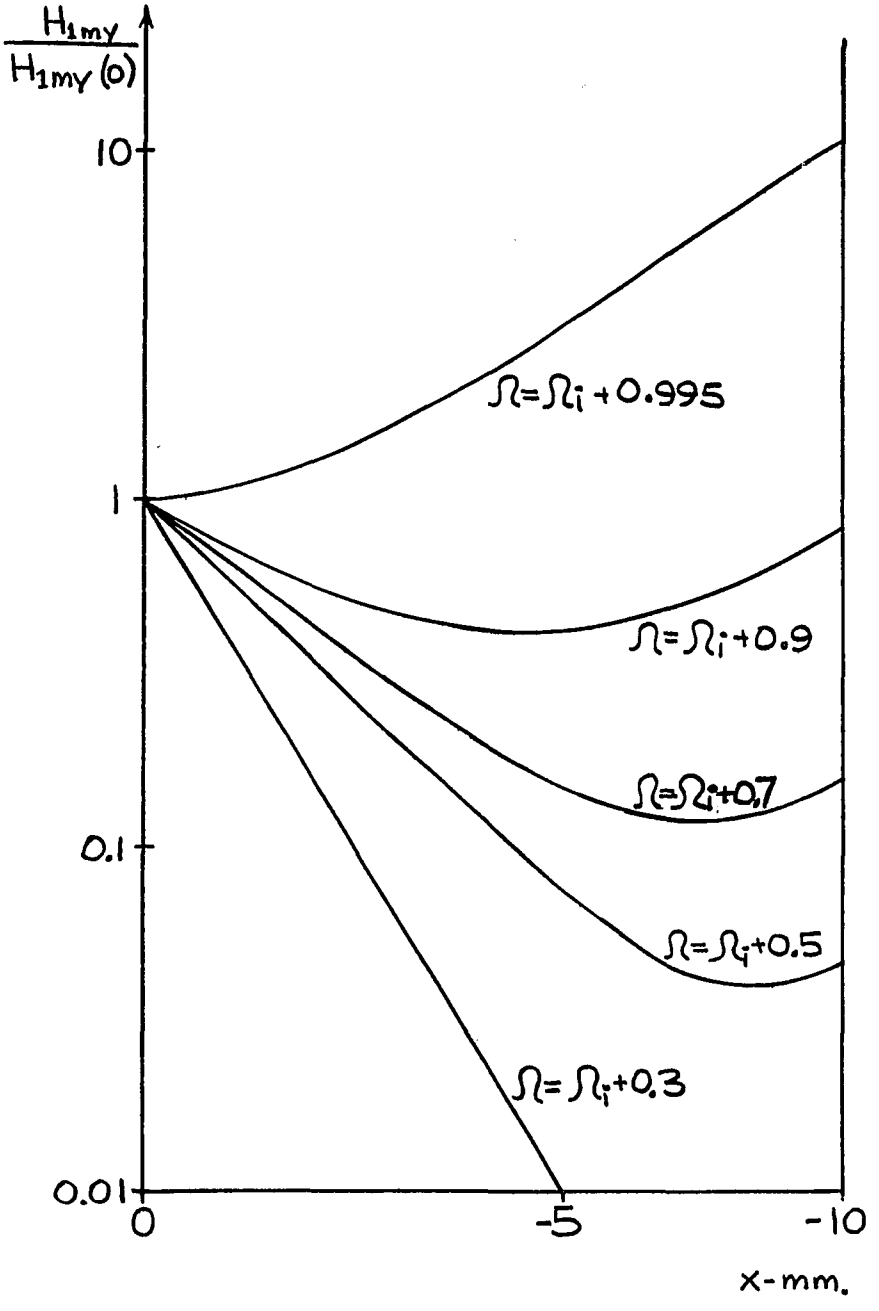

Figure 3-14 - Variation of the Magnitude of H_{1my} Across The Thickness of 10mm. Grounded Ferrite Slab

and thus subject to the deletive effects of ferrite losses.

Immediatedly above the s=-1 mode resonance, there is a frequency range, shown in greater detail in Figure 3-15, for which a surface wave solution does not exist. If the ferrite is sufficiently thick, this cutoff region is of limited extent; the ferrite grounded by a perfect conductor supports surface waves at frequencies greater than the ferrite-metal mode resonance, as illustrated by the upper branches of the 10mm. and 20mm. curves in Figure 3-12. These characteristics are observed to originate at the $\beta_d = 0$ curve and approach the semi-infinite dynamic mode solution as the wavenumber increases. However, the upper frequency limits (where the surface wave characteristic merges with the $\beta_m = 0$ curve) are lower than predicted by the semi-infinite model. Near the upper frequency limits, β_m is small and the fields vary only slightly across the sample's thickness. At the cutoff $(\beta_m = 0)$ the r.f. electric field is zero throughout the ferrite, the conductor, in effect, "shorting out" the surface wave at the opposite surface.

As the thickness of the grounded ferrite decreases, the pass band of the upper branch s=-1 surface mode decreases. As indicated by the 7 and 8mm. curves of Figure 3-15, the mode originates at the $\beta_m = 0$ curve (not at the $\beta_d = 0$ curve) where it couples to the oscillatory modes in the bulk. As the ferrite thickness is further reduced, the upper and lower frequency limits approach one another until, at approximately 6.38 mm., they merge resulting in the disappearance of this portion of the spectrum.

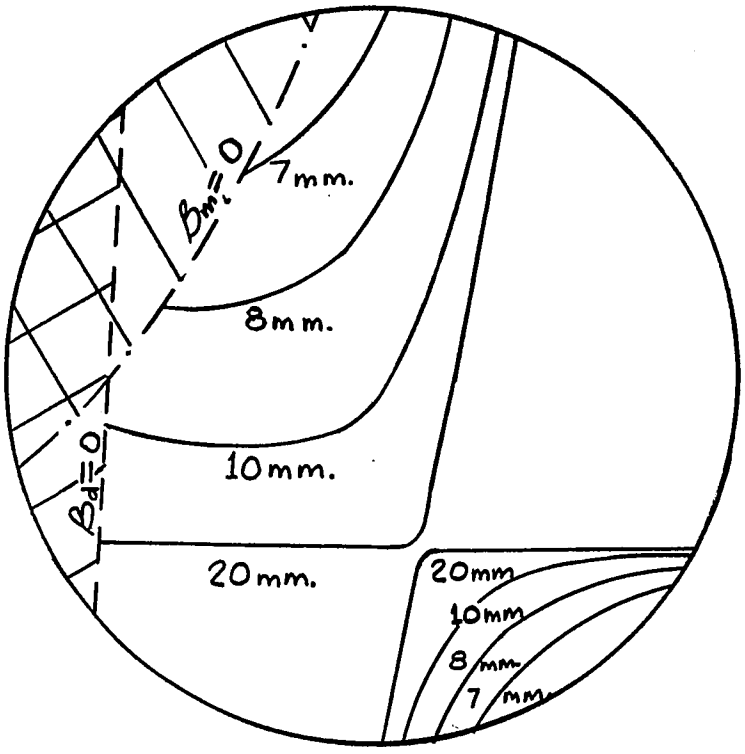

Figure 3-15 - Surface Electromagnetic Modes of a Grounded Ferrite Slab in the Transition Region

On the other hand, as the ferrite thickness increases the range for which the s=-1 mode is cutoff decreases. In the semi-infinite limit the upper and lower branches of the s=-1 mode spectrum coalesce with the result that both the cutoff and the resonance are eliminated.

It has been demonstrated in Sections 2.3, 2.4 and 3.1 that the frequency range of the "dynamic" modes may be altered and their character changed by varying the permittivity of the dielectric region(s) adjacent to the ferrite. It has also been shown that the s=-1 mode of a grounded ferrite has dynamic mode properties at the lower end of its frequency range. Thus it is expected that this portion of the grounded ferrite surface wave spectrum may be significantly modified by varying the permittivity of the dielectric medium. However, in the vicinity of the s=-1 mode resonance frequency, the mode becomes magnetostatic in character. In this region the behavior of the mode is not affected by the permittivity of the dielectric.

The characteristics of the surface waves supported by a .5mm. thick grounded ferrite slab are plotted in Figure 3-16 for various values of dielectric medium permittivity. (The ferrite parameters, internal magnetic field intensity, and normalization remain the same as in the previous figures.) It is observed that in the long wavelength regions of the spectrum, the wavelength of the s=+1 and s=-1 modes decrease as ϵ_d is increased. However, as the respective resonance frequencies are neared the permittivity of the dielectric medium has little effect on the dispersion characteristics. (Vaslow[79] analyzed the behavior of surface waves supported by

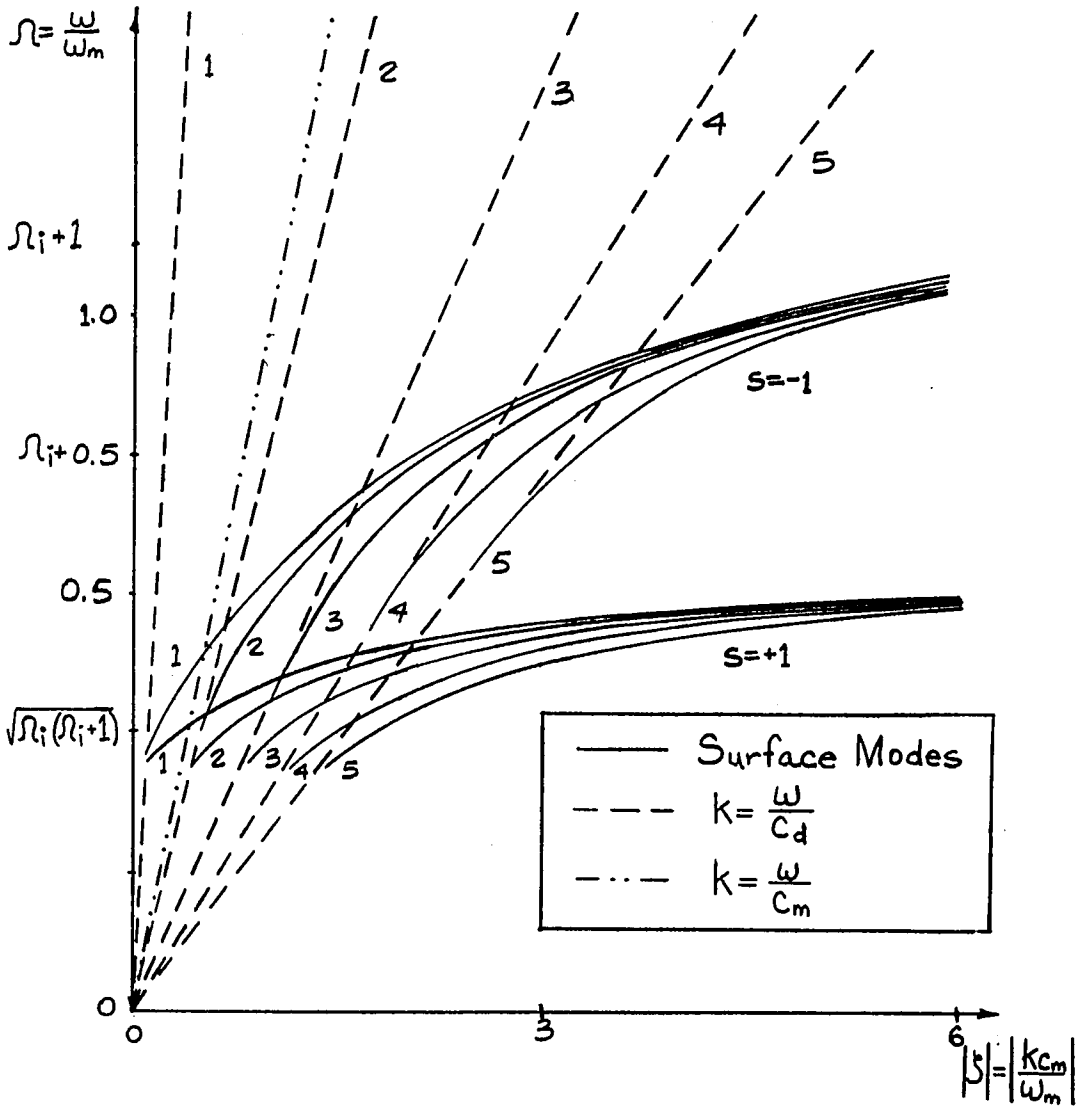

Figure 3-16 - Surface Electromagnetic Modes Of a 0.5mm Grounded Ferrite Slab as a Function of Dielectric Loading. 1. ϵ_d=1, 2. ϵ_d=21, 3. ϵ_d=70, 4. ϵ_d=140, 5. ϵ_d=210

Bongianni's [59] free space-ferrite-dielectric metal configuration. In analogy with the results described above, Vaslow found that the permittivity of the substrate only affects group delay times in the long wavelength region.) Further examination of the s=-1 mode spectra of Figure 3-16 reveals that as the permittivity of the dielectric is increased the lower frequency limit also increases. As can be seen from the figure, it is possible, with the appropriate choice of parameters, for the s=+1 and s=-1 modes of a grounded ferrite slab to propagate in separate non-overlapping frequency ranges. (This occurs when ϵ_d =196.8 for the parameters used in Figure 3-16.) This effect, demonstrated in Figure 3-17 for ϵ_d =210, becomes more pronounced as the distance between the ferrite-dielectric interface and the conductor increases. This important result, which is overlooked in making the magnetostatic approximation, makes it possible to study the s=+1 mode independently of the s=-1 mode. Furthermore, since the s=+1 and s=-1 mode spectra may be made to be non-overlapping, surface mode transmission may be made reflectionless.

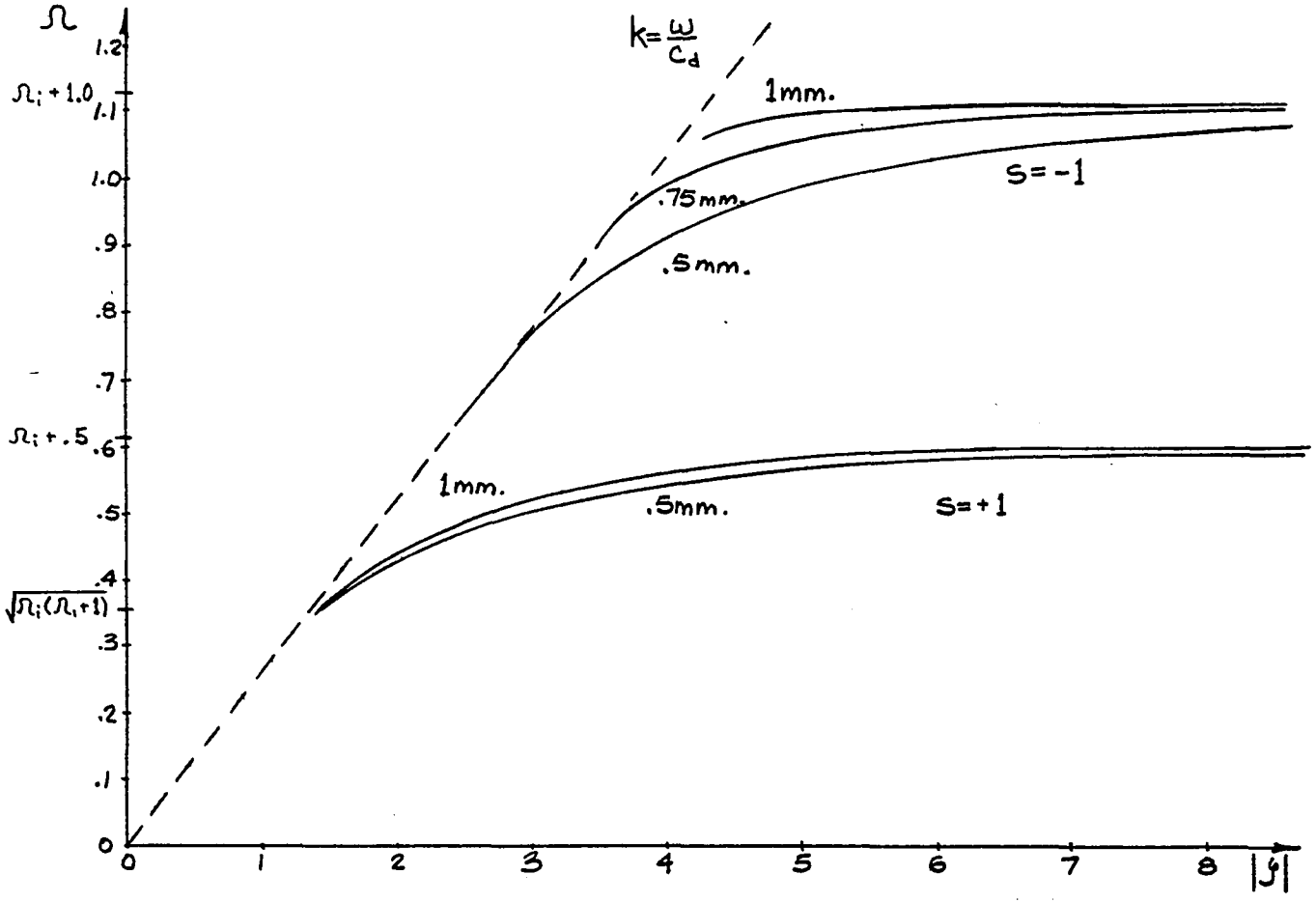

Figure 3-17 - Surface Electromagnetic Modes of a Grounded Ferrite Slab As A Function Of Ferrite Thickness For Large Dielectric Constant Case - ϵ_d=210

3.3 Experimental Results

In 1968 Brundle and Freedman[6] demonstrated the existence of magnetostatic surface waves. Their measurements at 3GHz verified the theoretical predictions of Damon and Eshbach and showed that

A. An insulating ferromagnetic slab could support a mode whose energy was localized at the surface,

B. The wave was localized at the surface where $\bar{k} \times \bar{B}_o$ ($\bar{k} \times \bar{H}_i$) was directed out of the ferrite

and C. The surface wave was a slow wave whose group velocity decreased as the resonance was approached.

The experimental arrangement used by Brundle and Freedman is shown in Figure 3-18. The slab is single crystal Yttrium Iron Garnet magnetized in the plane of its large surface as shown. Signal pulses, 15μsec. in duration, were launched at the input coupler labeled P and were detected at the output coupler Q, after having traveled the length of the slab. The group delay was measured and plotted as a function of the applied static magnetic field. The resultant curve compares favorably with that expected from theory - that is, near the resonance field the group delay increases, since $\frac{\partial \omega}{\partial k}$ becomes small as the resonance is approached. (Brundle and Freedman noted that exact correspondance between calculations based on the group velocity and experimental results cannot be expected because the energy velocity in a highly dispersive structure is not equal to the group velocity).

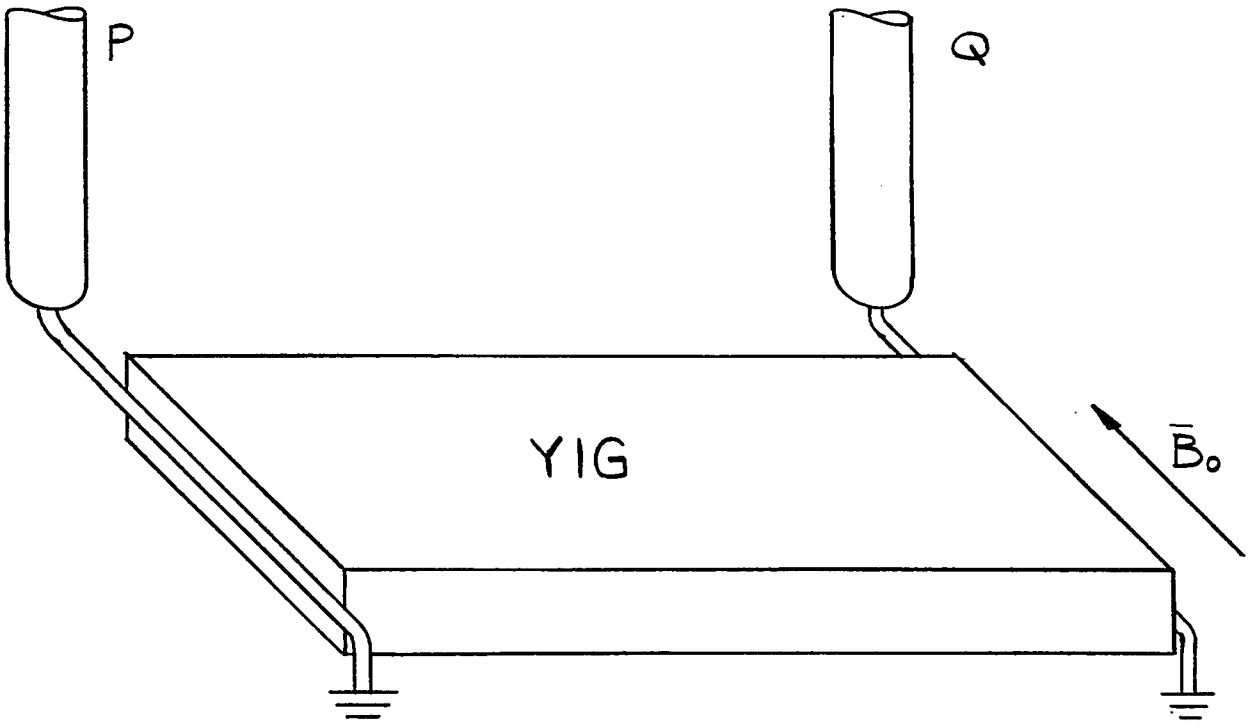

Figure 3-18 - Experimental Arrangement Used By Brundle and Freedman [6]

In seeking to show that the detected signals were surface waves, Brundle and Freedman placed a metal plate against one face (bottom) of the slab. They observed that the delayed signal was unaffected. However, when the metal plate was placed against the opposite (top) face, the delayed signal disappeared completely. It was therefore concluded that the wave depended on the conditions at one face only. Seshadri[7], however, pointed out that the surface wave mode structure is modified when a metal plate is placed in contact with one of the faces of the slab. As shown in Figure 3-12, waves travelling in the forward and reverse directions have different characteristics. If the opposite face of the slab is brought in contact with the metal plate, the directions of propagation of the two modes are interchanged. (This may be verified by substituting $-Q_m$ and $-\beta_d$, respectively, for Q_m and β_d in Equation 3-42). Thus, when the metal plate is in contact with the bottom face of the slab, the "ferrite-dielectric" mode resonant at $\omega = \omega_i + \frac{\omega_m}{2}$ propagates in the $+\hat{y}$ direction; and when the plate is in contact with the other face, the "ferrite-metal" mode, resonant at $\omega = \omega_i + \omega_m$ propagates in the $+\hat{y}$ direction.

Seshadri calculated the group delay times for the magnetostatic surface modes of grounded and ungrounded ferrite slabs as a function of applied field. He found that the group delay times are "practically unaffected if the ferrite is grounded at the bottom face" and that "the group delay becomes negligible if the ferrite slab is grounded at the top face." Seshadri goes on to say that as a result of this "negligible" delay, "the delayed signal cannot

be detected." Inherent in this statement is the assumption that the experimental set-up used by Brundle and Freedman was such that small delays could not be detected. However, it appears from the inset of Brundle and Freedman's Fig.2, that the time delay measurements were performed by displaying both the detected input and output waveforms. If this is the case then it would be unlikely that the "ferrite-metal" mode signal would not have been observed if it were sufficiently excited. As long as the input pulse is displayed, one could display the output pulse, if present and of sufficient magnitude, even for zero delay, by using the same trigger signal for both pulses. Unfortunately, Brundle and Freedman are not specific on this point. They indicate that "the delayed signal disappeared completely." This may be interpreted in either of two ways; either they observed no signal at all or they only considered signals delayed significantly with respect to the input signal.

Putting aside the question of the "ferrite-metal" mode, Brundle and Freedman's experiments demonstrated the existence of the "magnetostatic" (or "ferrite-dielectric) surface mode and verified the relationship between the direction of propagation and the surface with which the mode is associated. Furthermore, their pulsed r.f. experiments verified that the "magnetostatic" mode is not significantly altered when the opposite surface is placed in intimate contact with a metal plate.

Brundle and Freedman also studied the behavior of the "magnetostatic" modes under c.w. conditions. Using the same apparatus and signal frequency

as in their pulsed r.f. measurements they observed the transmission properties of the structure as a function of the applied static magnetic field. As the field was varied they observed a series of maxima of transmission (and corresponding minima of reflection). These, they reasoned, were traveling wave resonances which arose as a result of the wave traveling across one face and returning along the other as shown in Figure 3-19[6]. If after circumnavigating the slab the wave is in phase with the input, the wave is augmented corresponding to a maximum of transmission. If, on the other hand, they are out of phase, a minimum results. The resonances, therefore, may be related to the wavelength of the surface mode. Brundle and Freedman were thus able to compare their results with the magnetostatic theory of Damon and Eshbach[5]. While good agreement with the magnetostatic theory was experienced for the longer wavelength portions of the spectrum, the experimental results indicate that resonance occured at a lower value of applied field than anticipated. Brundle and Freedman point out that the agreement in the long wavelength region may be accidental "because the magnetostatic theory is less accurate at longer wavelengths." The pulsed measurement results also show that the resonance field does not coincide with that expected from the theoretical calculation. Thus, it is possible that either the applied field was not accurately measured (perhaps due to distortion of the field) or that the value of the effective anisotropy field used in the calculation was chosen too small.

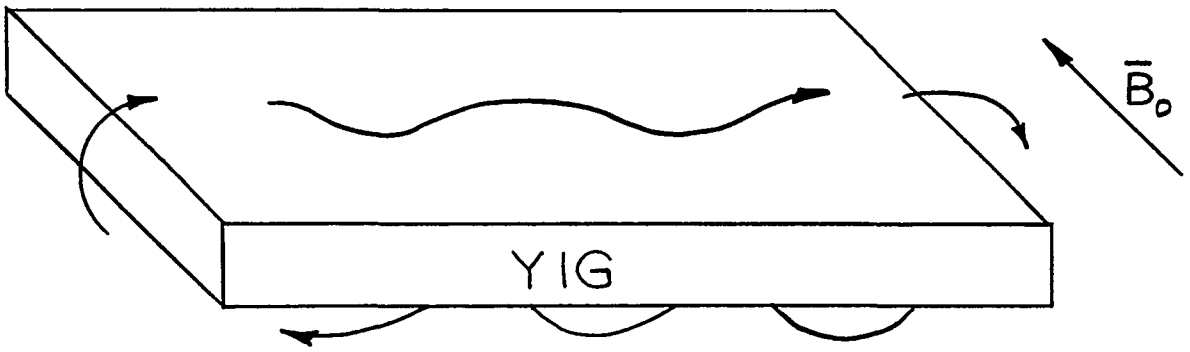

Figure 3-19 - Path of Surface Waves (After Brundle and Freedman [6])

Experiments involving "magnetostatic" surface wave propagation were performed to develop techniques to be used in the subsequent study of surface waves at the interface of a magnet insulator with a drifted semiconducting medium. An important aspect of this study was the gathering of information useful for the proper identification and classification of surface modes.

Figure 3-20 a and b are sketches of the experimental arrangement indicating the relationship of the couplers to the YIG slab. The slab, which is highly polished single crystal material, has the dimensions .393" x .105" x .033". A static magnetic field was applied parallel to the plane of the large surface as shown. Unlike the models considered in previous sections, the static magnetic field intensity within the slab is not uniform but varies as a result of the demagnetizing field. An expression for this field is obtained in Appendix I and is plotted versus distance along the center line of the large surface in Figure 3-21. As a result of this variation of demagnetizing field, the effective magnetic field intensity is higher at the slab's ends than at the center. This gradual variation in the internal field increases the coupling between the input signal and the relatively short wavelength "magnetostatic" modes[80]. This may be demonstrated qualitively by considering the behavior of the surface wave at a point along the surface to be represented by the dispersion relationship with ω_i taken as a value appropriate to H_i at that point. Since H_i, and therefore ω_i, varies along the surface, the wavelength at a particular excitation frequency also changes with position as depicted in Figure 3-22. It is observed that the wavelength

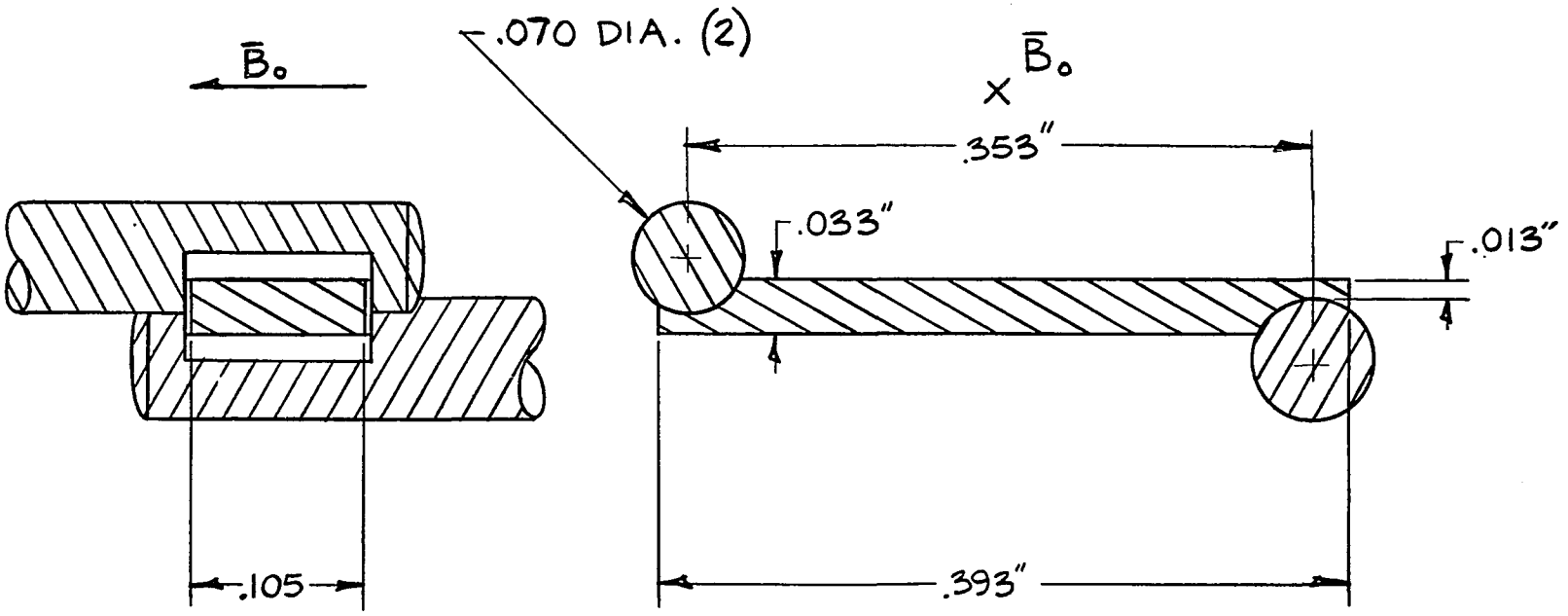

Figure 3-20 - Orientation of Applied Field and Couplers

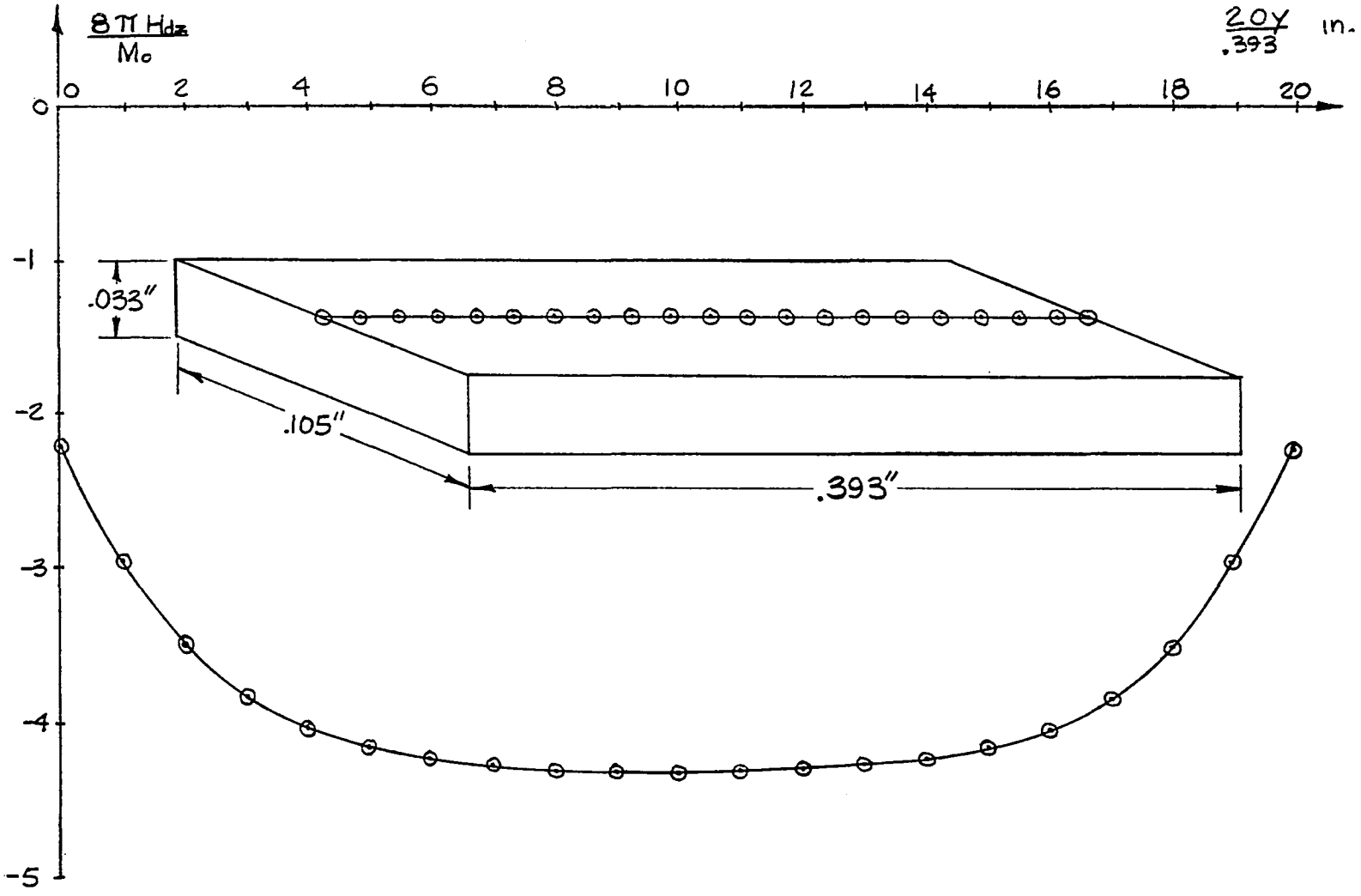

Figure 3-21 - Demagnetizing Field At The Surface Of The Ferrite Slab

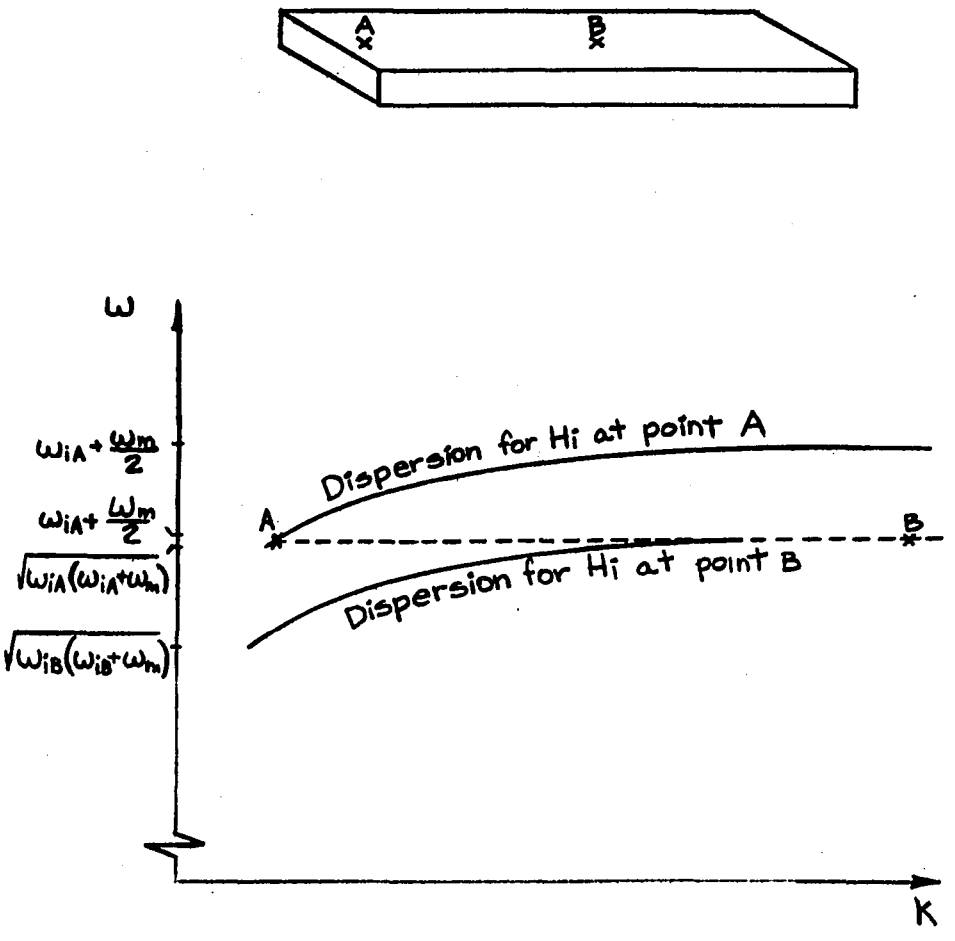

Figure 3-22 Coupling To Surface Waves Using The Non-uniform Internal Magnetic Field Intensity

of the surface wave is longer at the ends of the sample than at the center. Thus direct excitation of surface waves may take place near the ends of the slab where the surface wave energy, $\hbar\omega$, and momentum, $\hbar\bar{k}$ are approximately equal to those of the electromagnetic waves within the dielectric bulk. By exciting the relatively long wavelength surface wave at point A, power may then be coupled to the shorter wavelength "magnetostatic" mode at the center of the surface, point B. In a similar manner, the surface wave power may be extracted at the far end of the sample.

In addition to being positioned near the ends of the slab, the microwave couplers are placed on opposite sides to minimize direct coupling from input to output. The couplers, which are constructed of 70 mil. coax, Phelps- Dodge Type CT-07050, are shorted at their ends so that their magnetic fields have a maximum in the vicinity of the ferrite. Since these fields enclose the center conductor, their configuration resembles that of the r.f. magnetic field intensity components of the surface wave being excited. To increase the effectiveness of this coupling, part of the outer jacket and insulator of the coax is cut away bringing the center conductor to within 5 mils of the YIG.

The YIG slab is totally enclosed in a plexiglass housing, $\epsilon_d \cong 2.3$ as shown in Figure 3-23. Strips of teflon, .001 inch thick are inserted between the YIG and the plexiglass to insure a secure fit. Over most of the surface wave spectrum these teflon spacers ($\epsilon_d \cong 2.1$) are relatively thin when compared to $1/\beta_d$ and therefore have little effect

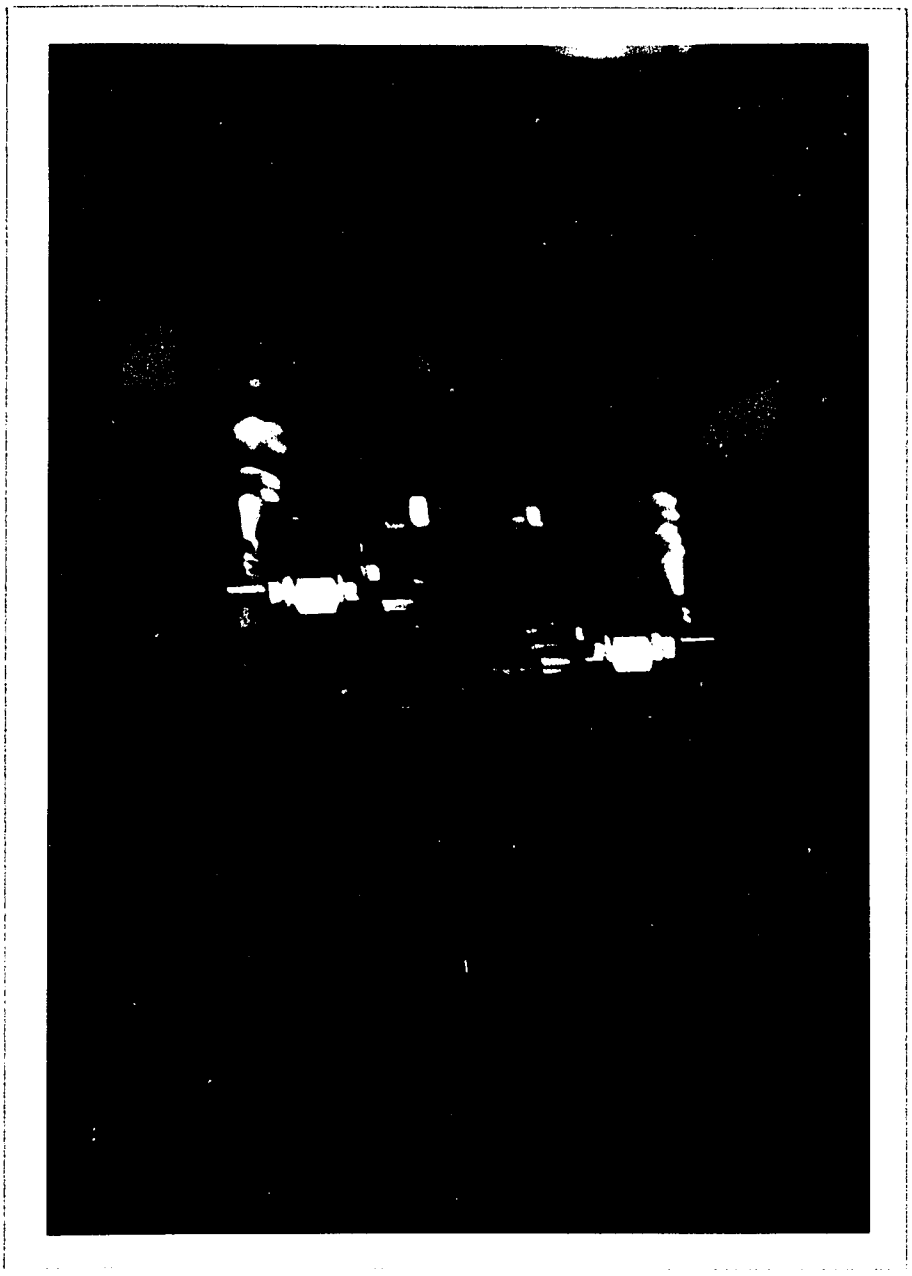

Figure 3-23 - Jig Used for Surface Wave Measurements

on the propagation characteristics. It has been demonstrated in Section 2.3 that near the "magnetostatic" mode resonance, where $1/\beta_d$ decreases rapidly, the permittivity of the dielectric region has little bearing on the behavior of the mode. Thus, the presence of the spacers may be neglected in computing the theoretical behavior of the structure. However, the relatively thick plexiglass may not be neglected. Its presence must be taken into account to determine the frequency ranges of the "dynamic" and "magnetostatic" modes. (Brundle and Freedman's [6] analysis was based on the magnetostatic theory of Damon and Eshbach[5] in which the effect of the permittivity of the medium surronding the slab is not considered. Thus, since no mention is made of the permittivity of the dielectric, it is assumed that the large faces of the slab were in contact with air).

In Chapter 2 it was shown that for $\epsilon_d < \epsilon_m$, the lower limit of the "dynamic" mode occurs at

$$\omega_1 \Big|_{s=-1} = \sqrt{\frac{(\epsilon_m - \epsilon_d)\,\omega_i^2 + \epsilon_m \omega_m \omega_i}{(\epsilon_m - \epsilon_d)}} \quad . \qquad 2\text{-}126$$

If the frequency ranges of the "dynamic" and "magnetostatic" modes do not overlap, the "magnetostatic" mode may be studied independently of the "dynamic" mode. For this to occur, ω_1 must be greater than the "magnetostatic" surface mode resonance.

$$\omega_{res} = \omega_i + \frac{\omega_m}{2} \quad , \qquad 2\text{-}114$$

or

$$\sqrt{\frac{(\epsilon_m - \epsilon_d)\,\omega_i^2 + \epsilon_m \omega_m \omega_i}{(\epsilon_m - \epsilon_d)}} > \omega_i + \frac{\omega_m}{2} \quad . \qquad 3\text{-}56$$

Squaring both sides of Equation 3-56 and solving for ω_i in terms of ω_m results in the conditon

$$\omega_i > \frac{\omega_m (\epsilon_m - \epsilon_d)}{4\epsilon_d} \quad . \qquad 3\text{-}57$$

Since the resonance frequency may be determined with a greater degree of accuracy than the effective value of the internal static magnetic field intensity, it is convenient to restate the inequality as a condition on the minimum value of the "magnetostatic" mode resonance frequency. Substitution of Equation 2-114 into Equation 3-57 yields

$$f_{res} > \frac{\omega_m (\epsilon_m + \epsilon_d)}{8\pi\epsilon_d} \qquad 3\text{-}58$$

Thus, for the "dynamic" and "magnetostatic" surface modes to propagate in non-overlapping frequency bands, the applied static magnetic field must be chosen such that the resonance frequency exceeds the value specified by the right side of Equation 3-58. For the parameters appropriate to the experimental arrangement described above, the resonance frequency condition is

$$f_{res} > 8.68 \text{ GHz.} \qquad 3\text{-}59$$

In the first series of tests the ω-k spectrum of the "magnetostatic" surface mode was measured. In contrast to the c.w. measurements of

Brundle and Freedman[6] which were performed at a fixed frequency, 3GHz., these tests were performed by making swept frequency measurements for several values of applied static magnetic field. The range of frequencies over which the tests were conducted was 7-9 GHz.

The tests were conducted by suspending the sample, encased in its plexiglass jig, in the field of an electromagnet. (The magnet poles and the tip of the fluxmeter are visible in Figure 3-23). The experimental setup is shown in block diagram form in Figure 3-24. The input signal was obtained from an HP 8690A sweep frequency oscillator with HO1-8694B r.f. plug-in whose output was levelled by means of an external feedback arrangement. This signal was transmitted through a waveguide set-up which had provision for monitoring the input to the sample as well as the reflected signal. The output was brought out through a waveguide section to a crystal detector. In the arrangement shown in Figure 3-25 a and b, the crystal detectors in the monitor and output sections are a matched pair, HP X424A, enabling the attenuator in the monitoring circuit to be used in determining relative power levels of the input and output. A wavemeter is also provided in the monitoring circuit permitting frequency measurements to be made within 0.08% over its range. At frequencies below the 8.2 - 12.4 GHz range of the HP 532B frequency meter, the frequency was measured using a Tektronix 535A Oscilloscope with a 1L30 Spectrum Analyzer plug-in.

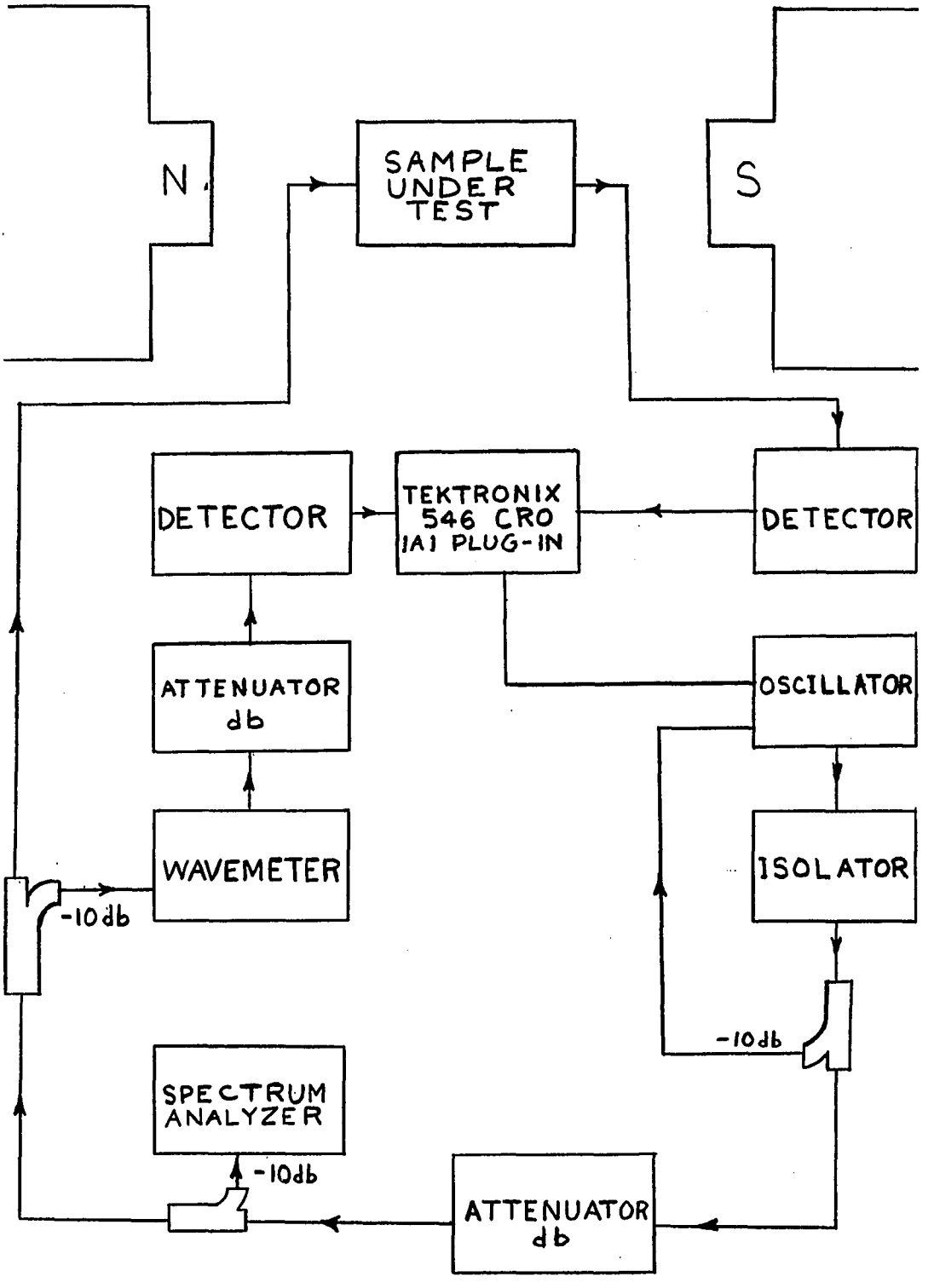

Figure 3-24 - Block Diagram of Experimental Set-up

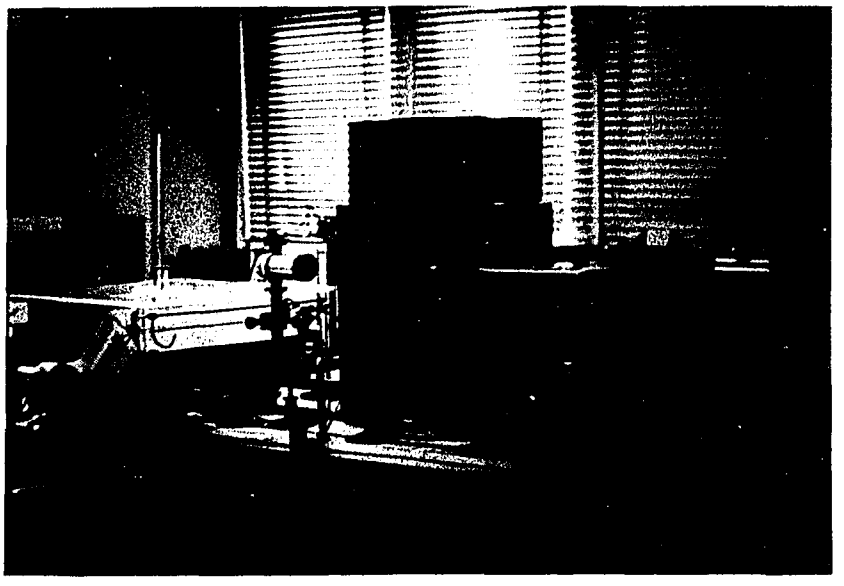

a

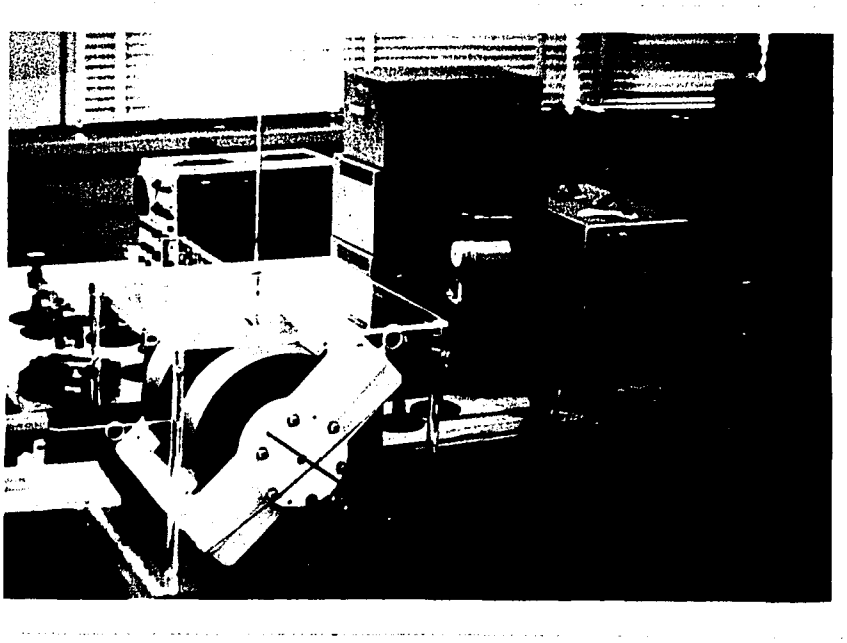

b

Figure 3-25 - Surface Wave Measurement Set-up

The magnet was adjusted until the rotating coil gaussmeter, Rawson-Lush Type 720S, indicated an applied field of 2300 Gauss. As the input frequency was swept, a series of resonances, corresponding to maxima of transmission of the type recorded by Brundle and Freedman[6], were observed at the output as shown in Figure 3-26. The trace is swept linearly across the screen, the frequency markers to the left and right of the graticule corresponding to 7.245 GHz. and 7.77 GHz. respectively. The waveform displayed across the center of the screen is obtained from the matched detector in the input circuit and is -10.6 db relative to the power incident upon the adaptors leading to the test sample. The waviness of this trace is caused by imperfect adaptor matching, VSWR $\approx$1.06. (This may be reduced by padding the input). Also noticeable on the input trace are small peaks which correspond to the output resonance peaks. It is observed that the input VSWR is reduced at these resonance frequencies since the transmission maxima correspond to minima of reflection.

The shape of the spectrum is "bell-like" with lower amplitude peaks occuring at the extremes. The lowest surface mode resonance peak, located 1cm. to the right of the edge of the graticule in Figure 3-26, is shown in greater detail in Figure 3-27. (The reference level in this figure is a -19.6 db .) This resonance peak, close to the lower frequency limit of the spectrum, disappears as the magnetic field is increased. Its relatively wide bandwidth is indicative of coupling to other modes caused by the variation of the magnetic field along the surface. A number of undulations

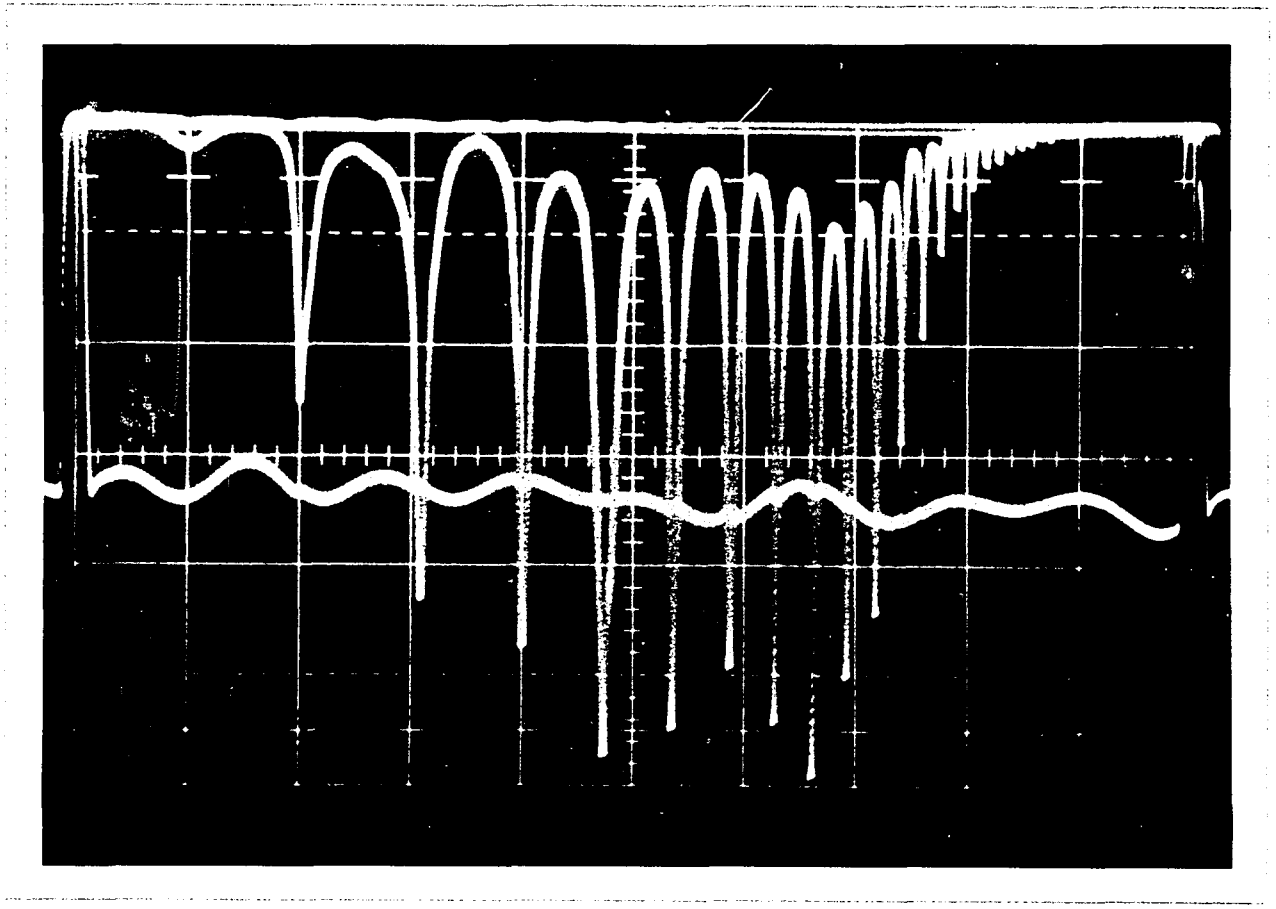

Figure 3-26 - Surface Wave Resonance Spectrum - B_c=-2300G.

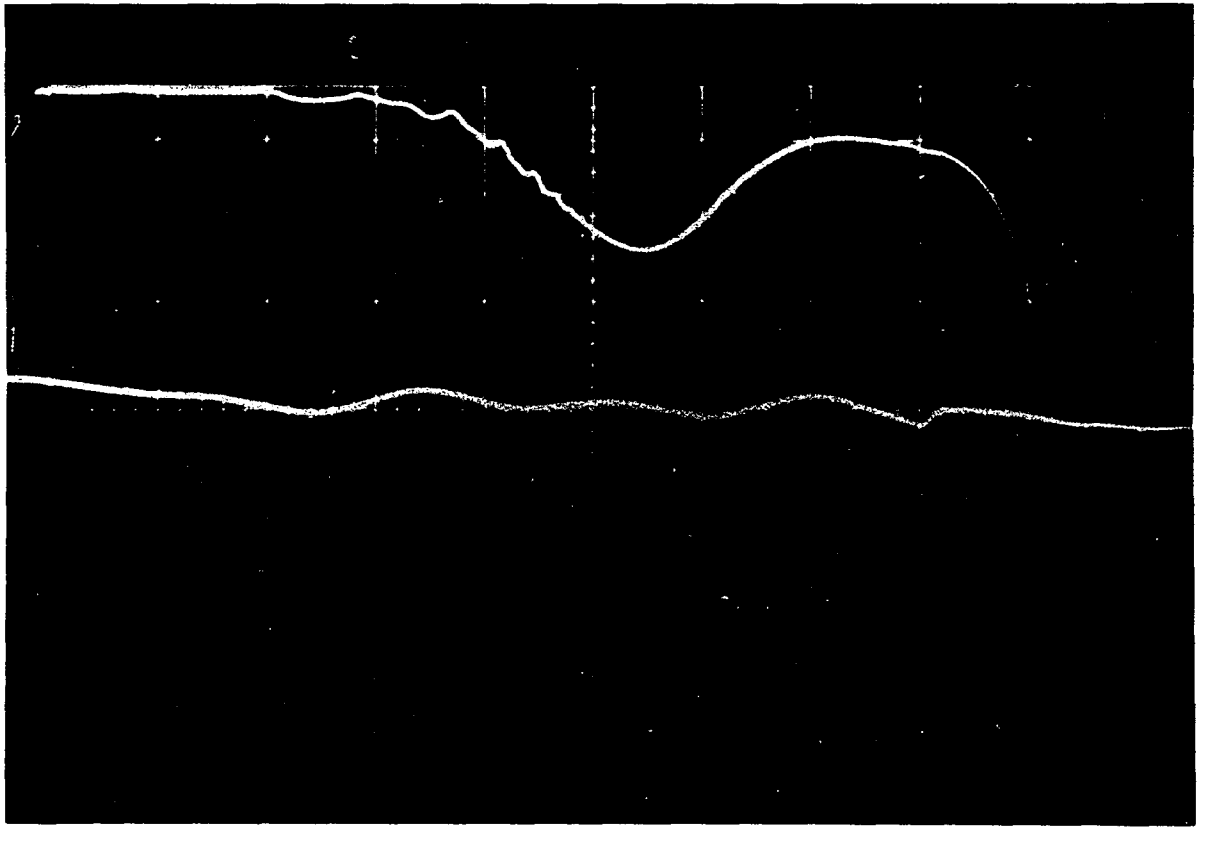

Figure 3-27 - N_r=1 Surface Wave Resonance - B_o=2300G

are observed on the low frequency portion of the resonance peak and are interpretable as bulk mode resonances. Sparks[81] calculated the theoretical magnetostatic mode spacings of a YIG slab for the Brundle and Freedman[6] case. Using Spark's notation, the bulk mode series beginning immediately to the right of the first surface mode resonance peak is labeled the $(n_L, 1)_{Bu}$ series. Other higher order bulk mode series may be observed at lower frequencies as shown in Figure 3-28. It is clear from this photograph that the experimental arrangement is such that coupling to the surface modes takes place more efficiently than coupling to the bulk modes.

A portion of the spectrum centered at the fifteenth resonance peak (7.683 GHz) is shown in Figure 3-29. The peaks which are clear and distinct become more closely spaced as the frequency is increased indicating that the wavelength and $\frac{\partial \omega}{\partial k}$ both decrease as the "magnetostatic" mode resonance is approached. Twenty-seven surface wave resonance peaks were classified and their frequencies recorded at this 2300 G. operating point. The "magnetostatic" surface wave resonance occurs at 7.751 GHz. for this operating point magnetic field.

As the magnetic field is increased the surface wave spectrum shifts to correspondingly higher frequencies. It is noted that while the appearance of the spectrum generally remains unchanged, the relative magnitude of the transmitted signal decreases, as shown by comparing Figure 3-30, corresponding to an applied magnetic flux density of 2500G., with that of Figure 3-26.

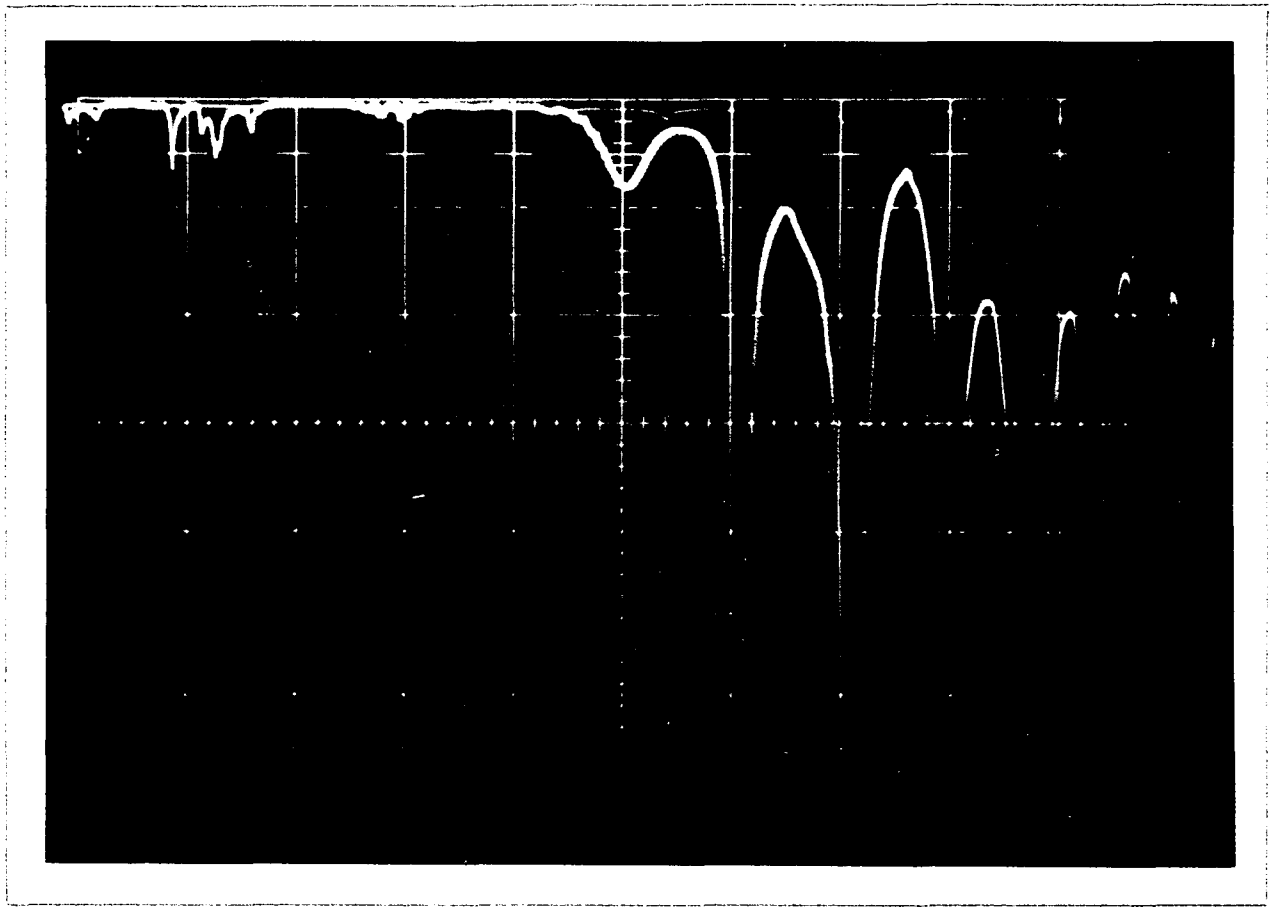

Figure 3-28 - Surface and Bulk Modes-N_r=1 Centered-B_o= 2300G.

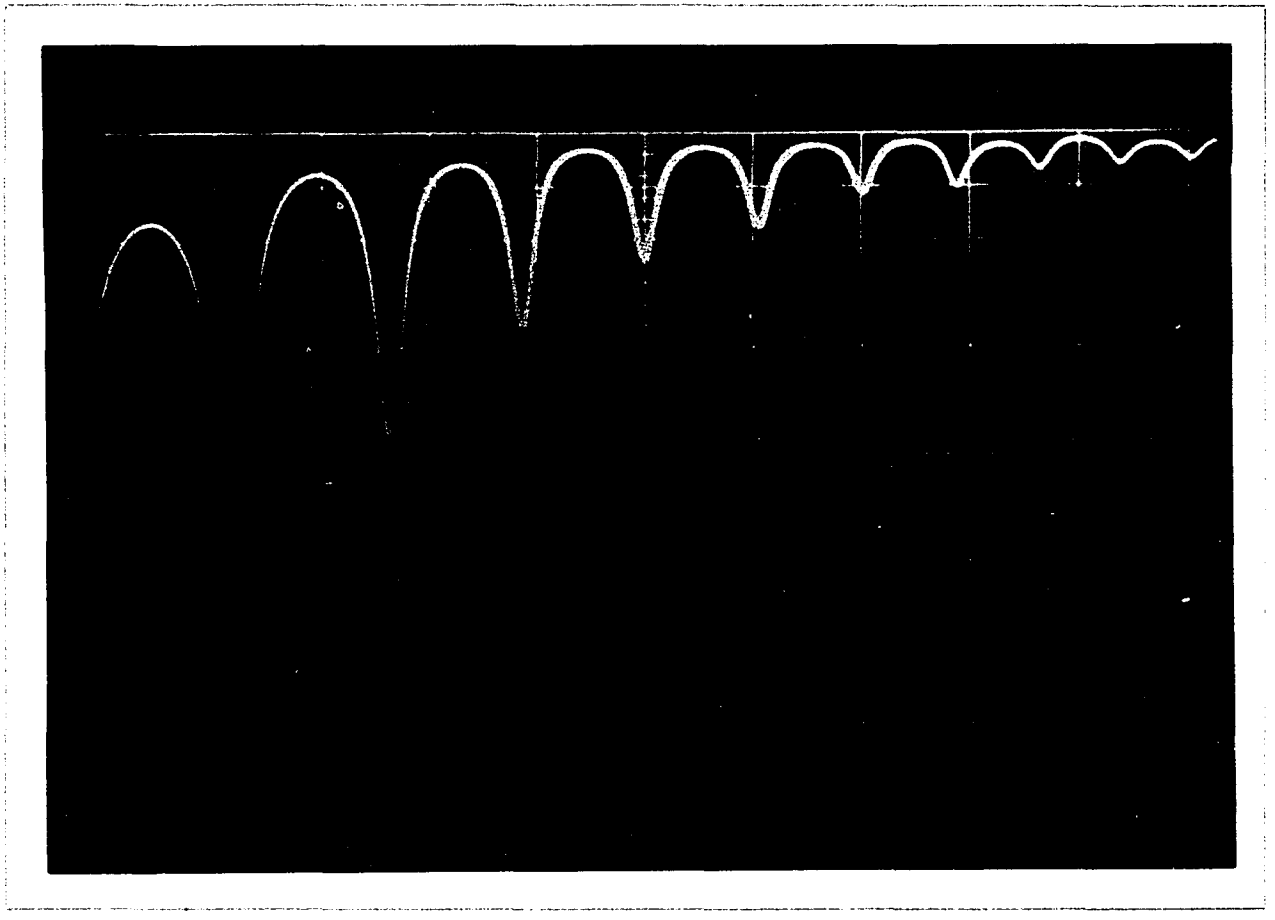

Figure 3-29 - Surface Wave Detail-N_r=15 Centered - B_o=2300G.

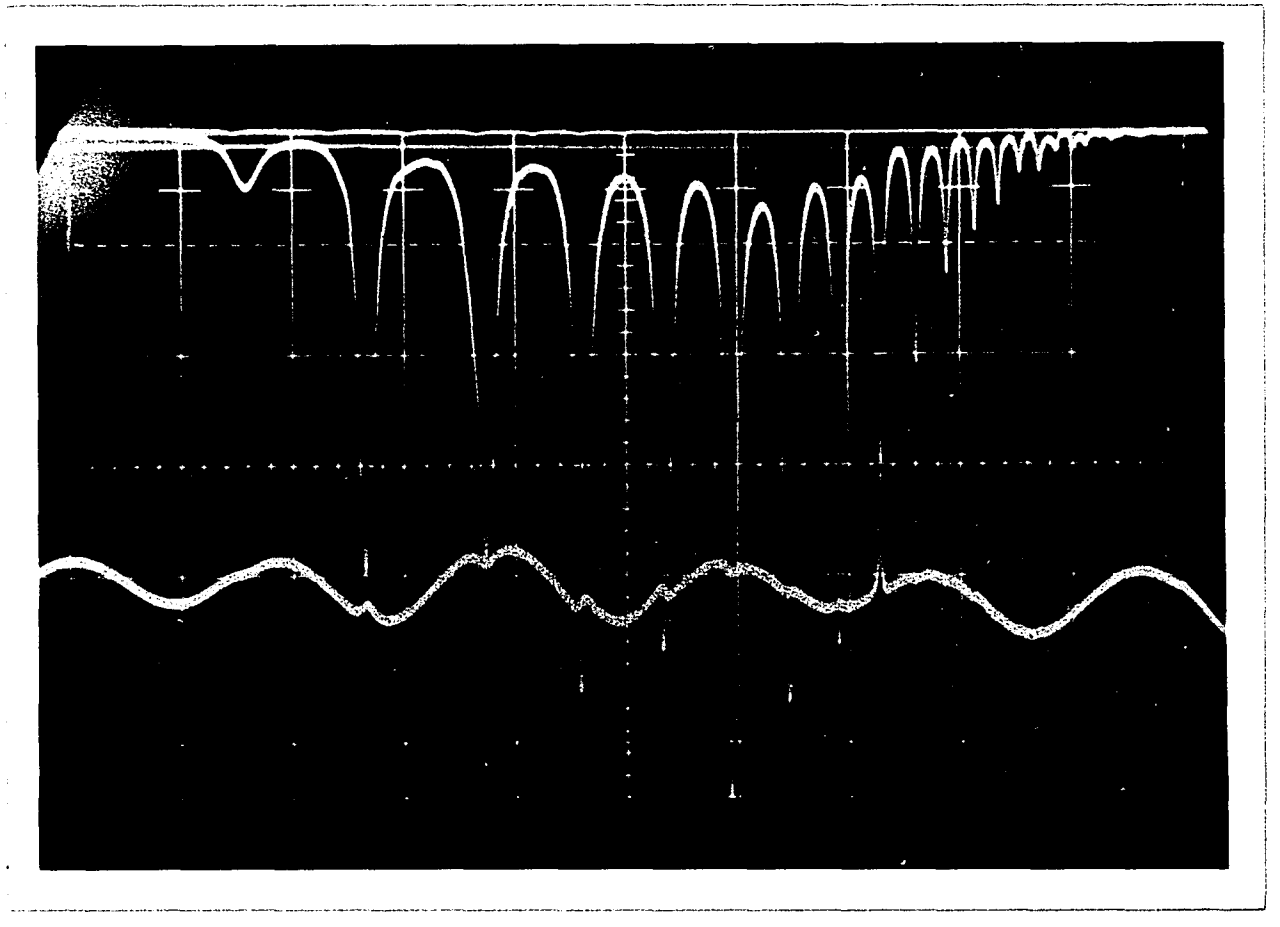

Figure 3-30 - Surface Wave Resonance Spectrum-B_o = 2500G.

In both cases the reference level is -10.6 db below the incident power level. In making the transition to higher frequencies the first peak diminished in magnitude unitl it could no longer be observed. Thus the lowest frequency surface mode resonance peak, located 1.6 cm. to the right of the edge of the graticul in Figure 3-30, does not correspond to the first peak in Figure 3-26, but rather to the second.

The sharp dip in the reference level approximately 6.3 cm. to the right of the graticule edge in Figure 3-30, is caused by the wavemeter in the monitoring circuit. Its position corresponds to a frequency of 8.2 GHz, the frequency of the resonance peak designated as N_r=10. The wavemeter in conjunction with the reference level attenuator was used to measure the width of the resonance peaks at their respective 3 db points, thus providing a measure of the losses. The width of peak numbers 11, 13 and 15 was found to be 6 MHz., 4 MHz.and 5.2 MHz. respectively, corresponding to a linewidth of approximately 1 to 2 Gauss. (It should be noted that this measurement only provides an upper limit on the linewidth of the YIG. Factors such as surface roughness and losses incurred in circumnavigating the slab also contribute to the width of the resonance peaks).

The surface wave spectrum obtained when the applied field was set at 2700 G. is shown in Figure 3-31. The reference line marker corresponds to 8.616 GHz., the frequency of the resonance peak labeled N_r=4. (The N_r=2 peak is small and cannot be distinguished on this photograph). The highest resonance peak distinguished at this operating point corresponds

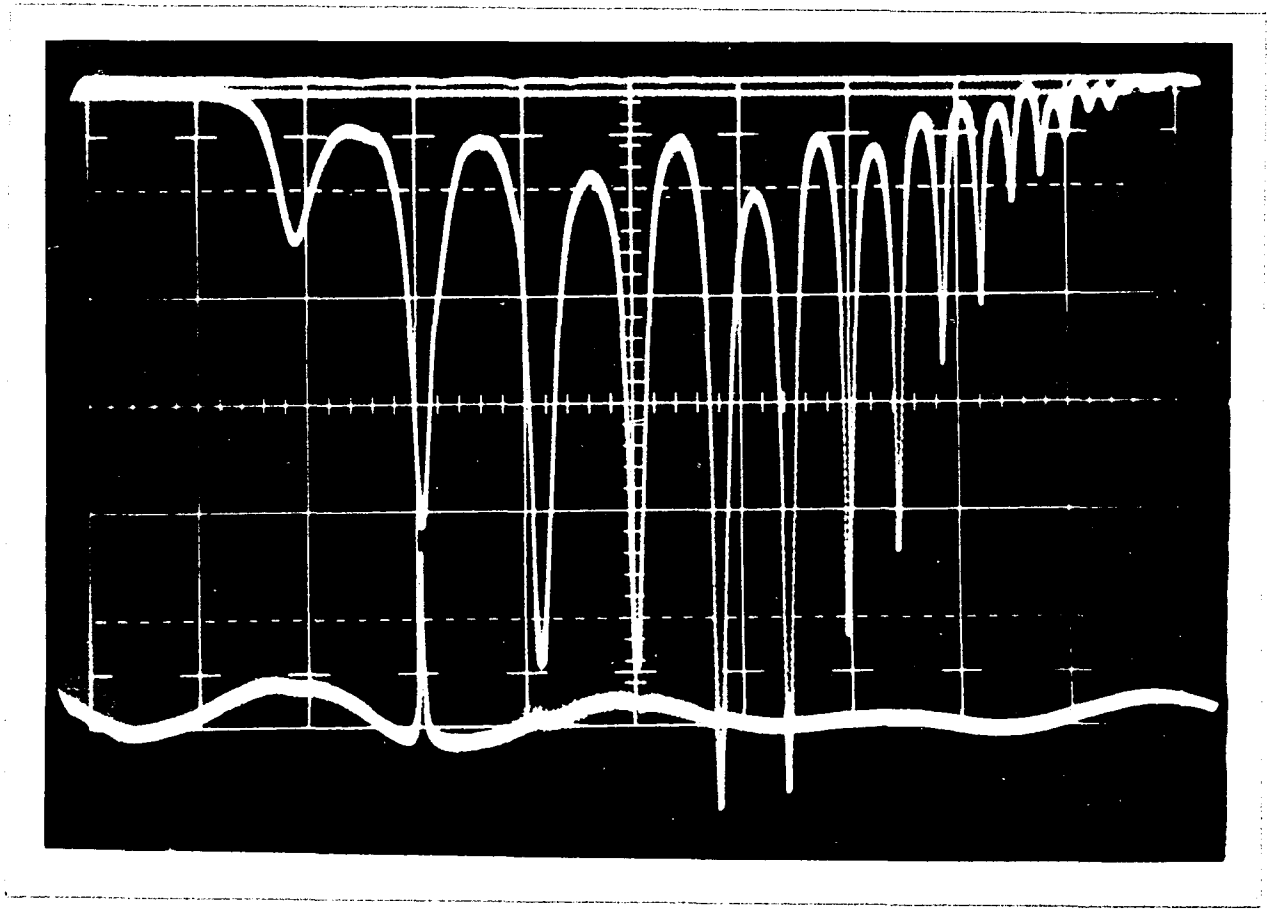

Figure 3-31 - Surface Wave Resonance Spectrum-B_o = 2700G.

to $N_r = 24$ at 8.8285 GHz. Reversal of the direction of the applied static magnetic field was found to have no significant effect on either the resonance frequencies or the amplitude of the spectrum. This is to be expected since the resonance frequencies are dependent on the size of the slab and are not influenced by whether the surface mode travels around the slab in either a clockwise or a counter-clockwise direction. Furthermore, since the distance between couplers is the same for both directions of travel no difference in amplitude results. In subsequent tests, however, a jig in which both couplers were mounted on the same side of the YIG was used. Here, there was a 2db difference in the amplitude of the spectrum when the "magnetostatic" surface wave traveled the long way (across the opposite face) as compared to the short way.

Dispersion characteristics for the ferrite slab may be determined from experimental results by relating the resonance peak numbers to the wavelength of the mode. Noting that at a maximum of transmission the wave completes an integral number of half cycles as it transverses the face of the slab, the wavelength may be related to the resonance peak number by

$$N_r \lambda = L_s \qquad 3\text{-}60$$

where L_s represents one half of the distance traveled by the wave in circumnavigating the slab, 0.426" in this case. Since the wavelength is related to the wavenumber through the expression,

$$k = \frac{2\pi}{\lambda} \qquad 3\text{-}61$$

the relationship between N_r and k is

$$k = \frac{\pi}{L_s} N_r = 290\, N_r \ \text{meter}^{-1} \qquad 3\text{-}62$$

Thus, an empirically derived ω-k diagram may be obtained by plotting the frequency of the resonance peaks versus their respective resonance numbers. (A similarl technique is used to experimentally determine the dispersion characteristics of slow-wave circuits [82]).

Dispersion characteristics calculated from the data obtained at the 2300 G., 2500 G. and 2700 G. operating points are shown in Figure 3-32. The solid curves are computed using Equations 2-94, 2-95 and 3-26, derived for the finite thickness ferrite model of Figure 3-1. The internal magnetic field intensity used in computing these curves is based upon the measured value of the applied field, the demagnetizing field attained at the center of the large face of the slab (Figure 3-21), and an anisotrophy field of -105 Oe, determined by equating the calculated resonance frequency at 2300 G. with that estimated at this operating point. The frequency ranges of the calculated and measured "magnetostatic" surface wave dispersion characteristics are seen to compare quite favorably with one another as the applied field is varied. The experimental and theoretical characteristics appear to be in close agreement near the upper and lower limits of the surface wave frequency band, the experimental disagreemen being greatest near midrange. This is primarily due to the non-uniformity of the

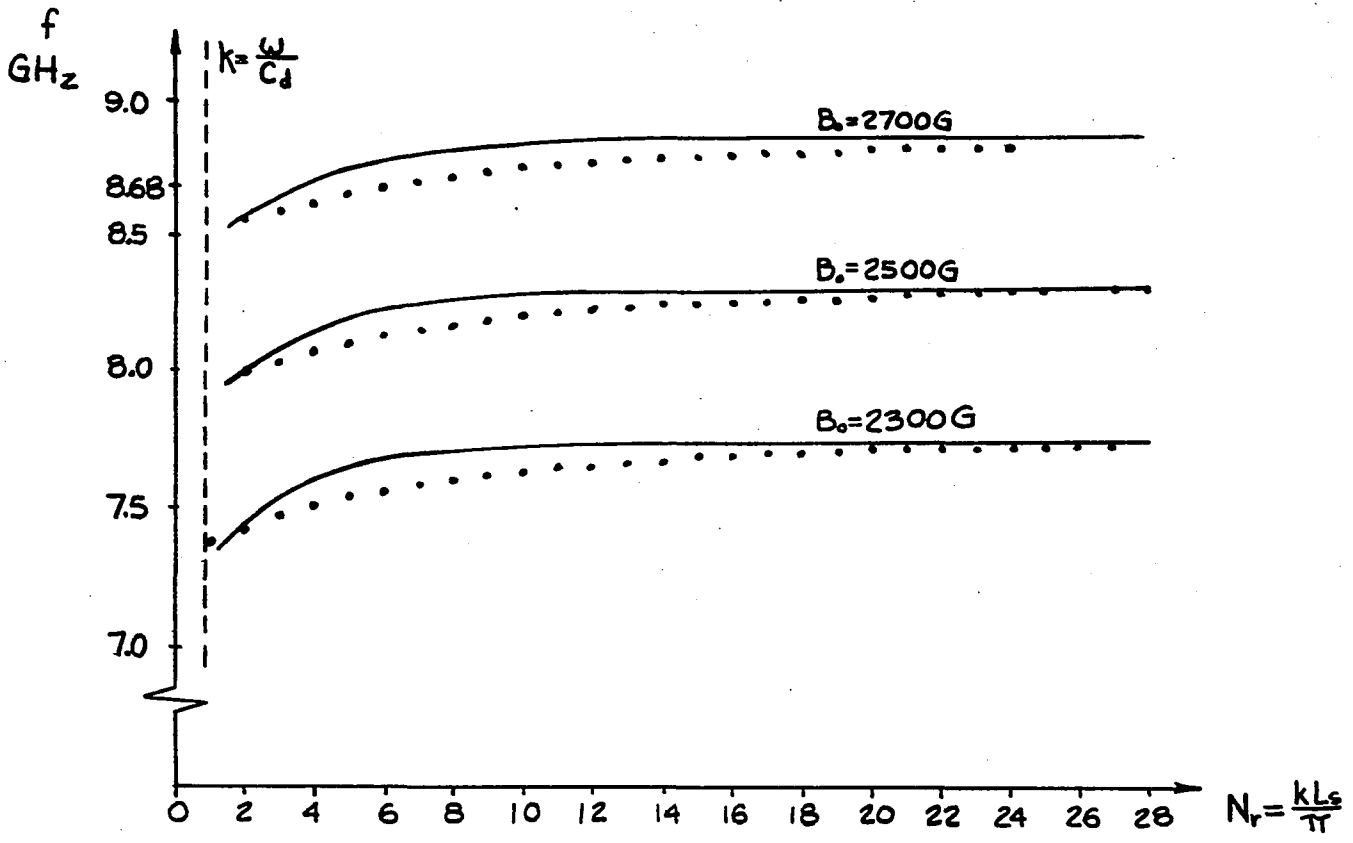

Figure 3-32 - Empirical "Magnetostatic" Surface Mode Spectra

internal magnetic field intensity of the slab. At the upper and lower limits of the pass band β_m is large causing the fields with the ferrite to be more closely confined to the surface than at mid-range. (This is illustrated by the relative energy density curves, Figure 3-6 and 3-7). As a result, the generally lower fields within the center of the ferrite are more effective in reducing the wavelength of the surface wave at the mid-range frequencies than at the extremes of the pass band.

It was noted previously, that the N_r=1 resonance peak, observed at the 2300 G. operating point, decreased in amplitude and disappeared as the magnetic field was increased. This result is supported by calculations which show that near its lower frequency limit the wavenumber of the resonance peak is very close to the value corresponding to N_r=1. The calculations further show that the wavenumber at the lower frequency limit increases as the applied magnetic field increases, resulting in the disappearance of the resonance peak. It was also noted that the N_r=1 peak had a relatively wide bandwidth, indicating that energy may be transmitted by other modes as changing magnetic fields are encountered. The location of the N_r=1 point between the 2300 G. "magnetostatic" surface wave curve and the curve corresponding to $k = \omega/c_d$ further supports this conclusion.

Of the three spectra plotted in Figure 3-32, only the 2700 G. spectrum has a resonance frequency exceeding 8.68 GHz. Thus, it is expected that the frequency ranges of the "dynamic" and "magnetostatic" modes do not overlap for this case. Comparing the photograph of the 2700 G. spectra with the spectra for 2300 G. and 2500 G., whose resonance frequencies fall below 8.68 Ghz., reveals no apparent differences that could be attributed to the "dynamic" mode.

An investigation of the time delay of the"magnetostatic" surface modes was conducted at the 2300 G., 2500 G. and 2700 G. operating points considered above. In preparing for each individual measurement, the surface wave was excited with a c.w. signal whose frequency was adjusted to correspond to one of the surface wave resonance peaks. The amplitude of the input signal was then modulated by using pulses of short duration. The time delay between the arrival of the pulse at the input and output crystal detectors is measured by comparing the signals on a dual trace oscilloscope. The input and output pulses are shown in Figure 3-33 for an applied field of 2300 G. and excitation frequency of 7.713 GHz. (This corresponds to N_r =19). The time scale is 0.1 μ sec./cm. The vertical amplifier sensitivities were adjusted so that both pulses were displayed with approximately equal amplitudes to facilitate the time delay measurement. (The time delay is taken as

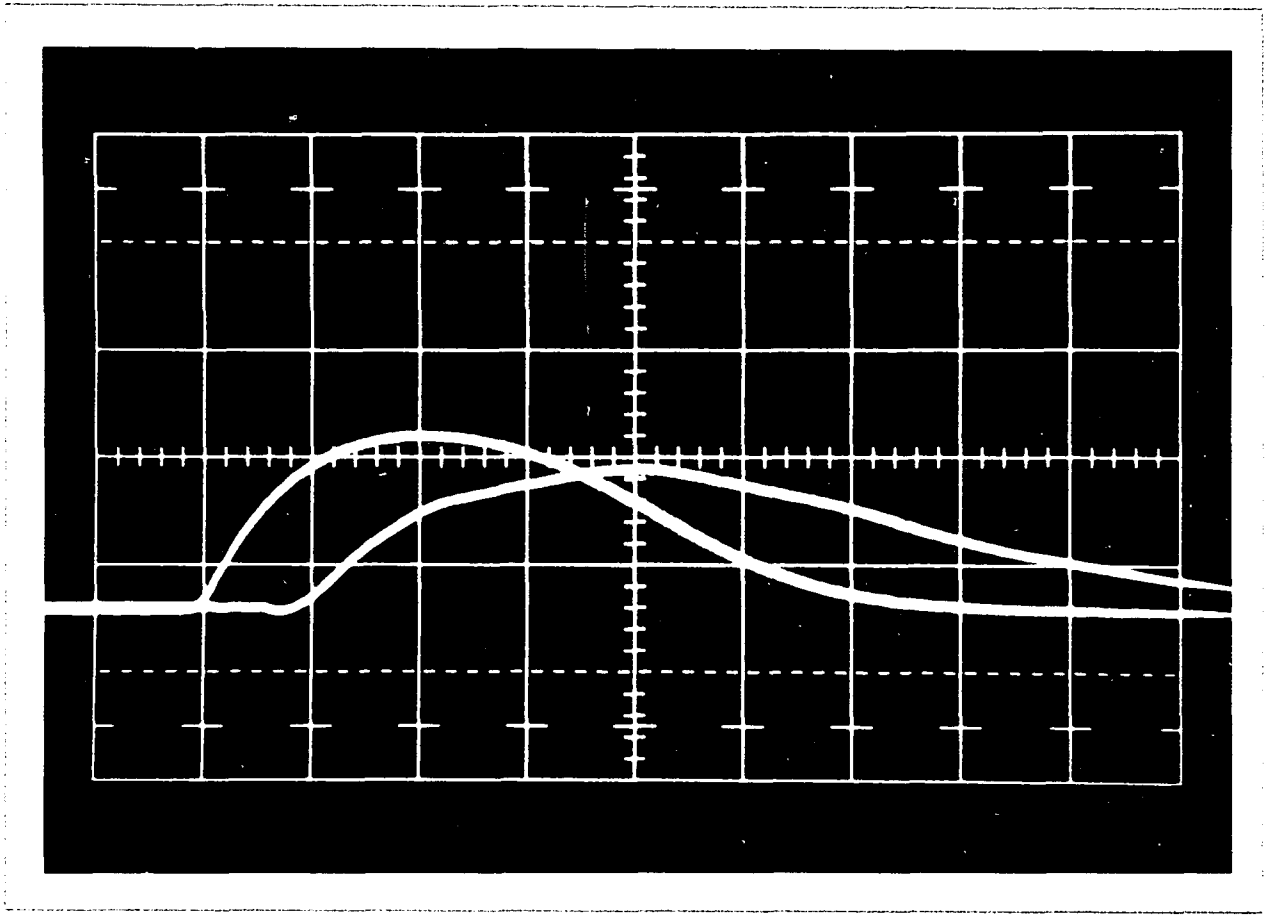

Figure 3-33 - Measurement of Time Delay Corresponding to N_r=19, B_o= 2300G.

the time duration between the maxima of the pulses). Comparison of the shape of the pulses indicates the dispersiveness of "magnetostatic" surface wave propagation.

The results of the time delay measurements are shown in Figure 3-34. The empirically determined curves clearly show that the time delay increases as the resonance frequency is approached. This is anticipated from theory and agrees with the results obtained by Brundle and Freedman [6] at 3GHz. It is interesting to note that the time delay corresponding to the lowest frequency peak in each case is significantly smaller than the delays associated with higher order resonances.

Futher experiments were conducted to study the behavior of the "magnetostatic" surface waves in the absence of the traveling resonance phenomena by severely attenuating the waves propagating along one of the large faces of the slab while permitting surface waves to propagate freely at the other. Attempts to accomplish this involved placing metallic materials in contact with one side of the YIG. Of the materials used, aluminum foil, brass shim stock and aluminized polyester tape, the latter proved to be the most effective. A photograph of surface wave transmission as a function of frequency is shown in Figure 3-35. The magnitude of the applied magnetic field density is 2300 G. and the edges of the graticule correspond to 7.3 and 7.7 GHz. The top image corresponds to the condition where

$$\bar{k} \times \bar{B}_o \longrightarrow \text{aluminized tape} \qquad 3\text{-}63$$

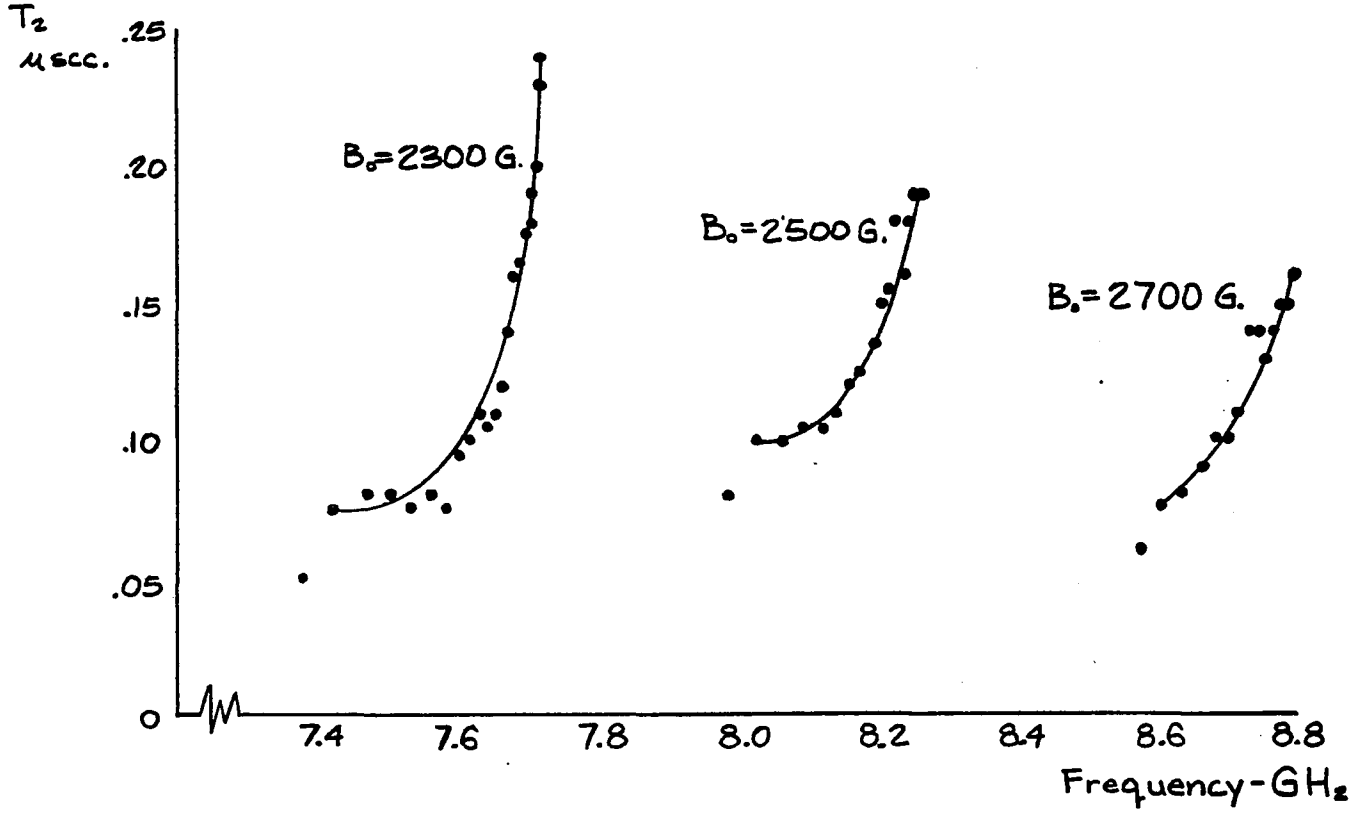

Figure 3-34 Time Delay Versus Frequency For "Magnetostatic" Surface Mode

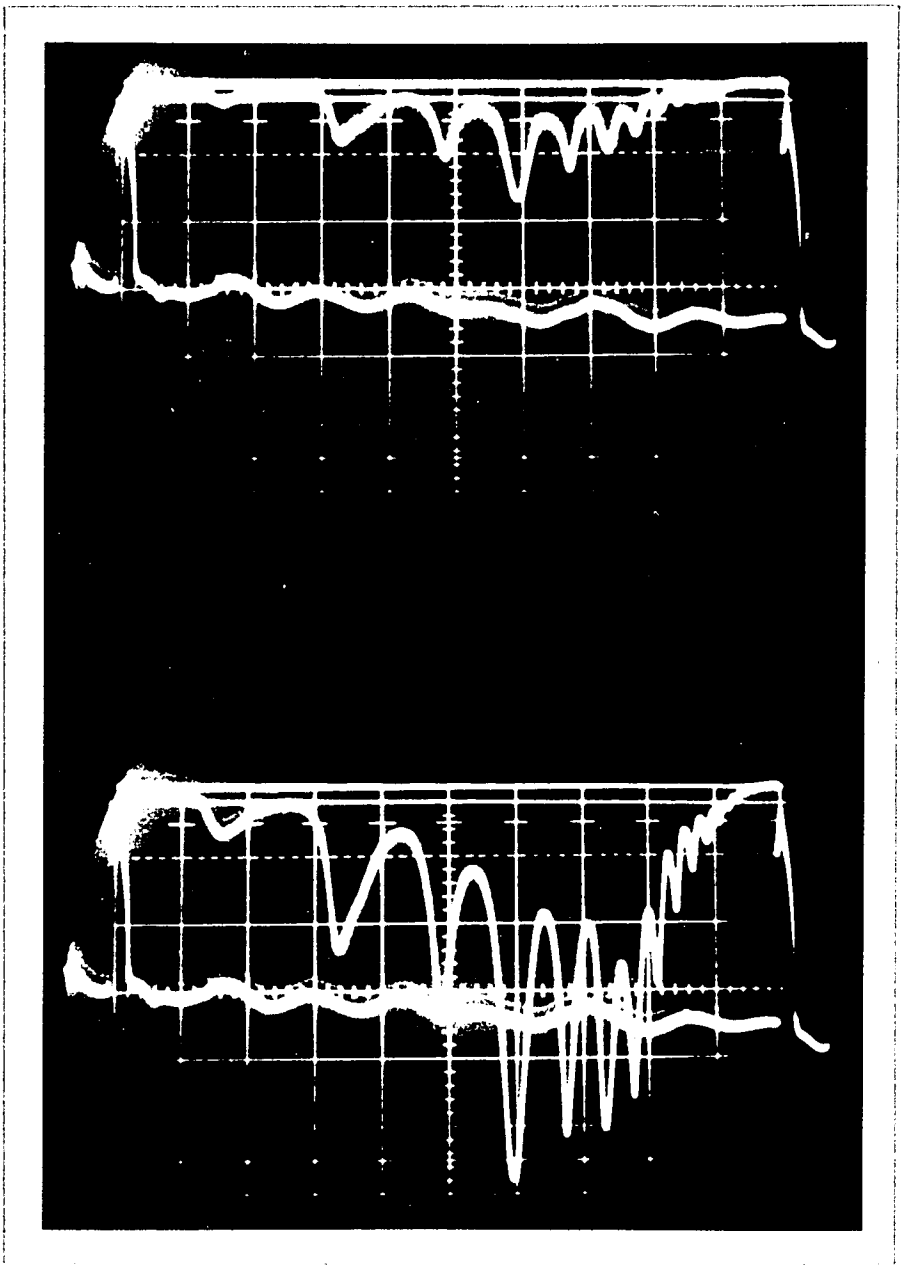

Figure 3-35 Surface Wave Transmission With One Side of Slab in Contact With Aluminized Tape - $B_o = 2300G$.

while the bottom image corresponds to

$$\bar{k} \times \bar{B}_o \longrightarrow \text{plexiglass.} \qquad 3\text{-}64$$

While it is apparent that the aluminum tape did not completely short out the surface wave at that face, the wave was attenuated sufficiently to cause the resonance peaks to broaden and result in the decrease in the difference between the resonance minima and maxima. The marked directivity indicated by the magnitude of the spectrum envelopes with respect to the -13.6 db. reference line clearly indicates the surface wave character and unidirectional properties of the "magnetostatic" surface mode.

To more effectively suppress the traveling wave resonance phenomenon another approach was taken. Instead of attempting to attenuate the wave at one of the faces by placing it in contact with a piece of metal, one side of the slab was completely covered with a coating of paint-on resistive material having a resistivity of 500 ohms/square. The effectiveness of this technique is clearly demonstrated in Figure 3-36. As in the previous photograph, the applied magnetic field density is 2300 G. and the edges of the graticule correspond to 7.3 and 7.7 GHz. The direction of applied field is opposite for the top and bottom images with the top one corresponding to

$$\bar{k} \times \bar{B}_o \longrightarrow \text{resistive material.} \qquad 3\text{-}65$$

It is observed that while the resonances have been largely suppressed, the envelope of the transmission spectrum retains the same general shape as when resonances are present. It is interesting to note also that although the lower frequency limit of the "dynamic" surface mode falls within the

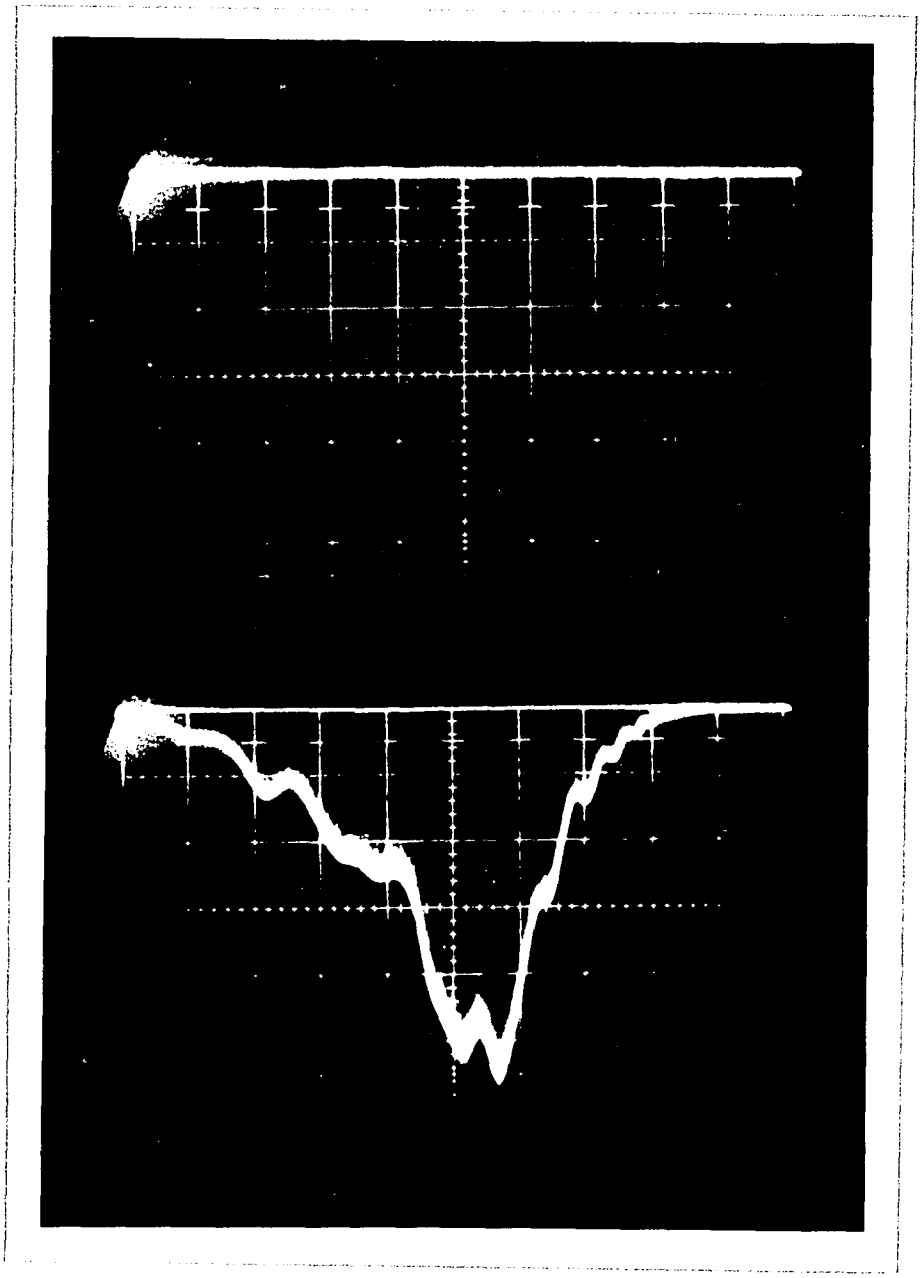

Figure 3-36 Surface Wave Transmission With One Side of Slab Covered With Resistive Coating - $B_o = 2300G$.

frequency range of the photograph, no mode having a direction of propagation opposite to that of the "magnetostatic" surface mode is observed.

Using the resistive paint to suppress the traveling wave resonances, as shown above, time delay measurements were again performed. Surface waves were excited with a 0.13 μsec. r.f. burst using a PIN diode modulator. The results for two values of frequency are shown in Figure 3-37. The top photograph, corresponding to a frequency of 7.39 GHz. indicates a delay of 0.045 μsec. . The bottom image, which clearly shows the dispersiveness of "magnetostatic" surface wave propagation, indicates that the delay is 0.25 μsec. . at 7.712 GHz. These results compare favorably with the time delay measurements conducted at the surface wave resonance peaks.

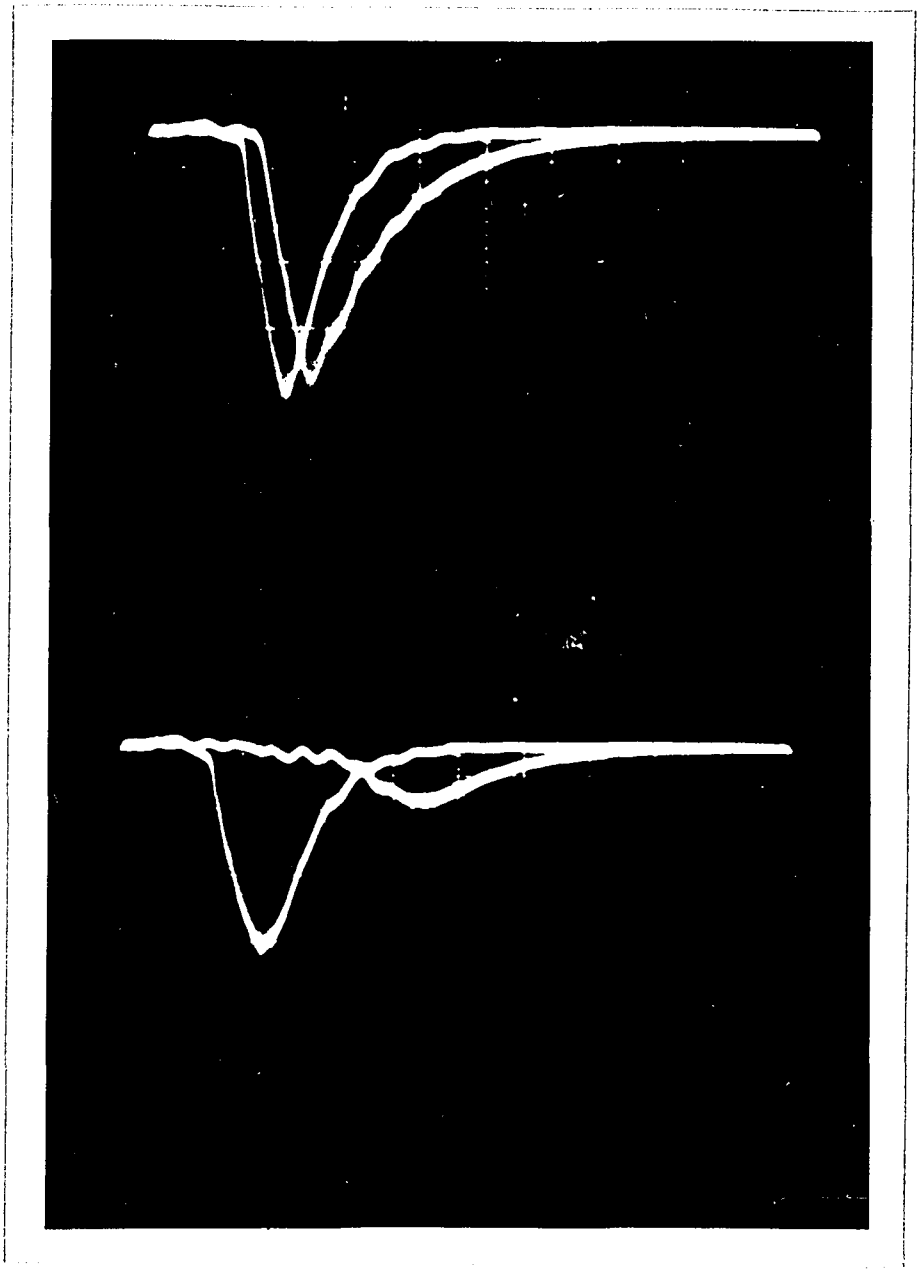

Figure 3-37 - Time Delay Measurements Showing Increase of Dispersion With Delay - B_o=2300G.

CHAPTER 4
ELECTROMAGNETIC SURFACE WAVE PROPAGATION AT THE BOUNDARY OF A SEMI-INFINITE FERROMAGNETIC INSULATOR AND A SEMI-INFINITE SEMICONDUCTOR

4.0 Introduction

The analytical investigation of electromagnetic phenomena occuring at the interface between a ferromagnetic insulator and a drifted semiconductor requires suitable characterization of the semiconductor medium in terms of observable quantities. Using a hydrodynamic model, the semiconductor parameters may be related to Maxwell's equations which describe the overall response of the system to electromagnetic excitations. Employing this model and the ferrite model developed in Chapter 2 a dispersion relationship is obtained and analyzed. These results are compared with the magnetostatic theory [23] which is extended to include the effects of multiple carrier species. An instability onset condition nomograph is developed showing material parameters for which a convective instability with net growth rate exists.

4.1 Characterization of Semiconducting Materials

The electromagnetic behavior of a semiconductor is related to Maxwell's equations, 2.1, 2.2, 2.3 and 2.4, through charge density, $\rho(\bar{r},t)$, and convection current density, $\bar{J}(\bar{r},t)$. An exact definition of these source terms requires knowledge of the position and velocity of each of the constituent carriers of the semiconductor plasma. For tractability, however, a statistical description is employed in which a distribution of carrier velocities is defined. This distribution function, $f(\bar{r},\bar{u},t)$, may be used to determine macroscopic properties of the semiconductor plasma. For example, the zeroeth moment of the velocity distribution function yields the average number density,

$$n(\bar{r},t) = \int_{\text{all } u} f(\bar{r},\bar{u},t)\, d^3\bar{u} \qquad 4\text{-}1$$

while taking the first moment leads to the average velocity,

$$\bar{v} = \frac{1}{n(\bar{r},t)} \int_{\text{all } u} \bar{u}(\bar{r},t)\, f(\bar{r},\bar{u},t)\, d^3u \qquad 4\text{-}2$$

Using these definitions of average number density and average velocity, the charge density and convection current density may be defined as

$$\rho(\bar{r},t) = \sum_{s=1}^{S} q_s n_s(\bar{r},t) \,, \qquad 4\text{-}3$$

and

$$\bar{J}(\bar{r},t) = \sum_{s=1}^{S} q_s n_s(\bar{r},t)\, v_s(\bar{r},t) \quad , \qquad 4\text{-}4$$

where the individual constituent carrier species are denoted by the subscript s, e.g. q_s is the charge of the s^{th} type carrier. The time variation of velocity distribution function is described by the Boltzman equation. For a multiconstituent plasma, such as the semiconductor under consideration, the Boltzman equation for each carrier species[83] is given by

$$\frac{\partial f_s}{\partial t} + \bar{u}\cdot\nabla_r f_s + \frac{q_s}{m_s^*}\left(\bar{E} + \bar{u}\times\bar{B}\right)\cdot\nabla_u f_s = \left(\frac{\partial f_s}{\partial t}\right)_c + \left(\frac{\partial f_s}{\partial t}\right)_{G\text{-}R} \qquad 4\text{-}5$$

where the effect of the periodic potential of the crystalline lattice is accounted for by using an effective mass, m_s^*[84]. The two terms on the right hand side of the equation represent, respectively, the rate of change of the distribution function due to collisions (scattering) and generation and recombination of carriers.

Moments of the distribution function are taken to determine the macroscopic properties of a plasma. Similarly, moments of the Boltzman equation yield equations describing the time variation of these properties. The zeroeth moment of the Boltzman equation yields the continuity equation,

$$\nabla_r\cdot\left(n_s\bar{v}_s\right) + \frac{\partial n_s}{\partial t} = S_s \qquad 4\text{-}6$$

which expresses conservation of s type particles. The terms S_s represents the rate at which particles of type s are gained (or lost). By summing over all possible current carriers the continuity equation (Equation 4-6) may be reexpressed as

$$\nabla_r \cdot \bar{J} + \frac{\partial \rho}{\partial t} = 0 \,, \qquad 4\text{-}7$$

Taking the first moment of the Boltzman equation leads to the momentum transfer equation [83, 86]

$$\frac{\partial \bar{v}_s}{\partial t} + \bar{v}_s \cdot \nabla_r \bar{v}_s = \frac{q_s}{m_s^*}(\bar{E} + \bar{v}_s \times \bar{B}) - \nu_s \bar{v}_s - \frac{\nabla_r \cdot \|P_s\|}{n_s m_s^*} \qquad 4\text{-}8$$

where $\|P_s\| = \int_{\text{all } u} m_s^* (\bar{u}_s - \bar{v}_s)(\bar{u}_s - \bar{v}_s) f(\bar{r}, \bar{u}, t)\, d^3u$ is the kinetic pressure tensor and $\nu_s \bar{v}_s = \frac{1}{n_s} \int_{\text{all } u} \bar{u} \left(\frac{\partial f_s}{\partial t}\right)_c d^3u$ represents impurity and lattice scattering loss. The evaluation of the pressure tensor depends on the energy transfer equation which is the second moment of the Boltzman equation. To terminate the equations at this point one usually assumes a form for $\|P_s\|$. If the distribution function is assumed to be isotropic [86] the tensor is diagonal with equal on-diagonal elements. These terms represent the energy departure of the carriers from the mean. Assuming that the velocity distribution function may be represented by a displaced Maxwellian distribution, the right-most term in Equation 4-8 may

be rewritten as

$$\frac{\nabla_r \cdot \| P_s \|}{n_s m_s^*} = \frac{\nabla_r (3 n_s k T_s)}{n_s m_s^*} = v_{T_s}^2 \frac{\nabla_r n_s}{n_s} \qquad 4\text{-}9$$

where $v_{T_s} = \sqrt{\frac{3 k T_s}{m_s^*}}$ is the themal velocity of the s^{th} type carrier.

Equation 4-7 and 4-8 are the hydrodynamic equations characterizing a semiconductor plasma. Such a macroscopic description may be used in studying electromagnetic phenomena in plasmas provided the phenomena of interest arise from the collective behavior of the system. A species will behave collectively when the wavelength of the response, λ , is much greater than the Debye Length,[87]

$$\lambda \gg \lambda_D = \left[\frac{k T_s \epsilon}{n_s q_s^2}\right]^{1/2} \qquad 4\text{-}10$$

In the above discussion the effect of the periodic lattice is accounted for by the introduction of an effective mass. At the surface of the semiconductor, however, the periodic potential abruptly terminates, an effect which Tamm[88] and Shockley[89] have shown leads to energy levels in the forbidden gap. These states, localized at the surface, have a bearing on the carrier concentrations and transport processes near the crystal boundary. Additionally, the rearrangement in crystal structure brought about by the surface discontinuity causes the surface atoms to readily interact with foreign atoms causing

oxide buildup (or impurity adsorption) which also influences the properties in the region of the surface.[90, 91]

In the absence of surface states and externally applied fields the energy bands of a uniformly doped semiconductor continue straight up to the surface and the surface concentration equals the bulk concentration. In the presence of surface states this is no longer the case. Localized states in the forbidden gap, in numbers approximately equal to the number of surface atoms in the crystal, have a profound influence on the shape of the energy bands and the carrier concentrations. Accumlation, depletion or even inversion layers may result depending on the concentration, energy level and type (donor or acceptor) of surface state present.

When an external electric field is applied normal to the surface, the potential variation and, hence, the carrier concentration near the surface are affected. Thus, an external field may be used to modulate the conductivity of the space charge region. When this is done, however, it is found that both fast and slow surface states exist. The relatively quick response of the fast states, relaxation times less than a microsecond [92], is attributed to surface states within the semiconductor crystal. The occupancy of these states can change rapidly due to their close proximity to the space charge layer. (These fast states, because of their intimate contact with the semiconductor and their location in the forbidden gap, are associated with recombination of carriers at the surface.[93]) The slow surface states, on the other hand, are associated with the oxide film and/or adsorbed impurities [92] and cannot

readjust as rapidly as the fast states. Their slow relaxation may, depending on surface treatment and temperature, range from seconds to days.[94]

In addition to the difference in conductivity between the space charge region and the bulk brought about by the surface potential, the mobilities of the carriers near the surface generally differ from those in the bulk. Carriers drifting in proximity to the surface are subject, not only to normal bulk scattering, but to scattering by the surface as well. This additional scattering reduces the mobility of carriers near the surface to values below that of the bulk. The degree to which this affects overall carrier transport depends on the thickness of the sample relative to the width of the surface layer as well as the type of space charge region[95].

The above illustrates how carrier transport is affected by the presence of the surface and its associated space charge layer. Additionally, the space charge region is affected by currents drifting in the semiconductor. Concern is primarily directed toward the case under consideration in this chapter, that of a semiconductor in which carriers are drifted in a direction parallel to the surface and normal to a static magnetic field lying in the plane of the surface. Under these conditions, carriers will be forced toward one side of the semiconductor setting up a Hall field and altering the distribution of carriers in the space charge layer. Determination of the charge distribution in this instance is extremely complicated. However, under moderate injection conditions when quasi-equilibrium can be assumed to prevail in the semiconductor, the general features of the space charge layers, discussed above,

remain essentially unaltered.

4.2 Semi-infinite Model of Semiconductor-Ferromagnetic Insulator Structure

In this section a model is developed of a structure consisting of a ferromagnetic insulator and a semiconductor. While the model is based on the media characteristics described in the preceding section and chapters, certain simplifications consistent with the physics of the problem are introduced.

The configuration that is to be studied is shown in Figure 4-1. The two media are assumed to be in intimate contact, the interface lying in the $\hat{y}$-$\hat{z}$ plane. Both the semiconductor and the ferrite are exposed to a static magnetic field which is $\hat{z}$ directed. Additionally, a d.c. electric field is applied to the semiconducting medium. The polarity of this field is such that the current within the semiconductor is caused to flow in the negative $\hat{y}$ direction.

In general, the lengths ($\hat{y}$ direction) and widths ($\hat{z}$-direction) of the semiconductor and ferrite are not equal. Considerable simplification can be achieved by assuming the width and length of both samples to be much larger than their thicknesses ($\hat{x}$ direction) and, more importantly, the excitation wavelength, λ , so that the effect of the presence of these transverse boundaries on the r.f. response is negligible.

Considering a centrally located region far removed from the boundaries in the $\hat{y}$ and $\hat{z}$ directions results in the magnetization within the ferrite being uniform in these directions. The carrier density in the semiconductor also does not vary in the $\hat{y}$ and $\hat{z}$ directions because of

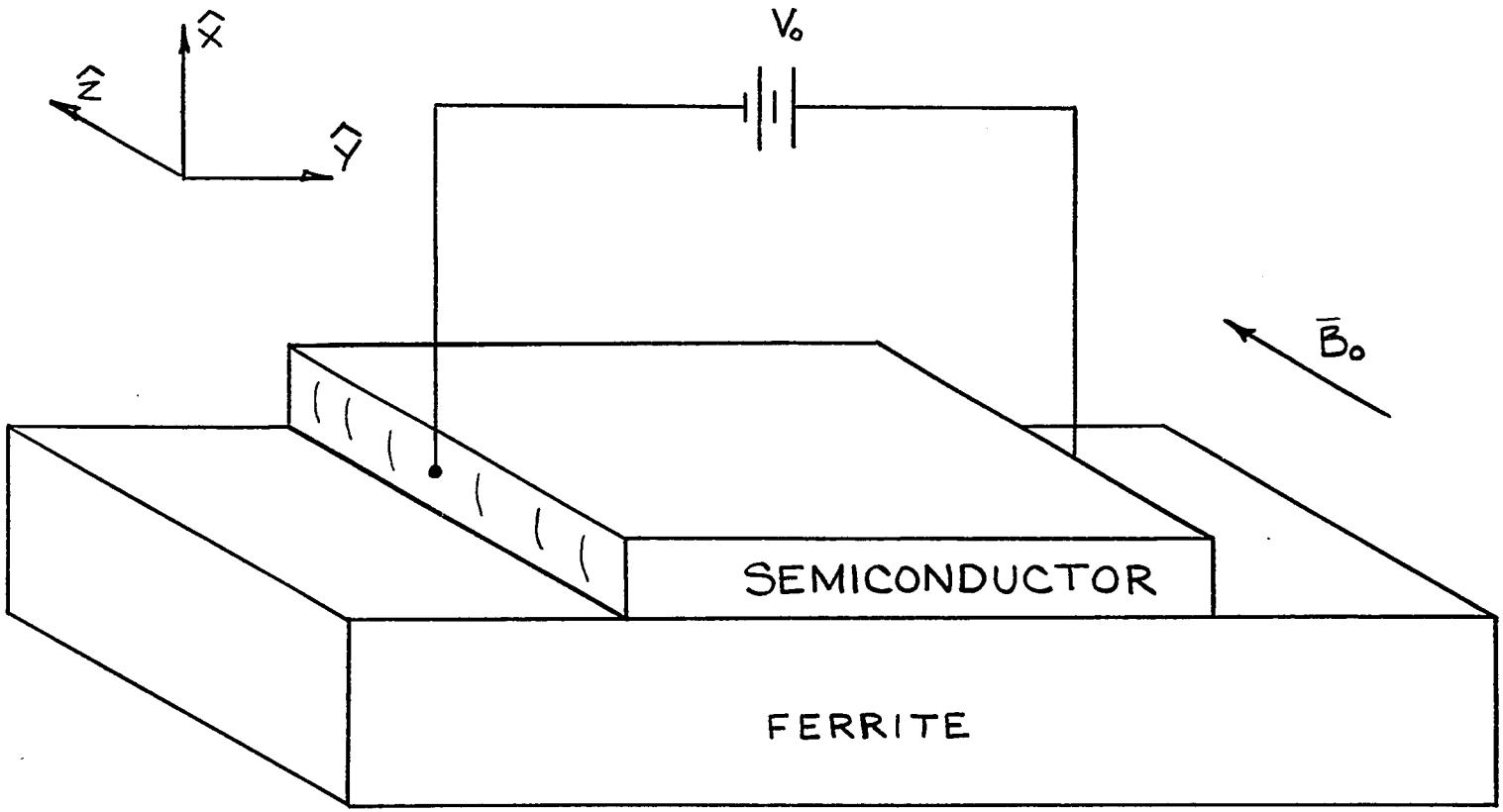

Figure 4-1 - Semiconductor-Ferromagnetic Insulator Structure

the remoteness of the surface regions and the current contacts. Thus, not only does this approximation dramatically reduce the number of boundary conditions that need be imposed, it additionally leads to a reduction in the complexity of the mode structure in the small signal limit.

Since attention is primarily directed toward the study of electromagnetic phenomena occuring at or near the interface between the semiconductor and the magnetic medium, it is convenient to begin the analysis by considering a semi-infinite model in which the boundaries in the positive and negative $\hat{x}$ directions are also assumed to be infinitely far from the interface. While such an approximation may not be appropriate if the magnetic material is very thin or the semiconductor is an epitaxial or highly non-uniformly doped material, it is a reasonable assumption if the materials are uniform over a distance which is large in comparison to the wavelength of the response.

In the semi-infinite model, the semiconductor bulk is characterized by uniform carrier concentrations and mobilities; near the interface with the magnetic material the semiconductor is characterized by a surface region whose conductivity and mobility differ from the bulk. Since the occupancy of the surface states cannot change as rapidly as the cyclic variations of the applied r.f. fields, the width and carrier density of the surface region are assumed to remain constant. As an approximation of the conditions existing near the surface, the semiconductor is assumed to consist of two adjacent regions, one semi-infinite and the other having a fixed finite width, with different carrier densities and different mobilities; these parameters being uniform in each region.

It may be determined from curves published in the literature[96,97] that the width of an accumulation region, as measured by the effective center of space charge,

$$L_c = \frac{\int_0^\infty \rho x \, dx}{\int_0^\infty \rho \, dx} , \qquad 4\text{-}11$$

is smaller than a Debye length. As the electromagnetic phenomena under consideration are associated with the collective responses of the semiconductor system, their wavelengths must exceed this distance. Thus, the width of an accumulation region is small in comparison to the system wavelength and its presence is at first neglected. Similarly, when the surface is depleted, the number of carriers available to interact with the surface wave is less at the surface than in the bulk. Thus, if the width of the depletion region is smaller than the wavelength of the surface wave, the active interaction is determined by the bulk carriers. Thus, as a further simplification, the semiconductor is considered to be uniform throughout with no variation in drift velocity, mobility or average density with distance from the interface. The validity of this assumption is investigated in Chapter 5 where the effect on the interaction of surface accumulation and depletion regions is considered further.

The semi-infinite model is shown in Figure 4-2. The semi-infinite ferrite, described in Section 2.2, is assumed to be uniform with no explicit pinning mechanism at the surface.

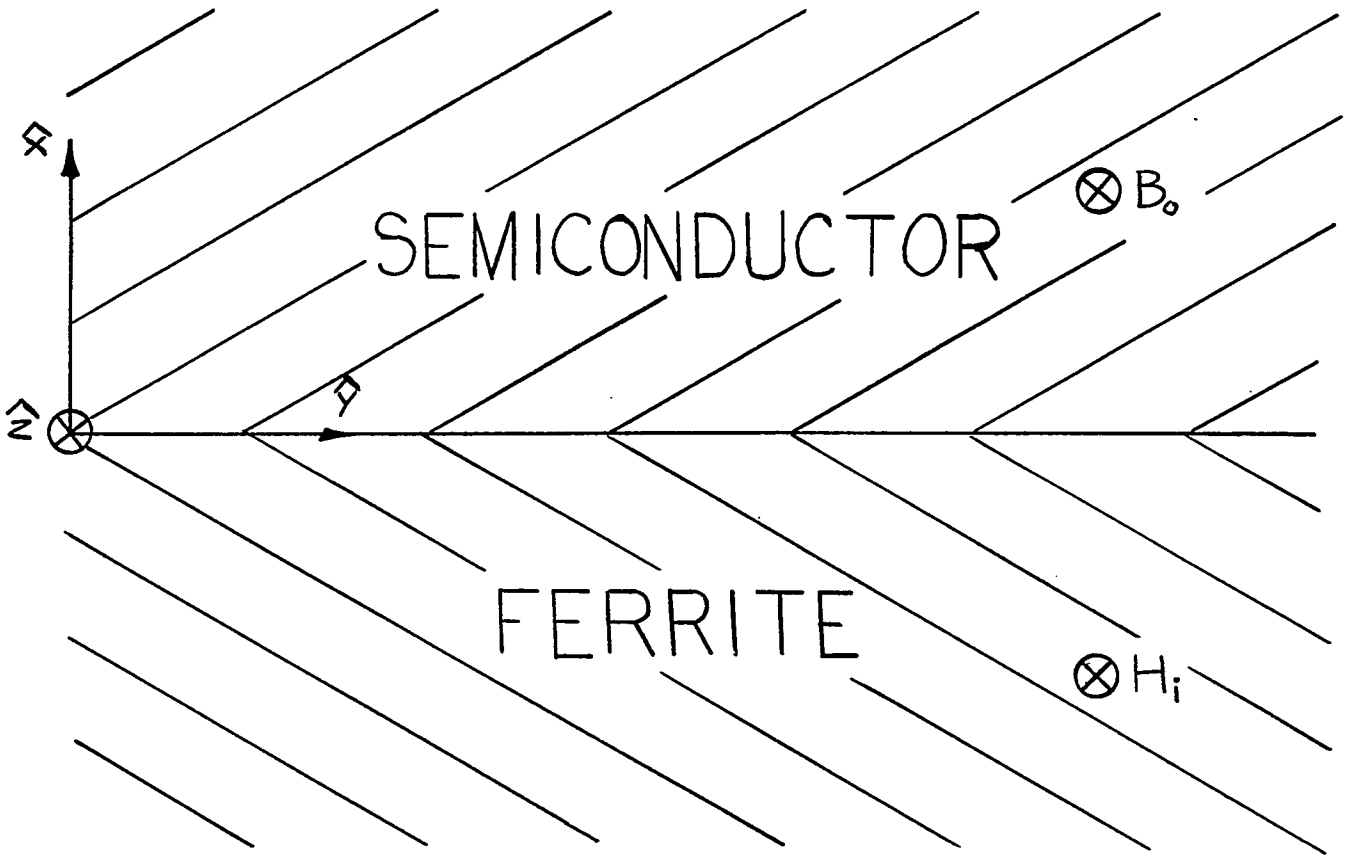

Figure 4-2 Semi-infinite Model of Semiconductor-Ferromagnetic Insulator Structure

4.3 Derivation of Dispersion Relation Describing Electromagnetic Surface Wave Propagation At The Interface Between a Semi-infinite Ferromagnetic Insulator And A Semi-infinite Semiconductor

In this section the dispersion characteristics of surface waves propagating along the interface between a semi-infinite semiconductor and an insulating ferromagnetic medium is determined. Assuming a solution of the appropriate surface wave form, the dispersion relationship is derived by satisfying Maxwell's equations in each medium as well as the boundary conditions at the interface.

The development of the equations describing the response of the structure of Figure 4-2 to electromagnetic excitations follows the procedures of Chapter 2. Since the ferrite occupies the lower half space, $x < 0$, the relations between the field quantities in this region are

$$E_{1mz} = G \exp[\beta_m x + j(\omega t - ky)] \qquad 4\text{-}12$$

$$H_{1mx} = \left[\frac{k\mu_{11} - \beta_m \mu_{12}}{\omega\mu_o(\mu_{11}^2 - \mu_{12}^2)}\right] E_{1mz} \qquad 2\text{-}74$$

and

$$H_{1my} = j\left[\frac{k\mu_{12} - \beta_m \mu_{11}}{\omega\mu_o(\mu_{11}^2 - \mu_{12}^2)}\right] \qquad 2\text{-}75$$

where consistancy with Maxwell's equations requires that β_m be related to k through the relation

$$D_k = k^2 - \beta_m^2 = \frac{\omega^2}{c_m^2}\left(\frac{\mu_{11}^2 - \mu_{12}^2}{\mu_{11}}\right) \qquad 2\text{-}95$$

The relations between the field quantities in the semiconductor are derived by assuming a traveling surface wave excitation of the form

$$\exp\left[-\beta_{sc}x + j(\omega t - ky)\right] \qquad 4\text{-}13$$

where β_{sc} must have a real part greater than zero since the semiconductor occupies the half space $x > 0$. Assuming small signal linearization

$$\bar{E}_{sc} = -E_o\hat{y} + \bar{E}_{1sc}\exp\left[-\beta_{sc}x + j(\omega t - ky)\right], \qquad 4\text{-}14$$

$$\bar{v}_s = -v_{os}\hat{y} + \bar{v}_{1s}\exp\left[-\beta_{sc}x + j(\omega t - ky)\right], \qquad 4\text{-}15$$

$$\bar{J}_s = -J_s\hat{y} + \bar{J}_{1s}\exp\left[-\beta_{sc}x + j(\omega t - ky)\right], \qquad 4\text{-}16$$

and

$$\rho_s = \rho_{os} + \rho_{1s}\exp\left[-\beta_{sc}x + j(\omega t - ky)\right], \qquad 4\text{-}17$$

where higher order terms are considered to be negligibly small. Maxwell's curl equations, 2-1 and 2-2, may be written for the first order quantities as

$$\nabla \times \bar{E}_{1sc} = -j\omega\bar{B}_{1sc} = -j\omega\mu_o\bar{H}_{1sc}, \qquad 4\text{-}18$$

and

$$\nabla \times \bar{H}_{1sc} = \bar{J}_1 + j\omega\epsilon_o\epsilon_{sc}\bar{E}_{1sc}, \qquad 4\text{-}19$$

where

$$\bar{J}_1 = \sum_{s=1}^{S}\bar{J}_{1s}, \qquad 4\text{-}20$$

since S individual carrier species are considered (e.g. electrons and holes, upper valley and lower valley electrons). The equation of motion for the s^{th} type carrier, Equations 4-8 and 4-9, may be reexpressed as

$$\frac{d\bar{v}_s}{dt} = \eta_s^* \left(\bar{E} + \bar{v}_s \times \bar{B} \right) - \nu_s \bar{v}_s - v_{th}^2 \frac{\nabla \rho_s}{\rho_s} \qquad 4\text{-}21$$

where

$$\eta_s^* = \frac{q_s}{m_s^*} \qquad 4\text{-}22$$

and

$$\rho_s = q_s n_s \ . \qquad 4\text{-}23$$

Substituting the linearized quantities, 4-14 through 4-17, into equation 4-21 one obtains to the first order

$$j(\omega + k v_{os} - j\nu_s) \begin{bmatrix} v_{1sx} \\ v_{1sy} \\ v_{1sz} \end{bmatrix} = \eta_s^* \begin{bmatrix} E_{1scx} \\ E_{1scy} \\ E_{1scz} \end{bmatrix} + \eta_s^* \begin{bmatrix} B_o v_{1sy} \\ -B_o v_{1sx} \\ 0 \end{bmatrix} + \eta_s^* \begin{bmatrix} -v_{os} B_{1scz} \\ 0 \\ v_{os} B_{1scx} \end{bmatrix} - \frac{v_{th}^2}{\rho_{os}} \begin{bmatrix} -\beta_{sc} \rho_{1s} \\ -jk\rho_{1s} \\ 0 \end{bmatrix} . \qquad 4\text{-}24$$

Noting that Equation 4-18 stipulates that the $\hat{x}$ component of $\bar{B}_{1sc}$ is related to E_{1scz} through the relation

$$B_{1scx} = \frac{k}{\omega} E_{1scz} \ , \qquad 4\text{-}25$$

the $\hat{z}$ component of Equation 4-24 is

$$v_{1sz} = -j \frac{\eta_s^* (\omega + k v_{os}) E_{1scz}}{\omega (\omega + k v_{os} - j\nu_s)} \ . \qquad 4\text{-}26$$

Therefore, the $\hat{z}$ directed current density may be written as

$$J_{1z} = -j \omega \epsilon_o \epsilon_{sc} \sum_{s=1}^{S} \frac{\omega_{ps}^2 (\omega + k v_{os}) E_{1scz}}{\omega^2 (\omega + k v_{os} - j\nu_s)} \ , \qquad 4\text{-}27$$

where

$$\omega_{ps} = \left[\frac{\rho_s \eta_s}{\epsilon_o \epsilon_{sc}}\right]^{1/2} = \text{plasma frequency of } s^{th} \text{ type of carrier.} \qquad 4\text{-}28$$

For this special case, where $\frac{\partial}{\partial z} = 0$, the fields are again separable into two uncoupled sets; one TE_y and the other TM_y. It was shown in Section 2.3 that TM_y waves propagating in a direction perpendicular to the direction of magnetization are, to the first order, unaffected by the spin system. This is equivalent to the case where a TM_y wave propagates along the interface between a semiconductor and a dielectric. The propagation characteristics of waves supported by a thin semiconductor bounded by dielectric media have been investigated by Swartz and Robinson[98]. Robinson and Swartz have also considered the properties of a structure consisting of alternating semiconducting and dielectric layers[99].

The TE_y components are obtained by assuming that

$$E_{1scz} = C \exp[-\beta_{sc} x + j(\omega t - ky)] \qquad 4\text{-}29$$

and substituting into Equation 4-18 resulting in

$$H_{1scx} = \frac{kC}{\omega\mu_o} \exp[-\beta_{sc} x + j(\omega t - ky)], \qquad 4\text{-}30$$

and

$$H_{1scy} = j\frac{\beta_{sc} C}{\omega\mu_o} \exp[-\beta_{sc} x + j(\omega t - ky)]. \qquad 4\text{-}31$$

Substitution of the expressions for the $\hat{z}$ directed current density, J_{1z}, and the TE_y field components into Equation 4-19 yields the dispersion relation describing wave propagation in the semiconducting medium

$$k^2 - \beta_{sc}^2 = \frac{\omega^2}{c_{sc}^2}\left[1 - \sum_{s=1}^{S} \frac{\omega_{ps}^2(\omega + kv_{os})}{\omega^2(\omega + kv_{os} - j\nu_s)}\right], \qquad 4\text{-}32$$

where c_{sc} is the velocity of light in the semiconductor

$$c_{sc} = \frac{1}{\sqrt{\mu_o \epsilon_o \epsilon_{sc}}} . \qquad 4\text{-}33$$

While the solutions obtained above satisfy Maxwell's equations in each medium, self-consistancy demands that the solutions satisfy Maxwell's equations at the interface as well. At x=0 the boundary conditions are given by

$$\hat{x} \cdot (\bar{D}_{1m} - \bar{D}_{1sc}) = \text{surface charge density}, \qquad 4\text{-}34$$

$$\hat{x} \times (\bar{E}_{1m} - \bar{E}_{1sc}) = 0, \qquad 4\text{-}35$$

$$\hat{x} \cdot (\bar{B}_{1m} - \bar{B}_{1sc}) = 0, \qquad 4\text{-}36$$

and

$$\hat{x} \times (\bar{H}_{1m} - \bar{H}_{1sc}) = \text{surface current density}. \qquad 4\text{-}37$$

Due to the interrelationships between the field quantities Equations 4-35 and 4-36 are equivalent and only the condition expressing the continuity of the tangential components of the electric field need be considered. Similarly, Equations 4-34 and 4-37 are equivalent. Since the modes under investigation are TE_y and contain no component of D_1 normal to the surface, Equation 4-37 is the remaining condition which must be satisfied at the interface. Due to the finite conductivities of the adjacent media, no surface current

exists at the boundary leading to

$$H_{1my} = H_{1scy} \quad . \tag{4-38}$$

Applying Equation 4-35 to the r.f. electric field and neglecting pinning coupled exchange effects

$$E_{1mz}(0) = G \exp[j(\omega t - ky)] = C\exp[j(\omega t - ky)] = E_{1scz}(0), \tag{4-39}$$

resulting in

$$G = C. \tag{4-40}$$

The boundary condition on the tangential component of the magnetic field intensity together with Equation 4-40 leads to

$$\beta_{sc} = \left[\frac{k\mu_{12} - \beta_m \mu_{11}}{(\mu_{11}^2 - \mu_{12}^2)}\right], \tag{4-41}$$

the dispersion equation relating the transverse wavenumbers in the semiconductor and ferrite.

Equations 2-95, 4-32 and 4-41 are the single mode exchange modified dispersion relations describing electromagnetic surface wave propagation along the interface between a semi-infinite semiconductor and a semi-infinite ferromagnetic insulator. Robinson et. al.,[23] who obtained similar equations for the single carrier species case, analyzed the dispersion relations in the magnetostatic limit. Using parameters approximately representative of a YIG-InSb composite structure at room temperature, they found that the system could support a convective instability at X-band

frequencies. Schlömann[18] also found that amplification of magnetstatic surface waves was possible in a structure consisting of a thin semiconductor (InSb) in contact with a semi-infinite ferrite (YIG) magnetized in the plane of the mutual interface. (Schlomann's results are described more fully in Chapter 5 where geometrical effects are considered). The initial numerical analysis of the exhange modified dispersion relation, including the effects of electromagnetic propagation, is also performed using YIG-InSb parameters. Information concerning the validity of the magnetostatic approximation as well as new information concerning the propagation of surface waves supported by a ferrite bounded by a semiconductor plasma is thereby obtained.

The dispersion characteristics are computed using a procedure similar to that outlined in Section 2.3. Whereas in Chapter 2 it was only necessary to solve the equations for real values of frequency, the analytic techniques employed in the present chapter to determine directions of propagation and classify instabilities require that the equations be solved for complex values of frequency. First the roots of Equations 2-95 are obtained and the solution corresponding to the value of D having the smallest magnitude is selected. (The other two roots correspond to exchange modes and are neglected). Using Equation 2-95, β_m is eliminated from Equation 4-41 resulting in

$$\beta_{sc\pm} = \frac{k\mu_{12} \mp \mu_{11}\sqrt{k^2 - D_k}}{(\mu_{11}^2 - \mu_{12}^2)}, \qquad 4\text{-}42$$

where the permeability tensor components are evaluated using the complex values of ω and D_K specified. Squaring both sides of Equation 4-42 and substituting the result into Equation 4-32 yields

$$\left[1-\frac{(\mu_{11}^2+\mu_{12}^2)}{(\mu_{11}^2-\mu_{12}^2)^2}\right]k^2+\frac{2\mu_{11}\mu_{12}k\sqrt{k^2-D_K}}{(\mu_{11}^2-\mu_{12}^2)^2}+\frac{\mu_{11}^2 D_K}{(\mu_{11}^2-\mu_{12}^2)^2}-\frac{\omega^2}{c_m^2}\left[1-\sum_{s=1}^{S}\frac{\omega_{ps}^2(\omega+kv_{os})}{\omega^2(\omega+kv_{os}-j\nu_s)}\right]=0, \quad 4\text{-}43$$

and

$$\left[1-\frac{(\mu_{11}^2+\mu_{12}^2)}{(\mu_{11}^2-\mu_{12}^2)^2}\right]k^2-\frac{2\mu_{11}\mu_{12}k\sqrt{k^2-D_K}}{(\mu_{11}^2-\mu_{12}^2)^2}+\frac{\mu_{11}^2 D_K}{(\mu_{11}^2-\mu_{12}^2)^2}-\frac{\omega^2}{c_m^2}\left[1-\sum_{s=1}^{S}\frac{\omega_{ps}^2(\omega+kv_{os})}{\omega^2(\omega+kv_{os}-j\nu_s)}\right]=0. \quad 4\text{-}44$$

Elimination of the radical term by the multiplication of Equation 4-43 by 4-44 results in the dispersion relationship describing surface wave propagation along the interface between a semi-infinite semiconductor and an insulating ferromagnetic material,

$$\left[(\mu_{11}^2-\mu_{12}^2)^2-2(\mu_{11}^2+\mu_{12}^2)+1\right]k^4$$

$$+2\left\{\frac{\mu_{11}^2 D_K\left[(\mu_{11}^2-\mu_{12}^2)-1\right]}{(\mu_{11}^2-\mu_{12}^2)}-\frac{\omega^2}{c_m^2}\left[1-\sum_{s=1}^{S}\frac{\omega_{ps}^2(\omega+kv_{os})}{\omega^2(\omega+kv_{os}-j\nu_s)}\right]\left[(\mu_{11}^2-\mu_{12}^2)^2-(\mu_{11}^2+\mu_{12}^2)\right]\right\}k^2$$

$$+\left\{\frac{\mu_{11}^2 D_K}{(\mu_{11}^2-\mu_{12}^2)}-\frac{\omega^2}{c_{sc}^2}\left[1-\sum_{s=1}^{S}\frac{\omega_{ps}^2(\omega+kv_{os})}{\omega^2(\omega+kv_{os}-j\nu_s)}\right](\mu_{11}^2-\mu_{12}^2)\right\}^2=0 \quad 4\text{-}45$$

Equation 4-45, which because of the non-zero carrier densities ($\omega_{ps}\neq 0$) is not biquadratic in k, may be solved to yield 4+2S values of k. In order to determine which of these roots correspond to surface modes, the

corresponding transverse wavenumbers must be examined. Using an algorithm similar to that shown in Figure 2-7, with $\beta_{d|1,2,3,4}$ replaced by $\beta_{sc|1,2,3,4}$, each of the 4+2S roots is tested in order to ascertain whether it is associated with transverse wavenumbers whose real parts are positive. Furthermore, each wavenumber set k, β_m, β_{sc} is checked to ensure that it self-consistantly satisfies the dispersion relations.

The above procedure is used to compute semi-infinite ferrite-semiconductor surface mode dispersion characteristics which are plotted in Figure 4-3 for the case where the semiconductor is assumed collisionless. In the absence of collisions the spin system and streaming carriers are uncoupled as may be verified by setting $\nu_s = 0$ in Equation 4-45. (An analogous situation occurs for TE_y propagation perpendicular to the internal magnetic field within an infinite magnetic semiconductor. This is demonstrated in Appendix II). The solid curve in Figure 4-3 is plotted for ferrite parameters appropriate to YIG, the saturation magnetization equal to 1750 Oe., $\epsilon_m = 14$, $T_C = 550^0$ K, $a_1 = 12.37$ A, and $\gamma = 2.0$. The uniform internal field is assumed to be equal to 1800 Oe and losses in the magnetic system are neglected. The semiconductor parameters are selected to correspond to intrinsic InSb at room temperature, having an electron concentration of approximately $10^{16}/cm^3$. [100] Since the effective mass of the electrons is much less than that of the holes, $m_e^* = .01\ m_o$ as compared to $m_h^* = .18\ m_o$, [101] only the presence of the electrons is considered. (The effect of the presence of holes is considered in more detail in the

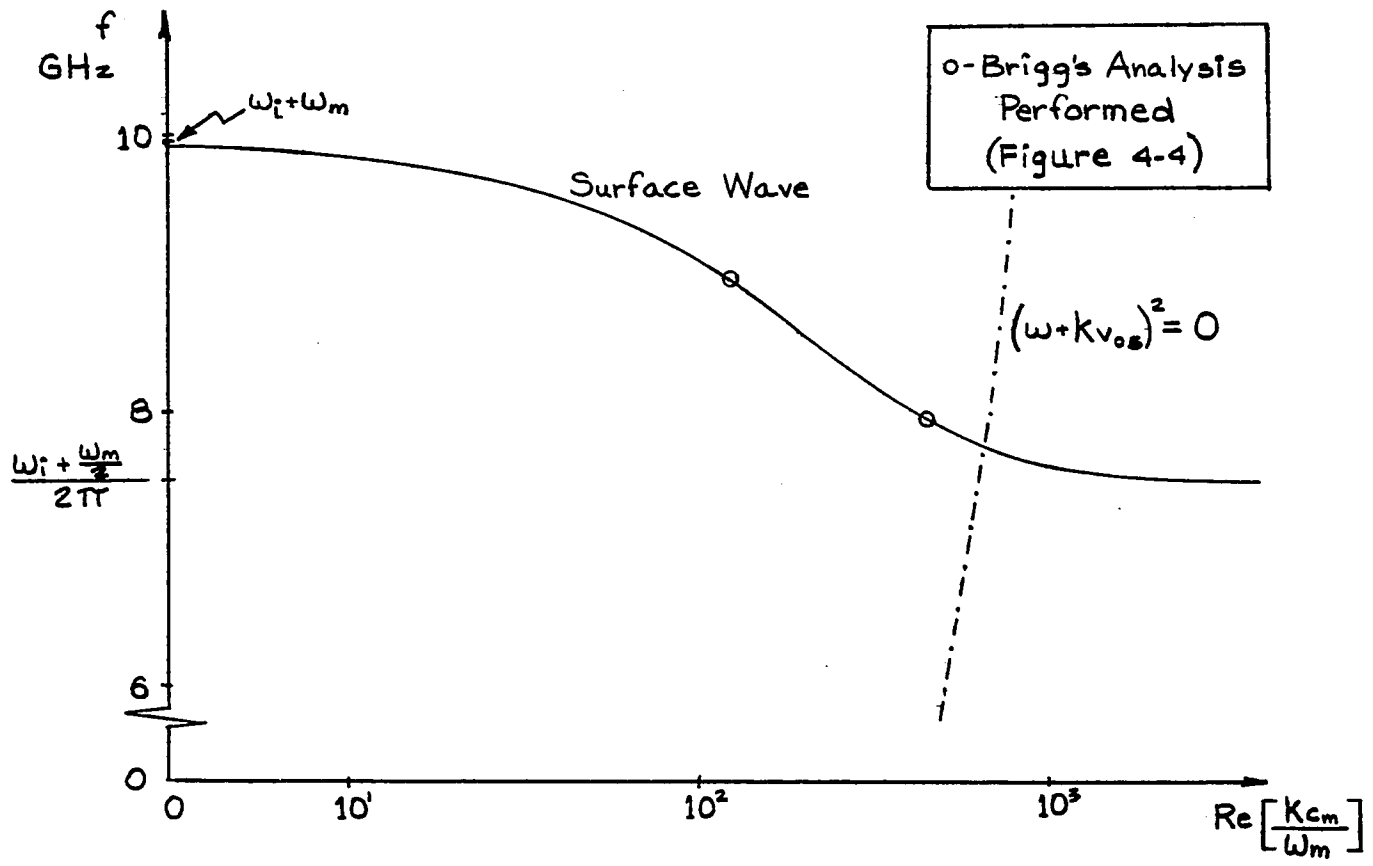

Figure 4-3 Semi-infinite Ferrite-Semiconductor Surface Mode Dispersion Characteristics - $\nu_s=0$, $\Delta H=0$.

following section). The relative permittivity of the semiconducting medium is taken to be 15.6.

Examination of the characteristics reveals that for the parameters selected there is only one surface mode, this mode having a positive phase velocity. While the surface wave has a resonance at $\omega_{res} = \omega_i + \frac{\omega_m}{2}$, as did the forward "magnetostatic" mode of Chapter 2, $\frac{\partial \omega}{\partial k}$ is negative, with the frequency range extending from the resonance to an upper limit of approximately $\omega_u = \omega_i + \omega_m$. Because of the negative group velocity it appears that signal flow in the lossless semi-infinite InSb-YIG structure, with a $\hat{z}$ directed static magnetic field, is in the negative $\hat{y}$ direction. This may be verified through the use of a modified version of Briggs' instability criteria.[102] The criteria, through which instabilities may be classified as to type, convective (growing with distance) or absolute (growing in time) instabilities, permit one to distinguish between amplifying and evanescent waves by determining the direction of signal flow. Briggs' instability analysis involves mapping the complex ω plane into the complex k plane, the shape of the resultant contours indicating how the system behaves.[103] Essentially, loss is introduced into the system through the imaginary component of the complex frequency. The direction of signal flow is then determined by observing the locus of the roots of the dispersion relation as the loss is varied. It the system exhibits a convective instability the imaginary part of the wavenumber changes sign as the imaginary part of the complex frequency is made negative. This

corresponds to sufficient loss being introduced into the system that the amplifying wave is transformed into a decaying wave. It the wave is evanescent the change in sign does not occur. On the other hand, an absolute or non-convective instability exists when the dispersion relation admits a double root of k for some complex value of frequency with negative imaginary part and, furthermore, as the imaginary part of the frequency is made more negative, the roots diverge such that one of them crosses the $\mathrm{Im}[k] = 0$ axis. [102]

The locus of roots obtained as the imaginary part of ω is made negative has been plotted in Figure 4-4 for two points on the characteristic of Figure 4-3 corresponding to frequency values $\omega = \omega_i + 0.6\omega_m$ and $\omega = \omega_i + 0.8\omega_m$. It is observed that the imaginary part of k becomes positive as the imaginary part of ω becomes negative. This indicates that the direction of signal flow is in the negative $\hat{y}$ direction, confirming the conclusions expressed above. (Robinson et. al. [23] indicate that the root should be followed as the imaginary part of ω goes to $-\infty$, however, it is found that as the loss is increased a point is reached where the surface wave no longer exists. When this occurs the search is concluded).

The line consisting of alternate dots and dashes in Figure 4-3 corresponds to the double root of the collisionless dispersion equation, $(\omega + kv_{os}) = 0$, for $v_{os} = -2 \times 10^{+7}$ cm/sec. These synchronous modes are not surface modes when the streaming carriers and the spin system are uncoupled, however, one of them couples to the surface mode and takes on surface wave properties when collisions are introduced. In this way energy may be transferred

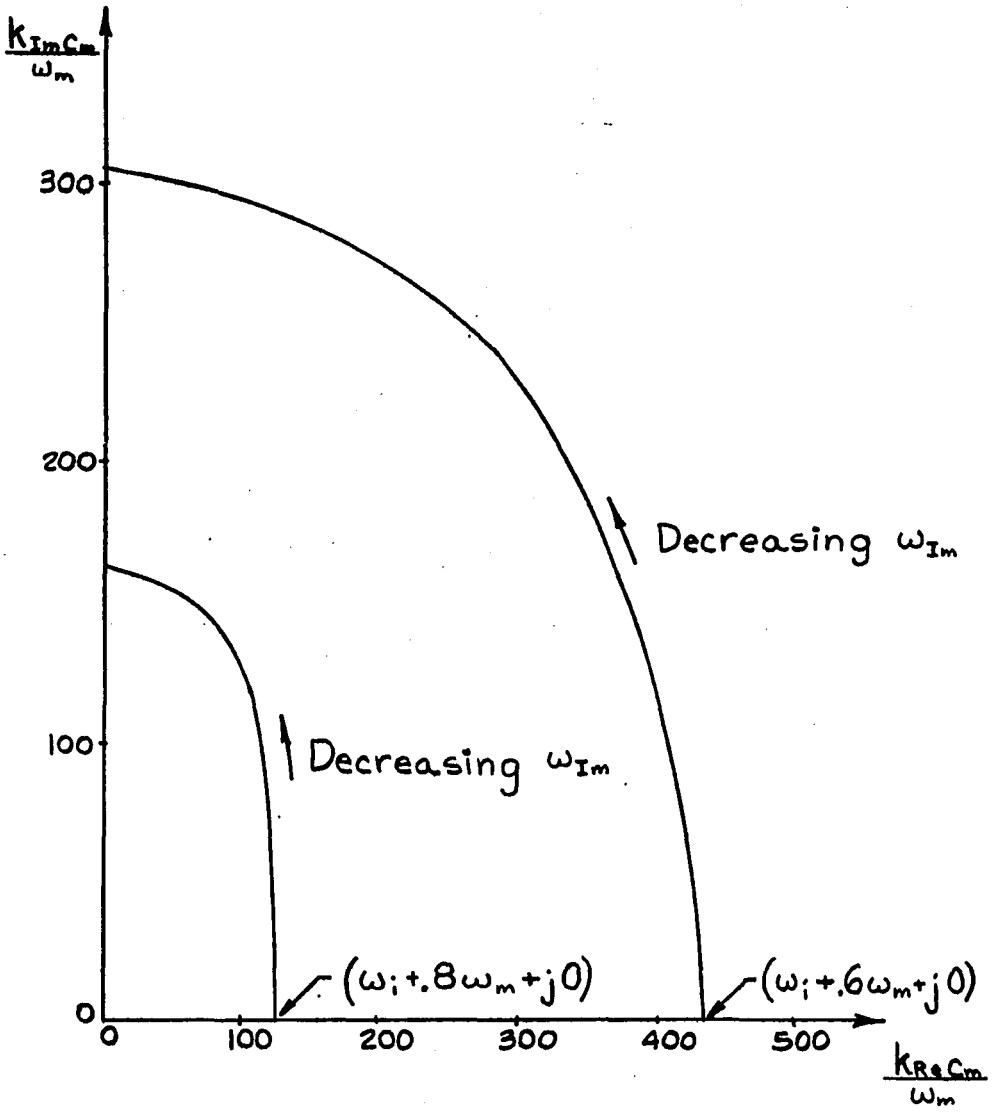

Figure 4-4 Locus of Roots Corresponding to $\omega_i + .6\omega_m + j\omega_{Im}$ **and** $\omega_i + .8\omega_m + j\omega_{Im}$; $\omega_{Im} < 0$, $\nu_s = 0$, $\Delta H = 0$.

from the carrier system to the spin system. Although the synchronous mode associated with the electron stream has a positive group velocity and the group velocity of the surface mode is negative, it cannot be inferred that active coupling of the modes leads to an absolute rather than a convective instability since the modes, when coupled, are appreciably altered and conclusions based on coupled mode theory would be inappropriate.[104]

When semiconductor and spin system losses are included in the dispersion relation computations, the dispersion characteristics are modified as shown in Figure 4-5, drawn for the same YIG and InSb parameters as in Figure 4-3 but with the ferrite linewidth changed to 0.35 Oe., the electron mobility ($\mu_e = \frac{e}{m_e^* \nu_e}$) of the semiconductor taken to be 80,000 cm^2/v-sec. corresponding to intrinsic InSb at room temperature[101] (This value is on the optimistic side, μ_e being given as 77,000 and 78,000 cm^2/v-sec. elsewhere.[100, 105, 106]) and the electron drift velocity set to zero. It is observed that with the introduction of losses the real part of the wavenumber no longer approaches infinity as the resonance is neared, but rather reaches a maximum at a finite value of k. Whereas the solutions for the lossless case indicate no wave propagation below the resonance, surface wave solutions are obtained below this frequency when losses are included. The additional surface mode branch, the lower frequency limit of which occurs at $\omega=\omega_i$, has a positive slope as did the "magnetostatic" surface modes investigated in Chapters 2 and 3. Whereas the imaginary part of the wavenumber of the portion of the surface wave spectrum above $\omega_i + \frac{\omega_m}{2}$ is

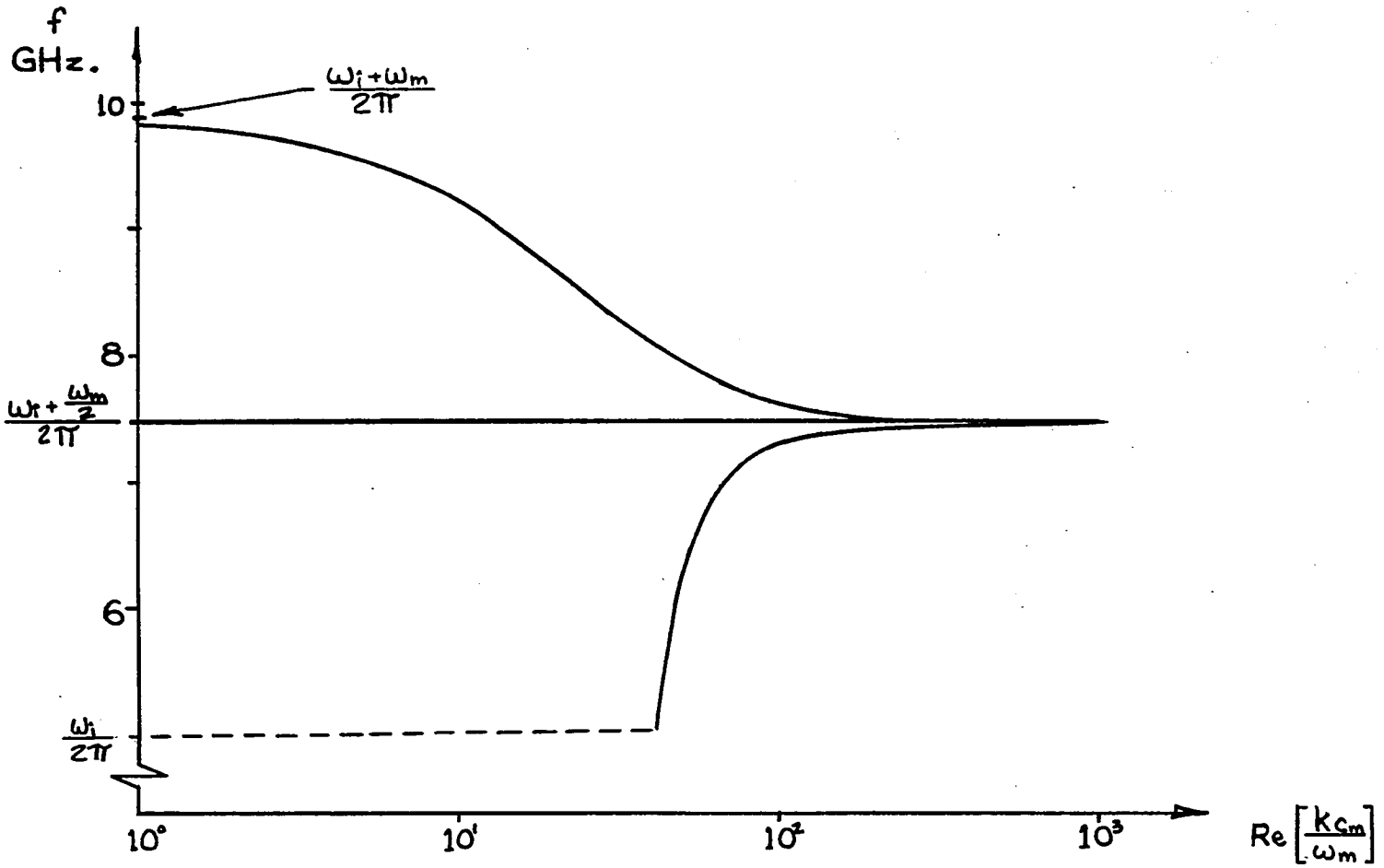

Figure 4-5 - Semi-infinite Ferrite-Semiconductor Surface Mode Dispersion Characteristics - $v_{os}=0$

positive, indicating propagation in the $-\hat{y}$ direction, Im [k] is negative below resonance. Applying the modified Briggs instability criteria confirms that the directions of propagation above and below the resonance are opposite.

As the resonance is approached from either the high frequency or low frequency portion of the spectrum, the real part of the wavenumber increases forming what appears to be a cusp at the resonance frequency. Close examination of this portion of the spectrum, Figure 4-6, reveals that as the resonance is approached from the low frequency end of the spectrum the real part of the wavenumber reaches a maximum below the resonance frequency and then decreases until the resonance frequency is reached. ($\frac{\partial \omega}{\partial k_{Re}} \longrightarrow \infty$ does not indicate that the signal energy travels at a velocity exceeding the velocity of light in the medium; the velocity of energy transport and the group velocity are not, in general, equal in dissipative dispersive media.[107] The correct direction of signal flow may be determined through the Briggs criteria.[102]) Over this portion of the spectrum, the imaginary component of the wavenumber remains negative, indicating that signal flow is in the positive $\hat{y}$ direction. This is confirmed by applying the modified Briggs criteria. At the resonance frequency the real part of the wavenumber reaches a local minimum, the sign of the imaginary part of the wavenumber becoming positive and remaining so as the frequency is increased, indicating signal flow in the negative $\hat{y}$ direction. Immediately above the resonance frequency the real part of the wavenumber increases until another maximum is reached whereupon any further increase in the

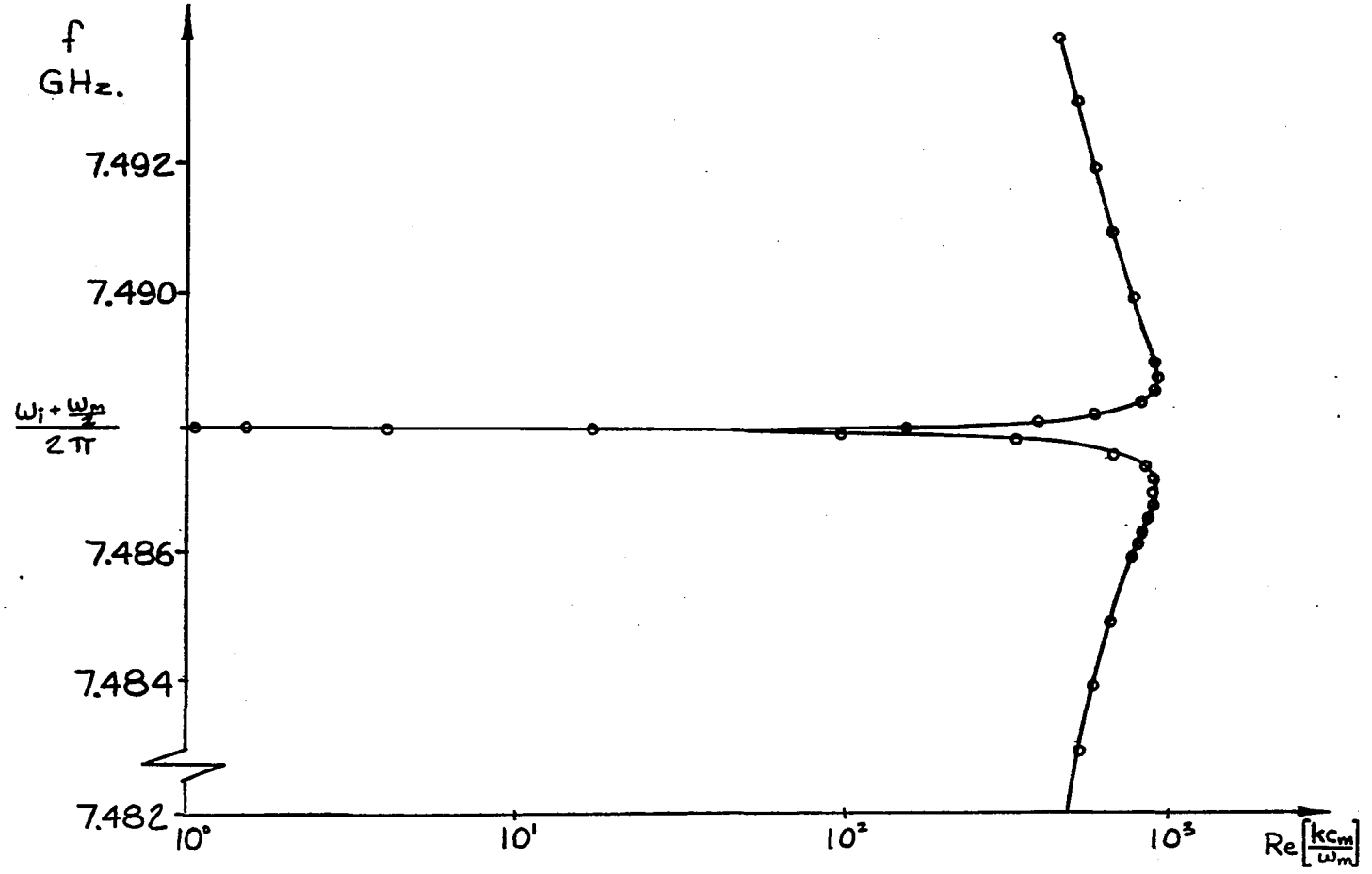

Figure 4-6 - Resonance Region of Semi-infinite Ferrite-Semiconductor Characteristics; $v_{os}=0$

frequency results in a decrease of the real part of the wavenumber.

When surface wave propagation along the interface of the semiconductor-magnetic insulator structure is considered with spin system and semiconductor losses included and the carrier stream drifted, a significant change in the dispersion characteristics results. The spectrum, which is plotted in Figure 4-7 for the same parameters as Figure 4-3 with $\Delta H = .35$ Oe., $\mu_e = 80,000$ cm^2/v-sec, $v_{os} = -v_{oe} = -2 \times 10^7$ cm/sec., indicates that in addition to a surface mode, which away from resonance is similar to that found for the undrifted case (referred to herein as the spin mode), a carrier stream mode, similar to the synchronous modes of Figure 4-3, also assumes surface mode properties. The frequency range of this carrier stream mode is smaller than the spin mode, having approximately the same lower frequency limit, $\omega = \omega_i$, but having an upper frequency limit at a frequency less than $\omega = \omega_i + \omega_m$, the upper limit of the spin mode (9.919 GHz versus 9.938 GHz for the parameters selected.) With the exception of the region near the resonance, both the spin mode and the carrier stream mode are evanescent, both modes propagating in the $+\hat{y}$ direction below the resonance region, while propagating in opposite directions above this region. Comparing the imaginary part of the spin mode wavenumber with that attained for the undrifted case, $v_{os} = 0$, at frequencies sufficiently far above and below the resonance region that such a comparison is valid, it is found that the loss rate experienced by the mode is reduced when electrons are drifted in the positive $\hat{y}$ direction as shown

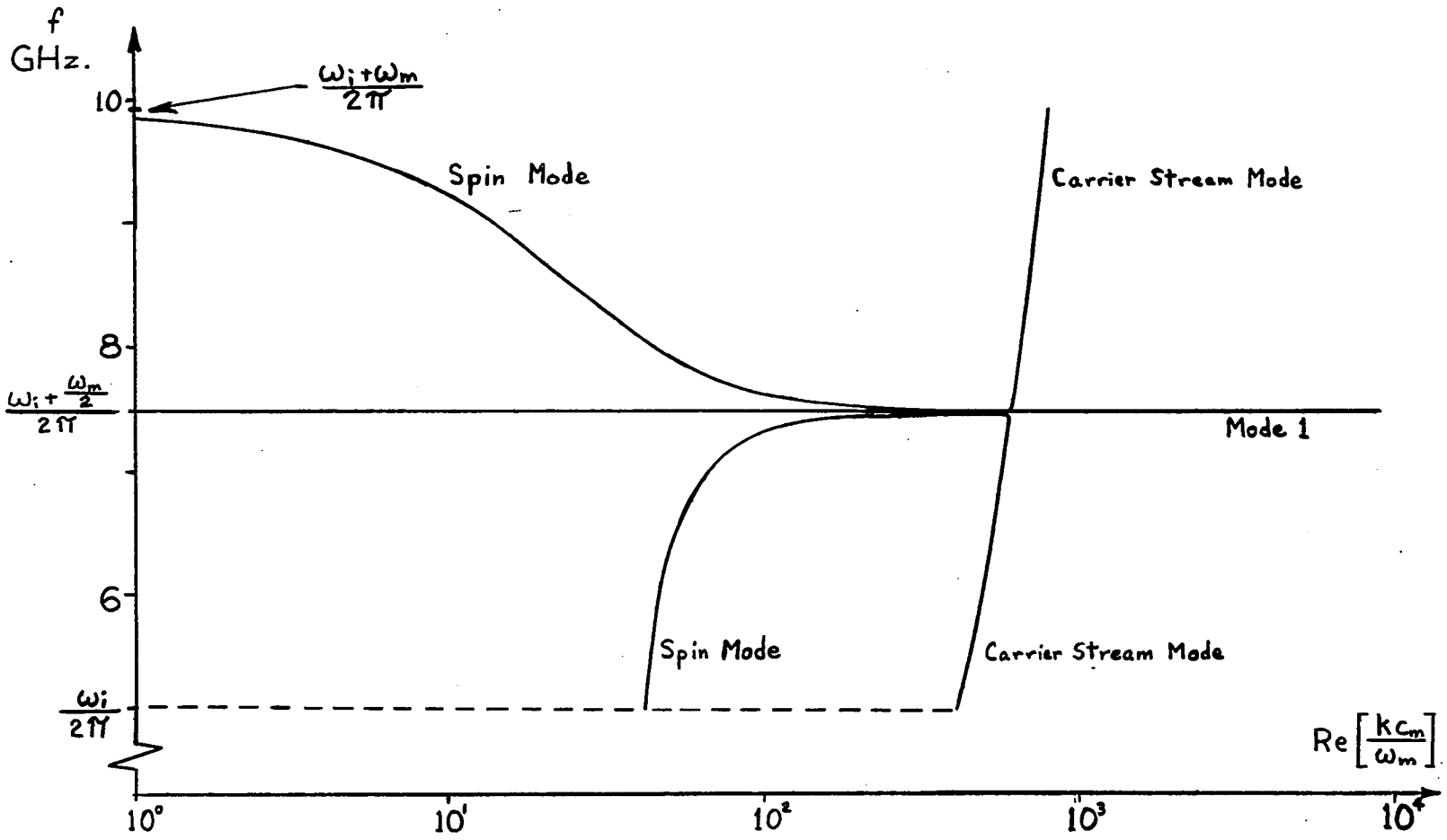

Figure 4-7 - Dispersion Characteristics of Electromagnetic Surface Waves Propagating Along the Interface Between a Magnetic Insulator and a Drifted Semiconductor; $V_{os} = -2 \times 10^7$ cm/sec.

in Figure 4-8. When the electrons are drifted in the opposite direction ($-\hat{y}$) it is found that the loss increases. (There is no surface carrier stream mode for this case). Thus, it is found that the losses associated with the propagation of surfaces waves along the interface between a semiconductor and an insulating ferromagnetic medium may be modified by drifting carriers within the semiconductor, even at frequencies and drift velocities where synchronism is not achieved.

Examining the region of the spectrum of Figure 4-7, near the resonance in detail, it is found that as the resonance is approached the real part of the wavenumber of the "spin" mode varies slowly as a function of frequency when compared to the wavenumber of the "carrier stream" mode which appears to be strongly influenced by the resonance, Figure 4-9. In this region where the modes are strongly modified, neither mode is classifiable as being exclusively associated with one system or the other, but are the result of the interaction between the constituent systems. Therefore, in order to clearly distinguish between the modes they are labelled modes 1 and 2, as shown on Figure 4-9. (This labelling is consistent with that used by Robinson et. al. [23] in their investigations).

Inspection of the complex wavenumbers of modes 1 and 2 reveals that in the narrow range between the frequency where the real part of the wavenumber of mode 2 reaches its maximum value (f=7.8795 GHz) and that where Re [k] of mode 1 reaches its maximum (f=7.8809 GHz) the imaginary parts of the wavenumbers of both modes are positive. Immediately above and

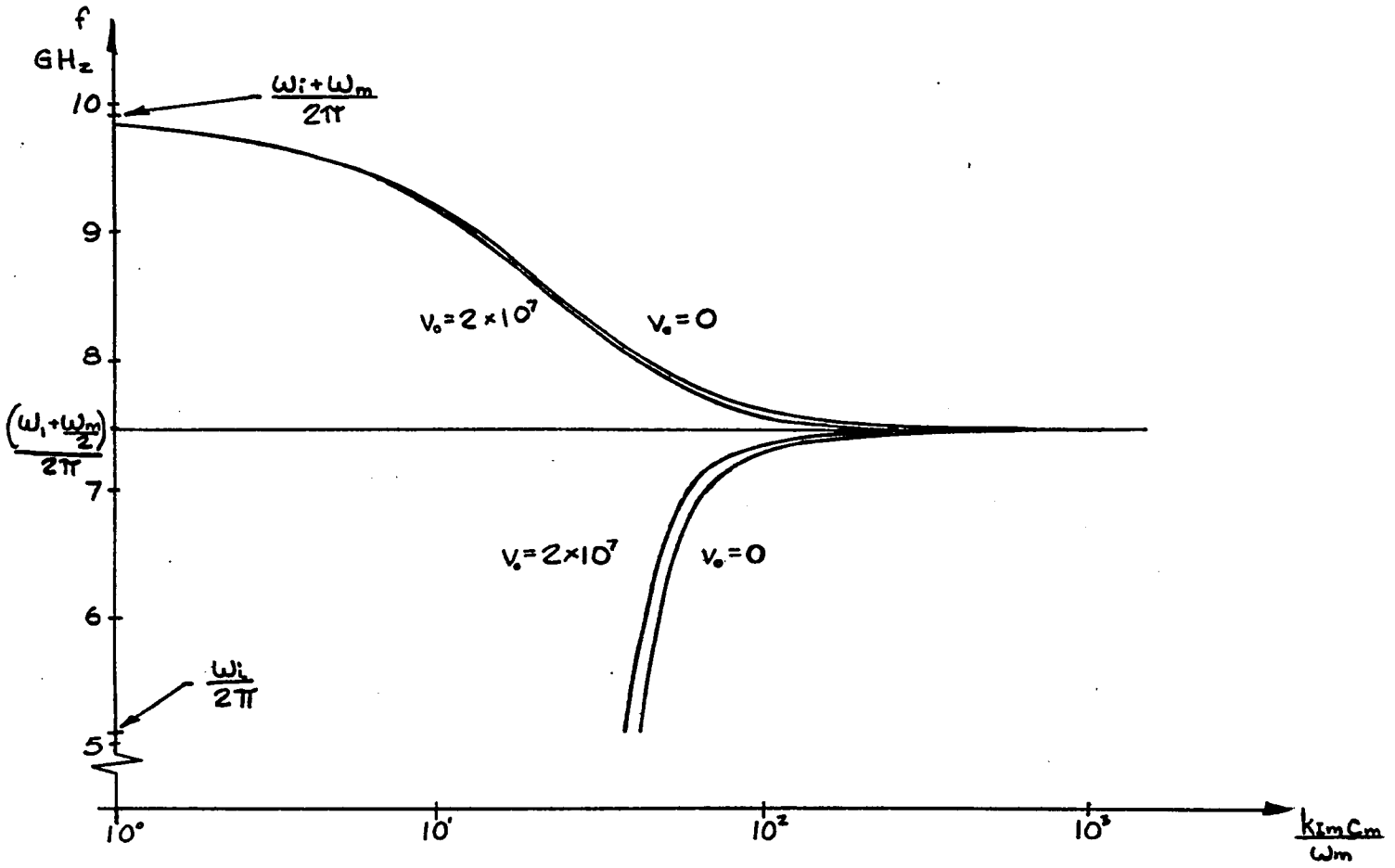

Figure 4-8 Comparison of Spin Mode Losses With and Without Drift

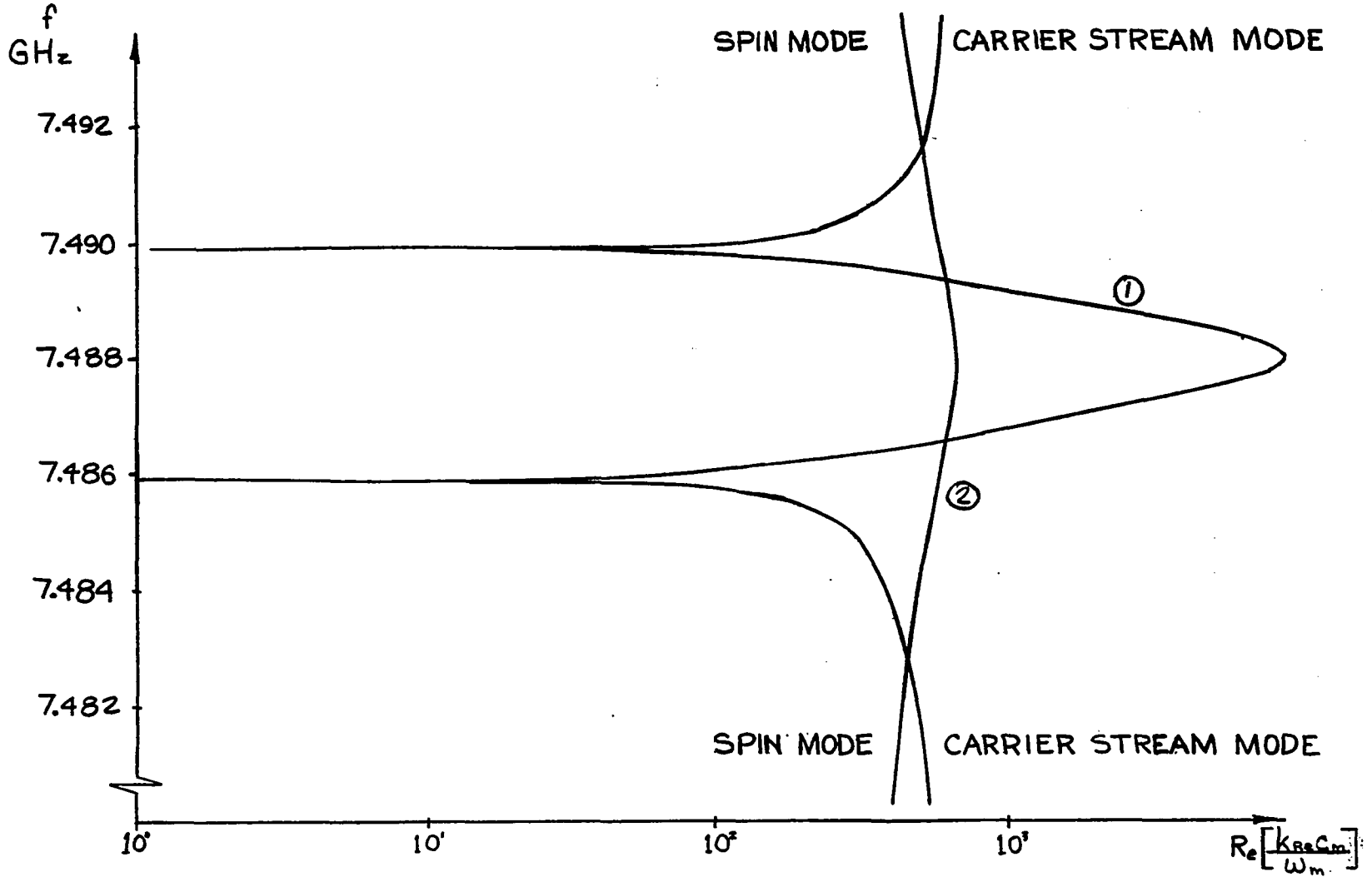

Figure 4-9 - Interaction Region of Surface Wave Characteristics

below this narrow band Im[k] of the modes are of opposite polarity. Examining the behavior of the modes in these regions using the modified Briggs [102] technique, it is found that the modes are evanescent. However, within the narrow band of frequencies where the imaginary parts of both wavenumbers are positive, it is found that an instability exists. Between the frequencies 7.48795 GHz and 7.487995 GHz, mode 2 is found to correspond to a weak convective instability with a maximum growth rate of approximately 1.38 nepers/mm. The type of instability is determined by noting that the imaginary part of the wavenumber changes sign from positive to negative as the imaginary part of the complex frequency is made negative. A saddle point is located at the complex frequency of $f=(7.487995-j1.605\times10^{-3})$GHz. The locus of roots about this point, shown in Figure 4-10, indicates the presence of an absolute instability. Beyond this frequency the instability again becomes convective with the instability now associated with mode 1. (Mode 2 now propagates in the $-\hat{y}$ direction). The maxium growth rate of this instability is approximately 708 nepers/mm. for the parameters chosen.

Robinson et. al. [23] obtained similar results investigating the interaction of streaming electrons with the surface wave by using the magnetostatic approximation in the ferrite. Comparing the transverse wavenumber within the ferrite with the longitudinal wavenumber in the instability region it is found that

$$\beta_m \cong k, \qquad 4\text{-}46$$

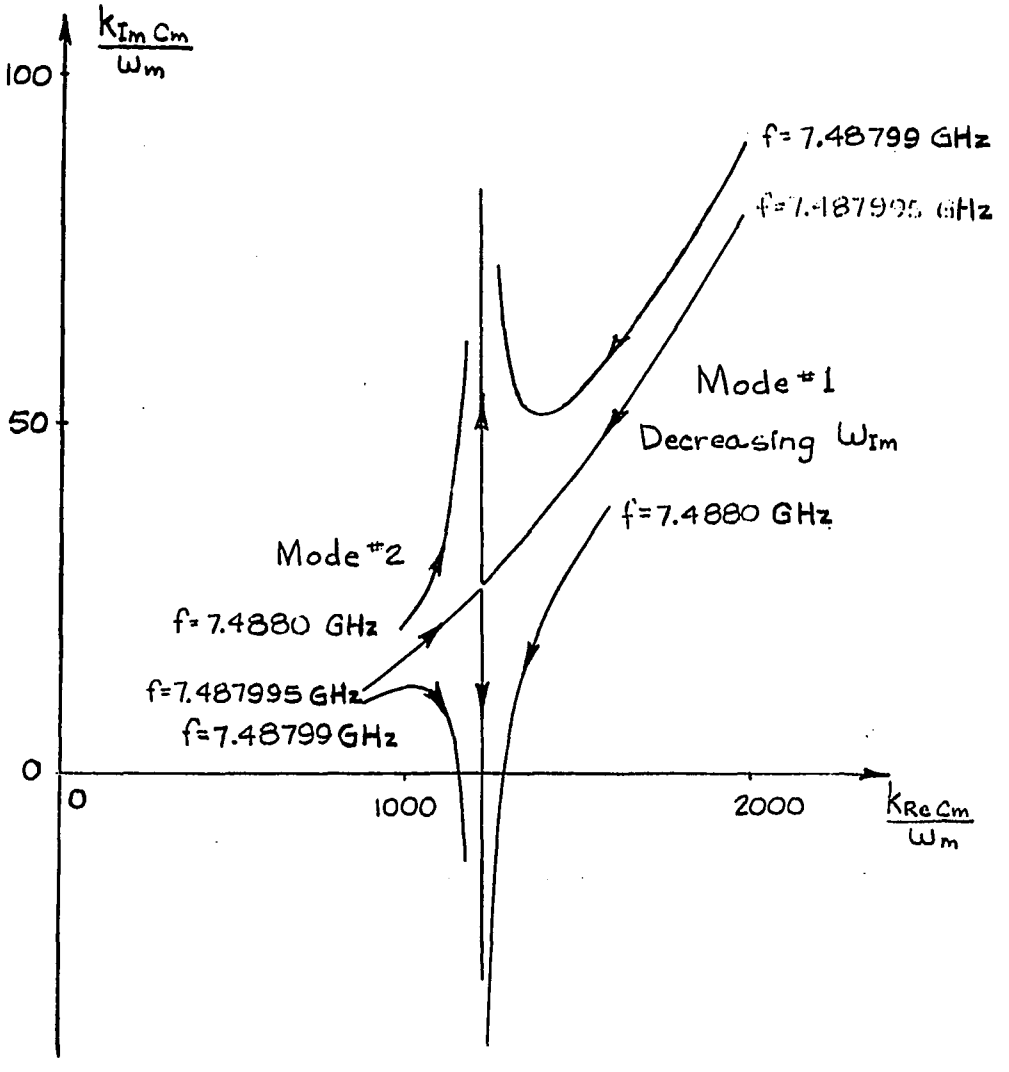

Figure 4-10 - Locus of Roots Corresponding to the Saddle Point at $f=(7.487995-j\,1.605\times10^{-3})$ GHz.

indicating that the magnetostatic approximation is appropriate in this region. Furthermore, comparing the longitudinal wavenumber with the transverse wavenumber within the semiconductor it is found that

$$Re[\beta_{sc}] \cong Re[k]. \qquad 4\text{-}47$$

The validity of Equations 4-46 and 4-47 in the interaction region simplify the investigation of an interaction in systems of greater complexity as discussed in Section 4-4 and Chapter 5.

4.4 Analysis Of Dispersion Relation Using Approximation Techniques

In the previous section the exchange modified dispersion relationship describing electromagnetic surface wave propagation along the interface between a semi-infinite drifted semiconductor and a semi-infinite ferromagnetic insulator was used to verify that the magnetostatic approximation provides a suitable description of the behavior of the fields in the ferrite when analyzing the interaction between the "magnetostatic" surface mode and the carrier stream. In the present section simplified dispersion relations obtained by making the magnetostatic approximation are used to develop a multiple carrier species instability onset criterion enabling the investigation of the effect on the interaction of the presence of holes. In addition, an instability onset condition nomograph is developed permitting the rapid determination of the suitability of materials for instability investigations. Using the nomograph, the relative merits of four commercially available semiconductors, Si, Ge, GaAs and InSb, are discussed. However, the existance of an instability is necessary but not sufficient to ensure that it can be observed. One must also determine whether the mode is excited sufficiently. Therefore, an expression for the relative excitation amplitudes and phases of the magnetostatic model mode solutions is derived and examined.

In Chapter 2 it was shown that in the magnetostatic limit,

$$k = \beta_m \ , \qquad 2\text{-}109$$

for modes with positive phase velocity (the real part of k positive) within the ferrite. In this limit Equation 4-53 may be written as

$$\beta_{sc} = \frac{k}{\mu_{11} + \mu_{12}} \ . \qquad 4\text{-}48$$

Squaring both sides, β_{sc} may be eliminated from Equation 4-32, resulting in the following dispersion relationship describing magnetostatic surface wave propagation along the drifted semiconductor-ferrite interface

$$k^2 - \frac{\omega^2}{c_{sc}^2}\left[\frac{(\mu_{11}+\mu_{12})^2}{(\mu_{11}+\mu_{12})^2 - 1}\right]\left[1 - \sum_{s=1}^{S} \frac{\omega_{ps}^2(\omega + k v_{os})}{\omega^2(\omega + k v_{os} - j\nu_s)}\right] = 0 \qquad 4\text{-}49$$

Noting that in the magnetostatic limit, the exchange term in the expression for Ω_e , Equation 2-57, is negligible with respect to ω_i the permeability tensor components may be written as

$$\mu_{11} = 1 + \frac{\omega_i \omega_m \left[1 + j\frac{\lambda_r \omega}{\omega_m \omega_i} + \left(\frac{\lambda_r}{\omega_m}\right)^2\right]}{\left[\omega_i^2 - \left(\omega - j\frac{\lambda_r \omega_i}{\omega_m}\right)^2\right]} \qquad 4\text{-}50$$

and

$$\mu_{12} = \frac{\omega_m \omega}{\left[\omega_i^2 - \left(\omega - j\frac{\lambda \omega_i}{\omega_m}\right)^2\right]} \ . \qquad 4\text{-}51$$

Defining a magnetic relaxation frequency, ν_m , as

$$\nu_m = \frac{\omega}{\omega_m}\lambda_r \ , \qquad 4\text{-}52$$

the permeability tensor components may be reexpressed as

$$\mu_{11} = 1 + \frac{\omega_m\left[\omega_i\left(1 + \frac{\nu_m^2}{\omega^2}\right) + j\nu_m\right]}{\left[(\omega_i + j\nu_m)^2 - \omega^2 + \nu_m^2\left(\frac{\omega_i^2}{\omega^2} + 1\right)\right]} \qquad 4\text{-}53$$

and

$$\mu_{12} = \frac{\omega_m \omega}{\left[(\omega_i + j\nu_m)^2 - \omega^2 + \nu_m^2\left(\frac{\omega_i^2}{\omega^2}+1\right)\right]} . \qquad 4\text{-}54$$

For narrow line widths, $\Delta H << H_i$, the relaxation frequency is much smaller than either ω_i or ω ($\omega = \omega_i + \frac{\omega_m}{2}$ near the "magnetostatic" mode resonance) and the above expressions further reduce to

$$\mu_{11} = 1 + \frac{\omega_m(\omega_i + j\nu_m)}{(\omega_i + j\nu_m)^2 - \omega^2} \qquad 4\text{-}55$$

and

$$\mu_{12} = \frac{\omega_m \omega}{(\omega_i + j\nu_m)^2 - \omega^2} . \qquad 4\text{-}56$$

This is the form that the permeability tensor components assume when derived from the Gilbert (2-27, 2-27b) rather than the Landau-Lifschitz (2-27, 2-27a) form of the equation of motion of the magnetization for, as was demonstrated in Chapter 2, the two forms are equivalent in the narrow line width case.

Substituting the simplified permeability tensor definitions, Equations 4-55 and 4-56 into Equation 4-49, the dispersion relationship becomes, upon simplification

$$k^2 = \frac{\omega^2}{c_{sc}^2}\left\{\frac{\left[\omega_i + \omega_m + j\nu_m - \omega\right]^2}{2\omega_m\left[\omega_i + \frac{\omega_m}{2} + j\nu_m - \omega\right]}\right\}\left[1 - \sum_{s=1}^{S}\frac{\omega_{ps}^2(\omega + kv_{os})}{\omega^2(\omega + kv_{os} - j\nu_s)}\right] \qquad 4\text{-}57$$

or

$$k^2 - \frac{\omega}{c_{sc}^2}\,\mu_{sw}\left[1 - \sum_{s=1}^{S} \frac{\omega_{ps}^2(\omega + k v_{os})}{\omega^2(\omega + k v_{os} - j\nu_s)}\right] = 0 \,, \qquad 4\text{-}58$$

where

$$\mu_{sw} = \frac{\left[\omega_i + \omega_m + j\nu_m - \omega\right]^2}{2\omega_m\left[\omega_i + \frac{\omega_m}{2} + j\nu_m - \omega\right]} \,, \qquad 4\text{-}59$$

which reduces to the equation obtained by Steele and Vural [22] and Robinson et. al. [23] for the case S=1, i.e. a single carrier stream. Steele and Vural note the similarity between the magnetostatic dispersion relation describing the behavior of the surface waves in the layered structure and that describing TE waves propagating perpendicular to a static magnetic field in the bulk of a ferromagnetic semiconductor. For the bulk ferromagnetic semiconductor case, the dispersion relation differs from Equation 4-58 only in the form of the effective permeability (See Appendix II.)

Robinson et. al. [23] have analyzed the single stream dispersion relationship and have developed a formulation expressing the necessary and sufficient conditions for instability onset. The criterion is developed by noting that an instability exists if for some real value of k, the dispersion relation has a root, ω, with a negative imaginary component. The instability onset condition for the case where more than one semiconductor carrier species is considered is derived using a similar approach.

Assuming that the interaction occurs near the system resonance and that the complex radian frequency differs from its resonant value by a small amount δ, defined by

$$\omega = \omega_i + \frac{\omega_m}{2} + j\nu_m + \delta = \omega_{res} + j\nu_m + \delta. \qquad 4\text{-}60$$

Equation 4-57 may be linearized to yield

$$k^2 c_{sc}^2 = \frac{\omega_m}{8\delta}\left[\sum_{s=1}^{S} \frac{\omega_{ps}^2(\omega + kv_{os})(\omega + kv_{os} + j\nu_s)}{(\omega + kv_{os})^2 + \nu_s^2} - \omega^2\right]. \qquad 4\text{-}61$$

Reformulating the above expression and considering two types of carriers, electrons, symbolized by the subscript e, and holes, symbolized by the subscript h, the following expression is obtained

$$\delta = \frac{\omega_m}{8k^2c_{sc}^2}\left[\frac{\omega_{pe}^2(\omega - kv_{oe})(\omega - kv_{oe} + j\nu_e)}{(\omega - kv_{oe})^2 + \nu_e^2} + \frac{\omega_{ph}^2(\omega + kv_{oh})(\omega + kv_{oh} + j\nu_h)}{(\omega + kv_{oh}) + \nu_h^2} - \omega^2\right]. \qquad 4\text{-}62$$

where v_{oe} and v_{oh} are defined as positive quantities. This expression may be simplified in the collision dominated limit,

$$\nu_e \gg \omega, kv_{oe}, \qquad 4\text{-}63$$

$$\nu_h \gg \omega, kv_{oh}, \qquad 4\text{-}64$$

yielding

$$\delta = \frac{\omega_m}{8k^2c_{sc}^2}\left[j\frac{\omega_{pe}^2(\omega - kv_{oe})}{\nu_e} + j\frac{\omega_{ph}^2(\omega + kv_{oh})}{\nu_h} - \omega^2\right]. \qquad 4\text{-}65$$

Since k is real, the imaginary part of this expression is

$$\delta_{I_m} = \frac{\omega_m}{8k^2 c_{sc}^2}\left[\frac{\omega_{pe}^2(\omega_{res} - k v_{oe})}{\nu_e} + \frac{\omega_{ph}^2(\omega_{res} + k v_{oh})}{\nu_h}\right], \quad 4\text{-}66$$

where it has been assumed that

$$\nu_m << \frac{\omega_{pe}^2}{\nu_e}, \frac{\omega_{ph}^2}{\nu_h} \quad 4\text{-}67$$

and

$$Re[\delta] << \omega_{res}. \quad 4\text{-}68$$

To satisfy the necessary and sufficient conditions for the existance of an instability δ_{I_m} must be negative and have a magnitude greater than ν_m. Inspection of Equation 4-66 reveals that a necessary condition for the onset of an instability is that the drift velocity of the electrons be greater than the phase velocity

$$v_{oe} > \frac{\omega}{k}. \quad 4\text{-}69$$

(Since the directions of drift of electrons and holes are opposite, similar results for holes may be obtained by reversing the direction of the applied electric field. However, since the mobility of electrons in a semiconductor is in general greater than that of holes, the velocities needed to achieve synchronism are more easily attained by electrons.)

Further examination of Equation 4-66 reveals that not only must the electrons attain velocities in excess of the phase velocity of the surface wave but that a definite threshold due to the presence of the holes must

additionally be overcome

$$v_{oe} > \frac{\omega}{k}\left[1 + C_{he}\right] + C_{he}\, v_{oh}\,, \qquad 4\text{-}70$$

where

$$C_{he} = \frac{\omega_{ph}^2\, \nu_e}{\omega_{pe}^2\, \nu_h}\,. \qquad 4\text{-}71$$

Noting that the ratio of v_{oh} to v_{oh} is to first order a constant, Equation 4-70 may be reformulated as

$$v_{oe} > \frac{\omega}{k}\,\frac{\left[1 + C_{he}\right]}{\left[1 - C_{he}\mu'\right]}\,, \qquad 4\text{-}72$$

where $\mu' = \mu_h/\mu_e$, the ratio of the hole and electron mobilities.

The conditions for which an instability may occur have been obtained by noting that $|\delta_{Im}|$ must be greater than ν_m for the imaginary part of ω to be negative. The lower limit for which this relationship may be satisfied is determined when the maximum of $|\delta_{Im}|$ just equals ν_m .

Differentiating Equation 4-66 with respect to k and equating the result to zero it is found that the maximum value of $|\delta_{Im}|$ occurs when

$$v_{oe} = \frac{2\omega}{k}\,\frac{\left[1 + C_{he}\right]}{\left[1 - C_{he}\mu'\right]}\,. \qquad 4\text{-}73$$

Substituting Equation 4-73 into Equation 4-66 and making use of the condition that $|\delta_{Im}|$ must be greater than ν_m , the instability onset condition is

$$\frac{\omega_m\, \omega_{pe}^2\, v_{oe}^2}{32\, c_{sc}^2\, \nu_e \left(\omega_i + \frac{\omega_m}{2}\right)\nu_m}\,\frac{\left[1 - C_{he}\mu'\right]^2}{\left[1 + C_{he}\right]} > 1\,. \qquad 4\text{-}74$$

It is observed that the holes have a detrimental effect on the interaction. If, however, $C_{he} << 1$, the holes have little influence on the interaction and the semiconducting medium may be treated as though only one carrier species, electrons, were present. For this case Equation 4-74 reduces to the instability condition given by Robinson et. al.[23]

$$\frac{\omega_m \omega_{pe}^2 v_{oe}^2}{32 c_{sc}^2 \nu_e (\omega_i + \frac{\omega_m}{2}) \nu_m} > 1. \qquad 4\text{-}75$$

Rearranging this single carrier onset condition a lower limit on the velocity that electrons are required to attain is obtained,

$$v_{oe} > \left[\frac{32 c_{sc}^2 \nu_e (\omega_i + \frac{\omega_m}{2}) \nu_m}{\omega_m \omega_{pe}^2} \right]^{1/2}. \qquad 4\text{-}76$$

Expressing the parameters within the brackets in terms of their definitions, the following simplified relation results

$$v_{oe} > 4 c_o \left[\frac{\epsilon_o \omega (\frac{\Delta H}{M_o})}{\sigma_n} \right]^{1/2}, \qquad 4\text{-}77$$

where

$$\sigma_n = N e \mu_e. \qquad 4\text{-}78$$

Thus, the minimum velocity required for instability onset is a function of only two material dependent quantities, the conductivity, σ , of the semiconductor and the linewidth to magnetization ratio of the ferrite.

At this point some conclusions concerning selection of materials to be used in obtaining the interaction may be drawn. Of the ferrites commercially available, a good choice is Yittrium Iron Garnet. The saturation magnetization of YIG is 1750-1785 Oe. at 300^0K making it suitable

for observing surface wave propagation in the widely used S and X microwave bands with moderate applied static magnetic fields (less than 4 kG). In addition, YIG is characterized by a linewidth to magnetization ratio of as little as 2×10^{-4} for highly polished samples at 300^0 K.[42]

The choice of a suitable semiconducting medium is somewhat more complex. As an aid in the selection process a nomograph is constructed by plotting the electron mobility required for instability onset versus carrier density with electron drift velocity as a parameter. The nomograph of Figure 4-11 is drawn for a frequency of 3 GHz. (middle of S band) and the linewidth to magnetization ratio of the neighboring ferrite is taken as 2×10^{-4}. The chart is used by locating the point corresponding to the mobility and density of the semiconductor under consideration. If this point lies above and to the right of the curve corresponding to the maximum drift velocity of electrons in this material, or, more precisely, the maximum velocity attainable with the transverse magnetic field required for resonance at the frequency under consideration, then it may be possible to obtain an instability. Since the maximum velocity decreases with increased transverse magnetic field, the frequency [$f_{res} = \frac{1}{2\pi}(\omega_i + \omega_m/2)$] should be chosen to be as small as is practicable (large enough to ensure that the magnetization is saturated by the applied magnetic field) thus allowing higher drift velocities to be obtained. It is observed from Equation 4-77 that operating at low frequencies also reduces the velocity required for instability onset.

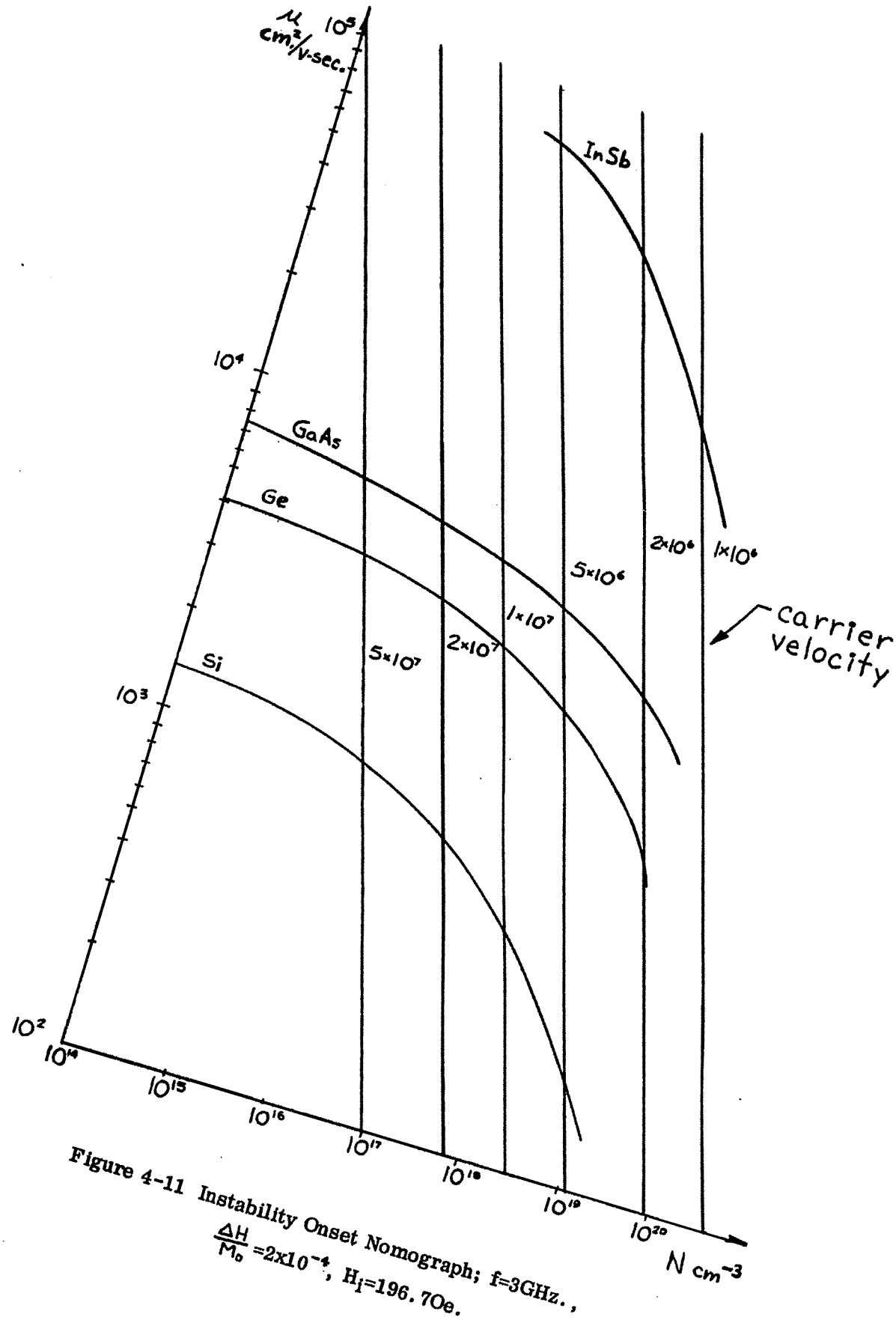

Figure 4-11 Instability Onset Nomograph; f=3GHz., $\frac{\Delta H}{M_o}=2\times10^{-4}$, H_i=196.7Oe.

As an example of the use of the instability onset nomograph, mobility-density relations[106, 107] are plotted on Figure 4-11 for four semiconductors, silicon, germanium, gallium arsenide and indium antimonide. The maximum drift velocities of these materials are listed in Table 4-1. (While conductivity changes due to the creation of electron-hole pairs begins at approximately 150v/cm. in InSb, Prior[108], using pulses of short duration, determined that there is no variation in electron mobility up to at least 800v/cm. This corresponds to a drift velocity in excess of 3×10^7 cm/sec. for the highest mobility specimen he examined.) It is noted that a region can be found for each of the four semiconductors where the minimum instability onset condition is satisfied. A check on C_{he} in these regions indicates that the assumption that the influence of the holes is small and may be neglected is valid.

The average power per unit volume dissipated by a current drifting through a semiconductor is

$$P_v = \bar{J}_o \cdot \bar{E}_o = \sigma E_o^2 \qquad 4\text{-}79$$

Using this expression, the instability onset relation, equation 4-77, may be reexpressed as a condition on the miniumum power per unit volume required to obtain an instability

$$P_v > \frac{16 c_o^2 \epsilon_o \omega \left(\frac{\Delta H}{M_o}\right) E_o^2}{v_{oe}^2} \qquad 4\text{-}80$$

For low electric field values,

$$v_{oe} = \mu_e E_o , \qquad 4\text{-}81$$

and Equation 4-80 may be rewritten as,

Table 4-1

Typical Values of Limiting Drift Velocity, Specific Heat Melting Point, and Thermal Conductivity For Various Semiconductor Materials (101, 108)

	Limiting Drift Velocity (B_0=0, T=300°K)	Specific Heat (T=300°K)	Melting Point	Thermal Conductivity (T=300°K)
	cm/sec	10^7 cm^2/sec°K	°C	w/cm°K
Silicon	1.1×10^7	0.71	1417	1.5
Germanium	8.0×10^6	0.34	937	0.6
Gallium Arsenide	1.7×10^7	0.31	1237	0.8
Indium Antimonide	$> 3.0 \times 10^7$	0.21	525	0.19

$$P_v > \frac{16 c_o^2 \epsilon_o \omega \left(\frac{\Delta H}{M_o}\right)}{\mu_e^2} \quad . \qquad 4\text{-}82$$

The minimum power per unit volume necessary for instability onset is greater than that predicted by Equation 4-82 because electron mobility decreases as the maximum drift velocity is approached. However, it is reasonable to assume that the mimimum power required for instability onset is smaller for a high mobility semiconductor such as indium antimonide than one such as silicon. (The minimum power per unit volume for instability onset for S_i, Ge, GaAs and InSb is tabulated in Table 4-2 for the conditions of Figure 4-11.)

Equation 4-82 gives an order of magnitude indication of the instantaneous power per unit volume which a semiconductor must be capable of dissipating if an instability is to be obtained. This power handling capability is dependent on several factors among which are the semiconductor's specific heat, thermal conductivity, melting point and surface to volume ratio as well as the thermal resistance of the mounting structure. The specific heat, melting point and thermal conductivity of the four semiconductors under consideration are listed in Table 4-1. It is noted that of the four, Silicon has the highest specific heat and thermal conductivity, however, referring to Figure 4-11, it is observed that of the four it has the lowest mobility and corresponds to the narrowest instability onset region. On the other hand, indium antimonide, which has the highest mobility of the semiconductors under consideration has the least desirable thermal char-

Table 4-2

Minimum Power Per Unit Volume
For Instability Onset
($f=3GHz$, $\frac{\Delta H}{M_o}=2\times10^{-4}$)

	$cm.^2/v.-sec.$	$w./cm.^3$
Silicon	1350	8.78×10^8
Germanium	3900	3.16×10^8
Gallium Arsenide	8500	6.65×10^7
Indium Antimonide	78,000	7.89×10^5

acteristics. Increasing the surface to volume ratio of the material through the use of thin films would permit operation at relatively high power to volume ratios while providing more surface area for cooling and, at the same time, lowering the power requirements demanded of the power supply. (The effect on the interaction of a semiconducting region of finite thickness is discussed in detail in Chapter 5.) While reports of the successful production, in limited quantities, of thin films of high mobility InSb have appeared in the literature,[109] epitaxial InSb is not commercially available. Gallium arsenide, which appears to represent a reasonable compromise material, having an electron mobility and thermal properties between those of silicon and indium antimonide, is commercially available is epitaxial form as a thin high conductivity layer on top of an insulating substrate. It should be noted however that due to its higher mobility and maximum drift velocity, epitaxial indium antimonide would be preferable.

In the preceding discussion the conditions necessary for instability onset were presented. Although satisfaction of these conditions ensures that the system in question exhibits an instability, the determination of whether the instability is convective or absolute requires the application of more stringent conditions as discussed in Section 4.3. If the system is found to have a mode which exhibits a convective instability, it must still be determined whether the mode is excited sufficiently for it to be observed. This requires knowledge not only of the exponential behavior of each of the modes, but their relative amplitudes and phases as well.[110] The latter

may be determined in the magnetostatic limit by modifying the semi-infinite model to include input and output couplers in the plane of the interface. The output coupler is assumed to be perfectly terminated so that no reflected wave is excited. Thus the only waves which must be considered are the three modes of the approximate single carrier model yielding

$$\sum_{l=1}^{3} E_{zl}\Big|_{y_{in}} = E_{in} \qquad 4\text{-}83$$

where E_{in} is the amplitude of the r.f. electric field excitation at the input coupler. Applying the boundary conditions of no r.f. velocity modulation and zero r.f. magnetization at the input, the following relations result

$$\sum_{l=1}^{3} v_{zl} = \sum_{l=1}^{3} j\frac{\eta_e^*(\omega - k_l v_{oe})E_{zl}}{\omega(\omega - k_l v_{oe} - j\nu_e)}, \qquad 4\text{-}84$$

and

$$\sum_{l=1} \bar{M} = \sum_{l=1}(\hat{x} - j\hat{y})\left[1 - \frac{1}{(\mu_{11} + \mu_{12})}\right]\frac{k_l E_{zl}}{\omega\mu_o} = 0 \qquad 4\text{-}85$$

Expressing the equations in matrix form, the equation relating the complex excitation amplitudes becomes

$$\begin{bmatrix} 1 & 1 & 1 \\ k_1 & k_2 & k_3 \\ \dfrac{(\omega - k_1 v_{oe})}{(\omega - k_1 v_{oe} - j\nu_e)} & \dfrac{(\omega - k v_{oe})}{(\omega - k_2 v_{oe} - j\nu_e)} & \dfrac{(\omega - k v_{oe})}{(\omega - k_3 v_{oe} - j\nu_e)} \end{bmatrix}\begin{bmatrix} E_{z1} \\ E_{z2} \\ E_{z3} \end{bmatrix} = \begin{bmatrix} E_{in} \\ 0 \\ 0 \end{bmatrix} \qquad 4\text{-}86$$

Evaluating the complex mode amplitudes in the vicinity of the instability for the parameters used in Section 4.3, it is found that mode 2 is strongly excited, its magnitude being approximately equal to E_{in}, while the power

level of mode 1 is approximately 24 db. lower upon excitation. (The third mode, less strongly excited than mode 1, does not correspond to a surface wave.) Due to the relatively large gain associated with mode 1 in the region where it exhibits a convective instability ($\cong$ 708 nepers/mm.), its magnitude would equal that of the excitation signal after the wave had traveled only 4.6 microns.

Due to the narrowness of the instability region a change in the value of the internal magnetic field of less than 0.1 Oe. (for the parameters selected) is sufficient to change the conditions from gain to loss with the rate of attenuation exceeding the maxium growth rate. Thus, if amplification is to be achieved or if the absolute instability is to be observed, the variation of the internal magnetic field along the ferrite-semiconductor interface should be as small as possible. This suggests the use of a thin ferrite plate whose dimensions are relatively large in the $\hat{y}$ and $\hat{z}$ directions. (The effect of the thickness upon the interaction is considered in Chapter 5.) However, it should be noted that the semiconductor should also be large in the $\hat{y}$ and $\hat{z}$ directions since the current in the semiconductor gives rise to a magnetic field and thus alters the total applied field. Additonally, heat generated as a result of the current flow may alter the saturation magnetization and the linewidth at the interface resulting in additional non-uniformities along the direction of propagation. The effects of heating and magnetic field shift due to the drifting carriers have been observed and are discussed further in Section 5.4 dealing with experimental results.

CHAPTER 5
THE EFFECTS OF GEOMETRY ON THE INTERACTION BETWEEN MAGNETOSTATIC SURFACE WAVES AND STREAMING CHARGE CARRIERS IN A SEMICONDUCTOR

5.0 Introduction

In Section 4.3 considerable simplification of the layered structure was achieved by assuming that both the magnetic and semiconducting media were uniform and extended semi-infinitely in the transverse direction. In this chapter equations are developed describing the effects of finite dimensions in either or both of the media. These deviations from the semi-infinite model may be used to determine the effects of finite dimensions, surface layers and dielectric spacing between the media.

In Section 5.4 empirical studies of the factors involved in the observation and interpretation of the transmission characteristics of composite structures consisting of adjacent semiconducting and magnetic insulating materials are described and discussed. On the basis of these investigations microwave transmission spectra are examined and the surface modes are identified.

5.1 Electromagnetic Surface Wave Propagation At The Boundary of a Ferrite Slab and a Semiconductor of Finite Thickness

The effect of finite dimensions upon the properties of electromagnetic surface waves propagating along the interface between a ferromagnetic insulator and a semiconductor is to be investigated. The model to be considered is shown in Figure 5-1. The ferrite, assumed to be infinite in extent in the $\hat{y}$ and $\hat{z}$ directions, is bounded at x=-a by dielectric # 2. and at x=0 by the semiconductor. A static magnetic field is applied in the $\hat{z}$ direction, resulting in a magnetic field intensity, $\overline{H_i}$, assumed uniform within the ferrite. The semiconductor, which occupies the region $0<x\leq d'$, consists of two portions, one extending from x=d to x=d' labelled semiconductor # 1, the remaining portion labelled semiconductor # 2. The two semiconducting regions are characterized by differing carrier densities and mobilities as would be the case of an epitaxial semiconductor, where the surface region $0<x\leq d$ is considered to be epitaxially grown material and the region $d<x\leq d'$ the bulk substrate. At x=d' the semiconductor is terminated by a dielectric medium, dielectric # 1, extending infinitely in the transverse directions. For simplicity it is assumed that both dielectric regions are perfect insulators and are characterized by equal permittivities.

The derivation proceeds by assuming an appropriate form for the r.f. electric field in each region. Then, using Maxwell's equations, 2-1 and 2-2, an expression for the r.f. magnetic field intensity as well as the dispersion equation relating the transverse wavenumbers are obtained.

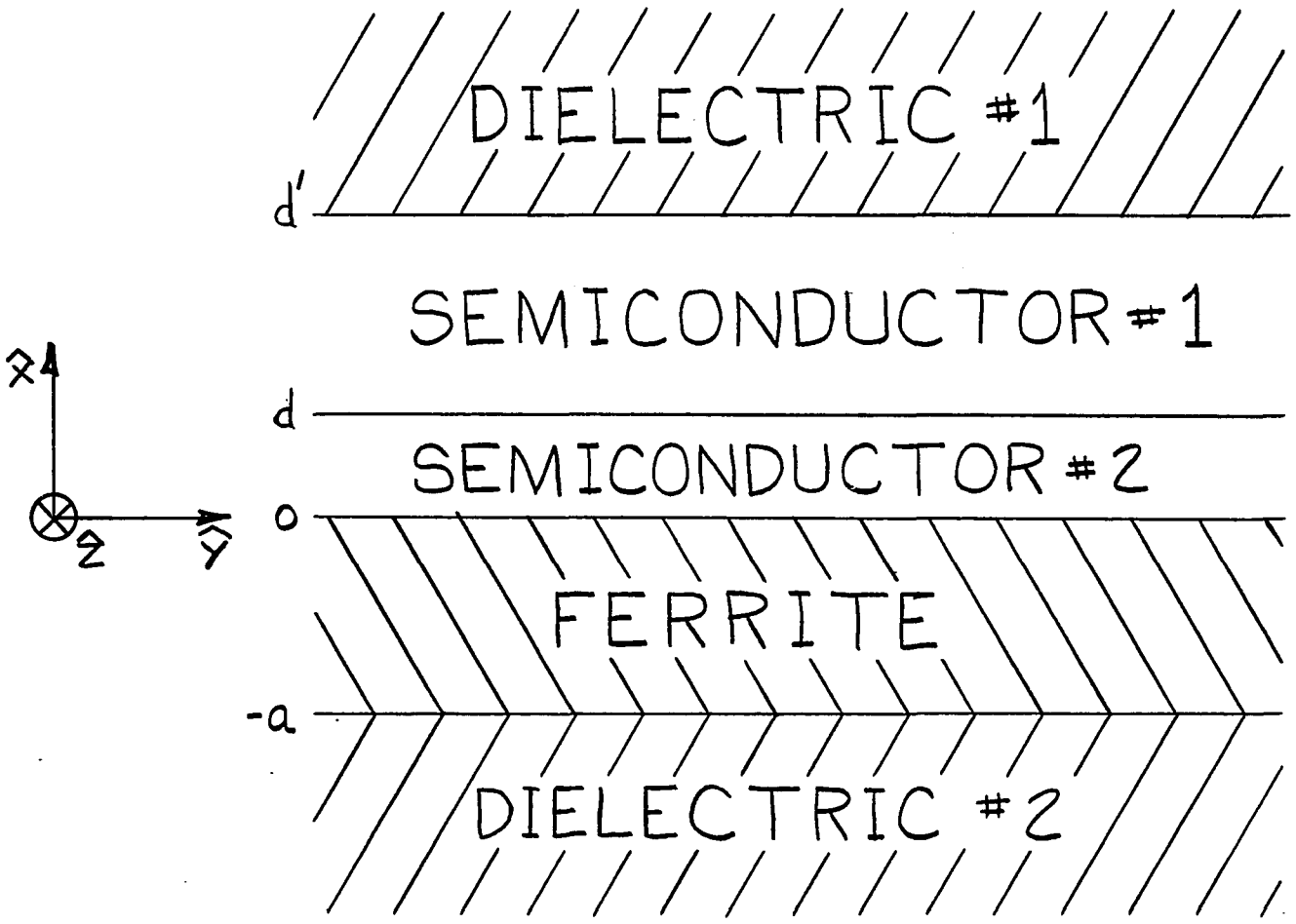

Figure 5-1 - Finite Ferromagnetic and Semiconducting Layered Structure

The relations between the field quantities in dielectric region # 1 are similar to the expressions obtained in Chapters 2 and 3 requiring only translation in $\hat{x}$ to reflect the new boundaries at x=d' yielding

$$E_{d1z} = A \exp\left[-\beta_d (x-d') + j(\omega t - ky)\right] \qquad 5\text{-}1$$

$$H_{d1x} = \frac{kA}{\omega \mu_o} \exp\left[-\beta_d (x-d') + j(\omega t - ky)\right] \qquad 5\text{-}2$$

and

$$H_{d1y} = j \frac{\beta_d A}{\omega \mu_o} \exp\left[-\beta_d (x-d') + j(\omega t - ky)\right] \qquad 5\text{-}3$$

where

$$k^2 - \beta_d^2 = \frac{\omega^2}{c_d^2} \qquad 2\text{-}94$$

For a plane wave solution to exist in the composite structure the waveform in each region must have the same phase velocity as the excitations in the adjacent media. The waveforms in the semiconducting media are therefore assumed to have the form

$$E_{sc1z} = \left[C_1 \sinh \beta_1 x + F_1 \cosh \beta_1 x\right] \exp\left[j(\omega t - ky)\right] \qquad 5\text{-}4$$

$$H_{sc1x} = \frac{k}{\omega\mu_o}\left[C_1 \sinh\beta_1 x + F_1 \cosh\beta_1 x\right]\exp\left[j(\omega t - ky)\right], \qquad 5\text{-}5$$

and

$$H_{sc1y} = -j\frac{\beta_1}{\omega\mu_o}\left[C_1 \cosh\beta_1 x + F_1 \sinh\beta_1 x\right]\exp\left[j(\omega t - ky)\right], \qquad 5\text{-}6$$

where

$$k^2 - \beta_1^2 = \frac{\omega^2}{c_1^2}\left[1 - \sum_{s=1}^{S_1}\frac{\omega_{p1s}^2(\omega + kv_{01s})}{\omega^2(\omega + kv_{01s} - j\nu_{1s})}\right], \qquad 5\text{-}7$$

for semiconductor # 1 and

$$E_{sc2z} = \left[C_2 \sinh\beta_2 x + F_2 \cosh\beta_2 x\right]\exp\left[j(\omega t - ky)\right], \qquad 5\text{-}8$$

$$H_{sc2x} = \frac{k}{\omega\mu_o}\left[C_2 \sinh\beta_2 x + F_2 \sinh\beta_2 x\right]\exp\left[j(\omega t - ky)\right], \qquad 5\text{-}9$$

and

$$H_{sc2y} = -j\frac{\beta_2}{\omega\mu_0}\left[C_2\cosh\beta_2 x + F_2\sinh\beta_2 x\right]\exp\left[j(\omega t - ky)\right], \qquad 5\text{-}10$$

where

$$k^2 - \beta_2^2 = \frac{\omega^2}{c_2^2}\left[1 - \sum_{s=1}^{S_2}\frac{\omega_{p2s}^2(\omega + kv_{02s})}{\omega^2(\omega + kv_{02s} - j\nu_{2s})}\right] \qquad 5\text{-}11$$

for semiconductor # 2.

In the region where $x < 0$ the geometry of the composite structure is identical to that considered in Section 3.1. Therefore the equations for the ferrite region are assumed to be of the form

$$E_{mz} = \left[G\cosh\beta_m x + L\sinh\beta_m x\right]\exp\left[j(\omega t - ky)\right], \qquad 3\text{-}9$$

$$H_{mx} = \frac{\left[(k\mu_{11}G - \beta_m\mu_{12}L)\cosh\beta_m x + (k\mu_{11}L - \beta_m\mu_{12}G)\sinh\beta_m x\right]}{\omega\mu_0(\mu_{11}^2 - \mu_{12}^2)}\exp\left[j(\omega t - ky)\right], \qquad 3\text{-}10$$

and

$$H_{my} = j\frac{\left[(k\mu_{12}G - \beta_m\mu_{11}L)\cosh\beta_m x + (k\mu_{12}L - \beta_m\mu_{11}G)\sinh\beta_m x\right]}{\omega\mu_0(\mu_{11}^2 - \mu_{12}^2)}\exp\left[j(\omega t - ky)\right] \qquad 3\text{-}11$$

where

$$k^2 - \beta_m^2 = \frac{\omega^2}{c_m^2} \frac{(\mu_{11}^2 - \mu_{12}^2)}{\mu_{11}}, \qquad 2\text{-}95$$

while those of dielectric region # 2 are

$$E_{d2z} = R \exp\left[\beta_d (x+a) + j(\omega t - ky)\right], \qquad 3\text{-}5$$

$$H_{d2x} = \frac{kR}{\omega \mu_o} \exp\left[\beta_d (x+a) + j(\omega t - ky)\right], \qquad 3\text{-}6$$

and

$$H_{d2y} = -j \frac{\beta_d R}{\omega \mu_o} \exp\left[\beta_d (x+a) + j(\omega t - ky)\right], \qquad 3\text{-}7$$

where as in dielectric region # 1,

$$k^2 - \beta_d^2 = \frac{\omega^2}{c_d^2} \qquad 2\text{-}94$$

The relationships between the transverse and longitudinal wavenumbers in each of the media have been determined. However, for the solution to be self-consistent the boundary conditions must be satisfied at the interfaces between each adjacent layer. The resultant self-consistency condition is

expressed as an equation relating the transverse wave numbers in each of the media.

At x=d', the interface between dielectric # 1 and semiconductor # 1, the r.f. tangential electric field must be continuous resulting in

$$A = C_1 \sinh \beta_1 d' + F_1 \cosh \beta_1 d'. \qquad 5\text{-}12$$

The field configurations in the adjacent media do not have displacement current terms in a direction perpendicular to the interfaces, hence no surface charge, or current, exists. Thus the tangential components of the magnetic field intensity must be continuous at each interface. Applying this boundary condition at x=d' yields

$$C_1 = F_1 \left\{ \frac{[\beta_d \cosh \beta_1 d' + \beta_1 \sinh \beta_1 d']}{[\beta_d \sinh \beta_1 d' + \beta_1 \cosh \beta_1 d']} \right\}, \qquad 5\text{-}13$$

where Equation 5-12 was used to eliminate the amplitude term A.

Applying the boundary conditions on the tangential components of the r.f. electric and magnetic fields at x=d and using Equation 5-13 yields

$$C_1 \left\{ \sinh \beta_1 d - \frac{[\beta_d \sinh \beta_1 d' + \beta_1 \cosh \beta_1 d']}{[\beta_d \cosh \beta_1 d' + \beta_1 \sinh \beta_1 d']} \cosh \beta_1 d \right\} = C_2 \sinh \beta_2 d + F_2 \cosh \beta_2 d \qquad 5\text{-}14$$

and

$$\beta_1 C_1\left\{\cosh\beta_1 d - \frac{[\beta_d \sinh\beta_1 d' + \beta_1 \cosh\beta_1 d']}{[\beta_d \cosh\beta_1 d' + \beta_1 \sinh\beta_1 d']}\sinh\beta_1 d\right\} = \beta_2[C_2\cosh\beta_2 d + F_2 \sinh\beta_2 d]. \quad 5\text{-}15$$

Combining Equations 5-14 and 5-15 and using well known identities results in

$$C_2 = -F_2 \frac{\{\beta_1[\beta_d\cosh Q_1 + \beta_1 \sinh Q_1]\cosh Q_2 + \beta_2[\beta_d \sinh Q_1 + \beta_1 \cosh Q_1]\sinh Q_2\}}{\{\beta_1[\beta_d\cosh Q_1 + \beta_1 \sinh Q_1]\sinh Q_2 + \beta_2[\beta_d \sinh Q_1 + \beta_1 \cosh Q_1]\cosh Q_2\}}, \quad 5\text{-}16$$

where

$$Q_1 = \beta_1(d'-d), \quad 5\text{-}17$$

and

$$Q_2 = \beta_2 d. \quad 5\text{-}18$$

Application of the boundary conditions on the tangential components of the r.f. electric and magnetic fields at x=0 yields

$$F_2 = G \quad 5\text{-}19$$

and

$$-\beta_2 C_2 = \frac{(k\mu_{12}G - \beta_m \mu_{11} L)}{(\mu_{11}^2 - \mu_{12}^2)}. \quad 5\text{-}20$$

Repeating this process at x=-a, the interface of the ferrite with dielectric # 2, leads to

$$R = G\cosh Q_m - L\sinh Q_m \quad 5\text{-}21$$

$$-\beta_d R = \frac{(k\mu_{12}G - \beta_m\mu_{11}L)\cosh Q_m - (k\mu_{12}L - \beta_m\mu_{11}G)\sinh Q_m}{(\mu_{11}^2 - \mu_{12}^2)} \qquad 5\text{-}22$$

where $Q_m = \beta_m a$ as defined by Equation 3-14. Combining Equations 5-19, 5-20, 5-21, and 5-22 the amplitude terms R, G, and L may be elimated yielding the following expression

$$C_1 = -\frac{F_2}{\beta_2}\left\{\frac{k\mu_{12}}{(\mu_1^2 - \mu_{12}^2)} - \frac{\beta_m\mu_{11}}{(\mu_{11}^2 - \mu_{12}^2)}\left[\frac{[k\mu_{12} + \beta_d(\mu_{11}^2 - \mu_{12}^2)]\cosh Q_m + \beta_m\mu_{11}\sinh Q_m}{[k\mu_{12} + \beta_d(\mu_{11}^2 - \mu_{12}^2)]\sinh Q_m + \beta_m\mu_{11}\cosh Q_m}\right]\right\}. \qquad 5\text{-}23$$

Equation 5-23 may be used to eliminate the amplitude terms in Equation 5-16 resulting in the self-consistency condition,

$$k\mu_{12} - (\mu_{11}^2 - \mu_{12}^2)\beta_2\left\{\frac{\beta_1[\beta_d + \beta_1\tanh Q_1] + \beta_2[\beta_d + \beta_1\coth Q_1]\tanh Q_2}{\beta_1[\beta_d + \beta_1\tanh Q_1] + \beta_2[\beta_d + \beta_1\coth Q_1]\coth Q_2}\right\}\coth Q_2$$
$$= \beta_m\mu_{11}\left\{\frac{[\beta_d(\mu_{11}^2 - \mu_{12}^2) + k\mu_{12}] + \beta_m\mu_{11}\tanh Q_m}{[\beta_d(\mu_{11}^2 - \mu_{12}^2) + k\mu_{12}] + \beta_m\mu_{11}\coth Q_m}\right\}\coth Q_m . \qquad 5\text{-}24$$

Equation 5-24, together with Equations 2-94, 5-7, 5-11 and 2-95 are the single mode exchange modified dispersion relationships describing electromagnetic surface wave propagation along the ferrite-semiconductor interface shown in Figure 5-1. Due to the complexity of this dispersion relationship it is convenient to consider the effects of finite semiconductor and finite ferrite dimensions independently. Thus, the dispersion relationship is analyzed in certain limiting cases in the following two sections.

5.2 Epitaxial Semiconductors, Surface Layers and Dielectric Spacing

In this section the model shown in Figure 5-1 is modified to illustrate the effect of finite semiconductor dimensions on the interaction. In the modified model, shown in Figure 5-2, semiconductor region # 1 and the ferrite are considered to be very thick, their boundaries with the dielectric regions being far from the ferrite-semiconductor # 2 interface. In this limit

$$\beta_m \coth Q_m \cong \beta_m \qquad 5\text{-}25$$

$$\beta_m \tanh Q_m \cong \beta_m \qquad 5\text{-}26$$

$$\beta_1 \coth Q_1 \cong \beta_1 \qquad 5\text{-}27$$

$$\beta_1 \tanh Q_1 \cong \beta_1 \qquad 5\text{-}28$$

and Equation 5-24 reduces to

$$\frac{k\mu_{12} - \beta_m \mu_{11}}{(\mu_{11}^2 - \mu_{12}^2)} = \beta_2 \coth Q_2 \left\{ \frac{\beta_1 + \beta_2 \tanh Q_2}{\beta_1 + \beta_2 \coth Q_2} \right\}, \qquad 5\text{-}29$$

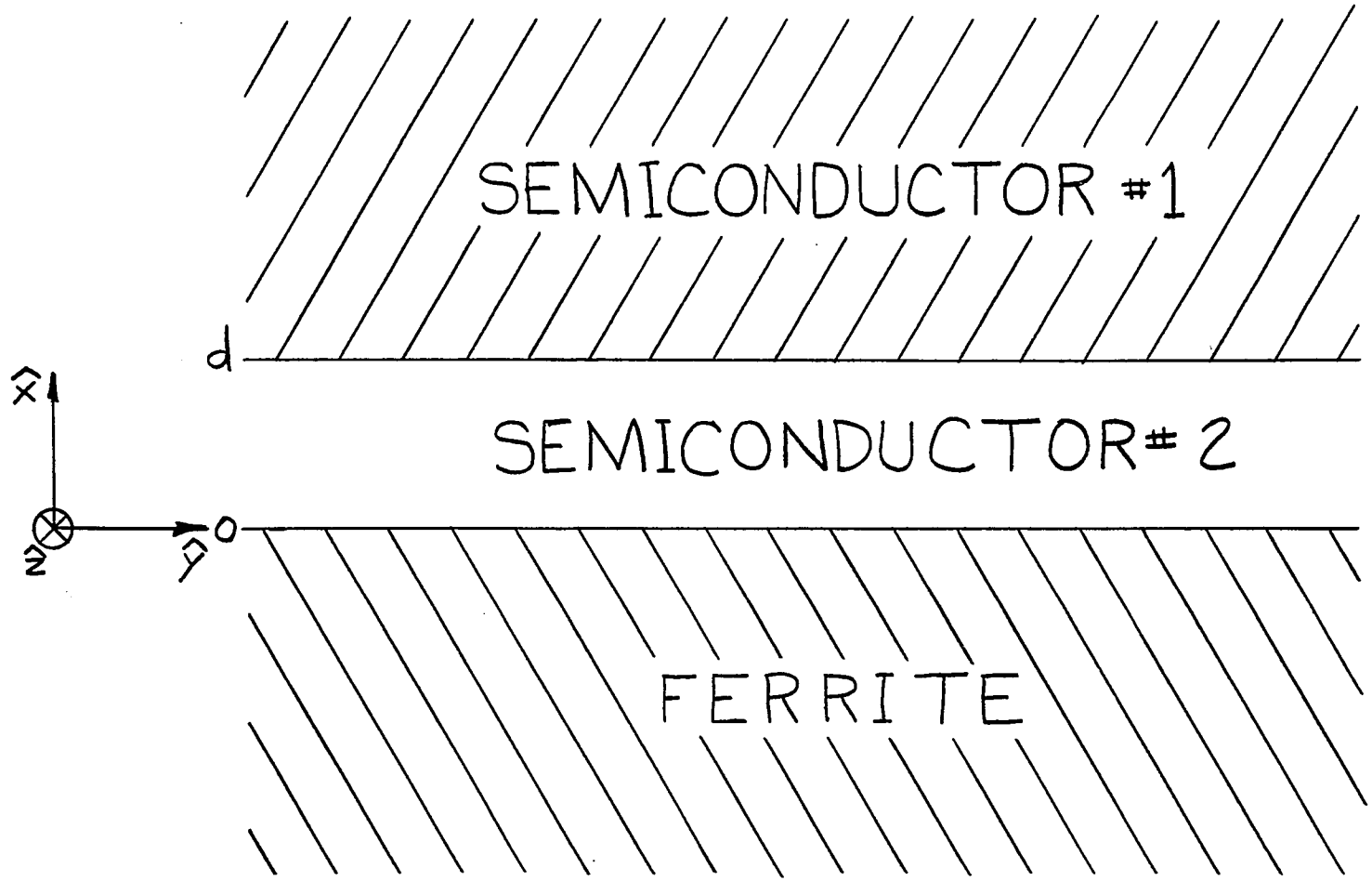

Figure 5-2 - Model For Determining Effects of Dielectric Spacing, Surface Layers and Finite Semiconductor Thickness

where

$$Re[\beta_m] > 0 \qquad 5\text{-}30$$

and

$$Re[\beta_1] > 0 \qquad 5\text{-}31$$

Equations 2-94, 5-7, 5-11, and 5-29 are the set of dispersion relationships describing surface wave propagation in the structure shown in Figure 5-2. This model may be used for an epitaxial semiconductor, where, the surface region, $0 < x \leq d$, is considered to be the epitaxial grown material and the region, $x > d$, as the substrate. The configuration may also be used to model the region in the vicinity of the surface of a semiconductor that is characterized by carrier densities and mobilities which differ from their bulk values as discussed in the previous chapter. Yet another case which the model of Figure 5-2 may be used to describe is that of a semiconductor and a ferrite separated by a uniform dielectric region, $\omega_{p2_i} = 0$, of thickness d. This dielectric region may represent an oxide layer on the semiconductor surface or a small separation between the media due to the roughness of the surfaces. Additionally, such a separation may intentionally be brought about by the insertion of a dielectric sheet between the media.

The similarities between the models for epitaxial semiconductors, surface layers and dielectric spacing permits initial analysis of surface wave behavior to be performed for the general case. Before proceeding with this

detailed analysis, some observations concerning the propagation characteristics may be made by inspection. If the thickness of semiconductor # 2 is allowed to become large such that

$$\beta_2 \coth Q_2 \cong \beta_2 \,, \tag{5-32}$$

$$\beta_2 \tanh Q_2 \cong \beta_2 \tag{5-33}$$

where

$$\mathrm{Re}[\beta_2] > 0, \tag{5-34}$$

then Equation 5-29 reduces to

$$\beta_2 = \frac{k\mu_{12} - \beta_m \mu_{11}}{(\mu_{11}^2 - \mu_{12}^2)} \tag{5-35}$$

indicating that semiconductor # 1 is sufficiently far from the x=0 interface that propagation along the ferrite-semiconductor # 2 interface is unaffected by it. Noting the similarity between Equation 5-35 and Equation 4-41 (or in the dielectric separation case Equation 2-94), the propagation characteristics are similar to those obtained for the semi-infinite ferrite-semiconductor (-dielectric) model. On the other hand, if the thickness of semiconductor # 2 is reduced to zero, Equation 5-29 becomes

$$\beta_1 = \frac{k\mu_{12} - \beta_m \mu_{11}}{(\mu_{11}^2 - \mu_{12}^2)} \tag{5-36}$$

indicating that surface wave behavior is determined by the properties of the ferrite and semiconductor # 1.

Analysis of the interaction between the spin and carrier systems for arbitrary semiconductor # 2 thicknesses is performed by observing the behavior of the complex radian frequency as the longitudinal wavenumber, k, is varied along the real axis. As noted in Chapter 4, an instability is indicated if there exists a root, ω, of the dispersion relation which has a negative imaginary component when k is real. Noting further that the magnetostatic approximation is appropriate when analyzing the interaction between the spin mode and the carrier stream, the analysis is restricted to the magnetostatic regime. In this limit the phase velocity is greater than the intrinsic velocities in the semiconducting (and dielectric) media and the transverse wavenumbers are related to the longitudinal wavenumber by the following expressions

$$\beta_m = k, \qquad 2\text{-}109$$

$$\beta_1^2 = k^2 [1 + j 2T_1], \qquad 5\text{-}37$$

and

$$\beta_2^2 = k^2 [1 + j 2T_2], \qquad 5\text{-}38$$

where

$$T_1 = \frac{1}{2kc_1^2} \sum_{s=1}^{S_1} \frac{\omega_{p1s}^2 (v_{ph} + v_{o1s})}{\nu_{1s}}, \qquad 5\text{-}39$$

$$T_2 = \frac{1}{2kc_2^2} \sum_{s=1}^{S_2} \frac{\omega_{p2s}^2 (v_{ph} + v_{o2s})}{\nu_{2s}}, \qquad 5\text{-}40$$

$$v_{ph} = Re\left[\frac{\omega}{k}\right] \cong \frac{\omega}{k}, \qquad 5\text{-}41$$

and it has been assumed that the carrier species in the semiconducting regions are collision dominated. If $|T_1| \ll 1$ and $|T_2| \ll 1$ Equations 5-37 and 5-38 become

$$\beta_1 = k[1 + j T_1], \qquad 5\text{-}42$$

and

$$\beta_2 = k[1 + j T_2], \qquad 5\text{-}43$$

to first order. Substituting these expressions for the transverse wavenumbers into Equation 5-29, the dispersion relation reduces to

$$\frac{1}{\mu_{11} + \mu_{12}} = -(1 + j T_2) \coth Q_2 \frac{[(1+jT_1) + (1+jT_2)\tanh Q_2]}{[(1+jT_1) + (1+jT_2)\coth Q_2]}. \qquad 5\text{-}44$$

Using the permeability tensor component definitions of Equations 4-55 and 4-56, the above relation may be reexpressed as

$$\frac{(\omega_i + j\nu_m - \omega)}{(\omega_i + \omega_m + j\nu_m - \omega)} = -(1+jT_2)\coth Q_2 \frac{[(1+jT_1)+(1+jT_2)\tanh Q_2]}{[(1+jT_1)+(1+jT_2)\coth Q_2]} . \quad 5\text{-}45$$

Solving for the complex radian frequency,

$$\omega = \omega_i + \omega_m \left\{ \frac{(1+jT_2)^2 + (1+jT_1)(1+jT_2)\coth Q_2}{(1+jT_1)+(1+jT_2)^2+(1+jT_1)(2+jT_1)\coth Q_2} \right\} + j\nu_m ; \quad 5\text{-}46$$

rearranging terms yields,

$$\omega = \omega_i + \omega_m \left\{ \frac{1}{[2+jT_1+2jT_2]} + j\frac{[2T_2+(T_1+T_2)\coth Q_2]}{[2+jT_1+j2T_2][1+\coth Q_2]} \right\} + j\nu_m , \quad 5\text{-}47$$

where higher order terms in T_1 and T_2 have been neglected. To the lowest order in T_1 and T_2 Equation 5-47 may be reexpressed as

$$\omega = \omega_i + \frac{\omega_m}{2}\left\{ 1 + j\frac{T_1}{2}\epsilon^{-2Q_2} + j\frac{T_2}{2}(1-\epsilon^{-2Q_2}) \right\} + j\nu_m . \quad 5\text{-}48$$

For there to be an instability,

$$\frac{\omega_m}{4}\left[T_1\epsilon^{-2kd} + T_2(1-\epsilon^{-2kd}) \right] < -\nu_m , \quad 5\text{-}49$$

the instability occuring at the magnetostatic mode resonance frequency,

$\omega_{res} = \omega_i + \frac{\omega_m}{2}$, as expected.

Examining first, the case of a non-conducting, non-magnetic layer of thickness d, sandwiched between a semiconductor and a ferromagnetic insulator, Equation 5-40 becomes

$$T_2 = 0 \qquad 5\text{-}50$$

The semiconductor is considered to have two types of carriers electrons and holes. If it is assumed that the electrons are drifting in near synchronism with the phase velocity of the excitation and that the magnitude of this velocity is much greater than the drift velocity of the holes, Equation 5-38 becomes

$$T_1 = \frac{-\omega_{pe}^2}{2kc_1^2\nu_e}\left[v_{oe} - (1 + C_{he})\, v_{ph} \right]. \qquad 5\text{-}51$$

Substituting Equations 5-50 and 5-51 into Equation 5-48 yields the imaginary component of the complex frequency

$$\omega_{Im} = \nu_m - \frac{\omega_{pe}^2\, \omega_m}{8kc_1^2\nu_e}\left[v_{oe} - (1 + C_{he})\, v_{ph} \right] \epsilon^{-2kd}. \qquad 5\text{-}52$$

It is observed, in agreement with the discussion of Chapter 4, that it is necessary but not sufficient for the drift velocity to exceed $(1+C_{he})\,v_{ph}$ for there to be an instability. Further, because of the exponential dependence upon the thickness of the dielectric, it becomes increasingly difficult for an instability to be achieved as the dielectric thickness increases.

To determine whether an instability exists for a specific combination of material parameters and dielectric thickness, Equation 5-52 must be

evaluated as a function of k. This relation has been plotted in Figure 5-3 for parameters appropriate to a YIG - Dielectric - In Sb structure, with static internal magnetic field intensity such that the resonant frequency is 3GHz. Assuming the saturation magnetization of the YIG to be 1750 Oe. and the linewidth 0.35 Oe. ($\Delta H/M_o = 2 \times 10^{-4}$), the instabiltity onset condition nomograph, Figure 4-11, is used to determine In Sb parameters corresponding to an instability in the semi-infinite case. Selecting the electron density and mobility as $10^{17}/\text{cm}^3$ and $50,000\,\text{cm}^2/\text{v-sec}$ respectively, a drift velocity of $4 \times 10^6 \frac{\text{cm}}{\text{sec.}}$ is observed to meet the instability onset conditions. The graph axes are normalized, the vertical axis being the imaginary component of the normalized frequency, $\Omega_{Im} = \frac{\omega_{Im}}{\omega_m}$, the horizontal axis being the normalized wavenumber, $k_n = Re\left[\frac{k v_{oe}}{2\omega}\right]$. (18) The curves correspond to various dielectric thicknesses and it is observed that Ω_{Im} is quite sensitive to variations in the thickness of the dielectric layer. For the parameters selected, the instability no longer exists if the dielectric separation is greater than $0.61\,\mu$. Thus, a separation between the semiconductor and ferrite, on the order of grit sizes used in the polishing of samples[42,111] is sufficient to suppress the instability in this case, underscoring the need for care in the preparation of surfaces used in surface wave propagation studies.

Considering the case of a space charge region at the surface of a semiconductor, where semiconductor # 2 represents the surface layer and semiconductor # 1 the bulk, it is assumed that carriers are drifted by an applied

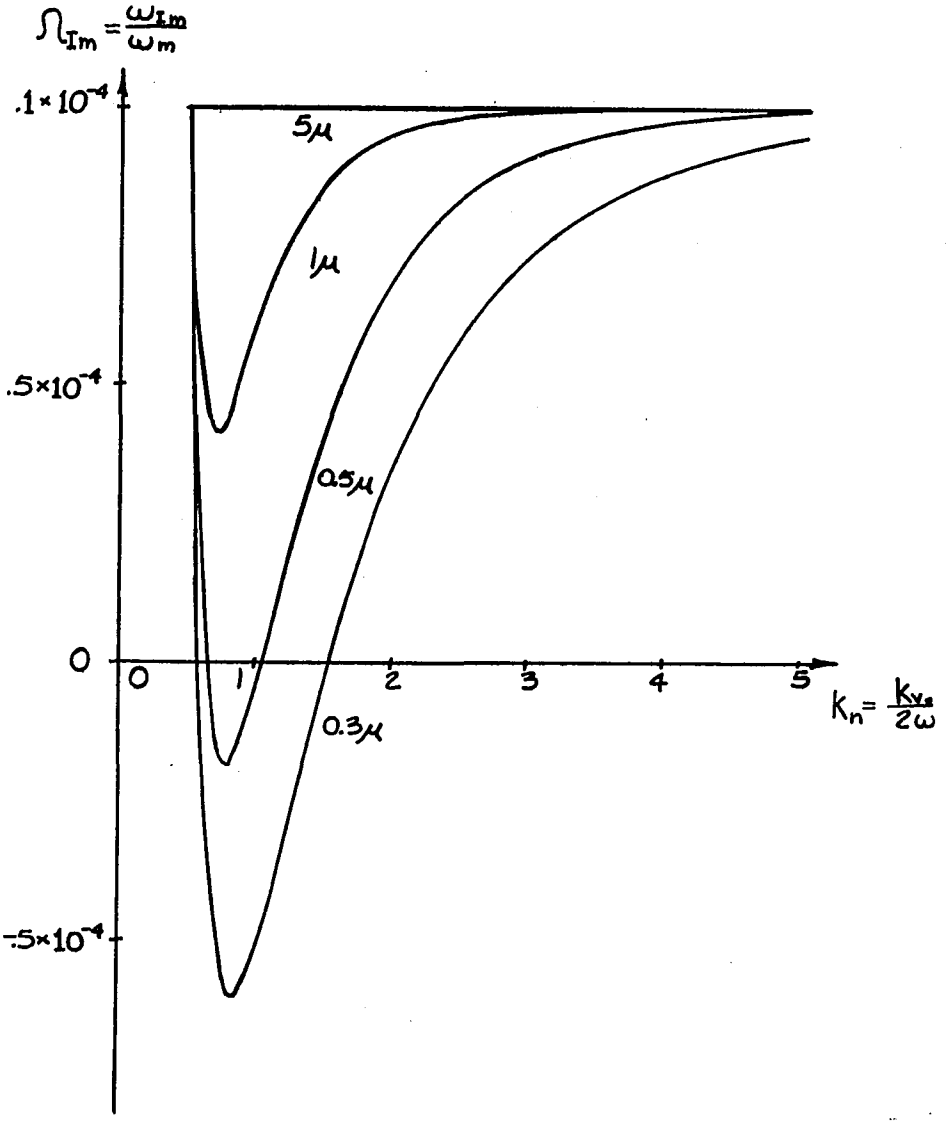

Figure 5-3 - Variation Of The Imaginary Component Of The Complex Frequency As A Function Of Wavenumber For Various Dielectric Separation Thicknesses

electric field of sufficient magnitude such that the highest mobility carrier in the bulk attains an average velocity exceeding synchronous velocity and that the concentration of these carriers is more than sufficient for there to be an instability in the absence of the space charge region. Further, the mobilites of carriers in the surface region are assumed to be sufficiently lower than those in the bulk such that the drift velocities of these carriers in the surface region are much smaller than the synchronous velocity. Under these conditions, Equation 5-11 becomes

$$k^2 - \beta_2^2 = \frac{\omega^2}{c_2^2}\left[1 - j\frac{\sigma_1}{\omega\epsilon_0\epsilon_2}\right], \qquad 5\text{-}53$$

where the conductivity of the surface region is defined as

$$\sigma_1 = \epsilon_0\epsilon_2 \sum_{s=1}^{S_2} \frac{\omega_{p2s}^2}{\nu_s} \quad . \qquad 5\text{-}54$$

Defining a complex permittivity,

$$\epsilon_2' = \epsilon_2\left[1 - j\frac{\sigma_1}{\omega\epsilon_0\epsilon_2}\right], \qquad 5\text{-}55$$

reduces the present problem to the previous case with the lossless dielectric replaced by one in which losses may no longer be neglected. Since the thickness of the space charge layer is approximately a Debye length and since it has been assumed that $\lambda_D << \lambda$, then

$$\epsilon^{-2kd} \cong 1 - 2kd , \qquad 5\text{-}56$$

and Equation 5-48 becomes

$$\omega = \omega_i + \frac{\omega_m}{2}\left\{1 + j\frac{T_1}{2}(1-2kd) + jT_2 kd\right\} + j\gamma_m \qquad 5\text{-}57$$

where

$$T_2 = \frac{V_{ph}\sigma_2}{2k c_o^2} , \qquad 5\text{-}58$$

and T_1, previously defined, is

$$T_1 = -\frac{\omega_{pe}^2}{2k c_1^2 \nu_e}\left[V_{oe} - (1 + C_{he})V_{ph}\right] , \qquad 5\text{-}51$$

for an electron-hole semiconductor plasma. Thus, in addition to the suppression (or reduction of the growth rate) of the instability caused by the physical separation of the ferrite and semiconductor bulk, the presence of the surface space charge layer introduces another term,

$$j\frac{\omega_m T_2 kd}{2} = j\frac{\omega_m V_{ph}\sigma_2 d}{4c_o^2} , \qquad 5\text{-}59$$

dependent on surface conditions and the applied fields. (The thickness and conductivity of the surface layer are functions of the applied electric and magnetic fields (Hall effect) as well as the surface state distribution.) Since T_2 is always greater than zero, the conductivity of the surface region is, as

expected, a debilitating effect on the interaction.

The case of an epitaxial semiconductor is considered next. Since the previous surface layer discussion leads to results which may be directly applied to the case of high resistivity epitaxial layers on low resistivity substrates, only the opposite situation, that of low resistivity material on high resistivity substrates, need be analyzed. Recognizing that the difference between this case and the previous one is that semiconductors # 1 and # 2 have interchanged their roles (i.e. semiconductor # 2 is now the major contributor to the instability, semiconductor # 1 having an insufficient number of carriers to interact strongly with the surface waves but serving as a lossy dielectric medium) T_1 and T_2 may be written as

$$T_2 = -\frac{\omega_{pe}^2}{2kc_1^2\nu_e}\left[v_{oe} - (1+C_{he})v_{ph}\right], \qquad 5\text{-}60$$

and

$$T_1 = 0, \qquad 5\text{-}61$$

where for simplicity the substrate losses are assumed negligible. Under these conditions, the expression for the complex radian frequency becomes

$$\omega = \omega_1 + \frac{\omega_m}{2}\left\{1 - j\frac{\omega_{pe}^2}{4kc_1^2\nu_e}\left[v_{oe} - (1+C_{he})v_{ph}\right]\left(1 - \epsilon^{-2kd}\right)\right\} + j\nu_m, \qquad 5\text{-}62$$

which, if only one carrier species is considered, is identical with the result of Schlömann.[18] Inspection of Equation 5-62 reveals that the growth rate is a maximum for infinitely thick films, the effect of finite semiconductor

thicknes being a reduction in the growth rate of the instability. This, in turn, leads to more restrictive instability onset conditions than those obtained for the semi-infinite model.

To determine whether an instability exists for a specific combination of materical parameters and dielectric thickness, the imaginary part of Equation 5-62 must be evaluated as a function of k. This has been plotted in Figure 5-4 for the YIG and InSb parameters used in Figure 5-3, with static internal magnetic field such that the resonant frequency is 3GHz. The normalization used in Figure 5-3 is used here as well. Examining the characteristics, it is observed that while reduction in the thickness of the epitaxial layer does have an adverse effect on the instability, the instability does exist for epitaxial layers in the submicron range, the minimum semiconductor thickness being approximately .19μ for the parameters used. Calculating the magnitude of T_2 corresponding to the point of minimum ω_{I_m} for a .19μ layer thickness, a value of $-8.02\text{x}10^{-4}$ is obtained, verifying that $|T_2| \ll 1$ as assumed in the derivation.

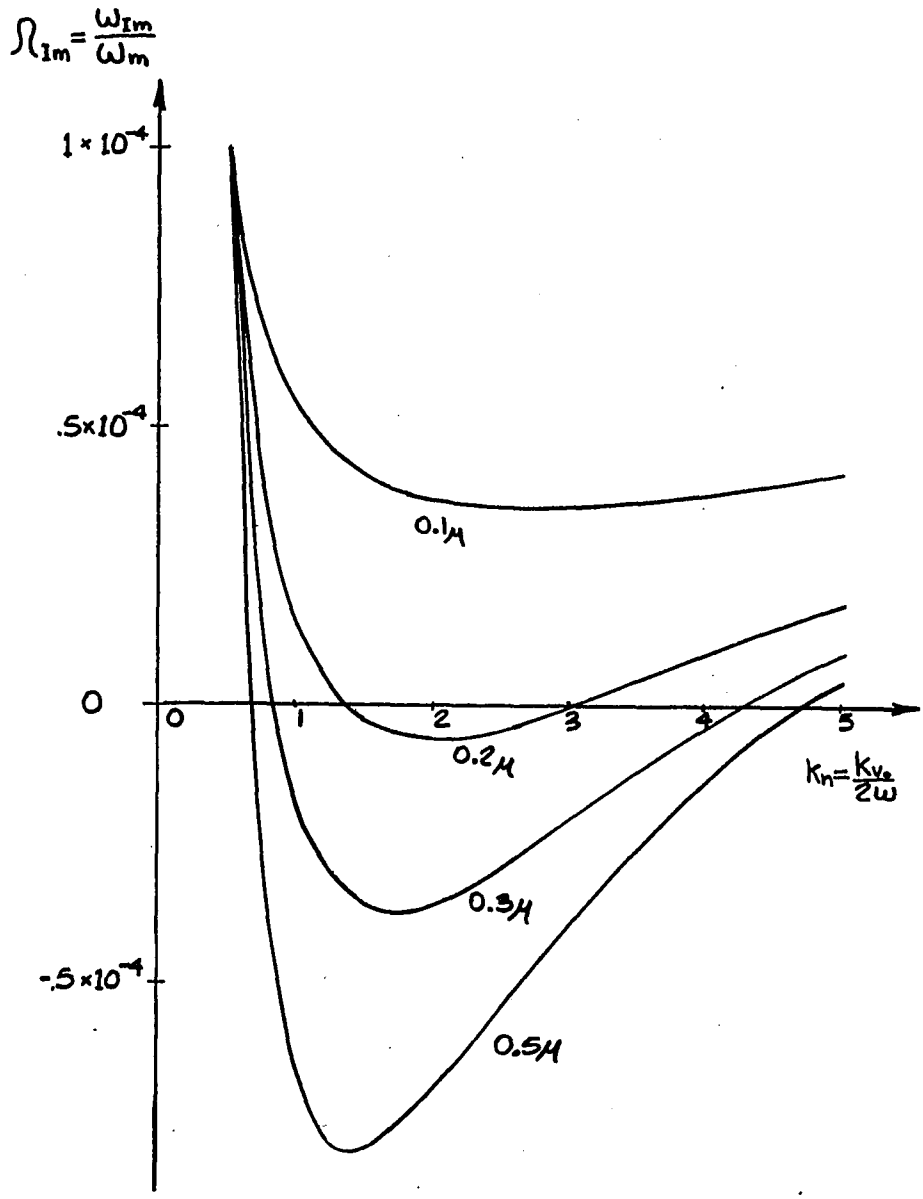

Figure 5-4 Effect Of Epitaxial Layer Thickness On The Imaginary Component Of Complex Frequency

5.3 Finite Magnetic Material

In the previous section the effect on the interaction of reducing the thickness of the semiconducting medium was discussed. The magnetic medium was assumed infinitely thick as in the semi-infinite model. In this section the alternate case is considered; the thickness of the ferrite is varied while the semiconductor is considered to be infinite in extent. The model, shown in Figure 5-5, is obtained from that of Figure 5-1 by assuming semiconductor # 2 to be very thick, such that

$$\beta_2 \coth Q_2 \cong \beta_2 , \tag{5-32}$$

and

$$\beta_2 \tanh Q_2 \cong \beta_2 , \tag{5-33}$$

where

$$\mathrm{Re}[\beta_2] > 0 . \tag{5-34}$$

In this limit Equation 5-24 reduces to

$$\mu_{12} k - (\mu_{11}^2 - \mu_{12}^2)\beta_2 = \mu_{11}\beta_m \left\{ \frac{[k\mu_{12} + \beta_d(\mu_{11}^2 - \mu_{12}^2)] + \mu_{11}\beta_m \tanh Q_m}{[k\mu_{12} + \beta_d(\mu_{11}^2 - \mu_{12}^2)] + \mu_{11}\beta_m \coth Q_m} \right\} \coth Q_m , \tag{5-63}$$

or, upon rearrangement of terms,

$$\beta_m \mu_{11} [\beta_d + \beta_2](\mu_{11}^2 - \mu_{12}^2)\cosh Q_m = [(k^2\mu_{12}^2 - \beta_m^2\mu_{11}) + k\mu_{12}(\beta_d - \beta_2)(\mu_{11}^2 - \mu_{12}^2) - \beta_d\beta_2(\mu_{11}^2 - \mu_{12}^2)]\sinh Q_m , \tag{5-64}$$

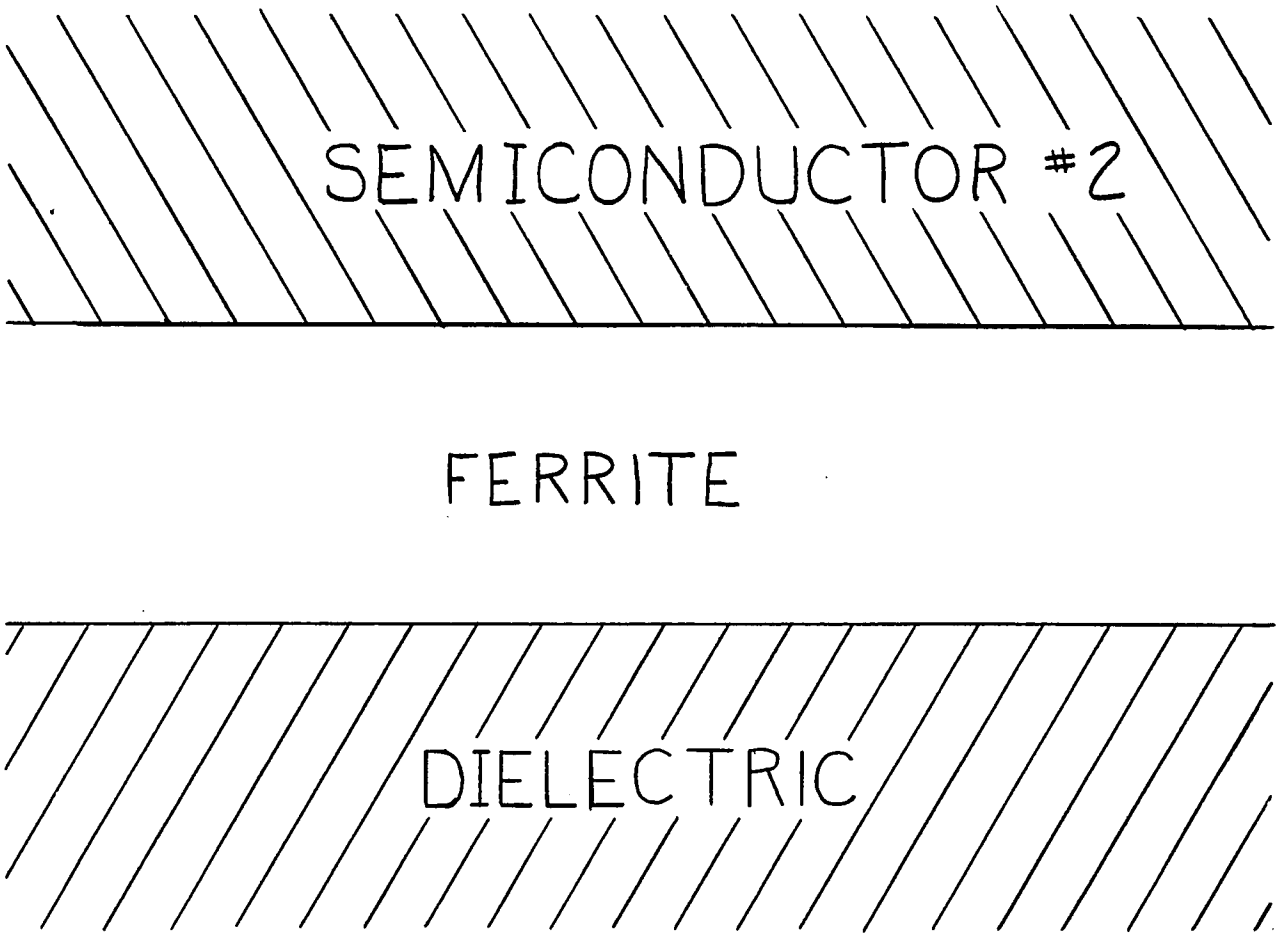

Figure 5-5 - Model Of Semi-infinite Semiconductor-Finite Ferrite Structure

which, with the exception of subscripts, is similar to Equation 3-17 obtained for a finite ferrite with dielectric loading.

If the thickness of the ferrite is large such that

$$\beta_m \cosh Q_m = \beta_m, \tag{5-25}$$

and

$$\beta_m \sinh Q_m = \beta_m, \tag{5-26}$$

where

$$\mathrm{Re}\,[\beta_m] > 0 \tag{5-30}$$

then Equation 5-64 may be reexpressed as

$$k^2\mu_{12}^2 - \beta_m^2\mu_{11}^2 + [k\mu_{12}(\beta_d - \beta_2) - \beta_m\mu_{11}(\beta_d + \beta_2)](\mu_{11}^2 - \mu_{12}^2) - \beta_2\beta_d(\mu_{11}^2 - \mu_{12}^2)^2 = 0, \tag{5-65}$$

or

$$[(\mu_{11}^2 - \mu_{12}^2)\beta_2 - k\mu_{12} + \beta_m\mu_{11}][(\mu_{11}^2 - \mu_{12}^2)\beta_d + k\mu_{12} + \beta_m\mu_{11}] = 0. \tag{5-66}$$

The terms in the left bracket of Equation 5-66 are recognized as the dispersion relationship describing surface wave propagation along a semiconductor - magnetic insulator interface where both media are semi-infinite,

$$\beta_2 = \left[\frac{k\mu_{12} - \beta_m\mu_{11}}{(\mu_{11}^2 - \mu_{12}^2)}\right], \tag{5-67}$$

this equation differing from Equation 4-41 only in the form of the subscript of the semiconductor medium transverse wavenumber. This solution corresponds to surface waves associated with and propagating along the x=0 interface. The terms in the right-hand bracket of Equation 5-66 correspond to a second mode set,

$$\beta_d = -\left[\frac{k\mu_{12} + \beta_m\mu_{11}}{(\mu_{11}^2 - \mu_{12}^2)}\right], \qquad 3\text{-}38$$

corresponding to waves propagating at the ferrite-dielectric interface at x=-a. Thus, in addition to the surface mode of interest propagating along the semiconductor-ferrite interface the ferrite may support up to two additional surface modes, a reverse "magnetostatic" mode, and possibly a forward or reverse "dynamic" mode as described in Chapters 2 and 3. Restricting the discussion to only those modes which may propagate in the immediate vicinity of the "magnetostatic" surface mode resonance, $\omega_{res} = \omega_i + \frac{\omega_m}{2}$, only the reverse "magnetostatic" and forward "dynamic" modes need be considered. The reverse "magnetostatic" mode, which may propagate at frequencies just below ω_{res}, provides a means whereby waves reflected at the far end of the slab may return along the x=-a interface. The waves returning along this "feedback path" give rise to traveling wave resonance phenomena similar to those described in Chapter 3 and discussed in connection with experimental observations in the next section. The forward "dynamic" mode, may propagate at the frequency of operation only if

$$\epsilon_d < \epsilon_m , \qquad 5\text{-}68$$

and

$$\omega > \sqrt{\frac{(\epsilon_m - \epsilon_d)\,\omega_i^2 + \epsilon_m \omega_m \omega_i}{(\epsilon_m - \epsilon_d)}} , \qquad 5\text{-}69$$

the latter condition having been obtained from Equation 2-126. If the inequalities expressed by Equations 5-68 and 5-69 are both fulfilled two surface waves may propagate in the $+\hat{y}$ direction simultaneously; one, the mode of interest, interacting with the semiconductor at x=0, and the other, a fast wave propagating along the alternate path at x=-a. While it was found in the experiments described in Chapter 3 that the "dynamic" mode was not as strongly excited as the "magnetostatic" mode, in the present configuration the "dynamic" mode travels along the relatively low loss ferrite-dielectric interface and may be significant at the output when compared to the mode of interest. It may therefore be of advantage to suppress the forward "dynamic" mode at x=-a when examining the transmission characteristics of the mode of interest. Furthermore, since the study of transmission properties may be complicated by traveling wave resonance phenomena caused by the x=-a feedback path, it may be desirable to suppress the reverse "magnetostatic" mode as well. This may be accomplished by coating the ferrite surface at x=-a with resistive paint as discussed in Chapter 3.

The interaction between the spin and carrier systems for the finite thickness ferrite is analyzed by observing the behavior of the complex radian frequency as the longitudinal wavenumber, k, is varied along the

real axis. Following the procedures of Section 5.2, it is assumed that the transverse wavenumbers are related to k as

$$\beta_m = k \qquad 2\text{-}109$$

$$\beta_d = k \qquad 2\text{-}110$$

and

$$\beta_2 = k[1 + j T_2], \qquad 5\text{-}42$$

where

$$T_2 = -\frac{\omega_{pe}^2}{2kc_1^2\nu_e}\left[v_{oe} - (1 + C_{he})v_{ph}\right] . \qquad 5\text{-}59$$

Substitution of Equations 2-109, 2-110 and 5-42 into Equation 5-64 yields,

$$\mu_{11}[2 + j T_2]\cosh Q_m + [1 + j T_2\mu_{12} + (1 + j T_2)(\mu_{11}^2 - \mu_{12}^2)]\sinh Q_m = 0. \qquad 5\text{-}70$$

Using the definitions for $\sinh Q_m$ and $\cosh Q_m$ as well as the permeability tensor component definitions, Equations 4-55 and 4-56, the above expression becomes

$$\omega^2[2 + j T_2] - \omega\left(j\frac{\omega_m}{2}T_2\right)(1 - \epsilon^{-2Q_m})$$
$$-\left(\omega_i + \frac{\omega_m}{2} + j\nu_m\right)\left[2\left(\omega_i + \frac{\omega_m}{2} + j\nu_m\right) + j T_2(\omega_i + \omega_m + j\nu_m)\right]$$
$$+\frac{\omega_m}{2}\left[\omega_m + j T_2(\omega_i + \omega_m + j\nu_m)\right]\epsilon^{-2Q_m} = 0. \qquad 5\text{-}71$$

In the limit where the ferrite is large such that

$$\epsilon^{-2Q_m} \ll 1, \qquad 5\text{-}72$$

Equation 5-71 reduces to

$$\omega^2\left[2+jT_2\right]-\omega\left[j\frac{\omega_m}{2}T_2\right]$$

$$-\left(\omega_i+\frac{\omega_m}{2}+j\nu_m\right)\left[2\left(\omega_i+\frac{\omega_m}{2}+j\nu_m\right)+jT_2\left(\omega_i+\omega_m+j\nu_m\right)\right]=0. \qquad 5\text{-}73$$

Rewriting this equation as

$$2\left[\omega^2-\left(\omega_i+\frac{\omega_m}{2}+j\nu_m\right)^2\right]$$

$$+jM\left[\omega^2-\frac{\omega\omega_m}{2}\left(\omega+\frac{\omega_m}{2}+j\nu_m\right)\left(\omega_i+\omega_m+j\nu_m\right)\right]=0, \qquad 5\text{-}74$$

factoring out the solution whose real part is negative and rearranging terms leads to

$$\omega=\omega_i+\omega_m\frac{\left[1+jT_2\right]}{\left[2+jT_2\right]}+j\nu_m, \qquad 5\text{-}75$$

which if, as has been assumed, $|T_2| \ll 1$ reduces to the following approximate solution for ω,

$$\omega=\omega_i+\frac{\omega_m}{2}\left[1+j\frac{T_2}{2}\right]. \qquad 5\text{-}76$$

This result is in agreement with the results of Section 5.2 in the limit where the semiconductor is uniform and extends infinitely from its interface with the ferrite.

Considering now the other extreme, where the ferrite thickness is small such that

$$\epsilon^{-2Q_m}\cong 1, \qquad 5\text{-}77$$

Equation 5-71 becomes

$$\omega^2 = (\omega_i + j\nu_m)(\omega_i + \omega_m + j\nu_m). \qquad 5\text{-}78$$

This result indicates that the instability has been suppressed by reducing the thickness of the ferrite layer. Furthermore, inspection of the numerator and denominator of Equation 2-95,

$$k^2 - \beta_m^2 = \frac{\omega^2}{c_m^2}\frac{(\mu_{11}^2 - \mu_{12}^2)}{\mu_{11}} = \frac{\omega^2}{c_m^2}\frac{[(\omega_i + \omega_m + j\nu_m)^2 - \omega^2]}{[(\omega_i + j\nu_m)(\omega_i + \omega_m + j\nu_m) - \omega^2]}, \qquad 5\text{-}79$$

reveals that β_m becomes large as this limit is approached. Thus, two of the conditions upon which this approximation is based may be violated when considering extremely thin ferrite layers. The first of these, the assumption that

$$\omega \gg \omega_{ex} a^2 \beta_m^2, \qquad 2\text{-}96$$

permitting pinning coupled exchange effects to be neglected, may no longer be satisfied. The second condition, that electromagnetic propagation may be neglected in the ferrite, the magnetostatic approximation, may also no longer be applicable. It is therefore necessary in applying Equation 5-71 to verify that both of the conditions mentioned above are satisfied. Furthermore, since the real part of the frequency is strongly dependent on Q_m, T_2 must be treated as a function of ω as well as k for a particular set of parameters.

Numerical evaluation of the approximate dispersion relationship proceeds by introducing the normalized parameters k_n and d_n, [18] defined as

$$k_n = Re\left[\frac{k\,v_{oe}}{2\omega}\right] \cong \frac{k\,v_{oe}}{2\omega} \quad , \qquad 5\text{-}80$$

and

$$d_n = Re\left[\frac{4\omega d}{v_{oe}}\right] \cong \frac{4\omega d}{v_{oe}} \quad , \qquad 5\text{-}81$$

into Equation 5-71 yielding

$$\omega^2\left[2 + jT_2\right] - \left(j\frac{\omega_m}{2}T_{2n}'\right)\left(1 - \epsilon^{-k_n d_n}\right)$$

$$-\left(\omega_i + \frac{\omega_m}{2} + j\nu_m\right)\left[2\left(\omega_i + \frac{\omega_m}{2} + j\nu_m\right) + jT_2\left(\omega_i + \omega_m + j\nu_m\right)\right]$$

$$+ \frac{\omega_m}{2}\left[\omega_m + jT_2\left(\omega_i + \omega_m + j\nu_m\right)\right]\epsilon^{-k_n d_n} = 0, \qquad 5\text{-}82$$

where

$$T_{2n} = -\frac{Ne\mu_e v_{oe}^2}{8\epsilon_o c_o^2}\left[\frac{2}{k_n} - (1 + C_{he})\frac{1}{(k_n)}\right] \quad , \qquad 5\text{-}83$$

and

$$T_2 = \frac{T_{2n}}{\omega} \quad . \qquad 5\text{-}84$$

Equation 5-82 is cubic in ω, T_2 being inversely proportional to ω. However, examining this expression in the quasi-quadratic form in which it is written, it is noted that since

$$|T_2| \ll 1 \quad , \qquad 5\text{-}85$$

T_2 causes only a small correction to the real part of the frequency in the region of interest, its effect being more pronounced on the relatively small

imaginary component of the complex frequency. As a result, if the third root of Equation 5-82 is neglected as being out of the frequency range of interest, a rapidly converging iterative technique may be used to solve for the one remaining root having a positive real part.

At each data point, corresponding to a specified value of k_n, a trial function equal to

$$\omega_{res} = \omega_i + \frac{\omega_m}{2} \qquad 2\text{-}114$$

is used to evaluate the initial value of T_2. Then, solving Equation 5-82 for the complex frequency root having a positive real part, an intermediate frequency value is determined. Reevaluating k_n, d_n, T_{2n} and T_2 using this intermediate frequency, Equation 5-82 is solved once more yielding the desired complex frequency solution, the real part of which corresponds to a frequency between $\omega_{res} = \omega_i + \frac{\omega_m}{2}$ $(a = \infty)$ and $\omega = \sqrt{\omega_i(\omega_i + \omega_m)}$ $(a = 0)$. The reason for the variation in the real part of the frequency becomes apparent when it is recalled that the "magnetostatic" mode suffers a decrease in wavelength over most of its spectrum due to the finite thickness of the ferrite (Chapter 3). Thus, as a result, synchronism is achieved at correspondingly lower frequencies as the ferrite thickness is decreased.

Having determined a frequency solution corresponding to the new value of k_n, Equations 2-95 and 5-38 are evaluated in order to obtain the corresponding values of β_m and β_2. These are then compared with k to determine whether the magnetostatic approximation is valid at that point.

In addition $\omega_{ex} a^2 \beta_m^2$ is also computed and compared with ω as a check on the appropriateness of neglecting pinning coupled exchange effects.

The technique outlined above has been used to evaluate and plot the real and normalized imaginary components of the complex frequency as a function of the normalized wavenumber as shown in Figure 5-6. The semiconductor and ferrite parameters selected are equal to the YIG and InSb parameters used in plotting Figures 5-3 and 5-4, with the static internal magnetic field intensity again chosen to correspond to a "magnetostatic" mode resonance frequency of 3GHz. It is observed that reduction of the thickness of the ferrite does have an adverse effect on the interaction, as anticipated from the analyses performed in the thin ferrite limit. Furthermore, as the ferrite thickness is decreased maximum gain occurs as larger values of normalized wavenumber and hence lower values of frequency. It is found that the instability no longer exists for ferrite thicknesses less than $.16\mu$ for the InSb-YIG parameters used. Calculations in the vicinity of the minimum Ω_{I_m} point show these results to be consistent with the magnetostatic and small exchange approximations employed.

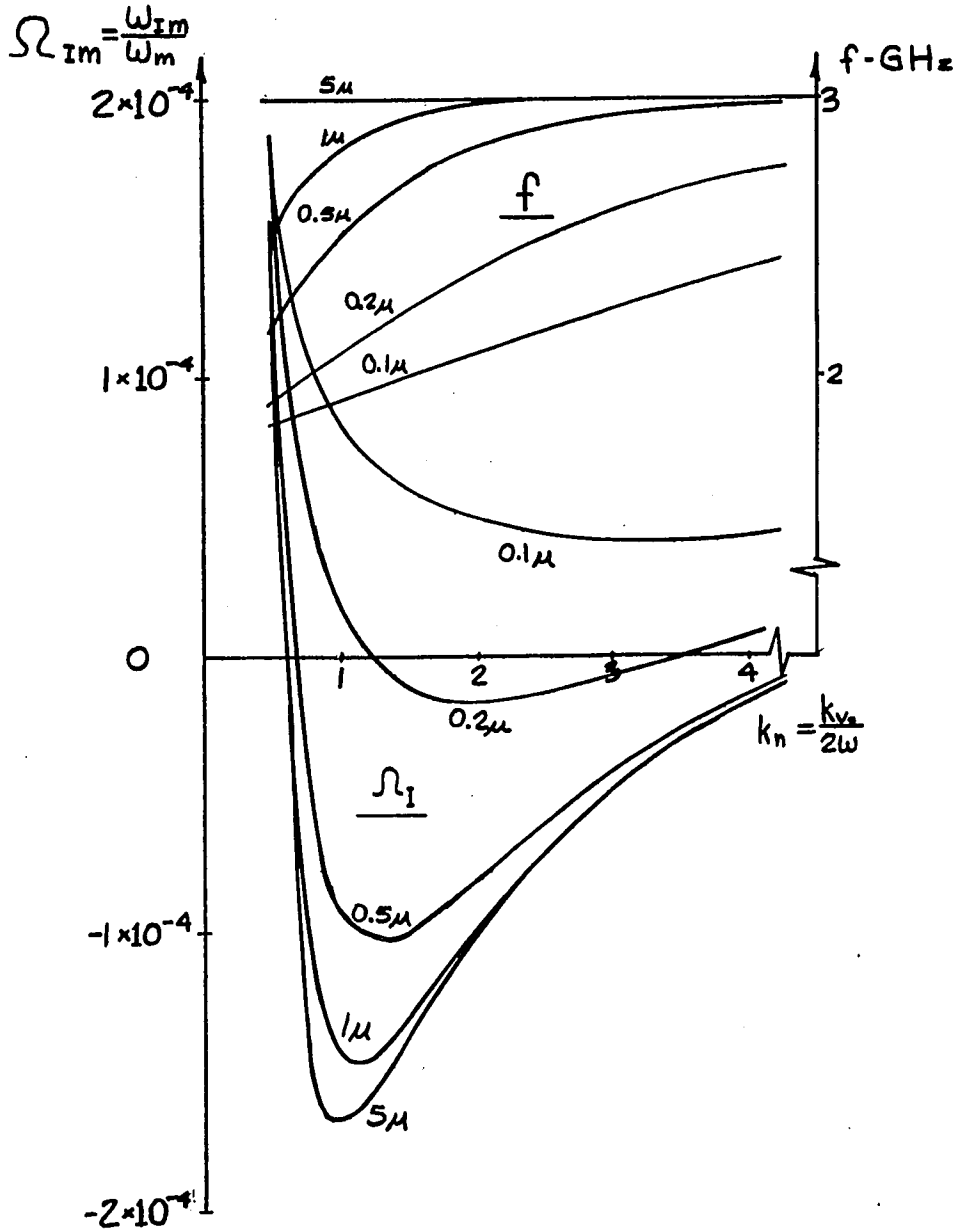

Figure 5-6 - Effect Of Finite Ferrite Thickness
On The Complex Frequency

5.4 Experimental Investigations

Empirical investigation of the transmission properties of surface waves propagating along the interface between a ferrite slab and a drifted semiconductor were conducted. Because of the complexity of the system studied numerous effects such as magnetic field shift, temperature variations and traveling wave resonance pehenomena were associated with the measurements. The techniques employed in accounting for and/or minimizing these effects are described and the results of the experiments are discussed.

The experiments were performed as the theoretical work was in progress and were subject to the availability of materials. The initial experiments were performed by placing a 10 x 55 x 206 mil sample of indium antimonide in contact with one of the large faces of the YIG slab described in connection with the experiments of Chapter 3. The YIG was supported in a plexiglass jig (an engineering sketch showing critical dimensions but not all details appears in Figure 5-7). The InSb was pressed against the YIG by a brass spring fastened at one end to the plexiglass and insulated from the InSb at its other by teflon and card stock. (These materials being sufficiently far from the YIG-InSb interface had little effect on the surface waves of interest). The relative positions of the InSb and YIG are as shown in Figure 5-8. The r.f. couplers, constructed of 70 mil coax, Phelps Dodge Type CT - 07050, are similar in design to those described in Chapter 3. In the present configuration they are located on the same side but at opposite ends of the ferrite, separated from it by a strip of 0.001 inch teflon. In

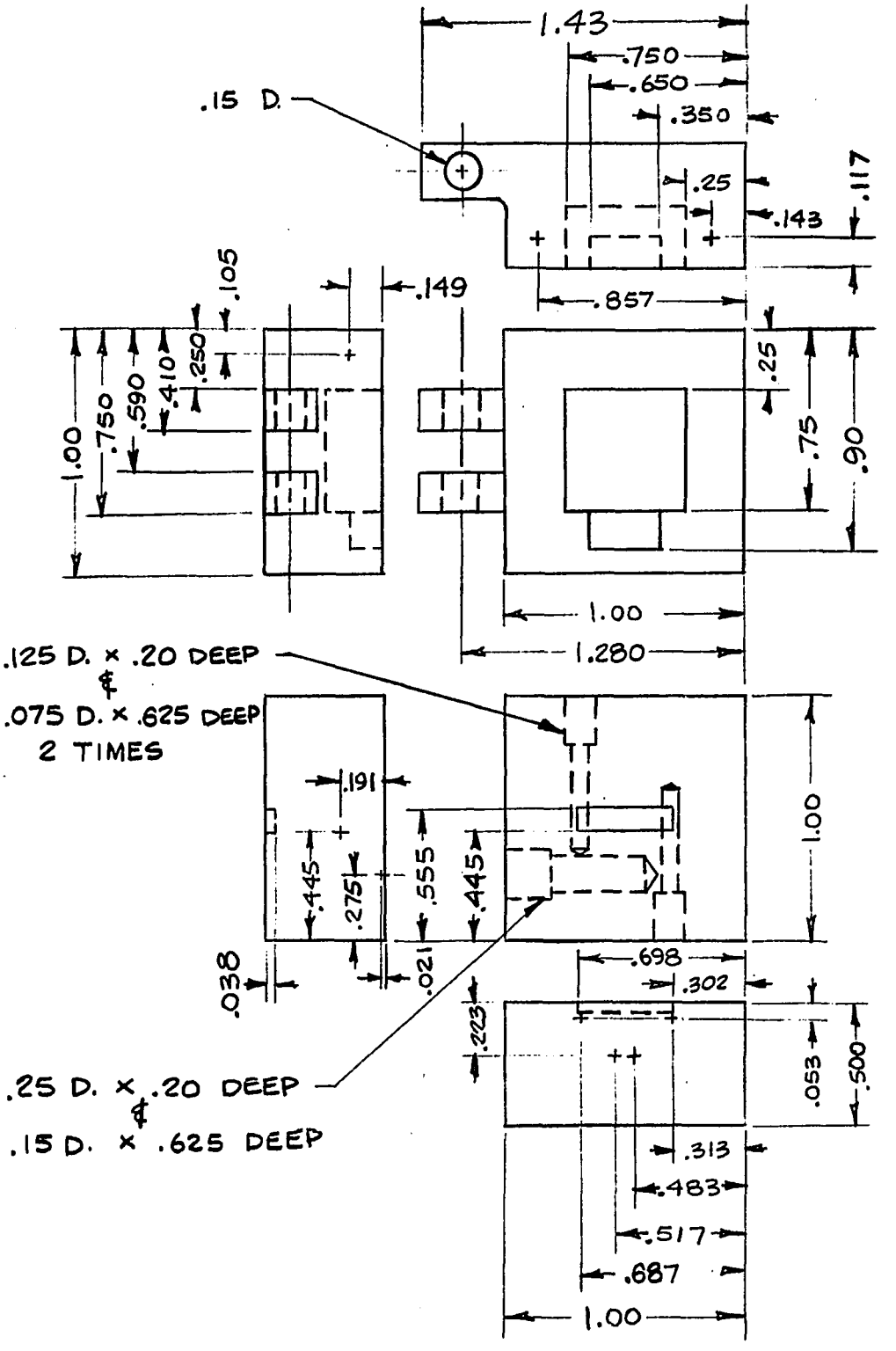

Figure 5-7 Engineering Sketch of Jig for YIG-InSb Transmission Experiments

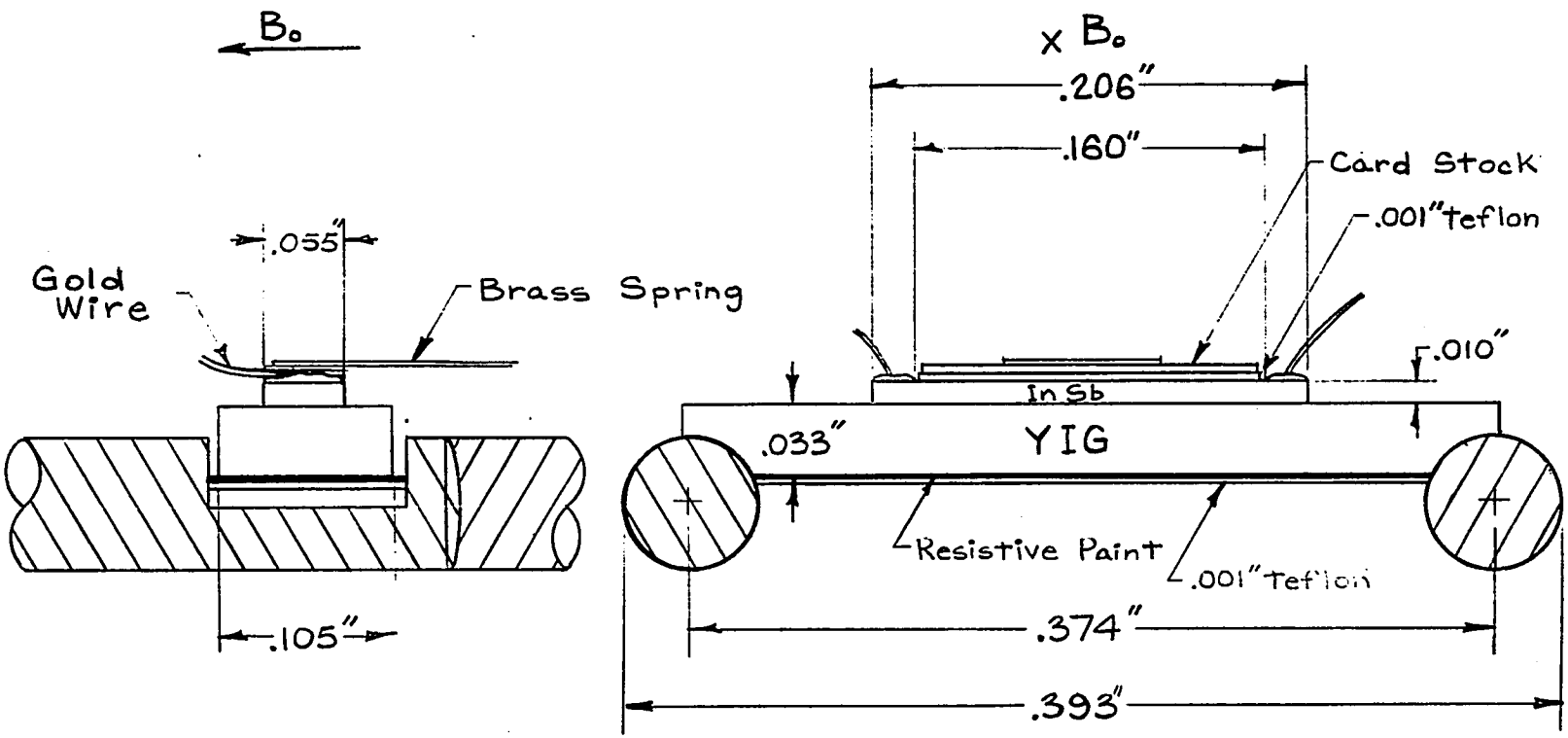

Figure 5-8 Relative Positions of InSb and YIG for Transmission Experiments

order to suppress the anticipated traveling wave resonances and surface wave coupling from input to output along the ferrite surface adjacent to the r.f. couplers, this surface of the ferrite was coated with resistive paint having a resistivity of 500 ohms/sq..

Drift fields were applied to the InSb at contacts placed at the sample's ends and connected to a 0.141 inch semirigid cable through 0.005 inch gold wires. The contacts, 0.160 inch apart, were fabricated by applying a 50-50 indium-tin solder to the indium antimonide with a low temperature soldering iron after the sample had been cleaned by immersing it in various hot and cold solvents. After tinning, the gold wires were attached by reheating the contacts until the solder melted. The sample contacts were tested and found to be ohmic. The room temperature resistance of the sample was measured to be 0.4 ohms.

Transmission experiments were performed with the YIG - InSb sandwich, housed in its plexiglass jig, lowered into a dewar filled with liquid nitrogen. In going from room temperature to that of liquid nitrogen, $77^{0}K$, the InSb carrier concentration decreases approximately two orders of magnitude to $N \cong 10^{14}$ cm.$^{-3}$, (data provided by supplier) while the electron mobility increases to approximately 280,000 cm^2/v-sec. (estimated on the basis of measurements; 2 μ sec., 25v pulse applied every 20 m sec.) As a result, the conductivity of the indium antimonide is decreased from its room temperature value, the sample presenting an increased resistance of R=26 ohms. The lowering of the temperature to that of liquid nitrogen

effects YIG properties as well. As the temperature decreases both the saturation magnetization and the linewidth increase, the saturation magnetization increasing from approximately 1760 G. to 2400 G.[30,112], while increases in the linewidth of as much as nine times have been reported[42]. (Observing the surface wave spectrum of the YIG slab as the temperature was lowered from room temperature to 77^0K, a shift of the spectrum to higher frequencies corresponding to an increased ω_m was seen. This increase in the frequency of the spectrum was accompanied by a decrease in the amplitude of the transmitted signal).

The schematic diagram of the experimental setup used in the transmission studies is shown in Figure 5-9. A continous wave signal, obtained from an HP 8690A sweep frequency oscillator with H01-8694B r.f. plug-in, is matched to the sample input by a single stub tuner, Microlab FXR X 311A. The r.f. output is brought out through another single stub tuner to a mixer-preamplifier, LEL Model XBH-3, where the signal is heterodyned to 30 MHz.. The local oscillator level is maintained at a constant level of 1mw ., and the attenuator in the input circuit is adjusted to insure that the mixer-preamplifier is operating sufficiently below saturation to ensure that its output is proportional to its input. After being attenuated by a precision variable attenuator, AIL Type 32, the output signal is displayed on an oscilloscope. The precision variable attenuator permits quantatative comparisons to be made between the output signal level when the electrons are drifted and that obtained without drift.

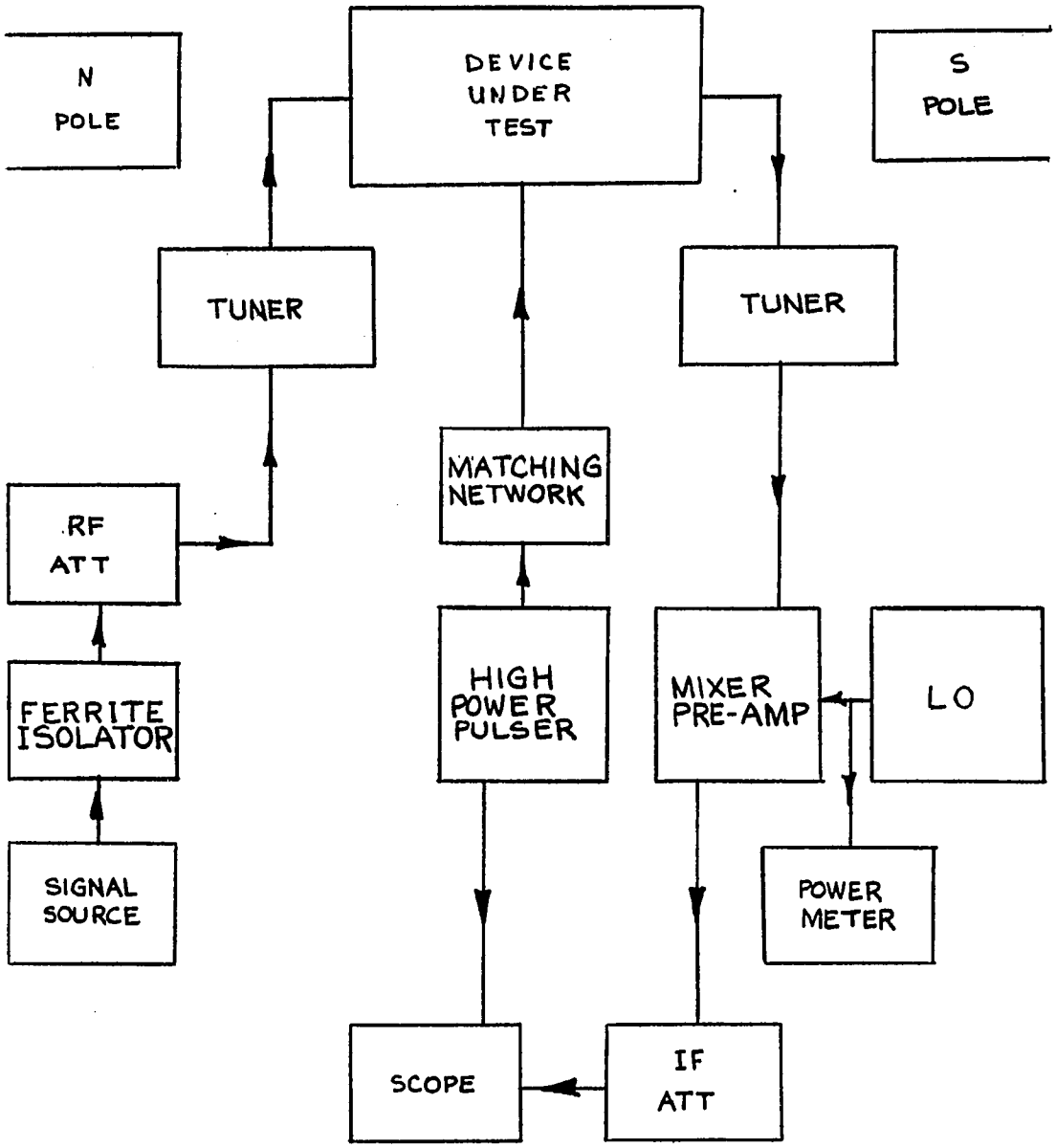

Figure 5-9 Experimental Set-up Used In Transmission Studies

In order to minimize heating effects caused by the application of high voltages to the indium antimonide, the electrons are drifted by low duty cycle pulses obtained at the output of a voltage divider network consisting of noninductive resistors and driven from the output of a Cober Model 605P high power pulser. The Cober pulse generator also provided a triggering signal for oscilloscope sweep initiation.

Investigations performed with the above set-up revealed certain difficulties involved with the comparison, in real time, of the structure's transmission properties as a function of drift field. It was determined that the current within the semiconductor resulted in significant changes in the static magnetic field in the YIG. Since, as noted in Chapter 3, a change in the applied magnetic field results in a frequency shift of the transmission spectrum, a new magnetic field operating point is established when the semiconductor is drifted. This may be demonstrated by observing the transmission characteristics in the vicinity of a bulk mode resonance peak. (In the configuration employed, the bulk mode resonance peaks are more pronounced (sharper) than the variations in the envolope of the surface mode spectrum because the bulk resonances are caused by reflections within the material and , hence, are less affected by the resistive paint than are the traveling surface wave resonances). With the frequency set to 8.052 GHz. and no voltage applied to the InSb, the applied magnetic field was adjusted to 2420 G. corresponding to the maximum of one of the bulk mode resonance peaks. When located at such a maximum point,

current flow through the indium antimonide sample in either direction resulted in a decrease in transmitted signal. When biased on the low magnetic field side of the resonance peak ($\bar{k} \times \bar{B}_o$ into YIG) a current pulse in the direction of propagation produced a decrease in transmission (lower field) while an increase in transmission was observed with the current direction reversed (higher field). On the other hand, when biased on the high field side of the peak an increase in transmission resulted from application of a colinear current pulse while current flowing in the opposite direction yielded a decrease in signal transmission. These results, which are consistent with Ampere's law[113]

$$\nabla \times \bar{B}_o = \mu \bar{J}_o \,, \qquad 5\text{-}86$$

demonstrate the necessity for using an experimental technique allowing for compenstation for the current dependent magnetic field shift. With the field shift thus taken into account, comparisons of transmission data with and without drift can be made for the same effective magnetic field.

If the static magnetic field data is not modified to reflect the current produced magnetic field shift, possible erroneous interpretations of transmission tests may result. As an example the following data corresponding to surface wave transmission is presented. With the sweep oscillator set for C.W. operation at 8.322 GHz. the applied static magnetic field was oriented such that $\bar{k} \times \bar{B}_o$ was directed into the semiconductor and adjusted to 2151 G. With the operating point thus established the indium antimonide sample was pulsed such that the electrons were

drifted in the direction of propagation. The differences in the level of the transmitted signal with and without drift were recorded and are plotted as a function of applied voltage in Figure 5-10. An initial enhancement of the transmitted signal is observed as the applied voltage is increased from zero. This enhancement increases with applied voltage, being 1.16 dB at an applied voltage of 10 v. (24.6 v/cm.). After reaching a maximum (approximately 1.25 dB) the enhancement decreases, the transmitted signal indicating a net loss between applied voltages of 26 v. and 50 v., the maximum voltage applied in this experiment.

Caluclation of the minimum conditions necessary for the instability onset indicates that the onset conditions cannot be satisfied with the materials and conditions employed in the above test. Thus the change in transmission with applied voltage that was observed was caused not by an exchange of energy between the drifting electrons and the surface wave, but rather by the change in magnetic field due to the semiconductor current.

In order to provide a means whereby the current produced magnetic field shift could be compensated for, the experimental arrangement was modified as shown in Figure 5-11 and 5-12a,b. Instead of applying a C.W. signal to the sample, the r.f. input was pulsed using an HP33102A PIN diode switch. The switching signal was obtained from a GR-Type 1391-B Pulse, Sweep and Time Delay Generator triggered by the Cober high power pulse generator. This arrangement permitted adjustments to be made in the delay between the initiation of the current pulse and the microwave pulse.

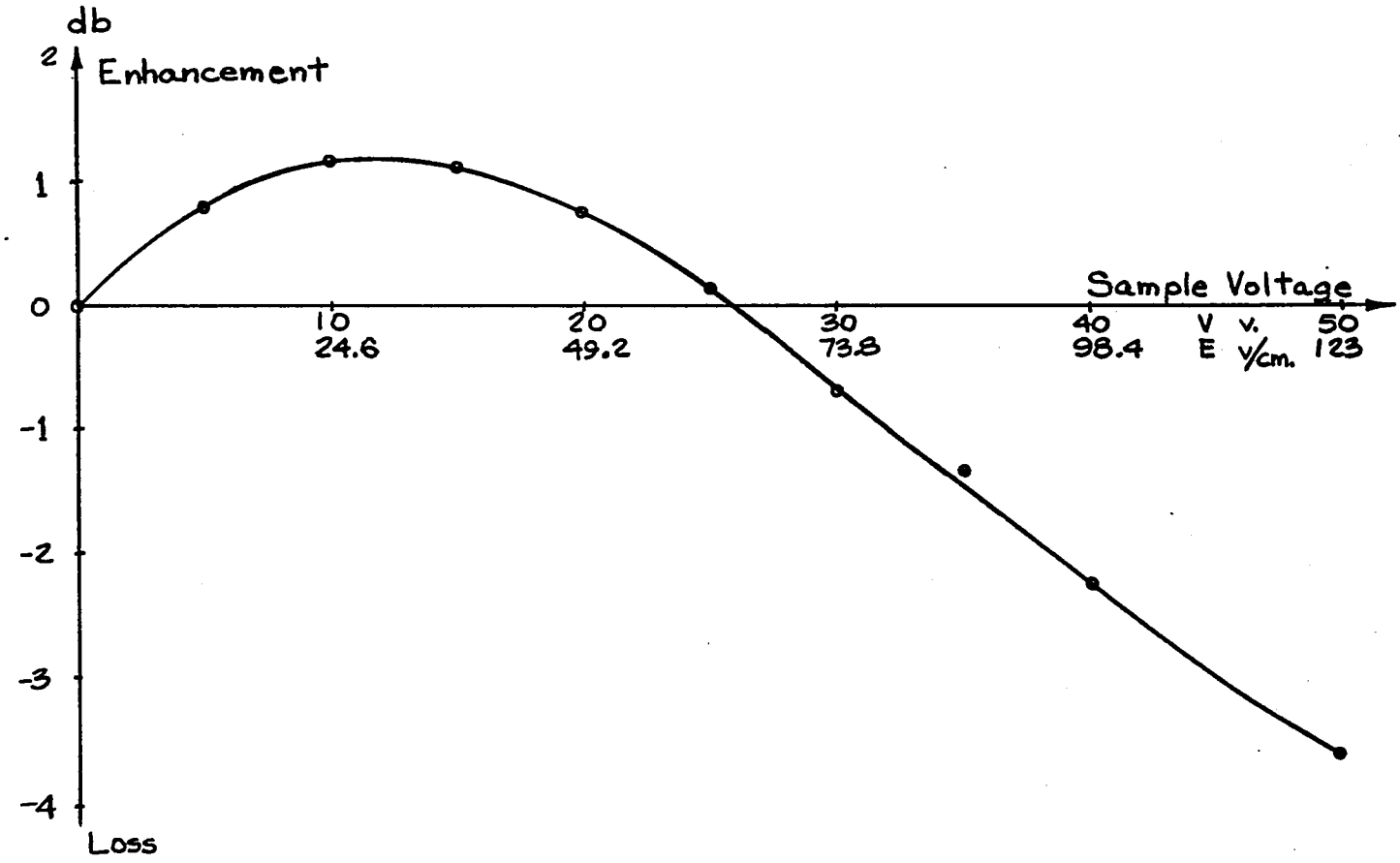

Figure 5-10 Signal Transmission Versus Applied Voltage

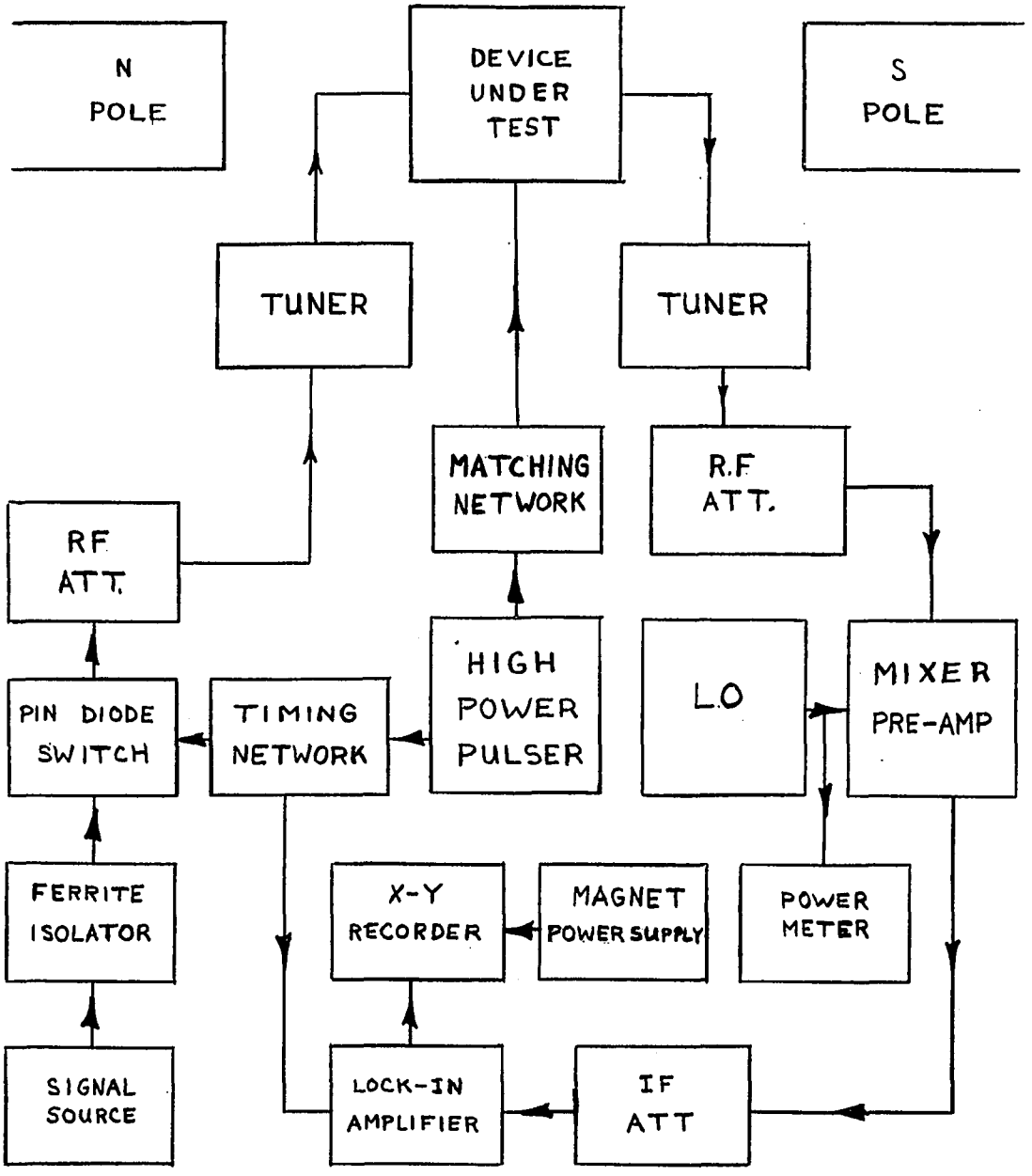

Figure 5-11-Modified Equipment Arrangement
For Transmission Studies

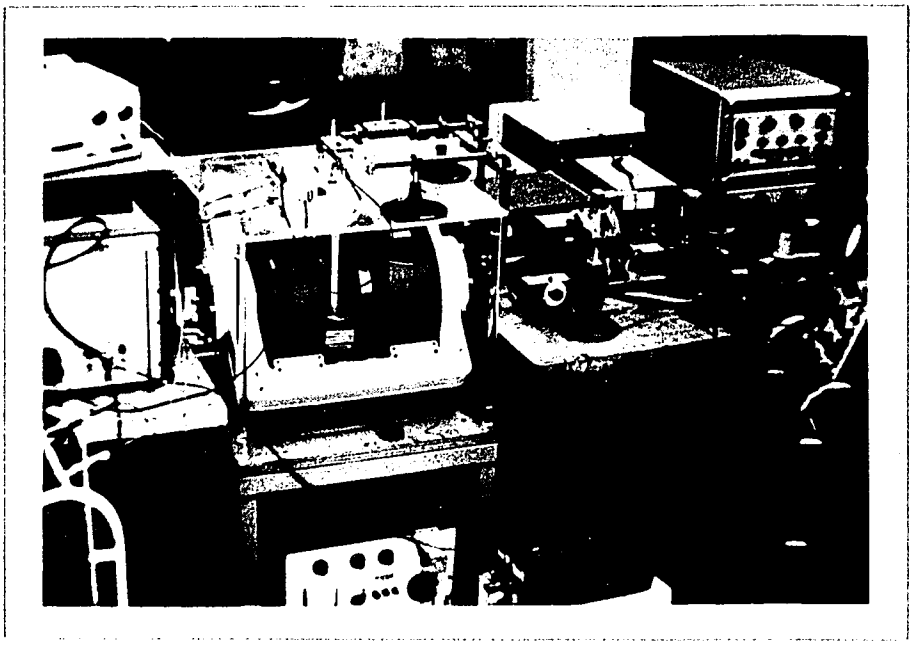

a

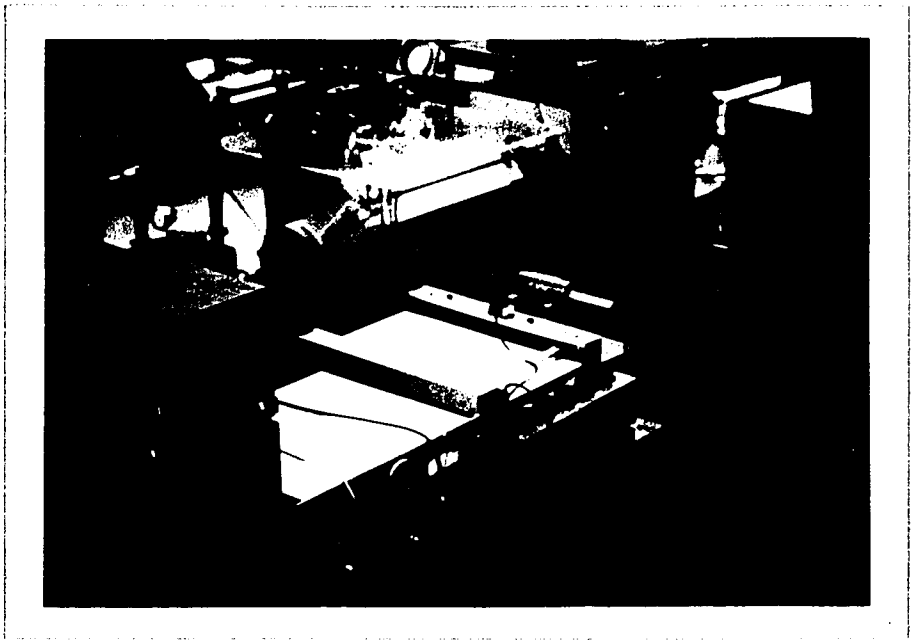

b

Figure 5-12 - Photographs of Experimental Set-up

Furthermore, the length of the microwave pulse could be adjusted so that it ended either subsequent or prior to termination of the current pulse as desired. This flexibility permitted visual comparisons between the transmitted signal with and without drift to be made as before and also provided the option of applying a microwave signal entirely within the period when carriers were drifted.

Additional modifications were made in the output circuitry. An X-band precision attenuator was inserted immediately ahead of the mixer-preamplifier and the 30 MHz. attenuator was removed from the mixer output. The envelope of the 30 MHz. signal was detected with an HP 424A crystal detector terminated in a 50 ohm load and was applied to the input of an HP 466 A amplifier used for impedance matching purposes as well as providing a gain of 40db. The output of the isolation amplifier was applied to the input of a P.A.R. HR-8 lock-in amplifier tuned to the Cober pulse generator's pulse repetition frequency. The output of the lock-in detector was applied to the Y terminals of an X-Y recorder.

To obtain an X-axis signal from which the value of the applied magnetic field may be calculated, a precision 10 turn potentiometer, Helipot SAJ 651, was coupled to the shaft of the Varian V-2900 electromagnet power supply's sweep circuit potentiometer. By applying 24v dc across the winding of the 10 turn potentiometer, a voltage related to the position of the sweep circuit potentiometer was obtained at the wiper arm of the 10 turn potentiometer. This voltage, applied to the X input of the X-Y

provided an X deflection related to the magnetic field in the gap. This deflection was calibrated in terms of kilogauss through the use of a Rawson-Lush Type 720 S rotating coil fluxmeter.

To avoid the increase in linewidth and the shift of the transmission spectrum associated with the decrease in operating temperature, measurements of surface wave transmission as a function of applied magnetic and electric field were conducted at room temperature using a gallium arsenide-YIG structure. The gallium arsenide consisted of a thin epitaxial layer on a 15 mil chromium doped, 10^8 ohm-cm. substrate; the epi layer, doped with sulfur to an electron carrier density of $1.27 \times 10^{17}/cm^3$, had an electron mobility of 4295 $cm^2/v\text{-sec}$. and was approximately 0.3μ thick after contacts had been applied. The method used in preparing the contacts is outlined in Appendix III.

The r.f. coupler and current contact arrangement used in the study of surface wave propagation along the interface of the GaAs with the single crystal YIG slab differs in several respects from the YIG-InSb configuration discussed previously. The fact that the GaAs is epitaxially grown on an insulating substrate makes it necessary for the YIG to be positioned between the GaAs contacts. To have the r.f. couplers near the ends of the YIG slab and positioned so as to be close to the YIG-GaAs interface it was necessary to place the r.f. connectors in contact with the GaAs substrate as shown in Figure 5-13. Due to the high resistance of the substrate and relatively small thickness

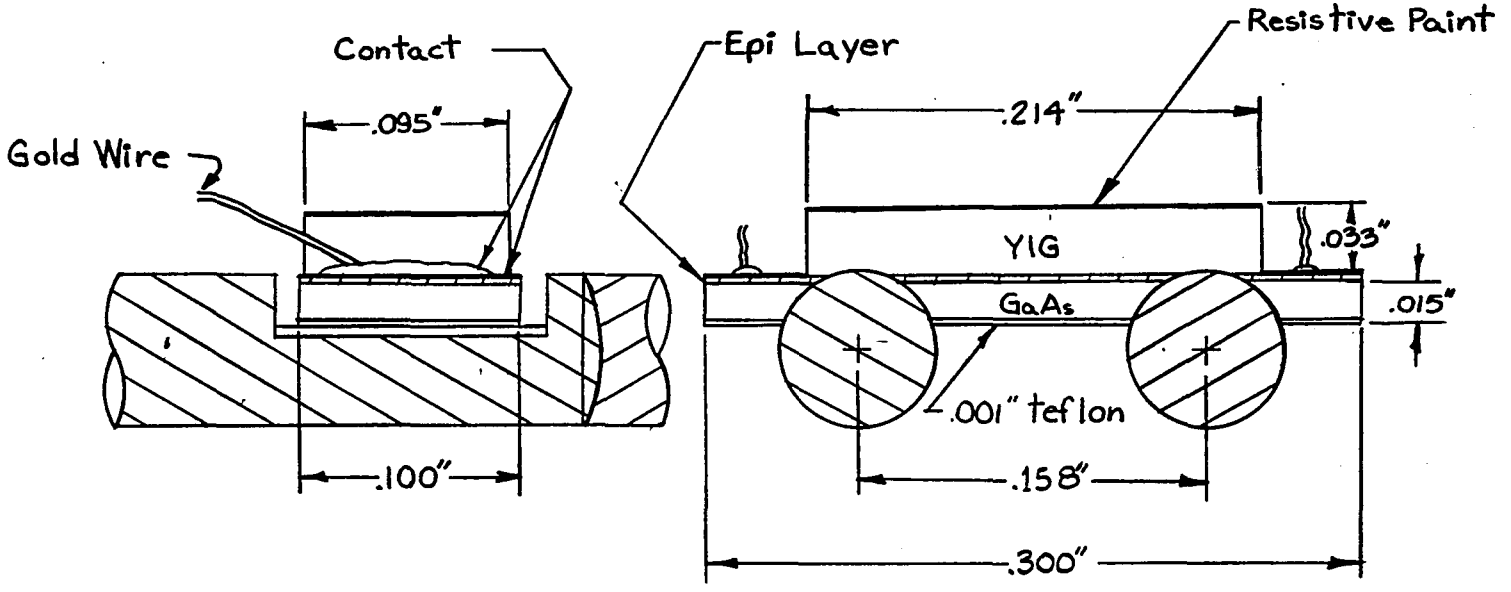

Figure 5-13-Relative Positions of Materials and Couplers

of the epitaxial layer surface waves could be launched at the YIG-GaAs interface in this manner.

The plexiglass jig which was used to hold the YIG-GaAs structure is shown assembled in Figure 5-14a and partially disassembled in Figure 5-14b. The GaAs is observed to be partially covering the r.f. couplers which are brought into the plexiglass jig from opposite sides. Electrical contact with the GaAs contacts is through 5 mil gold wires connected to the larger(141 mil) coaxial cable. The YIG slab, shown resistive paint side up, rests atop the GaAs between the electrical contacts. The YIG-GaAs sandwich is held in place by a brass spring attached at one end to the plexiglass jig. The spring may be seen in Figure 5-14a. (Card stock and teflon are used to protect the YIG from scratching.)

With the frequency set to 8.076 GHz. the input and output single stub tuners were adjusted for maximum signal transmission. The magnet was swept from 0.7 kG to 3.6kG once with $\bar{k} \times \bar{B}$. directed into the GaAs (S.C.) and again with $\bar{k} \times \bar{B}$. directed into the resistive paint (R) with no drift field appled to the GaAs in both cases. (Referring to the experimental data obtained for magnetostatic surface wave propagation at a YIG- dielectric interface, surface waves are expected to be observed for applied magnetic fields of approximately 2.5 kG.) The tracings recorded on the X-Y plotter for this operating condition have been reproduced in Figure 5-15. The vertical scale represents relative transmitted signal power in db while the abscissa is in units of kilogauss. A region of

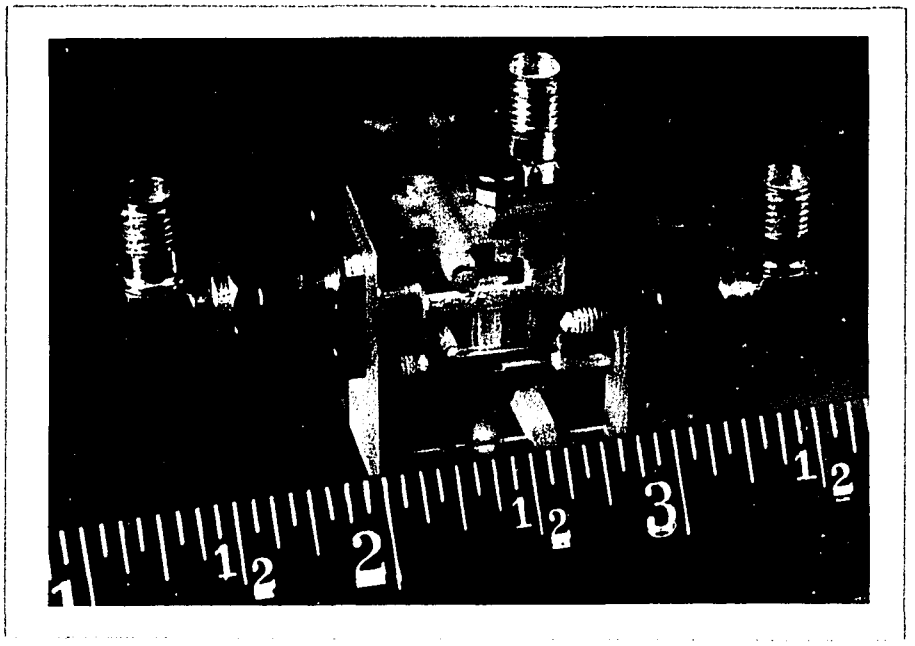

a

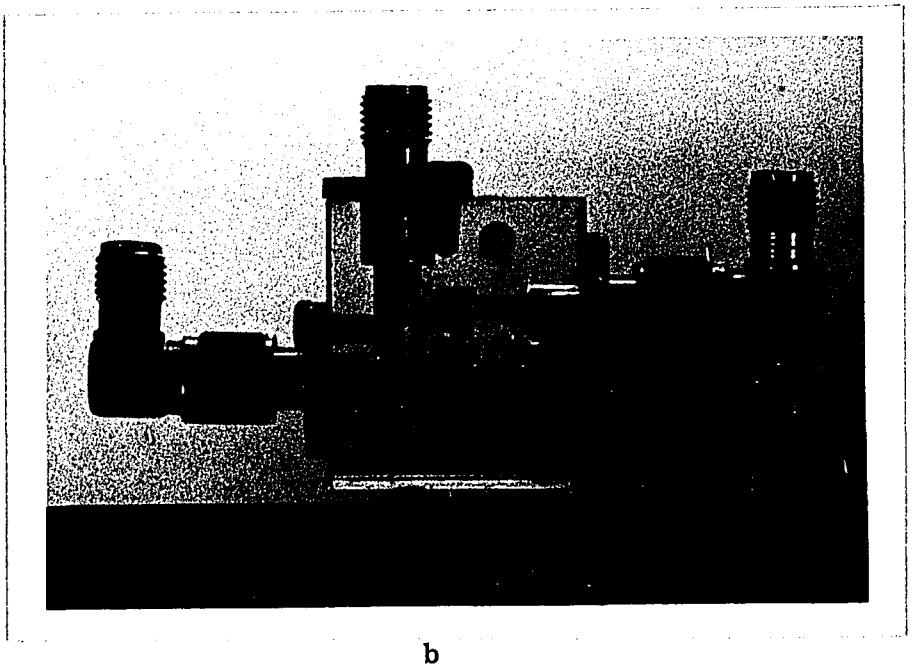

b

Figure 5-14 - Jig Used in GaAs-YIG Propagation Studies

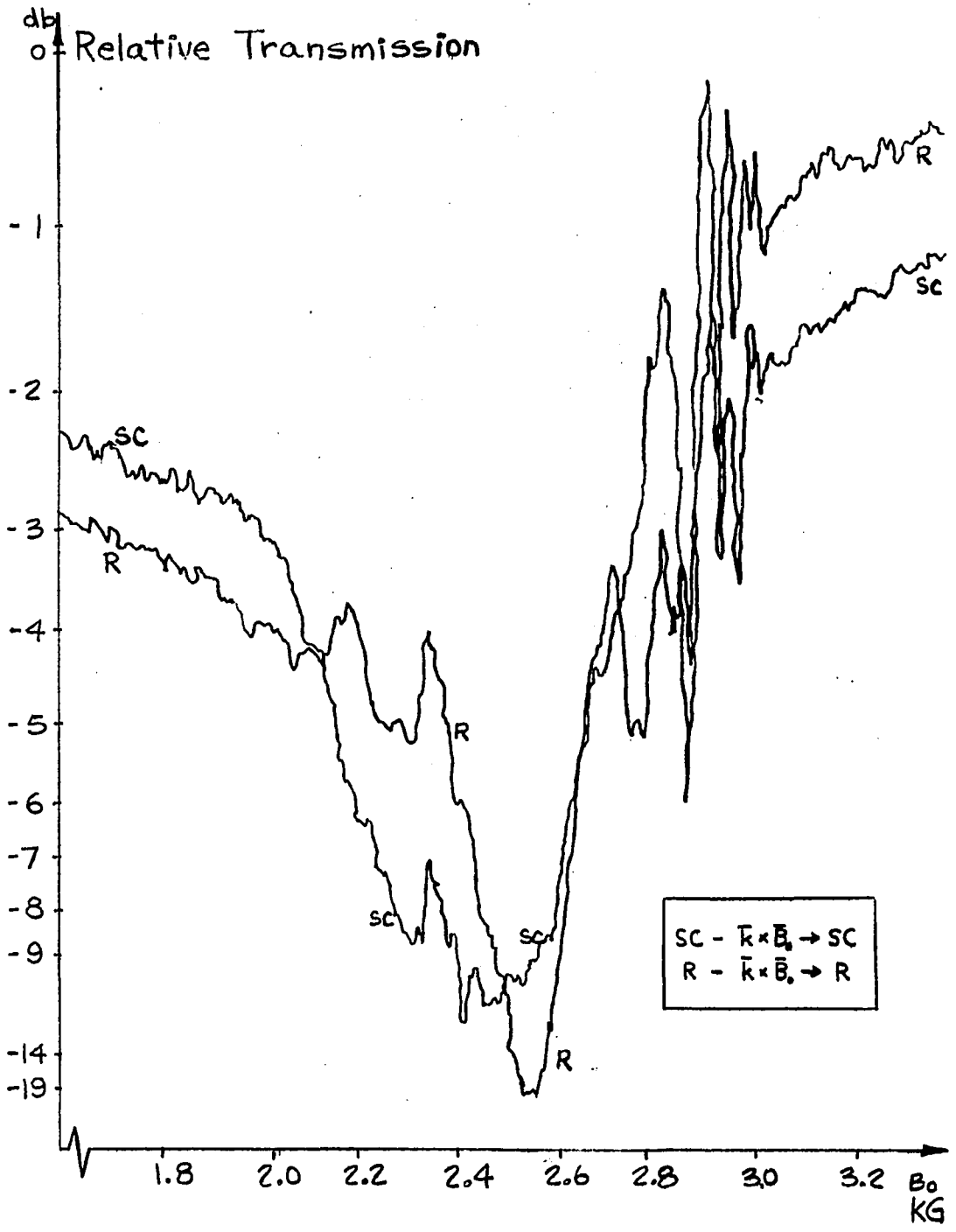

Figure 5-15 Microwave Transmission Spectrum of the GaAs - YIG Structure

relatively high loss is observed corresponding to applied field values between 2.0 and 2.9 kG, the region in which surface wave activity is anticipated. It is noted that the maximum loss experienced by curve R is greater than that experienced by curve SC. This indicates that the losses encountered by the "magnetostatic" surface wave in traveling from the input to the output are greater when the wave travels along the surface of the YIG slab coated with resistive paint than when it travels along the YIG-GaAs interface. Comparing Figure 5-15 with the results obtained in Chapter 3 for surface wave propagation at YIG-dielectric interface, it is noted that the surface wave passband is wider when the YIG is bounded by the GaAs. This is expected since it was shown in Chapter 4 that surface wave propagation along a ferrite-semiconductor interface may occur for field values (or if B_0 held constant, frequencies) both above and below the magnetostatic mode resonance. At the high field (or correspondingly, low frequency) end of the loss region a number of relatively sharp peaks are observed for both the R and S.C. traces. These peaks corespond to bulk mode resonances(refer to Figure 3-27) which, as noted previously, are primarily an internal phenomenon and, hence, are not suppressed to the extent that surface wave resonance peaks are by the resistive paint.

Examining the transmission spectra in the vicinity of the transmission minima (B_0=2533 G.) on an expanded scale, Figure 5-16, the difference between the losses experienced by the signal when $\bar{k} \times \bar{B}_0$ points into the semicon-

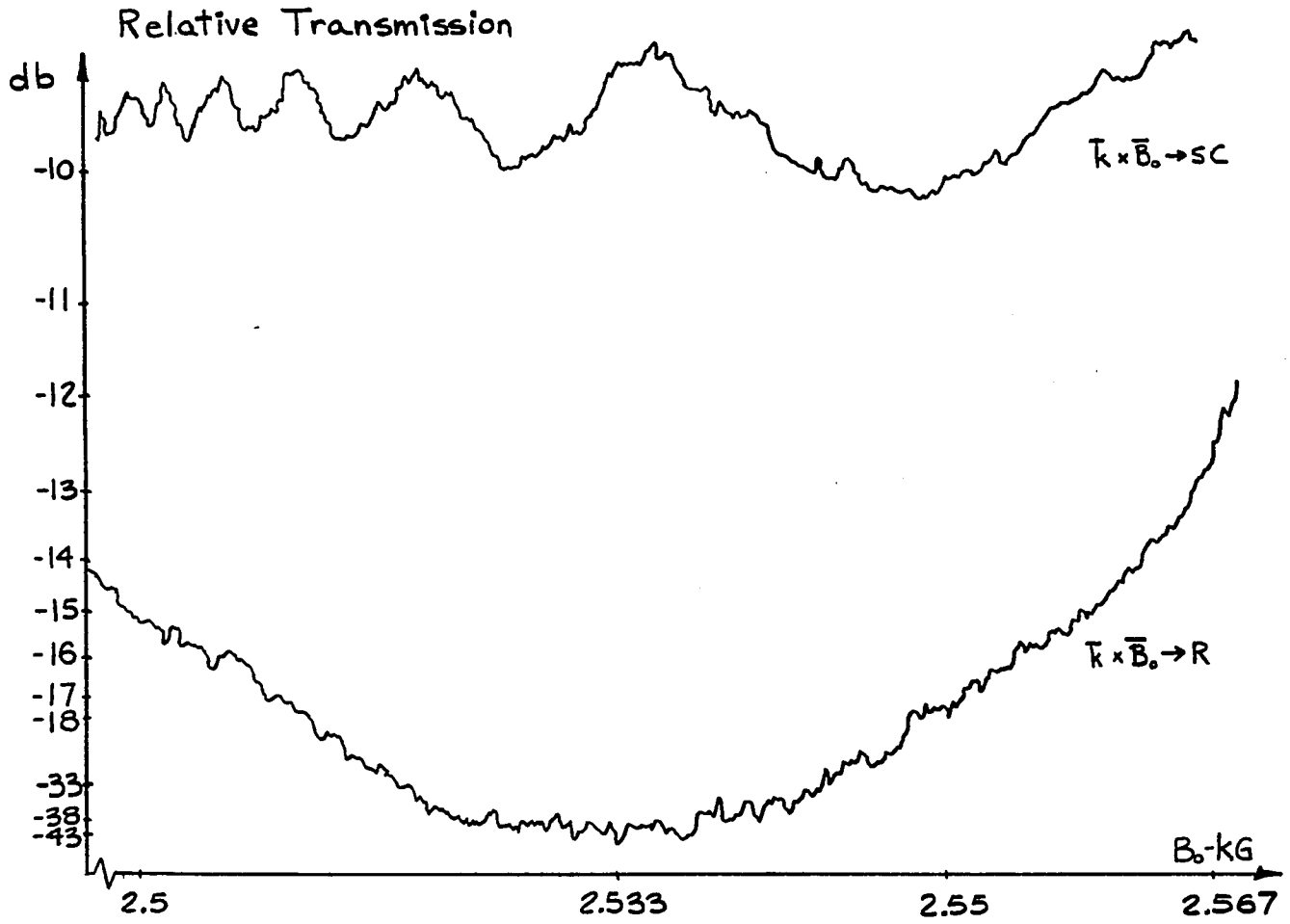

Figure 5-16 YIG-GaAs Surface Wave Transmission Spectrum

ductor relative to those experienced when $\bar{k}x\bar{B}_0$ is directed into the resistive paint is more clearly manifested. The R trace is observed to be at least 20db lower than that of the S.C. trace. (The minimum point of the R curve is at the system's noise level.) Observing the S.C. curve it is noted that it exhibits a series of relatively broad peaks and valleys. These peaks become more closely spaced as the applied magnetic field decreases (or if B_0 held constant, the frequency increases) corresponding to an increase in signal wavelength. This phenomenon is attributed to vestigial surface wave resonance peaks similar to those observed on the envelope of the "magnetostatic" surface wave transmission spectrum shown in Figure 3-36. The fact that the width of the peaks decreases as the magnetic field is reduced below bulk mode values is in agreement with predictions of increasing surface mode wavelength as the resonance is approached.

Other investigations of microwave propagation in ferrite-semiconductor structures have been reported previously[20, 21, 24]. Schneider[20], in his work, presents evidence of strong coupling between spin-wave volume modes in a YIG slab and electrons in an adjacent InSb sample. In both of the other references cited the ferrite used was also YIG. In neither of these cases, however, does the test frequency correspond to that expected for "magnetostatic" surface waves with the applied magnetic fields indicated. For instance, Vashkovskii et. al. reported observing the magnetostatic surface wave resonance at a frequency of 2 GHz. with an applied magnetic field of approximately 550 Oe. While

this frequency is 33.3% lower than that employed by Brundle and Freedman[6], the applied magnetic field at resonance is more than 100% higher. Furthermore, considering the lowest frequency for which the magnetostatic surface wave resonance may be obtained as being bounded by the condition that H_i, and hence ω_i, equals zero, a lower limit is found from $\omega_{res} = \omega_i' + \frac{\omega_m}{2}$ to be given by

$$f_{min} = \frac{1}{2\pi}\left(\frac{\omega_m}{2}\right) = 2.477\ \text{GHz.} \qquad 5\text{-}87$$

for the 1770 G. YIG material used by Vashovskii et.al. Since f_{min} is greater than 2GHz., it appears likely that the delayed signals observed by Vashkovskii et.al. were not surface waves but rather bulk waves. This would be consistent with the findings of Brundle and Freedman[6] who reported that "at higher d.c.fields, groups of delayed signals were also visible, sometimes to delays greater than 1μ sec."

In the above discussion experiments involving the transmission of microwave signals in a structure consisting of adjacent ferrite and semiconducting layers have been described. By observation of the transmission spectrum as a function of applied magnetic field both bulk and surface modes were identified and related to the corresponding modes for a ferrite bounded by a dielectric. It is believed that this is the first positive identification of "magnetostatic" surface wave propagation along a ferrite-semiconductor boundary.

The theory presented herein and in other works[18, 23, 120] predicts the possibility of obtaining active interactions in systems consisting of

adjacent semiconducting and ferromagnetic insulating regions. To experimentally verify these predictions, however, high mobility thin film semiconductors, such as thin epitaxial InSb would be required. As epitaxial InSb was not commercially available at the time the work reported herein was in progress, experiments for which the instability onset criterion was satisfied could not be performed.

CHAPTER 6

SUMMARY AND CONCLUSIONS

The electromagnetic propagation of surface waves at the interface between two semi-infinite insulators, one magnetic the other non-magnetic, has been investigated. By observing changes in the dispersion characteristics as the permittivity of the dielectric regions was altered, new information concerning the behavior of the "magnetostatic" and "dynamic" modes was obtained. It was found that an increase in the permittivity of the dielectric not only resulted in a decrease in wavelength for any given frequency of the "magnetostatic" mode but also modified the frequency range and character of the "dynamic" mode. While the "dynamic" mode is found to propagate in the reverse direction for $\epsilon_d < \epsilon_m$, it is cutoff entirely for the range of parameters $\epsilon_m < \epsilon_d < \epsilon_m \frac{(\omega_i + \omega_m)}{\omega_i}$, a result heretofore not reported. Furthermore, when the relative permittivity of the dielectric region exceeds $\epsilon_m \frac{(\omega_i + \omega_m)}{\omega_i}$, a new "dynamic" mode, guided along the ferrite-dielectric interface is found to exist. This mode, referred to as the forward "dynamic" mode propagates in the same direction as the magnetostatic mode of Damon and Eshbach[5].

The electromagnetic analysis has been extended to the case of finite ferrite slabs bounded by non-magnetic insulating regions as well. It was found that modes similar to the "magnetostatic" and "dynamic" modes, discussed in connection with the semi-infinite ferrite-dielectric

structure also exist when the ferrite is of finite thickness. By examining the ratio of surface wave energy densities at the top and bottom surfaces, it was demonstrated that a mode set consisting of a "magnetostatic" and a "dynamic" mode is associated with each surface. It was found that the frequency range over which the "dynamic" modes may propagate can be varied through a suitable choice of the adjacent dielectric media parameters in a manner similar to that described for the semi-infinite case. If desired, the neighboring insulating material may be chosen to entirely cut-off the "dynamic" modes, resulting in surface wave propagation solely by "magnetostatic" modes. The analysis has also shown that the new "dynamic" mode, which propagates in the same direction as the "magnetostatic" surface mode may exist on finite ferrite slabs as well.

In the initial investigations leading to these results, the effects of exchange were included in calculating the permeability tensor components, while pinning coupled exchange effects were neglected. When considering thin films, however, the transverse exchange term becomes significant and this approximation is no longer appropriate. Wolfram and DeWames[68], considering the effects of surface pinning have investigated the effects of exchange on the surface modes of YIG films. In assuming $\nabla \times \overline{H}$ to be zero, however, the details of the long wavelength region, such as the "dynamic" modes, the effects of neighboring media and the behavior of the modes in the vicinity of the lower frequency limit are not included in the analysis. Furthermore, it has been determined from the exchange modi-

fied electromagnetic surface wave analysis that the transverse wavenumber in the ferrite becomes large as the lower frequency limit is approached indicating that these solutions may be modified by exchange in this limit. Thus an interesting and informative extension to the present work would be a detailed electromagnetic analysis of the modes of a ferrite slab with pinning coupled exchange effects included.

The propagation of electromagnetic modes on the surface of a ferrite slab backed by a perfect conductor has been considered. It has been demonstrated that a close relationship exists between the magnetostatic "ferrite-metal" mode and the "dynamic" mode of the semi-infinite model. This has been established by showing the transition of the mode from a "ferrite-dielectric" field configuration near the lower frequency limit to a "ferrite-metal" configuration as the resonance is neared. Further verification was provided by observation of the mode as the ferrite thickness of the grounded slab was varied. It was found that when the ferrite is sufficiently thick, surface waves propagate at frequencies greater than the "ferrite-metal" mode resonance frequency, previously thought to be the upper limit.

DeWames and Wolfram[10] have studied the characteristics of magnetostatic surface waves on a slab backed by a lossy conductor. (Recently, Masuda et. al.[26] have published a similar study with the lossy metal replaced instead by a semiconductor treated in the collision dominated limit.) Examining the dispersion relationship of the ferrite-

metal mode as the metal becomes lossy, it is observed that the mode is no longer resonant at $\omega_i + \omega_m$; instead, its characteristic approches $\omega_i + \frac{\omega_m}{2}$ as the wavenumber becomes large. As losses are further increased the mode appears to closely resemble the $s=-1_m$ mode of the ungrounded slab. This behavior is intersting since the ferrite-metal mode and the s=-1 Damon and Eshbach mode are unrelated in the lossless case.

Considering the imaginary part of the complex frequency, through which the introduction of losses is also manifested, one finds that as losses are introduced attenuation of the mode initially increases. As losses are increased further, however, the imaginary part of the complex frequency attains a maximum such that the introduction of additional losses only serves to decrease the maximum rate of attenuation. In other words, it appears that the losses decrease as the metal becomes more lossy.

To better understand and clarify the circumstances surrounding these phenomena, it is suggested that further analysis of the case of a ferrite slab backed by a lossy conductor be performed without neglecting electromagnetic propagation effects. Since a close relationship has been established between the "ferrite-metal" mode and the "dynamic" mode, a mode which may only be calculated by including the effects of electromagnetic wave propagation, an increased understanding of the problem may be gained through such an analysis.

Swept frequency measurement techniques permitted real-time observation of the "magnetostatic" surface wave frequency spectrum as a function of applied static magnetic field. In this way it was possible to follow the traveling wave resonance peaks, leading to the observation that the lowest resonance peak disappeared as the frequency spectrum shifted to higher frequencies. Through the correlation of the data obtained from the resonance peak observations with calculations based on an electromagnetic analysis of the finite ferrite structure, it was possible to show that this behavior was caused by the increase in the wavenumber at the lower frequency limit as the magnetic field increased. This close correlation of theory and experiment would not have been possible had a magnetostatic analysis been performed instead.

The traveling wave resonance phenomenon observed in connection with the "magnetostatic" surface wave is caused by the additive and subtractive interferance of the wave as it circumnavigates the ferrite slab. It is also possible for the "dynamic" mode to exhibit traveling wave resonances provided the sample is of sufficient size with respect to the mode's relatively long wavelength. For a sample of the size used in the studies described in Chapter 3, one should be able to observe one resonance. A single resonance corresponding to a mode whose direction of propagation was opposite to that of the "magnetostatic" mode was observed albeit at a frequency somewhat lower than

anticipated. As the thrust of these experiments was development of techniques and gathering of information useful for the subsequent studey of "magnetostatic" surface modes at a ferrite semiconductor interface, confirmation of the possible "dynamic" mode resonance was not attemped and remains an open question.

The propagation of electromagnetic waves guided along the interface between a magnetic insulator and a semiconductor has also been considered. Using parameters appropriate to YIG and InSb at room temperature, the dispersion relationship was analyzed to determine directions of signal flow in the regions above and below resonance. Examining the imaginary part of the spin mode wavenumber, it was found that apart from the resonance region and its immediate vicinity, the mode's attenuation function exhibits little change as the electron drift velocity is varied. Within the interaction region itself the magnetostatic approximation is found to be appropriate and was used to extend the instability onset condition obtained by Robinson et. al. [23] to include the effects brought about by the presence of minority carriers. It was determined that while the presence of minority carriers has a detrimental effect upon the interaction, this effect is small and may be neglected in the ranges of material parameters required for an active interaction with the four commericially available semiconductors examined. The ranges of material parameters for which the instability onset criterion is satisfied may be quickly established through the use of the instability onset condition nomograph developed. The nomograph, which is drawn for a particular value of $\left(\frac{\Delta H}{M_o}\right)$ and frequency, is used by locating the point

corresponding to the carrier density and mobility of the semiconductor in question and noting whether the corresponding drift velocity may be obtained with this material.

Dispersion relationships describing electromagnetic wave propagation along a ferrite-semiconductor interface, where both the ferrite and the semiconductor are of finite extent were developed. These relationships were then examined in the magnetostatic limit for material parameters satisfying the instability onset criterion as determined by using the instability onset crierion nomograph. An interesting conclusion of this study is that a dielectric separation between the semiconductor and ferrite materials of the order of grit sizes used in the polishing of samples is sufficient to prevent instability onset. It was also determined that, in addition to the detrimental effect of ferrite thickness reduction on the interaction, the frequency at which an instability may be obtained is reduced as the ferrite thickness approaches the minimum value for which an instability may be obtained.

A series of experiments was described in which techniques required for proper evaluation of possible interaction between surface waves supported by a ferrite spin system and drifting carriers in a semiconductor were developed. Resistive coatings were used to suppress traveling surface wave resonances and to attenuate surface waves traveling along the large surface of the YIG slab directly opposite the semiconductor-ferrite interface of interest. Through the evaluation of the microwave transmission spectra obtained as a function of applied magnetic field, both

bulk and surface modes were identified and related to the corresponding modes for a ferrite bounded by a dielectric. It is believed that this is the first positive identification of "magnetostatic" surface wave propagation along a ferrite-semiconductor boundary.

Appendix I

The Demagnetizing Field Within A Rectangular Slab of Insulating Ferromagnetic Material

A rectangular parallelapiped of insulating ferromagnetic material, shown in Figure A-1, is of thickness a, length b, and width c and is bounded on all sides by free space. A uniform static magnetic field is applied in the $\hat{z}$ direction. It is assumed that the ferromagnetic material is such that the anisotropy field is small and may be neglected in comparison to the applied field, H_o.

Both within and without the slab the static magnetic fields are described by Maxwell's equations,

$$\nabla \cdot \bar{B} = 0, \qquad 2\text{-}4$$

and

$$\nabla \times \bar{H} = 0. \qquad A\text{-}1$$

In the interior region the magnetic flux density, B_i, is related to the magnetic field intensity, H_i, through the constitutive relation

$$\bar{B}_i = \mu_o(\bar{H}_i + \bar{M}), \qquad A\text{-}2$$

where $H_i = H_o + H_d$, H_d being the demagnetizing field and M the magnetization. Since it has been assumed that the applied static magnetic field is uniform

$$\nabla \cdot \bar{H}_o = 0, \qquad A\text{-}3$$

as well as

$$\nabla \times \bar{H}_o = 0. \qquad A\text{-}4$$

Taking the divergence of both sides of Equation A-2 and using Equations 2-4 and A-3 results in

$$\nabla \cdot \bar{H}_d = -\nabla \cdot \bar{M}. \qquad A\text{-}5$$

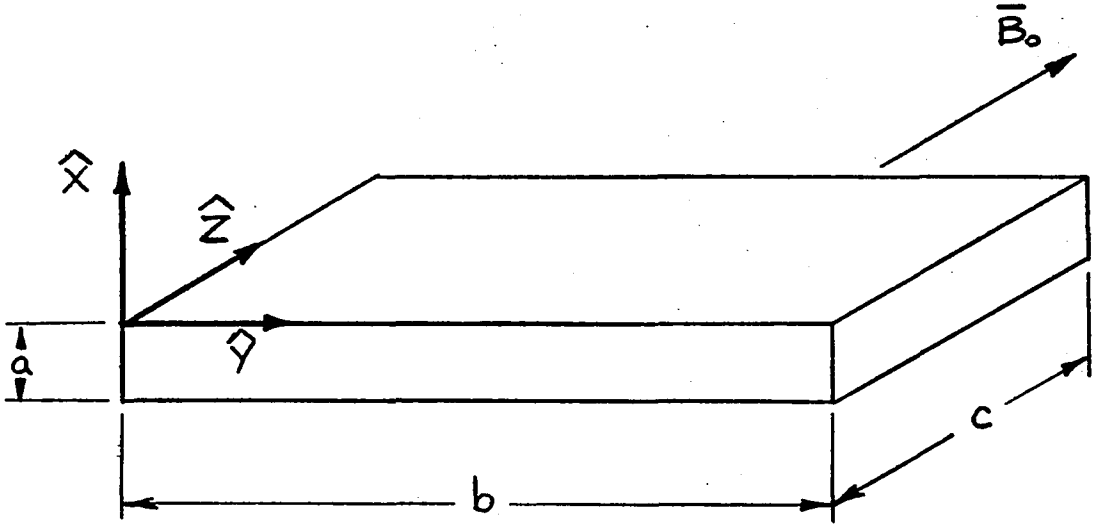

Figure A-1 - Insulating Ferromagnetic Slab

By employing the vector identity[114]

$$\nabla \times \nabla \Psi = 0, \qquad \text{A-6}$$

a scalar potential, Ψ may be defined such that[115]

$$\nabla \Psi = -\bar{H}_d \qquad \text{A-7}$$

Substitution of Equation A-7 into Equation A-5 yields

$$\nabla^2 \Psi \quad \nabla \cdot \bar{M} = -\rho_m . \qquad \text{A-8}$$

The solution to Equation A-8 may be expressed as[116]

$$\Psi(r) = \frac{1}{4\pi}\int_{v'} \frac{\rho_m(r')\, dv'}{|r-r'|} + \frac{1}{4\pi}\int_{s'} \frac{\delta_m(r')\, ds'}{|r-r'|}, \qquad \text{A-9}$$

where δ_m is the magnetic surface charge density. Expressing Ψ in terms of the magnetization of the slab, equation A-9 becomes

$$4\pi \Psi(r) = -\int_{v'} \frac{\nabla \cdot \bar{M}\, dv'}{|r-r'|} + \int_{s'} \frac{M_n\, ds'}{|r-r'|}, \qquad \text{A-10}$$

where M_n is the magnetization normal to the surface of the ferromagnetic slab.

In order to obtain an analytic expression for the demagnetizing field as a function of position within the ferromagnetic slab equation A-10 must be solved. Although the non-uniform demagnetizing field implies that the magnetization will not everywhere lie parallel to the applied field, it is a good approximation[117] to assume uniform magnetization in strong uniform applied fields since the transverse components are small.

Applying the uniform magnetization approximation, Equation A-10 may be written as

$$-4\pi\psi = \int_0^b \int_{-a}^{a} \frac{M_o \, dx'dy'}{\sqrt{(x-x')^2+(y-y')^2+z^2}} - \int_0^b \int_{-a}^{a} \frac{M_o \, dx'dy'}{\sqrt{(x-x')^2+(y-y')^2+(z-c)^2}} , \quad \text{A-11}$$

where M_n has been replaced by M_o , the $\hat{z}$ directed saturation magnetization. Since the integrals are well behaved in the region $\left|z - \frac{c}{2}\right| < \frac{c}{2}$, the derivation of the demagnetizing field is restricted to this central portion of the slab. It is evident from symmetry considerations that the transverse components of the demagnetizing field must be zero along the $z = c/2$ plane, so that an analytic expression for only the longitudinal component need be obtained.

The $\hat{z}$ component of the gradient of Equation A-11 is

$$\frac{4\pi H_{dz}}{M_o} = \int_0^b \int_{-a}^{a} \frac{-z \, dx'dy'}{\left[(x-x')^2+(y-y')^2+z^2\right]^{3/2}} + \int_0^b \int_{-a}^{a} \frac{(z-c) \, dx'dy'}{\left[(x-x')^2+(y-y')^2+(z-c)^2\right]^{3/2}} , \quad \text{A-12}$$

The integrals in Equation A-12 may be evaluated by repeated use of trigonometric substitutions. An angle θ is defined such that

$$\theta = \tan^{-1} \frac{(x - x')}{\sqrt{(y-y')^2 + z^2}} , \quad \text{A-13}$$

The differential element, dx', may then be expressed in terms of as

$$-dx' = \sqrt{(y-y')^2 + z^2} \; \sec^2\theta \, d\theta \quad \text{A-14}$$

Defining θ_1 as

$$\theta_1 = \tan^{-1} \frac{(x + a)}{\sqrt{(y-y')^2 + z^2}} , \quad \text{A-15}$$

and θ_2 as

$$\theta_2 = \tan^{-1} \frac{x}{\sqrt{(y-y')^2 + z^2}} , \quad \text{A-16}$$

the first integral on the right-hand side of Equation A-12 may be expressed as

$$I_1 = \int_0^b \int_{\theta_1}^{\theta_2} \frac{z \cos\theta \; d\theta dy'}{(y-y')^2 + z^2} \qquad \text{A-17}$$

Integrating with respect to θ yields

$$I_1 = \int_0^b \frac{\sin\theta_2 \, dy'}{(y-y')^2 + z^2} - \int_0^b \frac{\sin\theta_1 \, dy'}{(y-y')^2 + z^2} \; . \qquad \text{A-18}$$

Expressing this result in terms of x yields

$$I_1 = \int_0^b \frac{zx \quad dy'}{[(y-y')^2+z][x^2+(y-y')^2+z]^{1/2}} - \int_0^b \frac{z(x+a) \quad dy'}{[(y-y')^2+z^2][(x+a)^2+(y-y')^2+z^2]^{1/2}} \qquad \text{A-19}$$

Following a similar technique in evaluating the second integral on the right-hand side of Equation A-12, the following expression for H_{dz} is obtained,

$$\frac{4\pi H_{dz}}{M_0} = \int_0^b \frac{zx \quad dy'}{[(y-y')^2+z^2][x^2+(y-y')^2+z^2]^{1/2}} + \int_0^b \frac{(c-z)x}{[(y-y')^2+(z-c)^2][x^2+(y-y')^2+(z-c)^2]^{1/2}}$$
$$- \int_0^b \frac{z(x+a) \quad dy'}{[(y-y')^2+z^2][(x+a)^2+(y-y')^2+z^2]^{1/2}} - \int_0^b \frac{(c-z)(x+a)}{[(y-y')^2+(z-c)^2][(x+a)^2+(y-y')^2+(z-c)^2]^{1/2}} \qquad \text{A-20}$$

Defining now an angle ϕ such that

$$\phi = \tan^{-1} \frac{(y-y')}{\sqrt{x^2+z^2}} \; , \qquad \text{A-21}$$

the first term on the right-hand side of Equation A-20 may be expressed as

$$I_2 = -\int_{\phi_1}^{\phi_2} \frac{zx \sec\phi \; d\phi}{(x^2+z^2)\sec^2\phi - x^2} \; . \qquad \text{A-22}$$

The integrand of the above expression may be factored to yield,

$$I_2 = \frac{1}{2}\int_{\phi_1}^{\phi_2} \frac{z \sec\phi \; d\phi}{\sqrt{(x^2+z^2)}\sec\phi + x} - \frac{1}{2}\int_{\phi_1}^{\phi_2} \frac{z \sec\phi \quad d\phi}{\sqrt{(x^2+z^2)}\sec\phi - x} \; . \qquad \text{A-23}$$

Further manipulation results in

$$I_2 = \frac{1}{2}\frac{z}{\sqrt{x^2+z^2}}\int_{\phi_1}^{\phi_2}\frac{d\phi}{1+\frac{x}{\sqrt{x^2+z^2}}\cos\phi} - \frac{1}{2}\frac{z}{\sqrt{x^2+z^2}}\int_{\phi_1}^{\phi_2}\frac{d\phi}{1-\frac{x}{\sqrt{x^2+z^2}}\cos\phi} \quad \text{A 24}$$

The integrands in the above expression are in the form

$$I_3 = \int_{\zeta_1}^{\zeta_2}\frac{d\zeta}{1+N\cos\zeta}, \quad \text{A 25}$$

where $|N|<1$. From the integral tables of B.O. Pierce[118] and G. Petit Bois[119], the solution is given as

$$I_3 = \frac{1}{\sqrt{1-N^2}}\sin^{-1}\left\{\frac{\sqrt{1-N^2}\sin\zeta}{1+N\cos\zeta}\right\}\Bigg|_{\zeta_1}^{\zeta_2} \quad \text{A-26}$$

Thus the integrals of Equation A-24 may be evaluated as

$$2I_2 = \sin^{-1}\left\{\sqrt{\frac{z^2}{x^2+z^2}}\left[\frac{(y-b)}{\sqrt{x^2+(y-b)^2+z^2}+x}\right]\right\} - \sin^{-1}\left\{\sqrt{\frac{z^2}{x^2+z^2}}\left[\frac{y}{\sqrt{x^2+y^2+z^2}+x}\right]\right\}$$

$$- \sin^{-1}\left\{\sqrt{\frac{z^2}{x^2+z^2}}\left[\frac{(y-b)}{\sqrt{x^2+(y-b)^2+z^2}-x}\right]\right\} + \sin^{-1}\left\{\sqrt{\frac{z^2}{x^2+z^2}}\left[\frac{y}{\sqrt{x^2+y^2+z^2}-x}\right]\right\}. \quad \text{A-27}$$

Performing similar operations on the remaining integrals of Equation A-20 yields the following result for the demagnetizing field of the rectangular ferromagnetic slab in the region of the central plane z = c/2

$$\frac{8\pi H_{dz}}{M_o} = \sin^{-1}\left\{\sqrt{\frac{z^2}{x^2+z^2}}\left[\frac{(y-b)}{\sqrt{x^2+(y-b)^2+z^2}+x}\right]\right\} - \sin^{-1}\left\{\sqrt{\frac{z^2}{x^2+z^2}}\left[\frac{y}{\sqrt{x^2+y^2+z^2}+x}\right]\right\}$$

$$-\sin^{-1}\left\{\sqrt{\frac{z^2}{x^2+z^2}}\left[\frac{(y-b)}{\sqrt{x^2+(y-b)^2+z^2}-x}\right]\right\} + \sin^{-1}\left\{\sqrt{\frac{z^2}{x^2+z^2}}\left[\frac{y}{\sqrt{x^2+y^2+z^2}-x}\right]\right\}$$

$$+\sin^{-1}\left\{\sqrt{\frac{(z-c)^2}{x^2+(z-c)^2}}\left[\frac{(y-b)}{\sqrt{x^2+(y-b)^2+(z-c)^2}+x}\right]\right\} - \sin^{-1}\left\{\sqrt{\frac{(z-c)^2}{x^2+(z-c)^2}}\left[\frac{y}{\sqrt{x^2+y^2+(z-c)^2}+x}\right]\right\}$$

$$-\sin^{-1}\left\{\sqrt{\frac{(z-c)^2}{x^2+(z-c)^2}}\left[\frac{(y-b)}{\sqrt{x^2+(y-b)^2+(z-c)^2}-x}\right]\right\} + \sin^{-1}\left\{\sqrt{\frac{(z-c)^2}{x^2+(z-c)^2}}\left[\frac{y}{\sqrt{x^2+y^2+(z-c)^2}-x}\right]\right\}$$

$$-\sin^{-1}\left\{\sqrt{\frac{z^2}{(x+a)^2+z^2}}\left[\frac{(y-b)}{\sqrt{(x+a)^2+(y-b)^2+z^2}+(x+a)}\right]\right\} + \sin^{-1}\left\{\sqrt{\frac{z^2}{(x+a)^2+z^2}}\left[\frac{y}{\sqrt{(x+a)^2+y^2+z^2}+(x+a)}\right]\right\}$$

$$+\sin^{-1}\left\{\sqrt{\frac{z^2}{(x+a)^2+z^2}}\left[\frac{(y-b)}{\sqrt{(x+a)^2+(y-b)^2+z^2}-(x+a)}\right]\right\} - \sin^{-1}\left\{\sqrt{\frac{z^2}{(x+a)^2+z^2}}\left[\frac{y}{\sqrt{(x+a)^2+y^2+z^2}-(x+a)}\right]\right\}$$

$$-\sin^{-1}\left\{\sqrt{\frac{(z-c)^2}{(x+a)^2+(z-c)^2}}\left[\frac{(y-b)}{\sqrt{(x+a)^2+(y-b)^2+(z-c)^2}+(x+a)}\right]\right\} + \sin^{-1}\left\{\sqrt{\frac{z^2}{(x+a)^2+(z-c)^2}}\left[\frac{y}{\sqrt{(x+a)^2+y^2+(z-c)^2}+(x+a)}\right]\right\}$$

$$+\sin^{-1}\left\{\sqrt{\frac{(z-c)^2}{(x+a)^2+(z-c)^2}}\left[\frac{(y-b)}{\sqrt{(x+a)^2+(y-b)^2+(z-c)^2}-(x+a)}\right]\right\} + \sin^{-1}\left\{\sqrt{\frac{(z-c)^2}{(x+a)^2+(z-c)^2}}\left[\frac{y}{\sqrt{(x+a)^2+y^2+(z-c)^2}-(x+a)}\right]\right\}.$$

Appendix II

Normal Mode Formulation of the 90^0 Spin Wave-Carrier Wave Interaction in Magnetic Semiconductors

The interaction between TE waves supported by the spin system and carriers streaming within the bulk of materials possessing both magnetic and semiconducting properties is discussed. By expressing the equations describing the interaction in terms of the system's normal modes, the role played by collisions in coupling and mode modification is demonstrated.

A model of the magnetic semiconductor is considered in which the boundaries are far from the regions of interest and variations due to their presence are assumed negligible. The magnetic semiconductor is magnetized in the $\hat{z}$ direction by an externally applied static magnetic field resulting in a uniform internal magnetic field intensity, $\overline{H}_i$. Additionally a static electric field is applied in the $-\hat{y}$ direction causing electron drift in the positive $\hat{y}$ direction with average velocity v_{oe} . (Only a single carrier species, electrons, is considered in this investigation).

Electromagnetic propagation phenomena are described by Maxwell's equations given by Equation 2-1, 2-2, 2-3 and 2-4, where ϵ is equal to $\epsilon_o \epsilon_{ms}$ in the magnetic semiconductor. If it is assumed that the wavelength of the system response to electromagnetic excitation is larger than the Debye length of the medium, the carrier system may be treated hydrodynamically; furthermore, since the Debye length is orders of magnitude greater than atomic dimensions, the spin system is adaquately described

by a continuum model. If the amplitude of the response of the system to electromagnetic excitations is sufficiently small and of the form $\exp(j\omega t)$, the system equations may be written

$$\nabla \times \bar{E}_1 = -j\omega \bar{B}_1 , \qquad \text{A-29}$$

$$\nabla \cdot \bar{E}_1 = \frac{\rho_1}{\epsilon_0 \epsilon_{ms}} , \qquad \text{A-30}$$

$$\nabla \cdot \bar{B}_1 = 0 \qquad \text{A-31}$$

$$\nabla \times \bar{H}_1 = \bar{J} + j\omega \epsilon_0 \epsilon_{ms} \bar{E}_1 \qquad \text{A-32}$$

$$\bar{v}_{0e} \cdot \nabla_r \bar{v}_1 = -j(\omega - j\nu_e)\bar{v}_1 - \eta_e^*(\bar{E}_1 + \bar{v}_{0e} \times \bar{B}_1 + \bar{v}_1 \times \bar{B}_0) + \frac{v_{th}^2}{\rho_0} \nabla_r \rho_1 , \qquad \text{A-33}$$

and

$$\bar{B}_1 = \mu_0 \begin{Vmatrix} \mu_{11} & +j\mu_{12} & 0 \\ -j\mu_{12} & \mu_{11} & 0 \\ 0 & 0 & 1 \end{Vmatrix} \bar{H}_1 , \qquad \text{A-34}$$

where

$$\mu_{11} = 1 + \frac{\omega_m(\omega_i + j\nu_m)}{(\omega_i + j\nu_m)^2 - \omega^2} , \qquad \text{4-55}$$

and

$$\mu_{12} = \frac{\omega_m \omega}{(\omega_i + j\nu_m)^2 - \omega^2} . \qquad \text{4-56}$$

Assuming that the response is TE_y and, hence, propagating perpendicular to the direction of the static internal field, as shown in Figure A-2, Equation A-31 may be rewritten as

$$\nabla \cdot \bar{B}_1 = \frac{\partial B_y}{\partial y} = 0 , \qquad \text{A-35}$$

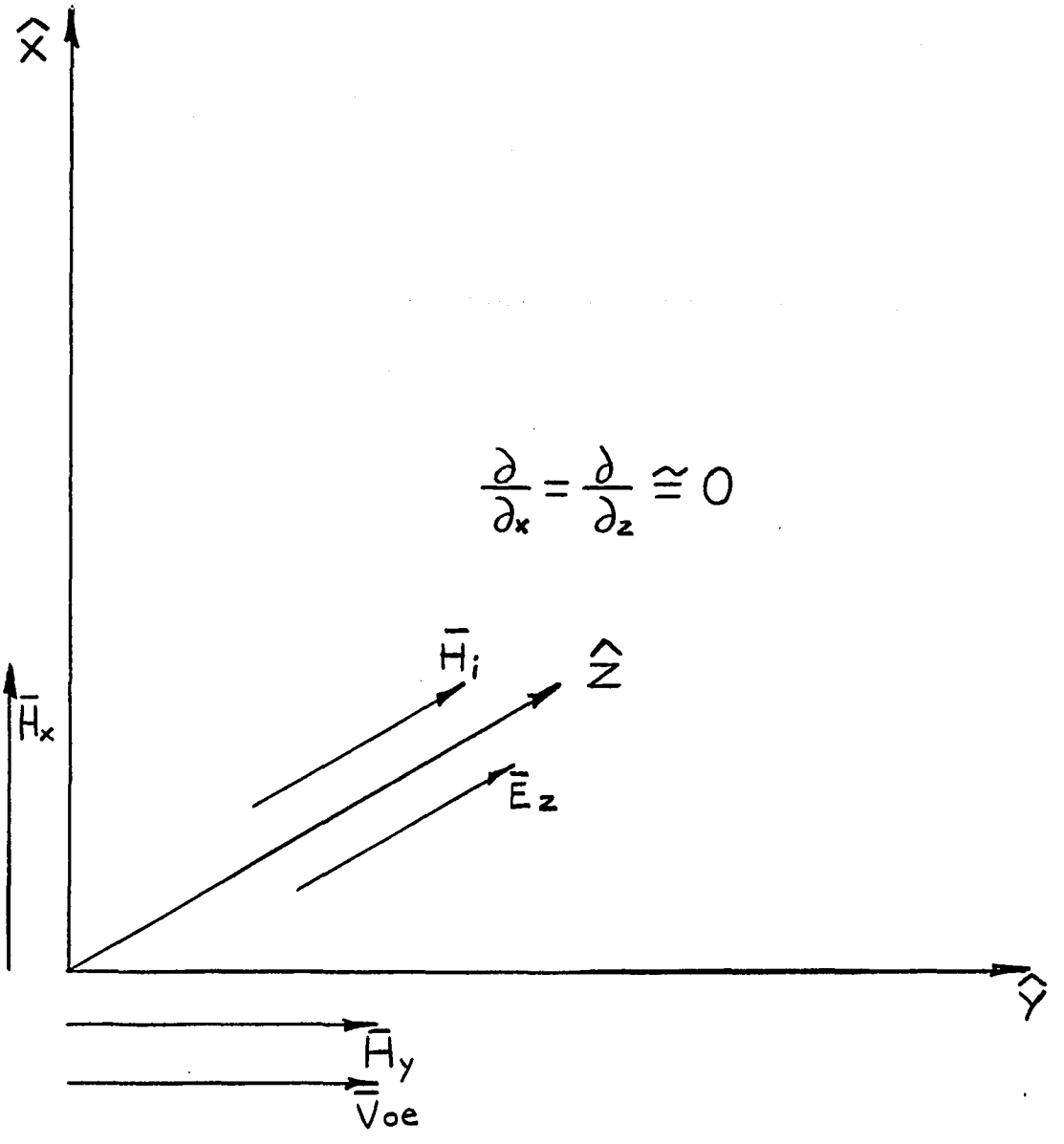

Figure A-2 Magnetic Semiconductor Coordinate System

indicating that the first order $\hat{y}$ directed component of the magnetic flux density is zero. Substituting this result into Equation A-34, the following expression for B_x is obtained,

$$B_x = \mu_o \frac{(\mu_{11}^2 - \mu_{12}^2)}{\mu_{11}} H_x = \mu_o \mu_b H_x \qquad \text{A-36}$$

Additionally, noting that the space charge density is zero in the first order

$$\nabla \cdot \bar{E}_1 = 0 = \frac{\rho_1}{\epsilon_o \epsilon_{ms}} , \qquad \text{A-37}$$

Equations A-29, A-32 and A-33 may be reexpressed as

$$\frac{\partial E_z}{\partial y} = -j\omega B_x , \qquad \text{A-38}$$

$$\frac{\partial H_x}{\partial y} = \rho_o v_z - j\omega \epsilon_o \epsilon_{ms} E_z \qquad \text{A-39}$$

and

$$v_{oe} \frac{\partial v_z}{\partial y} = -j(\omega - j\nu_e) - \eta^* E_z + \eta v_{oe} B_x . \qquad \text{A-40}$$

Thus the system of equations has been expressed as a set of first order linear differential equations which may be written in matrix form as

$$\bar{w}' = \frac{\partial}{\partial y} \begin{bmatrix} E_z \\ B_x \\ J_z \end{bmatrix} = \begin{Vmatrix} 0 & -j\omega & 0 \\ -j\frac{\omega \mu_1}{c_{ms}^2} & 0 & -\mu_o \mu_1 \\ \frac{i\omega_{pe}^2 \epsilon}{v_{oe}} & -\omega_{pe}^2 \epsilon & -j\frac{(\omega - j\nu_e)}{v_{oe}} \end{Vmatrix} \begin{bmatrix} E_z \\ B_x \\ J_z \end{bmatrix} , \qquad \text{A-41}$$

where

$$\epsilon = \epsilon_o \epsilon_{ms} \qquad \text{A-42}$$

$$c_{sm}^2 = \frac{1}{\mu_o \epsilon_o \epsilon_{ms}}, \qquad \text{A-43}$$

and

$$J_z = -\rho_o v_z \qquad \text{A-44}$$

The characteristic equation may be obtained by evaluating the determinant

$$|jkI - S| = 0, \qquad \text{A-45}$$

leading to

$$k^2 - \frac{\omega^2 \mu_b}{c_{ms}^2}\left[1 - \frac{\omega_{pe}^2(\omega - kv_{oe})}{\omega^2(\omega - kv_{oe} - j\nu_e)}\right] = 0. \qquad \text{A-46}$$

Hence the modes (in the absence of collisions) have the characteristic values

$$k = \frac{\omega}{v_{oe}}, \qquad \text{A-47}$$

and

$$k = \pm\sqrt{\frac{(\omega^2 - \omega_{pe}^2)\mu_b}{c_{ms}^2}}. \qquad \text{A-48}$$

It is noted that for this case, $\nu_e = 0$, the carrier mode is independent of the spin system and the modes are uncoupled.

In order to better observe the role that collisions play in this system the vector $\bar{w}$ is transformed into the vector $\bar{p}$ where the p_n are the normal modes of the system. A modal matrix, R is defined as

$$\bar{p} = R^{-1}\bar{w}, \qquad \text{A-49}$$

such that if $\nu_e = 0$,

$$\Upsilon = U|_{\nu_e=0} = R^{-1} S|_{\nu_e=0} R \,, \qquad \text{A-50}$$

where Υ is a diagonal matrix; the elements of Υ are the characteristic values, k , determined above. Performing the algebraic manipulation one finds

$$R = \frac{\begin{Vmatrix} \left[\frac{\omega_{pe}^2 \mu_b}{c_{ms}^2 \alpha_1}(f_- - f_+)\right] & \left[\frac{\omega f_+ g_-}{\alpha_2}\right] & \left[\frac{-\omega f_- g_+}{\alpha_3}\right] \\ \left[\frac{\omega_{pe}^2 \mu_b}{c_{ms}^2 \alpha_1}(g_- - g_+)\right] & \left[\frac{\omega g_+ g_-}{\alpha_2} - \frac{\omega_{pe}^2 \mu_b g_-}{c_{ms}^2 \alpha_2}\right] & \left[\frac{\omega_{pe}^2 \mu_b g_+}{c_{ms}^2 \alpha_3} - \frac{\omega g_+ g_-}{\alpha_3}\right] \\ \left[\frac{\omega_{pe}^2 \epsilon}{\alpha_1}(f_- g_+ - f_+ g_-)\right] & \left[\frac{\omega_{pe}^2 \epsilon f_+ g_-}{\alpha_2}\right] & \left[\frac{-\omega_{pe}^2 \epsilon f_- g_+}{\alpha_3}\right] \end{Vmatrix}}{\left\{ \frac{\omega_{pe}^2 \mu_b}{c_{ms}^2}[f_- - f_+] - [g_+ f_- - f_+ g_-] \right\}}$$

A-51

where

$$f_\pm = \left[\frac{\omega}{V_{oe}} \pm \sqrt{\frac{(\omega^2 - \omega_{pe}^2)\mu_b}{c_{ms}^2}} \right] , \qquad \text{A-52}$$

$$g_\pm = \left[\frac{\omega \mu_b}{c_{ms}^2} \pm \frac{1}{V_{oe}} \sqrt{\frac{(\omega^2 - \omega_{pe}^2)\mu_b}{c_{ms}^2}} \right] , \qquad \text{A-53}$$

and the α_n are arbitrary constants.

Performing the transformation without neglecting collisions

$$\bar{P}' = U\bar{P} = R^{-1}\bar{w}' = R^{-1} S R R^{-1} \bar{w} = R^{-1} S R \bar{P} \,. \qquad \text{A-54}$$

and

$$U = -j \begin{Vmatrix} \left(\frac{\omega}{V_{oe}} + j\frac{\nu_e \omega [f_- g_+ - f_+ g_-]}{V_{oe} Z_d}\right) & \left(j\frac{\nu_e \omega f_+ g_-}{V_{oe} Z_d}\right) & \left(-j\frac{\nu_e \omega f_- g_+}{V_{oe} Z_d}\right) \\ \left(j\frac{\nu_e \omega_{pe}^2 \mu_b [f_- g_+ - f_+ g_-]}{c_{ms}^2 g_- V_{oe} Z_d}\right) & \left(\sqrt{\frac{(\omega^2 - \omega_{pe}^2)\mu_b}{c_{ms}^2}} + j\frac{\nu_e \omega_{pe}^2 \mu_b f_+}{c_{ms}^2 V_{oe} Z_d}\right) & \left(\frac{-j\nu_e \omega_{pe}^2 \mu_b f_- g_+}{c_{ms}^2 V_{oe} Z_d g_-}\right) \\ \left(j\frac{\nu_e \omega_{pe}^2 \mu_b [f_- g_+ - f_+ g_-]}{c_{ms}^2 g_+ V_{oe} Z_d}\right) & \left(j\frac{\nu_e \omega_{pe}^2 \mu_b f_+ g_-}{c_{ms}^2 V_{oe} Z_d g_+}\right) & \left(-\frac{(\omega^2 - \omega_{pe}^2)\mu_b}{c_{sm}^2} - j\frac{\nu_e \omega_{pe}^2 \mu_b f_-}{c_{sm}^2 V_{oe} Z_d}\right) \end{Vmatrix}, \quad \text{A-55}$$

where

$$Z_d = \frac{\omega_{pe}^2 \mu_b}{c_{sm}^2}\left[f_- - f_+\right] - \omega\left[f_- g_+ - f_+ g_-\right] . \quad \text{A-56}$$

As can be seen from the above matrix, collisions have the effect of modifying the normal modes by coupling one to another. Thus, collisions not only provide a loss mechanism in this system but also couple the carrier mode to the modified spin wave modes. In the region of synchronism,

$$\frac{\omega}{V_{oe}} \cong \sqrt{\frac{(\omega^2 - \omega_{pe}^2)\mu_b}{c_{ms}^2}} , \quad \text{A-57}$$

this coupling results in a collision induced instability.[22]

Appendix III

Preparation of Contacts to Epitaxial Gallium Arsenide Used In Surface Wave Transmission Studies

The gallium arsenide was cut into 0.300" x 0.100" x 0.015" sections and contacts were prepared using a method similar to that described by Cohen et. al.[121] First the gallium arsenide was cleaned in trichloro-ethelyne, acetone and isopropyl alcohol. After a quick dip in an etching solution consisting of $H_2O_2 - H_2SO_4 - H_2O$ in a 1:3:5 ration (the etch rate of a 1:3:1 solution is 5 μ/min.[122]) the sample was rinsed in distilled water and briefly washed in EDTA solution (44 gm. of NaOH and 44 mgm. of ethylenediaminetetraacetic acid dissolved in 1 liter of H_2O) 1:3 H_2O. After rinsing in distilled water and isopropyl alcohol the GaAs sample was dried with nitrogen and inserted into a stainless steel mask.

Contacts to the gallium arsenide were formed from a mixture of silver, indium and tin in a 8:1:1 ratio . The silver was obtained by cutting a piece of 0.010 inch diameter silver wire to a length of 12 inches. It was cleaned by etching for 10 seconds in an $NH_4OH:H_2O$, 5:2 solution and then rinsed with distilled water. The indium and tin were obtained from a 1/3 of an inch length of 0.030 inch diameter 50-50 In-Sn wire. The wire was etched for 10 seconds in a 5:2 solution of H_2O and HCL, rinsed in distilled water and then placed together with the silver in a crucible in a vacuum deposition unit where they were melted together in an Argon ambient at a pressure of 1 atm..

After the sample, housed in the stainless steel mask, was mounted in the vacuum deposition unit, it was exposed to 5 minutes of ion bombardment in a 0.35 tor (mm. Hg) Argon atmosphere. Following the ion bombardment, the chamber pressure was reduced to 1.5×10^{-5} tor and the gallium arsenide was heated to 160^0 C. After an initial outgassing period, during which the GaAs was protected by a shutter, the Ag-In-Sn mixture was evaporated coating the contact surfaces.

After cooling, the pressure within the chamber was allowed to return to atmospheric, whereupon the gallium arsenide sample was removed. The contacts were then alloyed by heating the sample to 550^0 C in an Argon atmosphere for two minutes. After the alloying process the contacts were checked and found to be ohmic. The sample resistance was measured to be 835 ohms corresponding to an average epitaxial layer thickness of approximately 0.3 μ between the contacts spaced 210 mils apart.

REFERENCES

1. J. Helszajn, "Principles of Microwave Ferrite Engineering", Chapter 6, Wiley-Interscience, 1969.

2. Ibid, Chapter 8.

3. Ibid, Chapter 10.

4. M.E. Hines, "Reciprocal and Nonreciprocal Modes of Propagation in Ferrite Stripline and Microstrip Devices", IEEE Trans. MTT, Vol. 19, pp. 442-451, 1971.

5. R.W. Damon and J.R. Eshbach, "Magnetostatic Modes Of A Ferromagnetic Slab", J. Phys. Chem. Solids, Vol. 19, pp. 308-320, 1961.

6. J. K. Brundle and N.J. Freedman, "Magnetostatic Surface Waves On A Y.I.G. Slab", Electronics Letters, Vol. 4, pp.132-134, 1968.

7. S.R. Seshadri, "Surface Magnetostatic Modes of a Ferrite Slab", Proc. IEEE, Vol. 58, pp. 506-507, 1970.

8. P. Young, "Efficient Broadband Excitation Of The n=0 Surface Magnetostatic Waves In A Y.I.G. Slab", Electronics Letters, Vol. 4, pp.566-568, 1968.

9. Idem, "Effect Of Boundary Conditions On The Propagation Of Surface Magnetostatic Waves In A Transversely Magnetized Thin Y.I.G. Slab", Electronics Letters, Vol. 5, pp. 429-431, 1969.

10. R.E. DeWames and T. Wolfram, "Characteristics of Magnetostatic Surface Waves For A Metalized Ferrite Slab", J. Appl. Phys., Vol. 41, pp. 5243-5246, 1970.

11. A.D. Bresler, "TE_{n0} Surface Waves At Ferrite-Air Interfaces", Microwave Research Institute Memo 48, R-723-59, PIB-651, Polytechnic Institute of Brooklyn, 1959.

12. L. Courtois, G. Declercq and M. Peurichard, "On The Non-reciprocal Aspect Of Gyromagnetic Surface Waves", AIP Conf. Proc. No. 5, Part 2, pp. 1541-1545, 1971.

13. F.W. Schott, T.F. Tao and R.A. Freibrun, "Electromagnetic Waves In Longitudinally Magnetized Ferrite Rods", J. Appl. Phys., Vol. 38, pp.3015-3022, 1967.

F.W.Schott and T.F.Tao, "On The Classification of Electromagnetic Waves In Ferrite Rods", IEEE Trans.MTT, Vol.16, pp.959-961, 1968.

T.F.Tau and J.W.Tully, "Nonmagnetostatic Volume and Surface Wave Modes On Gyromagnetic Y.I.G. Rod Waveguides", Appl.Phys.Lett., Vol.16, pp.194-196, 1970.

14. E.A.Stern and E.R.Callen, "Helicons and Magnons In Magnetically Ordered Conductors", Phys.Rev., Vol. 131, pp. 512-516, 1963.

15. A.I.Akhiezer, V.G.Bar'yakhtar and S.V.Peletminskii, "Coherent Amplification of Spin Waves", Soviet Phys., JETP, Vol.18, pp.235-238, 1964.

16. J.Spector and A.W.Trivelpiece, "Slow Waves In Ferrites And Their Interactions With Electron Streams", J. Appl.Phys., Vol.35, pp. 2030-2039, 1964.

17. H.N.Spector and T.N.Casselman, "Interaction Of Alfven Waves And Spin Waves In A Ferromagnetic Metal", Phys. Rev., Vol. 139, pp. A 1594-1597, 1965.

18. E.Schlömann, "Amplification of Magnetostatic Surface Waves By Interaction With Drifting Charge Carriers In Crossed Electric And Magnetic Fields", Ratheon Tech.Memo, T-789, 1968.

Idem, "Amplification Of Magnetostatic Surface Waves By Interaction With Drifting Charge Carriers In Crossed Electric And Magnetic Fields", J.A.P., Vol. 40, pp. 1422-1424, 1969.

19. B.Vural and E.E.Thomas, "Helicon-Spin Wave Interactions In The Magnetic Semiconductor $Ag_xCd_{1-x}Cr_2Se_4$", Appl. Phys.Lett., Vol. 13, pp.405-407, 1968.

20. B.Schneider, "Interaction Between Spin Waves And Electrons In A Hybrid Structure Of YIG and InSb", Appl. Phys. Lett., Vol. 13, pp. 405-407, 1968.

21. M.C.Steele and B.Vural, "Wave Interactions In Solid State Plasmas", Chapter 9, McGraw-Hill, 1969.

22. Ibid, Chapter 10.

23. B.B.Robinson, B.Vural and J.P.Parekh, "Spin-Wave/Carrier-Wave Interactions", IEEE Trans.ED, Vol.17, pp.224-229, 1970.

24. A.V. Vashkovshii, V.I. Zubkov, V.N. Kil'dishev and B.A. Murmushev, "Interaction of Surface Magnetostatic Waves With Carriers On A Ferrite-Semiconductor Interface", Sov. Phys. JETP Lett., Vol. 16, pp. 2-4, 1972.

25. L.J. Abella and B. Vural, "Normal Mode Formulation Of Spin Wave-Helicon Wave Interactions In Ferromagnetic Semiconductors, IEEE Trans ED, Vol. 19, pp. 928-932, 1972.

26. M. Masuda, N.S. Chang and Y. Matsuo, "Magnetostatic Surface Waves In Ferrite Slab Adjacent To Semiconductor", IEEE Trans. MTT, Vol. 22, pp. 132-135, 1974.

27. H.W. Lehman, "Semiconducting Properties Of Ferromagnetic $CdCr_2Se_4$", Phys. Rev., Vol. 163, pp. 488-498, 1967.

28. R.E. Collin, "Foundations For Microwave Engineering", Chapter 2, McGraw-Hill, 1966.

29. D.H. Martin, "Magnetism In Solids", Chapter 1, The MIT Press, 1967.

30. W.H. Von Aulock, "Handbook Of Microwave Ferrite Materials", Chapter 1, Academic Press, 1965.

31. G.A. Smolenski, C. Tszun, and A.K. Stankevich, "Influence Of Electron Diffusion On The Radio-Frequency Dispersion Of the Magnetic Permeability Of Ferrites With A Garnet Type Structure", Sov. Phys. Sol. State, Vol. 3, p. 486, 1961.

32. R.F. Soohoo, "Theory and Application of Ferrites", Chapter 1, Prentice-Hall, 1960.

33. Ibid, Chapter 5.

34. D.H. Martin, "Magnetism In Solids", Chapter 2, The MIT Press, 1967.

35. C. Kittel, "Introduction To Solid State Physics", Chapter 14, John-Wiley & Sons, 1967.

36. A.F. Ahkiezer, V.G. Bar'yakhtar and S.V. Peletminskii, 'Spin Waves", Chapter 1, John Wiley & Sons, 1968.

37. L.V. Azároff and J.J. Brophy, "Electronic Processes In Materials", Chapter 13, McGraw-Hill, 1963.

38. M. Javid and P.M. Brown, "Field Analysis and Electromagnetics", Chapter 6, McGraw-Hill, 1963.

39. S. Chikazumi, "Physics Of Magnetism", Chapter 7, John Wiley & Sons, 1964.

40. M. Sparks, "Ferromagnetic-Relaxation Theory", Chapter 2, McGraw-Hill, 1964.

41. C. Kittel, "Introduction To Solid State Physics", Chapter 15, John Wiley & Sons, 1967.

42. E. G. Spencer, R. C. LeCraw and A. M. Clogston, "Low-Temperature Line-Width Maximum In Yttrium Iron Garnet", Phys. Rev. Lett., Vol. 3, pp. 32-33, 1959.

43. R. F. Soohoo, "Magnetic Thin Films", Chapter 10, Harper & Row, 1965.

44. M. S. Cohen, "Ferromagnetic Properties Of Films", in "Handbook Of Thin Film Technology", Chapter 17, L. I. Maisel and R. Glang ed., McGraw-Hill, 1970.

45. G. V. Skrotskii and L. V. Kurbatov, "Phenomenological Theory Of Ferromagnetic Resonance", in "Ferromagnetic Resonance", Chapter II, S. V. Vonsovskii ed., Pergamon Press, 1966.

46. M. Sparks, "Ferromagnetic Resonance In Thin Films. III Theory Of Mode Intensities", Phys. Rev. B, Vol. 1, pp. 3869-3880, 1970.

47. R. F. Soohoo, "Magnetic Thin Films", Chapter 11, Harper & Row, 1965.

48. M. Sparks, "Effect Of Exchange On Magnetostatic Modes", Phys. Rev. Lett., Vol. 24, pp. 1178-1180, 1970.

49. P. E. Wigen, C. F. Kooi, M. R. Shanabarger and T. D. Rossing, "Dynamic Pinning In Thin-Film Spin-Wave Resonance", Phys. Rev. Lett., Vol. 9, pp. 206-208, 1962.

50. A. M. Portis, Low-Lying Spin Wave Modes In Ferromagnetic Films", Appl. Phys. Lett., Vol. 2, pp. 69-71, 1963.

51. M. Sparks, "Spin-Wave Energy And Source Of Inhomogeneities In Thin Films", Sol. State Comm., Vol. 8, pp. 659-663, 1970.

52. C. Kittel, "Excitation Of Spin Waves In A Ferromagnet By A Uniform r.f. Field", Phys. Rev., Vol. 110, pp. 659-663, 1970.

53. P. Pincus, "Excitation Of Spin Waves In Ferromagnets: Eddy Current And Boundary Condition Effects", Phys. Rev., Vol. 118, pp. 658-664, 1960.

54. G.T.Rado and J.R.Weertman, "Spin-Wave Resonance In A Ferromagnetic Metal", J.Phys.Chem.Solids, Vol.11, pp.315-333, 1959.

55. M.Sparks, B.R.Tittman, J.E.Mee and C.Newkirk, "Ferromagnetic Resonance In Epitaxial Garnet Thin Films", J.Appl.Phys., Vol. 40, pp. 1518-1525, 1969.

56. P.E.Wigen, C.F.Kooi and M.R.Shanabarger, "Evidence Of Unpinned Surface Spins From Parallel Spin-Wave Resonances In Permalloy Films", J.Appl.Phys., Vol.35, pp.3302-3311, 1964.

57. R.E.DeWames and T.Wolfram, "Surface Spin-Waves In A Semi-infinite Ferromagnet Including Exchange And Dipolar Fields", Sol. State Comm., Vol.7, pp.1451-1452, 1969.

58. T.Wolfram and R.E.DeWames, "Linewidth and Dispersion Of The Virtual Magnon Surface State In Thick Ferromagnetic Films", Phys.Rev.B., Vol.1, pp.4358-4360, 1970.

59. W.L.Bongianni, "Magnetostatic Propagation In A Dielectric Layered Structure", J.Appl. Phys., Vol.43, pp.2541-2548, 1972.

60. J.P.Parekh, "Magnetostatic Surface Waves On A Partially Metallized YIG Plate", Proc. IEEE (Letters). Vol. 61, pp.1371-1373, 1973.

61. F.A.Pizzarello, J.H.Collins and L.E.Coerver, "Magnetic Steering Of Magnetostatic Waves In Epitaxial YIG Films", J.Phys., Vol.41, pp. 1016-1017, 1970.

62. M.Sparks, "Magnetostatic Modes In An Infinite Circular Disk", Sol. State Comm., Vol.8, pp.731-733, 1970.

63. B.Desormiere and H.LeGall, "Magnetostatic Mode Excitation In YIG Rods Containing A Turning Point", J.Appl.Phys., Vol.40, pp. 1191-1192, 1969.

64. R.E.DeWames and T.Wolfram, "Magnetostatic Surface Modes In An Axially Magnetized Elliptical Cylinder", Appl.Phys.Lett., Vol.16, pp.305-308, 1970

65. L.R.Walker, "Magnetostatic Modes In Ferromagnetic Resonance", Phys. Rev., Vol. 105, pp.390-399, 1957.

66. M. Sparks, "Ferromagnetic Resonance in Thin Films. I Theory Of Normal-Mode Frequencies", Phys.Rev.B., Vol.1, pp.3831-3856, 1970.

67. W.S.Ament and G.T.Rado,"Electromagnetic Effects Of Spin Wave Resonance In Ferromagnetic Metals", Phys.Rev., Vol.97, pp.1558-1566, 1955.

68. T.Wolfram and R.E.DeWames, "Effect Of Exchange On The Magnetic Surface States Of Yttrium Iron Garnet Films", Sol.State Comm., Vol.18, pp. 191-194, 1970.

69. D.M.Bolle and L.Lewin, "On The Definitions Of Parameters In Ferrite-Electromagnetic Wave Interactions", IEEE Trans MTT, Vol. 21, p.118, 1973.

70. M.Sparks, "Theory Of Surface-Spin Pinning In Ferromagnetic Resonance", Phys. Rev. Lett., Vol.22, pp.1111-1115, 1969.

71. J.R.Eshbach and R.W.Damon, "Surface Magnetostatic Modes and Surface SpinWaves", Phys.Rev., Vol.118, pp.1208-1210, 1966.

72. S.D.Conte and C.deBoor. "Elementary Numerical Analysis", Chapter 2, McGraw-Hill, 1972.

73. B.Lax and K.J.Button, "Theory Of New Ferrite Modes In Rectangular Wave Guide", J.Appl.Phys.,Vol.26, pp.1184-1185, 1955.

74. K.J.Button and B.Lax, "Theory Of Ferrites In Rectangular Waveguides", IRE Trans. AP, Vol.4, pp.531-537, 1956.

75. M.L.Kales, H.N.Chait and N.G.Sakiotis, "A Nonreciprocal Microwave Component", J.Appl.Phys., Vol. 24, pp. 816-817, 1953.

76. B.Lax, K.J.Button and L.M.Roth, "Ferrite Phase Shifters In Rectangular Wave Guide", J.Appl.Phys., Vol.25, pp.1413-1421, 1954.

77. H.Seidel and R.C.Fletcher, "Gyromagnetic Modes In Waveguide Partially Loaded With Ferrite", BSTJ,Vol.38, pp.1427-1456, 1959.

78. R. Pauchard, B.Désormière and J.Guidevaux, "Electromagnetic Surface Waves In A Metallised Ferrite Slab", Electronics Letters, Vol.7, pp. 428-430, 1971.

79. D.F.Vaslow, "Group Delay Time For The Surface Wave On A YIG Film Backed By A Grounded Dielectric Slab", Proc. IEEE, Vol. 61., pp.142-143, 1973.

80. E.Schlömann, "Generation Of Spin Waves In Non-uniform Magnetic Fields I. Conversion Of Electromagnetic Power Into Spin-Wave Power and Vice Versa", J.Appl.Phys., Vol. 35, pp. 159-166, 1964.

81. M.Sparks, "Magnetostatic Surface Modes Of A YIG Slab", Electronics Letters, Vol. 5, pp. 618-619, 1969.

82. C.C.Johnson, "Field And Wave Electrodynamics", Chapter 7, McGraw-Hill, 1965.

83. E.H.Holt and R.E.Haskell, "Foundations Of Plasma Dynamics", Chapter 6, The Macmillan Co., 1965.

84. S.Wang, "Solid-State Electronics", Chapter 4, McGraw-Hill, 1966.

85. M.C.Steele and B.Vural, "Wave Interactions In Solid State Plasmas", Chapter 4, McGraw-Hill, 1969.

86. M.A.Uman, "Introduction To Plasma Physics", Appendix A, McGraw-Hill, 1964.

87. D.Pines and D.Bohm, "A Collective Description Of Electron Interactions: II. Collective vs. Individual Partical Aspects Of The Interactions", Phys. Rev.,Vol.85, pp.338-353, 1952.

88. I.Tamm, "Uber Einen Mogliche Art Der Electronenbindung An Kristalloberflachen", Physik. Zeits. Sowjetunion, Vol.1, pp. 773-746, 1932.

Idem, "Uber Einen Mogliche Art Der Electronenbindung An Kristalloberflachen", Zeits. Physik,. Vol.76,pp.849-850,1932.

89. W.Shockley, "On The Surface States Associated With A Periodic Potential", Phys. Rev., Vol. 56, pp. 312-323, 1969.

90. L.V.Azaroff and J.J.Brophy, "Electronic Processes In Materials", Chapter 4, McGraw-Hill, 1963.

91. A.Many, Y.Goldstein and N.B.Grover, "Semiconductor Surfaces", Chapter 1, North-Holland Publishing Company, 1965.

92. Ibid, Chapter 9.

93. J.P.McKelvey, "Solid State and Semiconductor Physics", Chapter 10, Harper & Row, 1966.

94. Ibid, Chapter 16.

95. A.Many, Y.Goldstein and N.B.Grover, "Semiconductor Surfaces", Chapter 8, North-Holland Publishing Company, 1965.

96. Ibid, Chapter 4.

97. D.R.Frankl, "Electrical Properties Of Semiconductor Surfaces" Chapter 2, Pergamon Press, 1967.

98. G.A.Swartz and B.B.Robinson, "Electromagnetic Generation Techniques (Phase II)", Final Report, RCA Laboratories, 1967.

99. B.B.Robinson and G.A.Swartz, "Two-Stream Instability In Semiconducting Plasmas", J.Appl. Phys., Vol.38, pp.2461-2465, 1967.

100. C.A.Hogarth, "Materials Used In Semiconductor Devices", Chapter 6, Interscience Publishers, 1965.

101. H.Wolf, "Semiconductors", Chapter 1, John Wiley & Sons, 1971.

102. R.J.Briggs, "Electron-Stream Interaction With Plasmas" Chapter 2, MIT Press, 1964.

103. H.Hartnagel, "Semiconductor Plasma Instabilities", Chapter III, American Elsevier Publishing Co., 1969.

104. W.H.Louisell, "Coupled Mode And Parametric Interactions", Chapter 1. John Wiley & Sons, 1960.

105. C. Hilsum and A.C.Rose-Innes, "Semiconducting III-V Compounds, Chapter 6, Pergamon Press, 1961.

106. O.Madelung, "Physics Of III-V Compounds", Chapter 4, John Wiley & Sons, 1964.

107. E.O.Schulz-DuBois, "Energy Transport Velocity Of Electromagnetic Propagation In Dispersive Media", Proc. IEEE, Vol. 57, pp.1748-1757, 1969.

108. A.C.Prior, "Avalanche Multiplication And Electron Mobility In Indium Antimonide At High Electric Fields", J.Electron and Control, Vol. 4, pp. 165-168, 1968.

109. M.Ohsita, "High Mobility InSb Films Prepared By Source Temperature Programed Evaporation Method", Jap. J. Appl. Phys., Vol. 10, pp.1365-1371, 1971.

110. M.Ettenberg and J.S.Nadan, "The Theory Of The Interaction Of Drifting Carriers In A Semiconductor With External Traveling-Wave Circuits", IEEE Trans. ED, Vol. 17, pp.219-223, 1970.

111. R.Brown, "Thin Film Substrates", in "Handbook Of Thin Film Technology", Chapter 6, L.I.Maisel and R.Glang ed., Pergamon Press, 1966.

112. M.A. Gilleo and S. Geller, "Magnetic And Crystallographic Properties Of Substituted Yttrium Iron Garnet, $3Y_2O_3\ xM_2O_3\ (5-x)\ Fe_2O_3$", Phys. Rev., Vol. 110, pp. 73-78, 1958.

113. C.C. Johnson, "Field And Wave Electrodynamics", Chapter 1, McGraw-Hill, 1965.

114. Ibid, Appendix IV.

115. A. Sommerfield, "Electrodynamics", Chapter 12, Academic Press, 1952.

116. M. Javid and P.M. Brown, "Field Analysis and Electromagnetics", Chapter 8, McGraw-Hill, 1963.

117. J.R. Eshbach, "Spin-Wave Propagation And The Magnetoelastic Interaction In Yttrium Iron Garnet", J. Appl. Phys., Vol. 34, pp. 1298-1304, 1963.

118. B.O. Pierce, "A Short Table of Integrals", The Anthenaeum Press, 1910.

119. G. Petit Bois, "Tables Of Indefinite Integrals", Dover Publications, 1961.

120. B. Vural, J.P. Parekh and E.E. Thomas, "Observation Of A Collision Induced Instability In An Semiconductor-Magnetic Composite Structure-Private Communication.

121. M.S. Cohen, S.N. Cutler and C.N. Klahr, "GaAs Doping For Microwave Application", Tech. Rep. AFAL-TR-68-42, 1968.

122. R.K. Willardson and H.L. Goering, "Compound Semiconductors", Vol. 1, "Preparation Of III-V Compounds", Reinhold Publishing, 1962.

123. H. Wolf, "Semiconductors", Chapter 3, John Wiley & Sons, 1971.

AUTOBIOGRAPHICAL STATEMENT

Thomas James Gerson was born in New York City on November, 1942. A recipient of a New York State Regents Scholarship, Mr. Gerson attended the City College of the City University of New York where he majored in electrical engineering. Graduating in February of 1965, Mr. Gerson continued his education while employed at the Environmental Testing Laboratory of GPL Div. of General Precision, Inc. Receiving a National Defense Education Act Fellowship in September of 1966, Mr. Gerson returned to the City University as a full time student and was awarded the Master's degree in electrical engineering from the City College in June of 1967.

From 1968 to 1972 Mr. Gerson was a member of the instructional staff in the Electrical Engineering Department and Bachelor of Technology Division of the School of Engineering of the City College of the City University of New York. Presently, he is an Instructor in the Department of Electrical Technology of Queensborough Community College of the City University of New York. Mr. Gerson is a member of Eta Kappa Nu, Tau Beta Pi, Sigma Xi, the Institute of Electrical and Electronics Engineers and the American Society for Engineering Education.

Mr. Gerson resides in Brooklyn with his wife Maggie and son Adam.